UNIVERSITÀ
DEGLI STUDI
DI PADOVA

SEDE AMMINISTRATIVA: UNIVERSITÀ DEGLI STUDI DI PADOVA
CISAS – CENTRO D'ATENEO DI STUDI ED ATTIVITÀ SPAZIALI G. COLOMBO

SCUOLA DI DOTTORATO DI RICERCA IN: Scienze Tecnologie e Misure Spaziali
INDIRIZZO: Misure Meccaniche per l'Ingegneria e lo Spazio
CICLO XXVII

DEVELOPMENT AND CHARACTERIZATION OF STANDARDIZED DOCKING SYSTEM FOR SMALL SPACECRAFT

Direttore della Scuola: Ch.mo Prof. Giampiero Naletto
Coordinatore d'indirizzo: Ch.mo Prof. Stefano Debei
Supervisore: Ch.mo Prof. Alessandro Francesconi

Dottorando: Lorenzo Olivieri

"Nothing is impossible. Not if you can imagine it. That's what being is a scientist is all about."

H. J. Farnsworth

"There is perhaps no better demonstration of the folly of human conceits than this distant image of our tiny world. To me, it underscores our responsibility to deal more kindly with one another, and to preserve and cherish the pale blue dot, the only home we've ever known."

C. Sagan (Pale Blue Dot: A Vision of the Human Future in Space)

UNIVERSITA' DI PADOVA

Abstract

CISAS – Centro d'Ateneo di Studi ed Attività Spaziali G. Colombo

DEVELOPMENT AND CHARACTERIZATION OF STANDARDIZED DOCKING SYSTEM FOR SMALL SPACECRAFT

by Lorenzo Olivieri

Since the first mating manoeuvre in space, performed in 1966, many different docking mechanisms were developed, mainly for large manned spacecraft. The few systems recently conceived for small satellites have never been verified in space nor scaled to CubeSat size. In the near future, small spacecraft docking procedures could acquire great importance due to the need to share resources between clusters of low-weight and low-cost vehicles: in fact, small spacecraft market is rapidly growing, focusing on commercial low risk application, low budget scientific and educational missions. In this context, this document presents a novel docking mechanism to provide small spacecraft with the ability to join and separate in space, to realize multi-body platforms able to rearrange, be repaired or updated, thus overcoming the actual on board limitations of single small-scale satellites. As for now, the few proposed docking ports present (1) simple probe-drogue interfaces, unable to dock with same-gender ports, or (2) androgynous geometries, that can overcome that problem, but usually employing complex and non-axis-symmetric latches to perform the docking manoeuvre, that would demand robust and stringent navigation and control systems. The proposed solution overcomes the aforementioned drawbacks, using a semi-androgynous shape-shifting mechanism that actuating one interface changes the port into a "drogue" configuration, letting the other port penetrate it and closing around to create a solid joint. The mechanism design through the requirement definition and a trade-off between different concepts is presented, followed by the analysis of the dynamic behaviour of the selected solution, with particular attention to two aspects, i.e. the loads transmitted between the mating ports and the alignment tolerances requested to perform successful docking manoeuvres. Such analysis led to the definition of an instrumented prototype to verify the solution through simple validation tests, which demonstrated the mechanism operations and defined the alignment ranges, that lie in the range of ± 15 mm and up to 6 degrees. Last, a comparison with SPHERES UDP is presented, as part of the activities performed during a visit period at MIT Space Systems Laboratory.

Summary

The continuously growing interest in small satellites and CubeSat missions is related to the significant potential to drastically cut the costs to access space, thus encouraging the development of space activities for educational purposes as well as low-cost, low-risk commercial applications and low budget scientific and technological missions. However, important technical restrictions related to the limited on board available resources are still preventing the employment of nanosatellites for complex and high performance missions, while the development of rendezvous and joining technologies could provide miniature space vehicles with the capability to aggregate in larger structures, thus addressing the volume and power needs for complex payloads. Giving small satellites docking abilities would enable scenarios where independent vehicles like CubeSats can join together to generate multipart space systems with the possibility to rearrange, be repaired or updated on orbit. Large structures such as segmented mirrors telescopes or solar arrays fields can be realized through the mechanical connection of many small satellites. These peculiarities would allow to optimally meet any variable mission requirements and to extend the practical duration of missions. Most noticeably, this improvement is a crucial step in the direction of making nanosatellite platforms competitive with traditional space vehicles. Deep-space exploration programs could also need the design of docking or at least capturing systems: for example, sample and return missions from Mars or other planets and moons would involve several spacecraft that can dock and separate.
In parallel, joining capabilities with non cooperative bodies (i.e. small asteroids, old satellites and their fragments) or operative spacecraft without docking interfaces are conditioned and limited by the state of the art technology of docking and capture systems. In the design of small commercial and scientific automatic spacecraft, docking operations were not considered, thereby possible refuelling and servicing missions for LEO and GEO satellites are subjected to compatibility problems.
The goals of this work are (1) the design of a novel docking mechanism, starting from state of the art analysis (Chapter 1) and constraints and requirements definition (Chapters 2-3), (2) the realization of an instrumented prototype (Chapter 4) and (3) its test on a dedicated test-bed (Chapter 5). In parallel, the activities performed during a visiting period at MIT are presented in Chapter 6.
To be more precise, Chapter 2 presents a numerical study of the loads transmitted between two mated spacecraft, defining a series of mechanical constraints that characterize the docking interface and evaluating some possible configurations of the control strategy of the assembled body. A simple analytical model allowed to define the docking joint required mechanical resistance in function of estimated disturbances, parametrized on the satellites mass: for example, two 20 kg spacecraft would require an axial resistance of 1 N and torsional and flexional resistances of about 0.1 Nm due to the disturbances

and the loads acting on a 700 km high orbit. As regards the stiffness, it was shown its dependence with the assembled structure requirements in terms of relative alignment and position of the composing vehicles: in case of optical payloads without dedicated pointing systems, such values would be around 10^{-7} m, hardly satisfiable for satellites larger than CubeSats. More complex simulations determined that damping ratios higher of 0.001 help to reduce transmitted vibrations of about 50% respect to configurations with ratios under 10^{-4}.

Chapter 3 describes the preliminary design of a new concept docking system, based on State of the Art analysis, practical considerations and requirements and constraints definition. The description of the main requirements the mating interface had to satisfy led to the definition of different level conflicts between them. The hardest conflicts were related to androgyny, rotational symmetry and simplicity; information from the conflict analysis helped to define relaxing requirements and the effect of different design solutions on the docking subsystem characteristics. At the same time, small spacecraft have restricted on-board resources, limiting the possible payload mass, volume and electrical power, that shall be taken in account in the design process. In order to establish a good compromise solution, three different classes of requirements were defined, weighting the influence of these three features; on these basis, a conceptual solution has been developed for each class, analysing and comparing characteristics and weaknesses. The first mechanism is directly inspired to the standard ISS androgynous interfaces and presents a three petals structure with an external soft docking ring. It consequently benefits from the consolidated design aspects but also presents some minor disadvantages of power consumption and mass budget. The second concept has axis-symmetric interfaces with a "probe and drogue" configuration with new-concept totally passive latches: the capture mechanism is designed to perform docking manoeuvres demanding only a well-defined chaser approach velocity and to separate using only spacecraft propulsion abilities. The mechanism main feature, the capability to do not consume electric power, may be the source of its main drawback: well-defined approach velocities and propulsion capabilities can be too stringent for spacecraft and may cause high impact forces and transmitted loads. The third solution is designed to combine the advantages of an androgynous system with the simplicity of a gender mating mechanism, using a shape-shifting structure. Far from the existing interfaces, the presented solution does not employ active latches for hard docking and uses only one electric motor for activation and docking: the internal stiffness and pre-load in the docked configuration creates the solid joint. A comparison between the three concepts and their requirements and constraints suggested that the third solution seemed a good compromise and it was therefore selected for further developments.

In Chapter 4 the docking interface detailed design is presented, introducing three different topics: geometric development, dynamic analysis and components manufacturing

and procurement. The proposed solution implements an actuating disk able to open and close eight peripheral petals, creating a semi-androgynous port capable to wrap around a twin one and to capture it. The petals opening mechanism was investigated, comparing two solutions, using respectively a rotational joint and a translational cam; a trade-off between the two solutions indicated that the cam was the more simple and reliable one. In this basis, the whole port is described and its working principle is briefly explained. Dynamical simulations allowed to analyse the port behaviour starting from simple models to evaluate the cams design and adding more complex characteristics to perform more accurate and specific investigations. Results permitted to define the amount of friction acting in the cam mechanisms and its effect on the petals opening and closing process, and then to verify the whole interface actuation, the transmitted loads and, last, a simplified docking procedure. At the end of the chapter,a brief risk analysis was performed and some technical solutions to increase the mechanism reliability were analysed, although they were not implemented in the tested prototype.

Chapter 5 introduces the test campaign performed on the developed prototype. The test-bed is a simple open-loop 1-DoF platform, in which the target is fixed on an instrumented structure and the chaser can approach it moving on a rail system. A partial freedom to rotate is also given to the chaser, thanks to suspension strings connecting it to the frame moving on the rail. The experimental verification, in order, aimed to (1) validate the prototype geometry and the opening-closing mechanism through functional tests, (2) determine the loads transmitted to the framework system during nominal docking procedures, and (3) evaluate the working range of the port, in terms of maximal allowable linear and angular displacements with respect to the nominal docking operation.

Results demonstrated the mechanism operation, and verified that collected loads were always under 3 N, never affecting the mechanism action. Last, the misalignment test defined the interfaces mechanical ranges in terms of allowed lateral and angular misalignments to perform complete docking procedures.

As depicted in Chapter 6, at the MIT Space Systems Laboratory, in the framework of the SPHERES programme, the Universal Docking Port (UDP) is in development, consisting of a new androgynous interface compatible with the test platforms and planned to fly on ISS in 2015. The SPHERES ground test bed consists in a low friction glass table, on which it is easy to test the developed hardware and control software to verify it before in-space experimental validation. A visiting period of about two months allowed to understand the methodology behind the UDP development and management and more generally the advantages to use a fast-available test bed for the continuous comparison between developed numerical investigation and its verification. In this period, some control codes for the SPHERES were developed, to test the rendezvous and docking on the low friction facility. Simulations demonstrated the goodness of the proposed manoeuvres

and the reliability of both collision avoidance and close rendezvous controllers; unfortunately, some issues related to the SPHERES state determination affected the system during the test campaign, preventing the complete verification of the developed code. Last, a comparison between the UDP and our semi-androgynous port showed that the latter has a larger working range in terms of accepted angular and lateral misalignments at docking.

In Chapter 7, the whole work is summarized and some conclusions are presented. The semi-androgynous port is evaluated to have reached a Technology Readiness Level of 3-4. Some observations are exposed, related to the test in a more relevant environment and the design of dedicated sensors for close navigation and docking. In parallel, other activities related to docking are reported. First, an improved version of the semi-androgynous port is presented, with rotating actuation instead of the linear motor to reduce the interface bulk. Second, the concept of tethered soft docking is described, consisting in employing a magnetic tether probe to perform the soft docking procedure, significantly simplifying the spacecraft joining operations and reducing the system complexity; preliminary activities on such topic included the FELDs experiment, aiming to assess the automatic self-alignment of the probe in 0-g environment.

In conclusion, a long research work is still to be performed, aiming to reach higher TRLs; some indications on future development are introduced, considering the continuously increasing interest on small spacecraft rendezvous, docking and, more generally, proximity operations. The run for space is at its beginning, and joining technologies are already a fundamental and unique enabler for most of the servicing activity, with positive and increasing opportunities for the next and far future, both in research and commercial fields. It is only matter of time before humankind will realize fleets of small spacecraft able to self assemble and repair each others or larger ones, or to move on interplanetary routes, transporting fuel, resources and scientific samples.

Sommario

Negli ultimi anni si nota un crescente interesse nel campo dei piccoli satelliti e CubeSat, grazie alla consistente riduzione dei costi d'accesso allo spazio per tali veicoli, che ha incoraggiato tanto lo sviluppo di missioni nel settore "Educational" quanto l'investimento da parte di realtà commerciali e gruppi di ricerca per lo sviluppo di esperimenti scientifici e dimostrazioni tecnologiche. Allo stesso tempo, vincoli tecnici legati alle limitate risorse presenti a bordo rendono ancora marginale l'utilizzo di nanosatelliti per missioni di elevata complessità: lo sviluppo di tecnologie di rendez-vous e docking viene considerato come possibile soluzione, in quanto darebbe ai veicoli la capacità di aggregarsi in strutture più grandi, risolvendo le limitazioni in termini di volume e potenza disponibili, e consentendo di realizzare payload condivisi aventi elevata complessità. La possibilità di eseguire operazioni di aggancio e sgancio porterebbe quindi alla realizzazione di scenari di missione fino ad ora inimmaginabili, in cui veicoli indipendenti come CubeSat potrebbero unirsi per generare sistemi eterogenei capaci di riorganizzarsi, autoripararsi ed espandersi tramite l'aggiunta o la sostituzione di alcuni elementi. Strutture quali specchi telescopici modulari o campi di pannelli solari potrebbero quindi essere realizzati tramite la connessione meccanica di più satelliti di piccole dimensioni. Inoltre, queste capacità di docking renderebbero possibile tanto l'aumento della durata delle missioni (consentendo la sostituzione di elementi vetusti o malfunzionanti) quanto la possibilità di variarne gli obiettivi, grazie alla maggiore elasticità di missione. In base a queste considerazioni, lo sviluppo di tecnologie per il docking è considerato come un passo necessario verso l'obiettivo di rendere CubeSat e piccoli satelliti competitivi sul mercato, erodendo quote normalmente riservate a piattaforme ben più grandi, complesse e costose. Infine, vi sarebbe una positiva ricaduta anche nell'ambito dell'esplorazione scientifica del Sistema Solare: per esempio, nelle previste missioni di "sample-and-return" da Marte o da altri corpi celesti è stato più volte considerato fondamentale l'impiego di sistemi di docking, per consentire il trasporto ed il trasferimento dei campioni raccolti, così da utilizzare sonde più piccole e meno complesse per le differenti attività di estrazione, inserimento in orbita e ritorno alla Terra.

Parallelamente, le ricerche sulle tecnologie di aggancio con corpi non cooperativi quali asteroidi, detriti o satelliti vecchi o non più funzionanti, oppure privi di interfacce di docking, sono al momento limitate e condizionate dall'attuale assenza di un solido background sperimentale. Nella progettazione di satelliti commerciali o scientifici, lo sviluppo di meccanismi di aggancio non è mai stato preso in considerazione, per cui al momento vi sono insormontabili limitazioni tecniche che impediscono la realizzazione di missioni di refuelling e manutenzione per veicoli già in orbita.

Gli obbiettivi del lavoro presentato in questo documento sono nell'ordine:

- l'analisi dello stato dell'arte delle tecnologie di docking e cattura per piccoli satelliti (capitolo 1);
- la definizione di una serie di requisiti per tali sistemi e un confronto tra possibili soluzioni progettuali (capitoli 2 e 3);
- la realizzazione ed il test di un prototipo semplificato (capitoli 4 e 5).

In parallelo, nel capitolo 6 sono descritte le attività di ricerca eseguite durante un periodo di soggiorno presso il Massachusetts Institute of Technology.
Più precisamente, il capitolo 2 presenta lo studio numerico dei carichi trasmessi tra due satelliti agganciati, definendo una serie di vincoli meccanici che caratterizzino l'interfaccia di docking e valutando possibili strategie di controllo del sistema assemblato. Un semplice modello analitico ha permesso di definire le rigidezze e le resistenze meccaniche del giunto di docking, in funzione dei disturbi esterni, stimati e parametrizzati sulla massa dei satelliti. Per esempio, due satelliti in orbita di 700 km di altitudine, aventi masse di 20 kg, richiederebbero una resistenza ai carichi assiali di 1 N e ai carichi torsionali e flessionali di circa 0.1 Nm. Riguardo alla rigidezza, si è dimostrata una dipendenza con i requisiti di allineamento e posizione propri dei singoli veicoli: nel caso di payload ottici non autoconsistenti dal punto di vista del puntamento, tali requisiti sarebbero nell'ordine di $10^{[}-7]$ m, difficilmente soddisfabili per satelliti di classe maggiore dei CubeSat. Simulazioni più avanzate hanno anche permesso di determinare che coefficienti di smorzamento più alti di 0.001 consentono di ridurre le vibrazioni trasmesse dal meccanismo di circa il 50% rispetto a configurazioni con smorzamenro pari a $10^{[}-4]$.
Il terzo capitolo descrive la progettazione preliminare del sistema di docking, basata sulle soluzioni attualmente esistenti, su considerazioni pratiche e sulla definizione dei requisiti e dei vincoli. La descrizione di tali requisiti ha inoltre portato alla discussione di possibili conflitti che possono nascere tra di essi. Per esempio, le contrapposizioni più onerose sorgono tra androginia, simmetria rotazionale e semplicità; l'analisi di tali conflitti è stata necessaria per definire il rilassamento di alcuni requisiti e l'effetto di differenti soluzioni progettuali. Allo stesso tempo, le risorse diponibili a bordo di piccoli satelliti sono usualmente limitate, con la conseguente ridotta capacità di ospitare carichi voluminosi, di massa elevata, o con alte richieste di potenza elettrica; tali vincoli devono essere tenuti in considerazione durante la fase progettuale. Per queste ragioni, con lo scopo di realizzare una soluzione ottima, sono state definite tre diverse classi di requisiti, dando diverso peso alle tre caratteristiche di androginia, simmetria e semplicità; in tale modo, per ogni gruppo è stata sviluppata una soluzione concettuale, così da studiarne e compararne i punti di forza e debolezza. Il primo meccanismo è direttamente ispirato alle interfacce standard installate sulla Stazione Spaziale Internazionale,

e utilizza una struttura a tre petali con un disco esterno per il soft-docking. Di conseguenza, beneficia di consolidate soluzioni progettuali, ma allo stesso tempo presenta alcune problematiche legate all'elevato consumo di potenza e alla non trascurabile massa. La seconda soluzione esposta presenta una logica "maschio-femmina", utilizzando interfacce assialsimmetriche, e con un sistema di aggancio totalmente passivo: il meccanismo di cattura è progettato per funzionare grazie all'energia cinetica scambiata durante la fase di docking, avendo quindi come requisiti solo una ben definita velocità di approccio per eseguire l'aggancio e capacità propulsive per lo sgancio. Questa caratteristica, il non consumare potenza elettrica, è forse l'origine dei principali svantaggi di questa interfaccia: l'intervallo di possibili velocità e spinte propulsive per eseguire le manovre potrebbe essere troppo stringente per i satelliti e potrebbe causare eccessivi impatti e carichi trasmessi. Infine, il terzo meccanismo è progettato per unire i vantaggi di sistemi androgini con la semplicità di quelli "maschio-femmina", usando una struttura mutaforma. Al contrario dalle soluzioni attualmente esistenti, questa soluzione non utilizza sistemi di aggancio attuati ma solo un motore elettrico per l'attivazione e il docking: la rigidezza della connessione viene realizzata solo grazie al precarico che si viene a realizzare durante l'aggancio. Il paragone tra le tre soluzioni e il confronto con requisiti e vincoli individua nel terzo meccanismo le migliori possibilità di sviluppo, presentate nel capitolo successivo.

Nel capitolo 4 viene presentato lo sviluppo dell'interfaccia, introducendo tre differenti argomenti: progettazione geometrica, analisi dinamiche e realizzazione di un prototipo. Il meccanismo qui sviluppato utilizza un disco attuato da un motore elettrico, che movimenta otto petali periferici, aprendoli e chiudendoli; la logica di semi-androginia permette quindi di avere un'interfaccia che, aprendosi, è capace di catturare una porta gemella ma non attuata, e di creare una connessione rigida chiudendosi attorno. Il meccanismo di apertura dei petali è quindi studiato, confrontando due possibili soluzioni baste rispettivamente su di un giunto rotativo e su di una camma lineare; dal confronto tra le due, si vede come il meccanismo a camma sia più semplice ed affidabile. Su queste premesse, l'intera interfaccia viene presentata ed il suo principio di funzionamento viene brevemente descritto. Una sere di simulazioni dinamiche consente poi di analizzare il comportamento della porta, partendo da un modello semplificato dedicato allo studio del meccanismo a camma e via via aggiungendo elementi ad accrescere la complessità così da realizzare analisi più specifiche ed accurate. I principali risultati permettono di valutare l'entità delle forze di attrito agenti sul meccanismo a camme, ed il suo effetto sul processo di apertura e chiusura dei petali, ed infine di verificare l'attuazione dell'intera interfaccia, i carichi trasmessi, e di simulare un'intera procedura di docking. Infine, una breve analisi di affidabilità viene introdotta, definendo le principali criticità del meccanismo e possibili soluzioni progettuali o operative a tali problematiche.

Il capitolo 5 introduce i test eseguiti sul prototipo sviluppato e precedentemente descritto. Il test-bed consiste in una semplice piattaforma a 1 grado di liberta traslazionale, nel quale il target è montato su di una struttura strumentata, mentre il chaser può muoversi su di una rotaia tramite un carrellino. Una ridotta mobilità rotazionale è allo stesso tempo concessa al chaser stesso, grazie ad un sistema di supporti che lo connettono al carrellino. Nell'ordine, i test hanno avuto come obiettivo (1) la validazione delle geometrie e del meccanismo di apertura e chiusura, (2) la determinazione dei carichi trasmessi alla struttura durante procedure nominali di docking, ed infine (3) la valutazione del campo di disallineamenti lineari ed angolari che le porte possono avere rispetto alle condizioni nominali riuscendo lo stesso ad eseguire una completa procedura di docking. I risultati hanno dimostrato la funzionalità dell'interfaccia, determinado le massime forze trasmesse alla struttura durante l'attuazione e l'aggancio. Infine, gli ultimi test hanno portato alla definizione dei sovracitati limiti massimi di disallineamento angolare e laterale.

Come descritto nel capitolo 6, presso il Space Systems Laboratory del MIT, all'interno del programma SPHERES, è in sviluppo la Universal Docking Port (UDP), una nuova interfaccia di docking compatibile con le piattaforme di test ivi sviluppate, che verrà testata a bordo della Stazione Spaziale Internazionale nel 2015. Il test-bed dedicato a SPHERES disponibile nei laboratori del MIT consiste in un tavolo a basso attrito, sul quale è facile testare tanto l'hardware quanto i codici di controllo sviluppati, prima di passare ai test sulla ISS. Un periodo di due mesi quale "visiting student" ha permesso di approfondire le metodologie di sviluppo della UDP e più in generale i vantaggi legati all'avere a rapida disposizione un test-bed facilmente utilizzabile per il confronto tra modelli numerici e risultati sperimentali. In tale periodo, sono stati sviluppati alcuni codici di controllo per le SPHERES, per testare il processo di rendez-vous e docking. Simulazioni numeriche hanno dimostrato la bontà delle manovre proposte e l'affidabilità dei codici di close-rendezvous e collison-avoidance; sfortunatamente, alcune problematiche legate al sistema di determinazione d'assetto e posizione di SPHERES hanno impedito di verificare tramite test il codice sviluppato. Infine, tramite un confronto tra la UDP e l'interfaccia semi-androgina, è stato dimostrato che l'ultima presenta un più ampio campo di funzionamento per quanto riguarda i disallineamenti lineari ed angolari accettabili durante la procedura di docking.

Nel capitolo 7 l'intero lavoro viene riassunto e alcune conclusioni vengono brevemente presentate. Si valuta che la porta semi-androgina abbia raggiunto un livello di sviluppo tecnologico pari a TRL 3-4. Tanto l'utilizzo di migliori setup sperimentali in ambienti più rilevanti quanto lo sviluppo di sensori dedicati sono indicati come necessari sviluppi futuri. In parallelo, vengono riportate altre attività in corso d'opera o concluse. Innanzi tutto, una versione migliorata del meccanismo descritto è brevemente introdotta, e il

suo principio di funzionamento viene riportato, assieme ai vantaggi legati al ridotto ingombro. Uno studio sulla nuova tecnologia di soft-docking bastata sull'utilizzo di sistemi "tethered" viene in seguito presentato: una sonda connessa al chaser tramite un cavo e controllata tramite navigazione magnetica viene usata per eseguire il primo aggancio, riducendo significamente le operazioni di docking e riducendo la complessità del sistema; alcune analisi preliminari sono state eseguite all'interno dell'esperimento FLEDs, che ha consentito di valutare l'effetto di allineamento automatico della sonda in condizioni di milligravità.

In conclusione, il lavoro qui introdotto presenta ancora elevati margini di ricerca, con l'obiettivo di raggiungere un più elevato TRL; alcune indicazioni sui possibili sviluppi futuri sono inoltre introdotte, considerando che l'interesse sulle tecnologie di docking e navigazione di prossimità è in continuo e costante aumento. La corsa per lo spazio è ancora al suo inizio, già ad oggi per la maggioranza delle operazioni di manutenzione queste tecnologie sono considerate insostituibili, e dimostrano ulteriori potenzialità d'investimento a breve e lungo termine, tanto nel settore commerciale quanto in quello della ricerca: in un futuro non troppo remoto flotte di piccoli satelliti solcheranno gli spazi interplanetari, consentendo il trasporto di propellenti, risorse e campioni scientifici, aggregandosi e autoriparandosi, portando la razza umana ad esplorare e sfruttare lo spazio immenso che circonda questo nostro piccolo puntino azzurro, chiamato casa.

Acknowledgements

In this three years long run I had the possibility to know a lot of people, to meet new friends and lose contact with old companions, but, as I am finally having a glimpse of the finish line, I feel that, at least, I would lime to remember you all. As it was once written, "I don't know half of you half as well as I should like; and I like less than half of you half as well as you deserve".

First of all, my colleagues in the SSG: Fren and Franz, they bore my bad character for three years with no complains, Livia, she cleverly ran away from us for one year, and Andrea, that was a good graduate student in Padova and a better friend in Boston. Gabriele "Asiago", no more a colleague but still a good friend and an incomparable story-teller: "Tosi, ve ne conto una".

My oldest friends Dona and Pietro, ex room-mates but still in contact; many of the best adventures in my life would not have happened without the insistence of Pietro and its restless work. Sky is not your limit.

Two of the oldest classmates, five years of University, and we are still friends: Lengo, always able to be in the right place at the right time (aperitif time), and Duzzo, starting his PhD research project while I am finishing: "in bocca al lupo!"

My summers cannot be so awesome without spending part of them in Caorle. The list of people I enjoy myself with is really long, but I shall start with Ruggero (how many good beers), his brother and my preferred barman Nicola, and their cousin Marco. And then Luca (cycling by night to PSM), Thomas (I totally miss our long talks in the dark hours before dawn), Red (you disappeared since you started working), Zambu (night photos on the beach), Moro (trying to teach me volleyball), Coppo (the best party-lawyer), Gianmarco (together "Tonto e Crucco") and the rest of those crazy Caorlotti; between them, a fundamental thanks to the staff of Dessart (Francesco, Silvia, Matilde, Davide): you fed both my body and my soul.

If my holidays are spent in Caorle, Padova is my home town for the rest of the year: and of all the apartments I lived in, only one I can call home. Via Roma 72 was an amazing place, sustained by the emotions of generations of students (more solid that those crumbling walls), soaked of their memory as much as the mattresses used by the landlord to absorb the rain seepages. I could not think to a worst house to live in (I had to change my mind visiting the US), but it was, simply, the right place. Five flat-mates, as different as only God can create, Lele, Steppo, Gallo, Dani and Brex, and as regular host FIFA14. Thanks, guys, for those eternal nights. And also thanks to our neighbours, Sabrina, Giulia, Mary and the new-entry Giuliana.

I am still in contact with many of my aerospace classmates, and I really want to thank them for the unofficial reunions we organize at least twice a year: Marco (Cesa), Riga, Michele, Abe, Scarpa, Marco (Coccon), Sergio, and all the others.

I also want to remember all the students I worked with, Stefano and Laura, examples of competence, and the two groups of POLARIS and FELDs: in the last year, you were the source of many enjoyable moments (and much more troubles), with your unlimited will and firm believe in the development of your experiments.
I want to thank the whole SCRAT team, able to organize unbelievable reunions in the farthest woods of Asiago. SCRAT is not only an experiment, but a way of life.
Out of those lists, but still in my mind, there are other good friends: Cisco, I miss Greanes and the good time all together, Tommaso, the man of unexpected meetings, Daniele and Teseo, so far but always close, Marco Barbetta, 10-minutes problem solver in every circumstance.
At CISAS, life would not be so crazy without the daily contribution of our secretaries Federica, Federica, Marika, Paola and Luciana, and the (not always) fast chats in the corridors with Alessio, Giacomo and Cinzia. Thanks also to Chiodo and Mitch, part-time members of our "Ufficio Arroganza", and to Riccardo: you are our new hermetic poets, able to describe the whole world with simple, aesthetic sentences.
I also want to thank professors Enrico Lorenzini, David Miller and Alvar Saenz-Otero, that after many difficulties were able to organize my visiting period at MIT, and the whole SPHERES group, above all Duncan and Bruno. I spent there one of the best periods of my life, growing both as a young professional and as a man; in those two months I discovered a new world and fresh motivations to continue my activity in the space sector.
One line shall be dedicated to my supervisor, professor Alessandro Francesconi, that worked to teach me not only how to be a good engineer and PhD, but also how to afford the other problems a young researcher has to fight day after day, with ethics, perspicacity and persistence.
Last, but first in my mind, I want to thank my family: their support is always beyond words, as only parents can be present before you need them. Thank you for your time, your help and your presence.

Contents

List of Figures

List of Tables

Abbreviations

ABS	**A**crylonitrile **B**utadiene **S**tyrene
AD	**A**ctuated **D**isk
ATV	**A**utomated **T**ransfer **V**ehicle
ADCS	**A**ttitude **D**etermination and **C**ontrol **S**ystem
ADR	**A**ctive **D**ebris **R**emoval
APAS	**A**ndrogynous **P**eripheral **A**ttach **S**ubsystem
ARCADE	**A**utonomous **R**endezvous **C**ontrol **A**nd **D**ocking **E**xperiment
BEXUS	**B**alloon-borne **EX**periments for **U**niversity **S**tudents
CSM	**C**ommand and **S**ervice **M**odule
DARPA	**D**efense **A**dvanced **R**esearch **P**rojects
DLR	**D**eutsches Zentrum für **L**uft- und **R**aumfahrt
DoF	**D**egree **o**f **F**reedom
EAP	**E**lectro**A**ctive **P**olymer
EE	**E**lastic **E**lement
EPOS	**E**uropean **P**roximity **O**perations **S**imulator
ESA	**E**uropean **S**pace **A**gency
FELDs	**F**lexible **E**lectromagnetic **L**eash **D**ocking **s**ystem
FFT	**F**ast **F**ourier **T**ransform
GEO	**G**eostationary **E**arth **O**rbit
GN&C	**G**uidance, **N**avigation **&** **C**ontrol
GNS	**G**lobal **N**avigation **S**ystem
GPS	**G**lobal **P**osition **S**ystem
GSP	**G**uest **S**cientist **P**rogram
HTV	**H**-II **T**ransfer **V**ehicle
IDSS	**I**nternational **D**ocking **S**ystem **S**tandard

IR	**I**nfra-**R**ed
ISS	**I**nternational **S**pace **S**tation
LEO	**L**ow **E**arth **O**rbit
LM	**L**unar **M**odule
MIT	**M**assachusetts **I**nstitute of **T**echnology
NASA	**N**ational, **A**eronautics and **S**pace **A**dministration
PWM	**P**ulse-**W**idth of **M**odulation
REXUS	**R**ocket-borne **EX**periments for **U**niversity **S**tudents
SAM	**S**emi-**A**ndrogynous **M**echanism
SPHERES	**S**ynchronized **P**osition **H**old **E**ngage and **R**eorient **E**xperimental **S**atellite
SSL	**S**pace **S**ystems of **L**abortatory
TRL	**T**echnology **R**eadiness **L**evel
UDP	**U**niversal **D**ocking **P**ort

Physical Constants

Speed of Light	c	$=$	$3 \cdot 10^8\ m \cdot s^{-1}$
Solar Constant	F_S	$=$	$1367\ W \cdot m^{-2}$
Standard Gravity	g	$=$	$9.81\ m \cdot s^{-2}$
Earth Magnetic Dipole	M	$=$	$7.96 \cdot 10^{15}\ T \cdot m^3$
Earth Standard Gravitational Parameter	μ	$=$	$398600.4418\ km^3 \cdot s^{-2}$

Symbols

A	Area	m^2
B	magnetic field	$\mathrm{T} = \mathrm{N}\cdot(\mathrm{m}\cdot\mathrm{A})^{-1}$
C_D	drag coefficient	
c_f	friction coefficient	
D	residual magnetic dipole	$\mathrm{A}\cdot\mathrm{m}^2$
e	error	
F	force	N
k	stiffness	$\mathrm{N}\cdot\mathrm{m}^{-1}$
K	arbitrary constant	
K_D	derivative gain	
K_P	proportional gain	
L	Young modulus	$\mathrm{N}\cdot\mathrm{m}^{-2}$
I	moment of inertia	$\mathrm{kg}\cdot\mathrm{m}^2$
m	mass	kg
M	magnetic dipole	$\mathrm{T}\cdot\mathrm{m}^3$
q	reflectance	
r	distance	m
t	time	t
T	torque	$\mathrm{N}\cdot\mathrm{m}$
v	velocity	$\mathrm{m}\cdot\mathrm{s}^{-2}$
x, y, z	position coordinates	
α, β	angles	rad
ϕ, θ, ψ	Euler angles	rad
ρ	distance radius	m

ω	angular frequency	rad s^{-1}
ω_i	rotation velocity	rad s^{-1}

Chapter 1

INTRODUCTION

In recent years there has been a continuously growing interest in space missions conducted with miniaturized spacecraft, down to nanosatellite and picosatellite classes. Such spacecraft have in fact demonstrated a significant potential to drastically cut the costs to access space, thus encouraging the development of space activities for educational purposes as well as low-cost, low-risk commercial applications. However, important technical restrictions related to the limited resources available on-board are still preventing the employment of nanosatellites for complex and high performance missions. One possible solution to this problem is the development of rendezvous and joining technologies that would provide miniature space vehicles with the capability to aggregate in larger structures, thus addressing the volume and power needs for complex payloads.
A docking system could provide small and nano-satellites assemblies with the capacity of self-expansion, reconfiguration, refurbishment through single units substitution and consequently increased fault-tolerance. In other words, docking could enable scenarios where small independent vehicles like CubeSats can join together to generate bigger multipart space systems with the possibility to rearrange, be repaired or updated on orbit. Large structures such as segmented mirrors telescopes or solar arrays fields are only two examples of the possible applications of the mechanical connection of many small satellites. Docking could allow to optimally merge variable mission requirements and to extend the practical duration of missions. Most noticeably, docking is a crucial step in the direction of making nanosatellite platforms competitive with traditional space vehicles.
Deep-space exploration programs could also need the design of docking or at least capturing systems: for example, a sample and return mission from Mars [1] or other planets and moons would involve several spacecraft that can dock and separate.
Last, joining capabilities with non cooperative bodies (i.e. small asteroids, old satellites and their fragments) or operative spacecraft without docking interfaces are conditioned

and limited by the state of the art technology of docking and capture systems.
Docking mechanisms have been employed in space mission for more than 50 years: since the Apollo project, docking ports became unavoidable subsystems to connect different spacecraft. Unlike on the ISS, where the participation of different contractors from various countries led to the definition of common design requirements [2], in the design of small commercial and scientific automatic spacecraft docking operations were not considered, thereby possible refuelling missions for LEO and GEO satellites (e.g. Orbital Express [3] and Space Infrastructure Service [4]) are subjected to compatibility problems.
Starting form these considerations, the objectives of this work, more accurately presented at the end of this chapter, can be stated as (1) the design of a novel docking mechanism, (2) the realization of an instrumented prototype and (3) its test on a dedicated test-bed.

1.1 Spacecraft joining operations

In-space rendezvous and joining of two bodies was one of the first technological challenges that space engineers dealt with; since the first active docking of two spacecraft during Gemini XIII mission under the command of Neil Armstrong [5], active joining of two or more bodies radically changed and evolved in different concepts of operations. Anyway, it is useful to introduce some common definitions; as is usual, the approaching spacecraft is denominated chaser, and the approached body is referred as target.

A preliminary classification can introduce the three main joining operations, depending on target attributes: capture, berthing and docking, as visible in figure 1.1. If the mission target is non cooperative (e.g.: uncooperative spacecraft, space junk or small bodies), the chaser shall approach and capture it, usually without the presence of joining interfaces or other useful grasping element; another common issue of this operation is the possible target tumbling motion. In case of cooperative bodies there is an ulterior classification between berthing (assisted joining), and docking (active mating): in the first case, the process needs the help of a grapple interface (such as ISS robotic arms) to bring one spacecraft and mate it to the other module; on the other hand, docking refers to the joining of two separate free flying spacecraft through active manoeuvres [6].

1.1.1 Geometry reference frame

In order to simplify the exposition of this research, this brief paragraph is dedicated to introduce the geometric parametrization that is employed in this thesis, as visible in figure 1.2. Nadir-pointing coordinates are centred in the spacecraft centre of mass, and

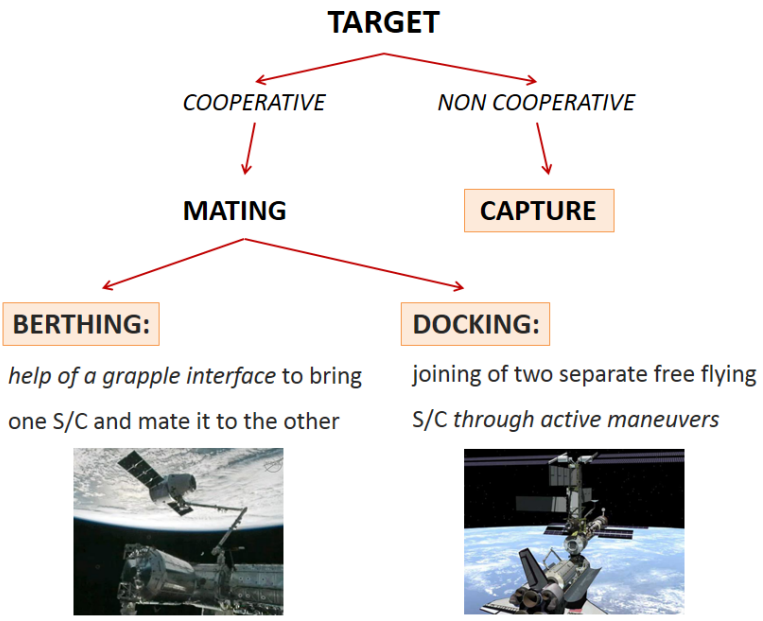

FIGURE 1.1: Joining operations classification

are based on these assumptions: the Z axis is pointed towards nadir, the X axis in the direction of satellite velocity and the Y axis completes the left-handed frame; rotation is parametrized through the 3-2-1 Euler Angles. Last, the direction normal to the docking port plane is defined as docking axis.

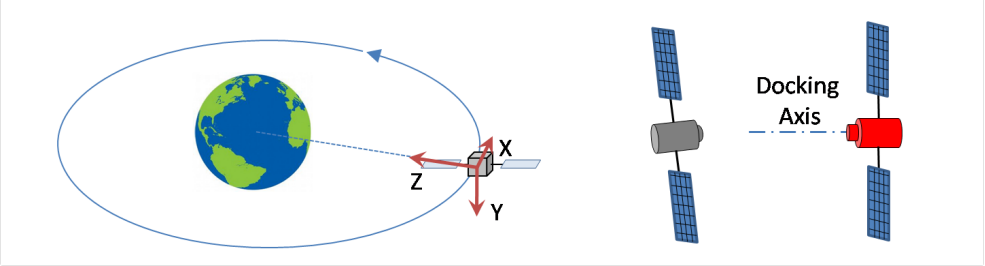

FIGURE 1.2: Geometry references: on the left, the nadir-pointing coordinates chosen in this document; on the right, the docking axis is defined as the direction normal to the docking port

1.1.2 Joining procedure description

A brief introduction of joining procedure follows, to present the motivations and the state of the art of capture and mating technologies.

A joining procedure for two satellites can be divided in four main parts (figure 1.3): phasing, far range rendezvous, close range rendezvous and mating [7]. During phasing, the objective is to reduce the phase angle between the two spacecraft rising and lowering

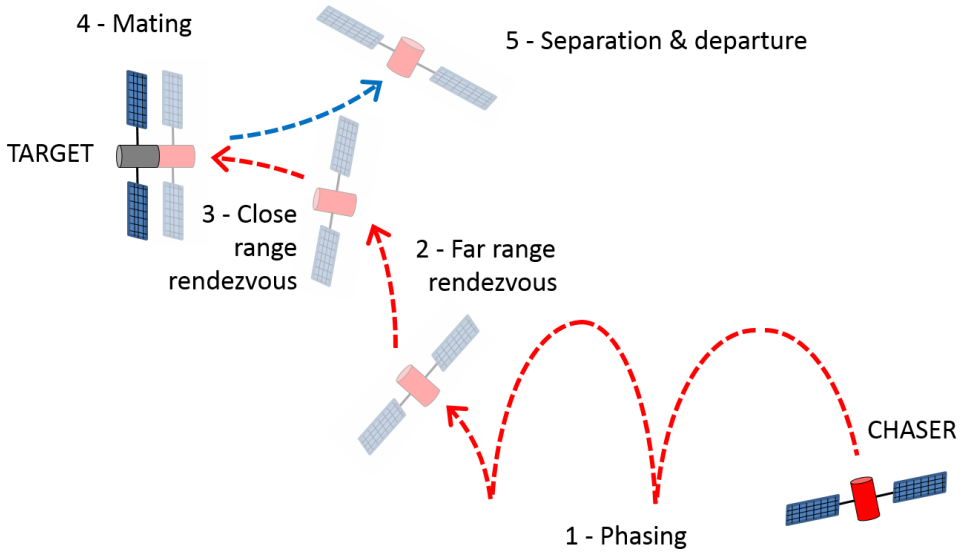

FIGURE 1.3: Approach procedure

the chaser orbit in order to modify its orbital period. At the end of this phase, the target is in a range of a few tens of kilometres from the chaser, and the far range rendezvous can start. Also called "homing", it aims to reduce the distance between target and chaser to a few kilometres. Relative navigation between satellites is monitored by relative measurements of distance (e.g. radar measurements) or by relative GPS positioning, with an accuracy of a few tens of meters. The third phase leads to the final reduction of the range to the target and to achieve chaser position and velocity conditions for a safe approach. Close range rendezvous therefore needs a class of sensors with an accuracy of about 1% of range or better. In the end, mating starts when the two bodies are in contact and aims to create a mechanical join between them through an interface. This phase can be often divided into two sub-phases: passive capture (recently developed as "soft capture"), when the bodies are connected by temporary joints like spring-actuated pins or electromagnets and no heavy mechanical loads can be transmitted, and hard capture, usually realized with structural latches. Last, a fifth phase could be considered: the separation and departure of the chaser at the end of its mission. After the opening of the mechanical joint, the chaser has to apply an impulse to separate from the target, with potentially dangerous effects on the target expose surfaces from the chaser propulsion subsystem.

Next paragraphs are better introducing the capture and the mating methods, describing the related technologies and their state of the art.

1.2 Capture of non-cooperative targets

In this section, an overview on capture systems for non cooperative objects is briefly presented. To date, a variety of grasping concepts have been studied (and some of them are under development) based on different technologies like: (1) robotic arms, (2) nets, (3) harpoons, (4) polymeric foams or (5) nozzle probes.
Nevertheless, none of the cited technologies has been flight qualified and all of them are still characterized by a low Technology Readiness Level (TRL).

1.2.1 Robotic arms

Robotic arms have already been employed and validated for several on-orbit operations, such as extra vehicular activities, ISS assembly and satellite servicing [8][9], and could represent a suitable option for debris removal (Figure 1.4). To this aim, few studies have suggested various solutions and outlined different concepts. Nishida and Kawamoto [10] proposed a system for braking and detumbling uncontrolled objects in space, based on a robot arm with a brush-type end-effector, although with no possibility to firmly hold the debris for further manoeuvres. The brush is used to brake most of the target object motion, while the arm is capable of buffering the residual movement thanks to its structural flexibility and active joint compliance control. Ueno et al [11] proposed a system which exploits several small-scale spacecraft equipped with robotic arms in order to grasp satellites for operations of recovering and disposal. Another solution is provided by the Aerospace Dual-Arm Manipulator (ADAM, [12]) that has been designed to identify and capture free-floating objects with unknown shape and position. Furthermore, the European Space Agency funded a project called ROGER (Robotic Geostationary orbit Restorer, [13]), for the development of a spacecraft which captures and transfers non-operational GEO satellites to graveyard orbits; in this case, one of the proposed configurations for the capture system comprehends a telescopic boom on which four tentacles are mounted; these tentacles are sufficient to encircle any potential target and

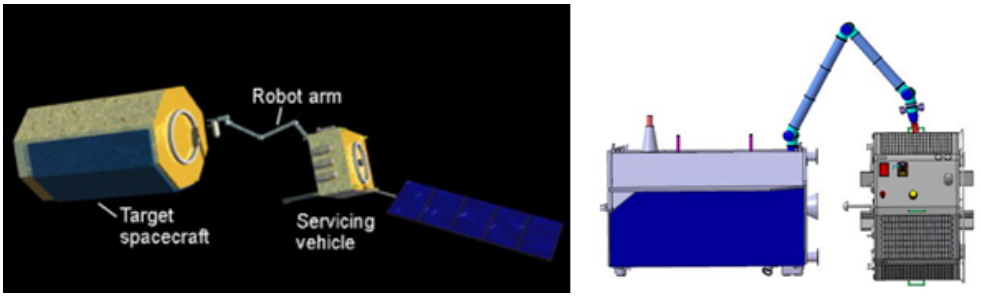

FIGURE 1.4: ADR by means of robotic arm (left) and DEOS berthing manoeuvre (right)

can be operated simultaneously or independently. Another example is represented by FREND (Front-end Robotics Enabling Near-term Demonstration, [14]), whose mission concept exploits a robotic arm to grabble standard satellite-launcher interfaces; in this case, autonomous rendezvous and docking operations have been successfully carried out in a laboratory environment that allows full-scale simulations of two satellites operating with six degrees of freedom in close proximity to each other. Finally, DEOS (Deutsche Orbital Servicing Mission, [15]) is a German Space Agency mission that aims to capture a client vehicle with a servicing spacecraft by means of a robotic arm that holds on handles the target object. The main disadvantage of all the mentioned solutions is the lack of research on appropriate end-effectors suitable to capture irregular shaped objects: robotic capture strategies typically assume that the target object offers structural features of known geometry, capable to withstand the handling loads and compatible with common hand grips. This approach is not general and, therefore, considerably constraints the operative flexibility of the solution since most times the only accessible features for grasping are delicate parts (e.g. solar panels, antennas, booms) that were not designed to sustain significant mechanical loads nor to provide a convenient handle for standard robotic manipulators, and not always satellite-launcher interfaces are easily reachable. Tentacle-based technologies avoid this problem but imply large volumes and masses to host the capture mechanism.

1.2.2 Nets

Nets appear a suitable solution since they offer a large contact surface and a good adaptability to irregular shapes. Also, the use of such devices guarantees a low load transmission from the captured object to the service vehicle, if a suitable deformable element is used to connect the net to the chaser. A promising design for this technology is the alternative configuration of ROGER capture mechanism, based on twenty deployable nets that are able to wrap around the target which is then pulled by the service satellite to graveyard orbits by means of a cable. Ground test were performed for the net deployment in 2009 and a microgravity test on a sounding rocket was planned for 2012. Another solution is provided by REDCROC (REsearch and Development for the Capture and Removal of Orbital Clutter, [16]), developed by University of Colorado, which is an inflatable net allowing to capture debris with minimal contact forces (figure 1.5, left). Another mission architecture based on a net system is described by Zhai and Zang [17], that proposed the employment of a flexible net equipped with a number of flight weights that are ejected towards the target by preloaded springs; the weights inertial forces pull the net out of its storage canister and let it fly to the target (figure 1.5, right). The bottom of the net is attached to the mother spacecraft through a connecting tether.

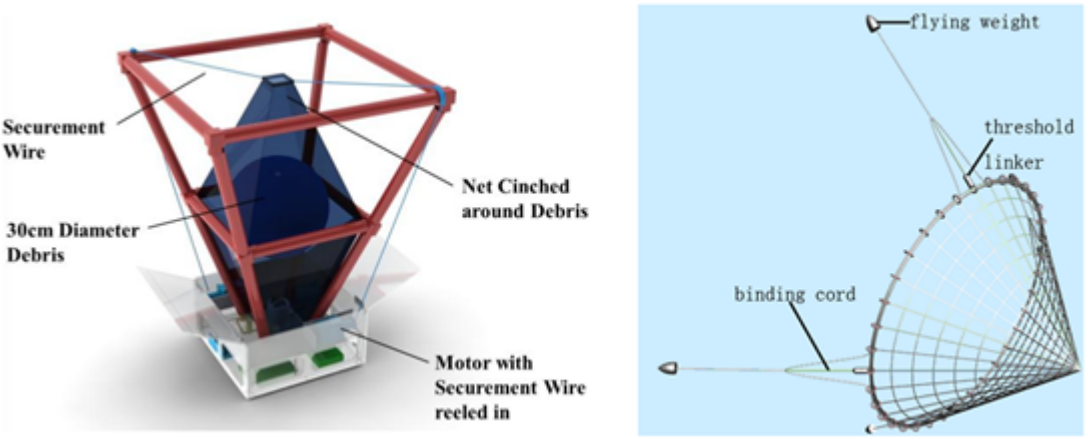

FIGURE 1.5: REDCROC system overview (left), and an example configuration of net capture (right)

When the net wraps around the target totally, the mouth tether is tightened by the flying weights and the net is closed behind the target.

Nets are a relatively cheap, reliable, and quite simple concept, but still have a low TRL and further study is required. The mentioned systems are in fact limited by the actual possibility to manage the deployment of the net and by the insufficient controllability of the target attitude after capture; moreover, although the low rigidity of the connection is advantageous in reducing the impulsive capture loads, it might not transmit the required control actions necessary to keep the correct attitude during re-entry. Further concerns are related to interaction between the debris and the net mesh, which can cause the fragmentation of delicate appendages such as solar panels or antennas.

1.2.3 Harpoons

Space harpoons shot by a servicing satellite towards the surface of the target object might be a solution compatible with a large amount of targets with different structures and shapes. One concept, developed by Reed et al. [18], is based on harpoons fired at any potentially threatening satellite from close range (Figure 1.6); after perforation, a barbs system is opened inside the debris body in order to secure the connection and apply a tightening force to rewind the linking cable.

In addition to concerns similar to those cited for net systems and related to the cable dynamics and debris control during manoeuvres, further drawbacks penalize this technique resulting in reduced employment flexibility and, possibly, even in harmful consequences. As a matter of fact, the impact between the harpoon and the target can generate dangerous small debris due to the fragmentation of the hit surface, setting a threat to the service spacecraft itself. The penetration depth should also be monitored, to avoid batteries rupture, tanks depressurization or similar hazards. Moreover, the impact

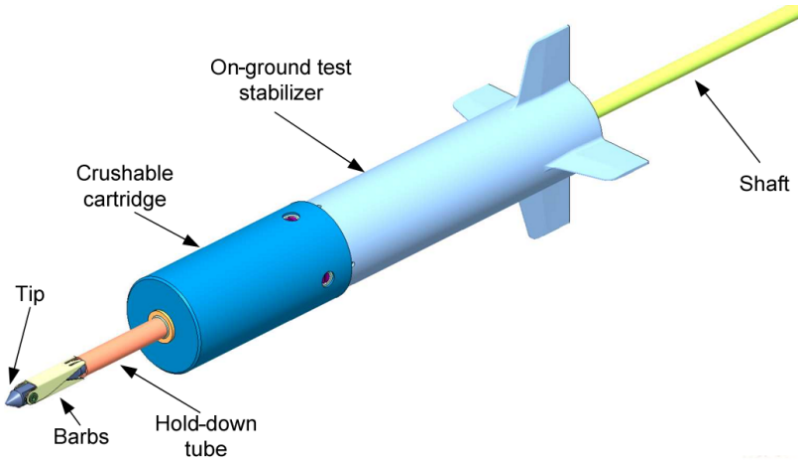

FIGURE 1.6: Ground-test prototype CAD view of an harpoon system[18]

necessarily transmits large dynamical disturbances to the object causing an uncontrolled attitude motion, that is particularly likely after off-axis impacts. Last, the target motion must be completely known, to avoid to hit external surfaces and appendix like solar arrays or antennas: sensors and navigation would require consistent system resources and should be able to estimate remover and target displacements and rotations between harpoon firing and hitting.

1.2.4 Polymeric foams

Polymeric foams as adhesive system have been proposed according to two different operational concepts. On one hand, such materials can be sprayed towards the debris to realize chemical bonding regardless of the target shape; the low rigidity of the created link limits the contact forces, thus relaxing the attitude control requisites and reducing the risk of debris structural damage [19]. On the other hand, these foams can also be employed to increase the atmospheric drag acting on the target object (i.e. increasing its ballistic coefficient) by enveloping the debris within a large volume of polymer.

In figure 1.7 the operative sequence of this de-orbiting technique is depicted: first the rendezvous with the target object is accomplished, then the polymeric foam is sprayed towards the debris and wraps it entirely, finally the large volume of the foam bubble augments the atmospheric drag action lowering the object orbit. However, capture systems based on polymeric foams show some weaknesses particularly connected to the employed material performances, in terms of solidification time/effectiveness in space, strength of solids[1] and interaction with the target surface material. This latter point is particularly crucial when brittle features/MLI are concerned.

[1] *the ability of solids to resist fracture (separation into parts) or an irreversible change in shape (plastic deformation) under the action of external loads*, The Great Soviet Encyclopedia, 3rd Edition (1970-1979).

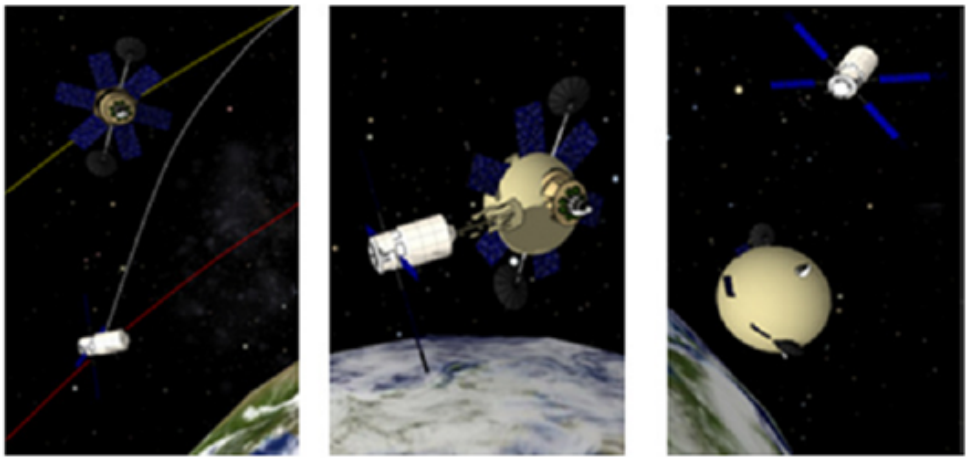

FIGURE 1.7: Representation of ADR by means of polymeric foam to increment debris ballistic coefficient

1.2.5 Nozzle probe docking

Finally, capture methods based on the use of nozzle probes to fit into target object nozzles have been studied since nozzles are common features available in most spacecraft and furthermore they have often enough strength to considerable loads such as those requested by orbital manoeuvres. An example of this concept is given by SMART-OLEV (SMART - Orbital Life Extension Vehicle, [20]), that is equipped with a mechanical probe appropriately shaped to mate with the nozzle of a GEO satellite (figure 1.8) and successively perform control maneuvers.

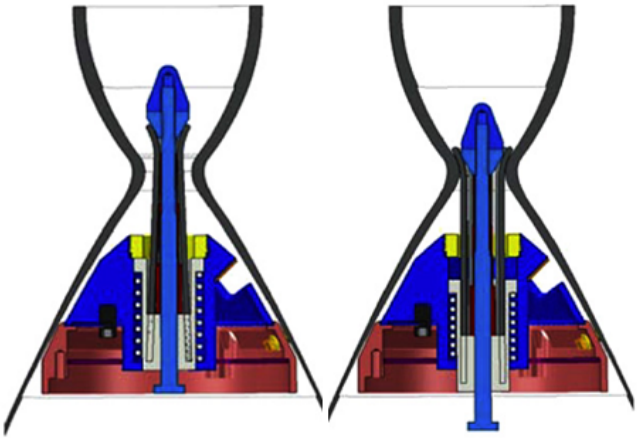

FIGURE 1.8: SMART-OLEV docking mechanism working principle: a probe penetrates the nozzle (left) and thanks to a shape shifting it wedges into the throat, creating a solid joint (right)

An alternative approach is proposed by Trushlyakov et al. [21], who conceived a remover composed by a mother ship and a small independent probe linked by means of a

cable. The small probe is provided with a docking mechanism able to capture a target securing to its nozzle. Rewinding and tightening the linking cable makes it possible to create a rigid joint and the system is then ready for deorbiting manoeuvres. The main disadvantage of these solutions is, once again, the lack of generality and the need of a nozzle suitable for capture; also, interesting targets for removal are often launch vehicle upper stages whose nozzle can be gimbaled and, therefore, not rigidly constrained to the vehicle structure. Furthermore, in case of tumbling motion of the debris, it may be extremely difficult to identify the target nozzle and to align with it for docking.

1.2.6 Comparison

A summary comparison between the capture devices considered so far is given in table 1.1 As it is visible in the table, at today there is no performing solution for the non-cooperative capture, although many research institutes and industries are funding the robotic arm technology, in order to overcame the aforementioned limitations.

1.3 Docking and berthing: state of the art

1.3.1 Large spacecraft

From the beginning of space era, both the US and the Soviet Union developed strategies for rendezvous and docking between spacecraft. The development of a safe procedure for spacecraft mating allowed scientist to design space-assemblies such as space stations through several missions of small launch vehicles, with consequent saving in money and advantages related to the modular design. During Gemini program US managed both to made the first space rendezvous (Gemini VI-A and Gemini VII) and the first docking (Gemini VIII and Agena Target Vehicle, March 16, 1966, figure 1.9 on the left) [5]. Gemini VIII mission, under the command of future Apollo 11 commander Neil Armstrong, was able to mate his target only for a brief amount of time, due to the failure of one of the spacecraft attitude control thrusters.

Less than two years later, on October 30, 1967, the Soviets carried out the first automatic docking between the two unmanned spacecraft Kosmos 186 and Kosmos 188 (figure 1.9, right, a commemorative soviet stamp). Due to a misalignment between the two satellites, the docking was not complete, with only a mechanical join instead of a complete connection; the following year, on April 14, Kosmos 212 and 213 realized a complete docking procedure and flew connected for about 4 hours [22].

In the same period NASA was developing the Apollo program to reach the Moon before

TABLE 1.1: Comparison between capturing devices

SYSTEM	MAIN FEATURES	LIMITS
Robotic arms	• Tracking of the object motion • Precise capture point interception • Angular momentum management	• Complexity • Absence of end-effector suitable for general object capture • Need for a grasping feature on the target object
Nets	• Adaptable to irregular shaped objects • Large contact surface	• Net deployment dynamics • Low rigidity of the connection after capture • Chaser/debris combined system control • Fragmentation of delicate appendages
Harpoons	• Compatibility with a large variety of targets	• Debris generation • Catastrophic damage hazard • Strong disturbance loads onto the target attitude (especially in case of off-axis impact point) • Chaser/debris combined system control
Foams	• Adaptable to irregular shaped objects	• Polymerization dynamics in vacuum • Low rigidity of the connection after capture • Adhesion to brittle features/MLI
Nozzle Probes	• Strong connection	• Not general solution • Need of extremely accurate rendezvous

FIGURE 1.9: Gemini VIII docking Agena (left - courtesy by NASA) and Kosmos 186-188 commemorative stamp (right)

the end of the sixties. To simplify the launch procedures, the Lunar Module (LM) was stored under the Command and Service Module (CSM) and was docked to the CSM only during the Lunar Transfer Orbit. Later in Lunar Orbit, it separated from the CSM to land on the Moon, and docked again after the end of Lunar activities. As visible in next figure, the interface on the LM (on the left) is composed by a hatch, a ring and a drogue. On CSM side it is visible a probe, another ring with mechanical latches and the other hatch. During mating, the probe is penetrating the drogue until it automatically fits in the middle hole; when softly docked, the CSM ring matches the LM ring and creates a mechanical junction with the activation of the latches. In a second time, the empty space is filled with air, and the probe-drogue system is hand-folded and stored in the CSM, to allow crew to move between the two crafts [23]. As all of the first docking

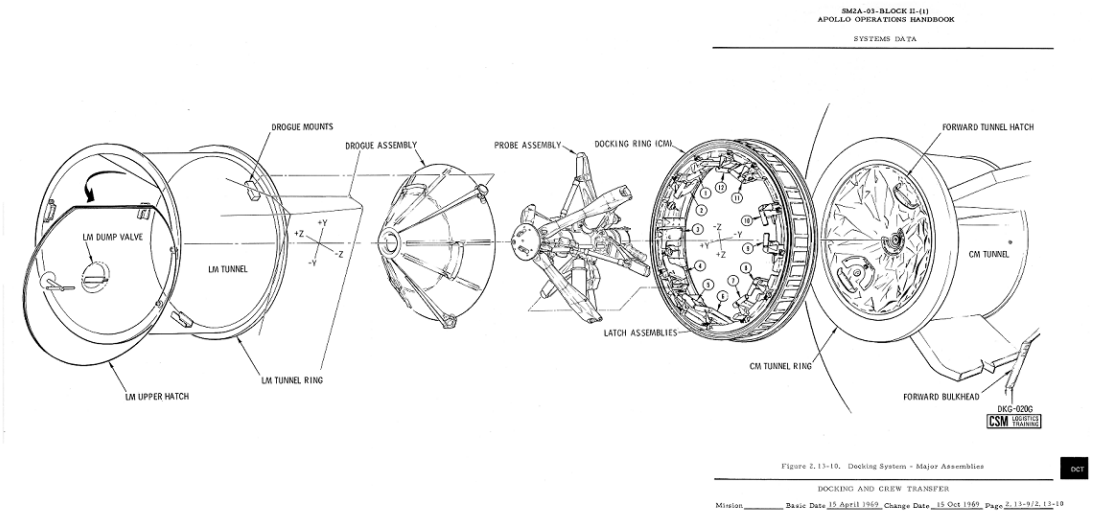

FIGURE 1.10: Apollo docking system (courtesy by NASA)

interfaces, Apollo docking system is not androgynous: each spacecraft has a unique design and can be mated only with the other interface, in a "gender-mate" configuration (figure 1.10).

Another milestone in docking evolution was the Apollo – Soyuz Test Project. In the détente atmosphere of '70s, US and Soviet Leaderships decided to celebrate the end of the Space Race with the first joint mission: the last Apollo mission and a Soyuz rendezvoused, cooperated and finally docked on July 17, 1975. Due to the different docking interfaces and the different atmospheres in the spacecraft (pure oxygen on Apollo, mixture of oxygen and nitrogen on Soyuz), a docking and airlock module was launched with the Apollo. On the Apollo side, the same "probe-drogue" system of LM was used, while its other end showed the new-designed Androgynous Peripheral Attach System (APAS-75) docking port. APAS was designed by Vladimir Syromyatnikov [24], a Soviet engineer. Syromyatnikov's docking mechanism is still used on ISS. The main feature of APAS-75 is its androgyny: unlike previous systems, each side can be active or passive and a spacecraft with APAS interface can mate with any other APAS port (figure 1.11, left).

The evolution of APAS-75 are APAS-89 (figure 1.11, right) and APAS-95 (US version

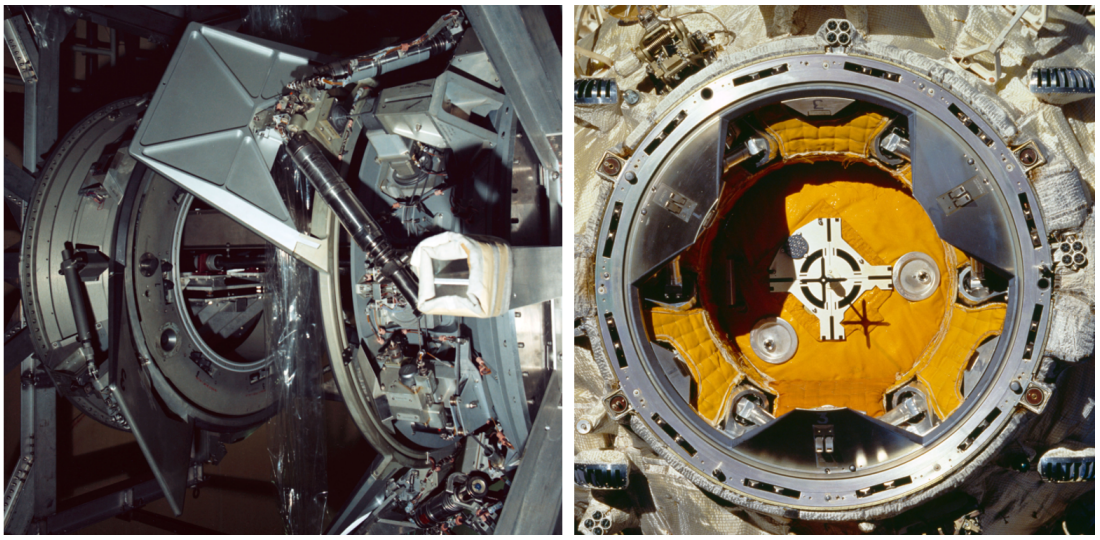

FIGURE 1.11: APAS-75 (left) and APAS-89 (right) Syromyatnikov's docking mechanisms (courtesy by NASA)

of -89), respectively designed for MIR-Buran and MIR-Shuttle programs. The main difference between the configurations is the position of the orienting petals: outward on -75 model, inward on -89 and -95; this led to the reduction of the passage diameter.

Currently three ISS docking modules are designed on APAS specifications and housed the Space Shuttles before retirement; Russian Soyuz and Progress and European ATV use probe-drogue docking modules. Chinese Shenzhou spacecraft uses an APAS-compatible

docking system. ISS docking requirements are defined by an international docking standard system (IDSS) document [2].
NASA is developing a new-concept androgynous docking interface (NASA Docking System, NDS) for both docking and berthing [25]. NASA port will not be compatible with APAS, and a new docking module shall be added to ISS.
Returning to the Soviets space technologies, the Soyuz docking interface is still the same since 1971. Called "System for docking and internal transfer" (SSVP - Sistema Stykovki i Vnutrennego Perekhoda), it shows a probe-drogue mechanism (figure 1.12) and it is currently implemented also on the Progress and ATV supply vehicles. To perform a docking procedure, an extended probe noise is at first passively captured by the drogue; retracting the nose, the probe body self-aligns with the drogue thanks to guide pins, until a solid joint can be created using mechanical latches.

Last, on the ISS the "Common Berthing Mechanism"[26] is used for the Japanese

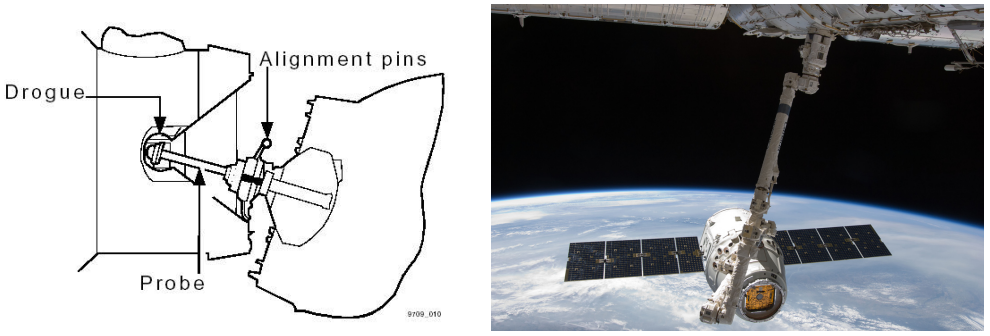

FIGURE 1.12: The Russian docking mechanism (left), still used on ATV and Progress cargo, and the Dragon spacecraft berthing with the ISS (right, courtesy by NASA), guided by Canadarm, showing the common berthing interface

HTV and the commercial supply spacecraft Cygnus and Dragon Cargo. It is composed by an active interface (on the ISS) and a passive one, both ring-shaped. In this case, petals are not implemented and the required alignment is reached using a robotic arm (the Canadarm on the ISS) to precisely guide the chaser to the target interface. All the aforementioned interfaces, with the exception of the Kosmos and, more recently, the ATV, need the active assistance of crew in at least one of the mating spacecraft to perform docking manoeuvres. Large satellites automatic rendezvous and proximity operations are still in a development stage, with only few studies and tests, such as the Japanese ETS-VII technology demonstrator of robotic berthing [27]; ATV technologies advances have recently given ESA a leading rule in this field.

1.3.2 Small satellites

As far as small scale vehicles are concerned, the issue of docking was not addressed at all since last decade; the state of the art of formation flight, relative navigation and

docking is represented by MIT SPHERES experiment on board the ISS [28]. The experiment is composed by three vehicles capable to perform precise relative navigation, gather in formation and accomplish synchronized manoeuvres and, in the framework of SWARM [29] and then UDP (Universal Docking Port) project, to connect to each other or to other servicing modules [30]. The SPHERES docking system, depicted in figure

FIGURE 1.13: SPHERES Universal Docking Port

1.13, features an androgynous pin-hole architecture that is common to each module and allows not only a rigid mechanical connection, but also power and data transfer. Its main drawbacks are represented by the exploitation of moving mechanical parts and the need for the modules to be oriented in a specific way about the roll axis in order to accomplish docking, as the interface is androgynous but not symmetric.

In addition to SPHERES, only few other connection systems for small-scale spacecraft

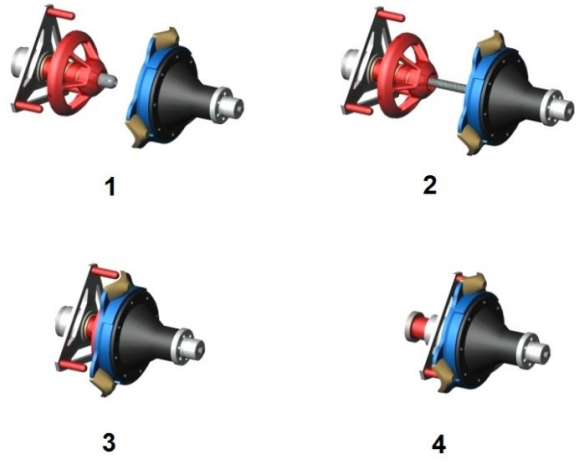

FIGURE 1.14: AMDS mechanism and docking sequence

have been developed to date, normally based on the probe-receptacle configuration. For instance, the Autonomous Microsatellite Docking System (AMDS, figure 1.14)[31] of Michigan Aerospace exploits an extendable probe which is captured by the drogue and then retracts, causing the two vehicles to mate before a series of mechanical latches secures the connection. AMDS underwent testing in a microgravity environment during a parabolic flight.

Another docking system (figure 1.15) was developed by the Laboratory for Space Sys-

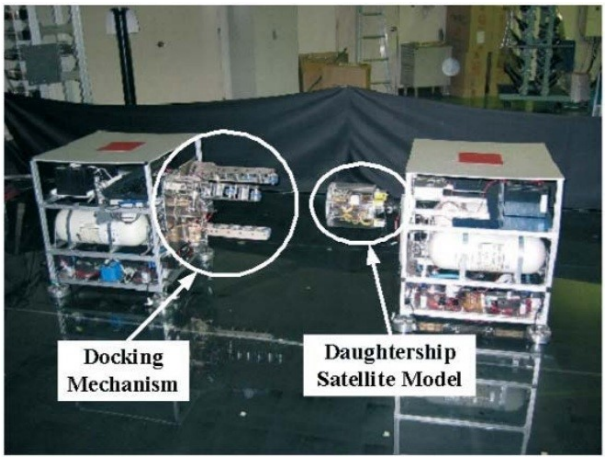

FIGURE 1.15: LSS Microgravity experiment setup of the docking system

tem (LSS) of the Tokyo Institute of Technology: a 100 kg mothership was capable to capture or release nanosatellite-class daughter-ships. The system was prototyped and tested in a microgravity environment [32]; main drawbacks of this solution are represented by the complexity of the grasping system and the limited dimensions and shape of the daughter-ships.

Another interesting mechanism has been design by Aachen, Berlin and Karlsruhe Universities in the framework of DLR iBOSS project [33], presenting an androgynous interface able to join replaceable modular components on a standard structure. It employs a simple cam mechanism, able to lock four latches through the rotation of a drive section. The interfaces doesn't show probing components, because misalignments are limited by the structure geometry and the interchangeable modules can fit on it in only one defined position. The simplicity of this solution is then counterbalanced by the limited possible operations that can be afforded: the interfaces can't be employed for complex rendezvous and docking procedures, but only for berthed joining.

Last, interfaces concept were designed for sample and return mission projects; an example is the WEB mechanism [34], designed by Honeybee Robotics for the Champollion Deep Space 4 Mission (cancelled in 1999), that implemented a net canister in order to compensate wide misalignments between the bodies and create a soft interface.

1.3.3 ARCADE and ARCADE-R2 experiments

At CISAS G. Colombo (University of Padova) the ARCADE and ARCADE-R2 experiment were developed to test a gender-mate interface in the framework of the REXUS-BEXUS programme [35]. The proposed mechanism is composed by a probe with a magnetic tip which is captured by an electromagnet placed at the end of the drogue; a linear actuator then controls the docking manoeuvre until the probe is locked by three latches. The experiments were part of a wider research program on docking mechanisms by CISAS: the results collected by ARCADE flighst together with the experience acquired in the design phase inspired further works on both gender mate [36] and androgynous [37] interfaces concepts as well as this work.

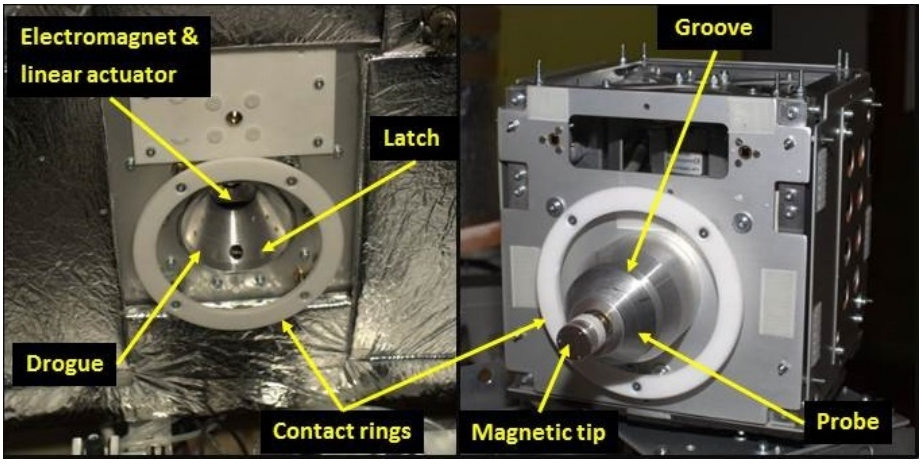

FIGURE 1.16: ARCADE experiment docking mechanism

1.3.3.1 Experiment description

The ESA BEXUS program [38] allows students from universities across Europe to perform scientific and technological experiments on research balloons, which can reach up to 35 km of altitude. Each year, two balloons are launched from ESRANGE (Sweden), carrying up the experiments fully designed and built by student teams. In this framework, in 2010 a group of students of the University of Padova proposed the ARCADE experiment, a technology demonstrator whose aim was to prove the feasibility of a small-scale gender-mate docking system, including automatic attitude determination and control capabilities, and to determine its performance under different atmospheric conditions. In more details, ARCADE, which stands for Autonomous Rendezvous, Control And Docking Experiment, was designed to perform relative proximity navigation, relative attitude control and docking between a small aerial vehicle and the balloon gondola and to correlate each subsystem performance to the disturbances due to the external environment. The development of such technologies is fundamental for future applications exploiting fleets of cooperative, automatic aerial unmanned vehicles, which possibly will be used

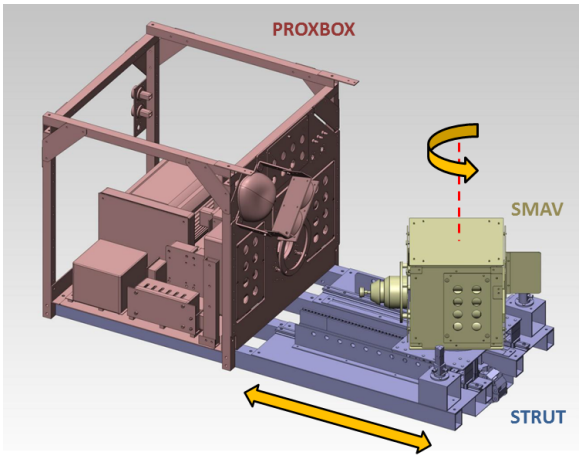

FIGURE 1.17: ARCADE overview

over the next decades in various scenarios, including mapping, surveillance, inspection and remote observation of hazardous environments that are inaccessible to ground vehicles (canyons, interior of buildings, etc...) As visible in figure 1.17, ARCADE was composed by a small vehicle (SMAV) provided with relative navigation sensors, attitude control actuators and a docking probe, mounted on a structure (STRUT) protruding outside the BEXUS gondola. Most of the electronics was placed inside a fixed assembly (PROXBOX), along with temperature and pressure sensors and the docking drogue.

The balloon was launched from the ESRANGE pad (figure 1.18) on a stratospheric balloon on September 28th, 2011, but an internal failure caused the ground base to lost the radio link with the experiment. An improved version of the experiment, ARCADE-R2,

FIGURE 1.18: ESRANGE balloon pad

was therefore proposed to ESA and was selected by the evaluation panel to participate to the 2013 BEXUS campaign, which took place in 2013, between the 4th and the 14th of October. ARCADE R-2 flew on BEXUS 17 on October 10th, 2013, performing two complete docking sequences and three release sequences before loosing radio contact due to BEXUS gondola problems.

1.3.3.2 Arcade docking mechanism overview

The ARCADE docking mechanism [35], visible in figure 1.19, comprises two mating interfaces to form a probe-drogue mechanism. The first interface is mounted in front of the SMAV and is totally passive. It shows a conical shape with a ferromagnetic tip mounted on a spring-damper to absorb contact forces during docking procedure. The drogue is attached on the PROXBOX external wall and present a conical shape to match the probe. To perform docking, the probe tip is softly captured by an electromagnet and thanks to a micro linear actuator it is pulled to its final configuration where the structural connection is achieved by means of three locking solenoids. The gondola and the SMAV interfaces are equipped with spring-mounted disks, creating a compressive force on the structure able both to secure the solenoids hard docking and to push away the SMAV during separation.

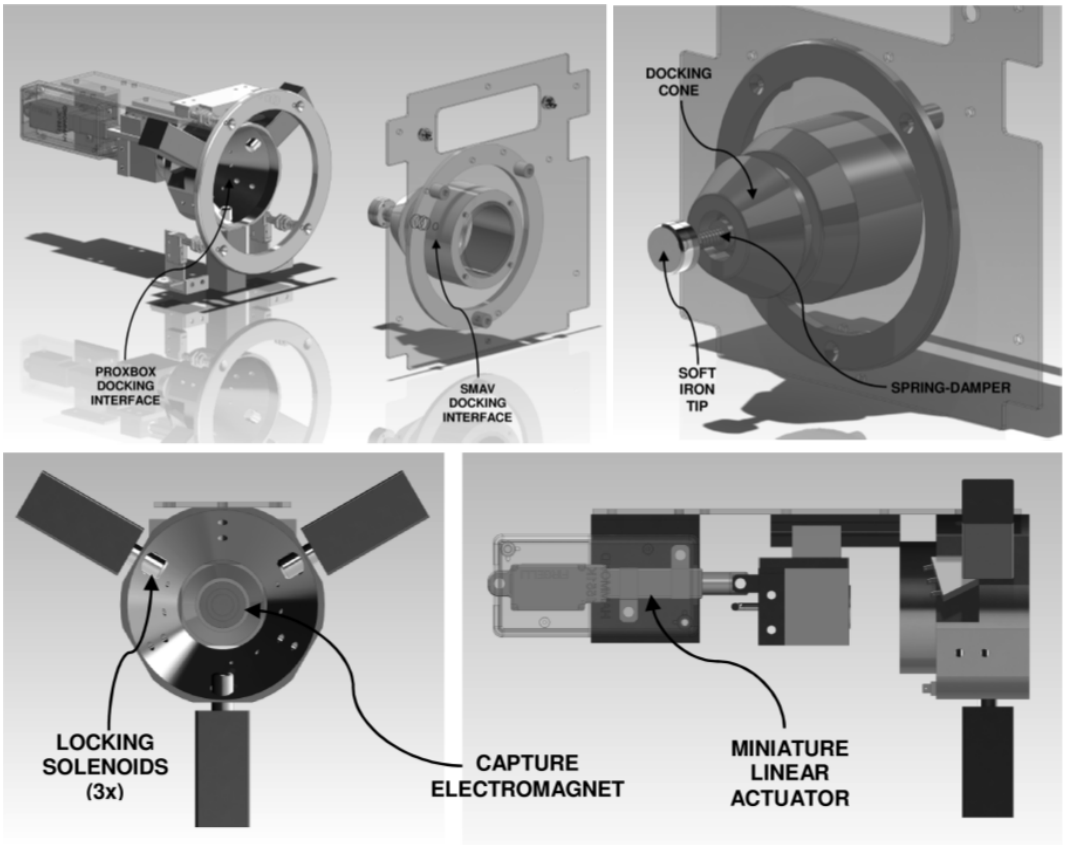

FIGURE 1.19: ARCADE docking system

FIGURE 1.20: ARCADE-R2 docking procedures during test (left) and flight (right)

1.3.3.3 Launch campaign results

The BEXUS 16/17 campaign lasted 10 days during the first half of October 2013; during the integration on the balloon gondola, ARCADE-R2 was continuously subjected to test. Data collected during such trials confirmed all the docking actuators and sensors functionality and permitted to check the perfect alignment between probe and drogue. Last, basic measurements were implemented to improve the docking automatic procedure, calculating the required actuation strokes for each motor.

ARCADE-R2 was launched the 10th of October, 2013, at 18.13 local time (16.13 UTC) and reached the maximal altitude of about 27 km. During the ascending phase, the E-Link connection was lost at 19.46 local time, causing ARCADE-R2 to stop communicating with the ground base. ARCADE-R2 softly landed at 00.01 in a forest in Finland and the PROXBOX electronics continued to work until it was switched off by the recovery team around noon.

During the flight, the experiment was subjected to random disturbances from the wind. Anemometers were dedicated to measure the relative wind speed acting on the experiment, to calculate the torque pushing on the chaser vehicle:

$$T_{dis} = \frac{1}{2}\rho \cdot C_D \cdot A \cdot v^2 \cdot d \tag{1.1}$$

with A the acting area, ρ the air density, C_D the drag coefficient, v the measured wind speed and d the distance between the centre of mass and the centre of pressure. Flight data permitted to calculate a maximal torque of about 0.035 Nm, negligible respect to actuators friction.

Another effect of the wind was the possible gondola inclination variation. It was calculated that ARCADE-R2 actuators could work up to 3.5° of inclinations respect to the horizontal direction, so an inclinometer was mounted on board the experiment; data collected before the communication loss showed, after some wider oscillations at launch,

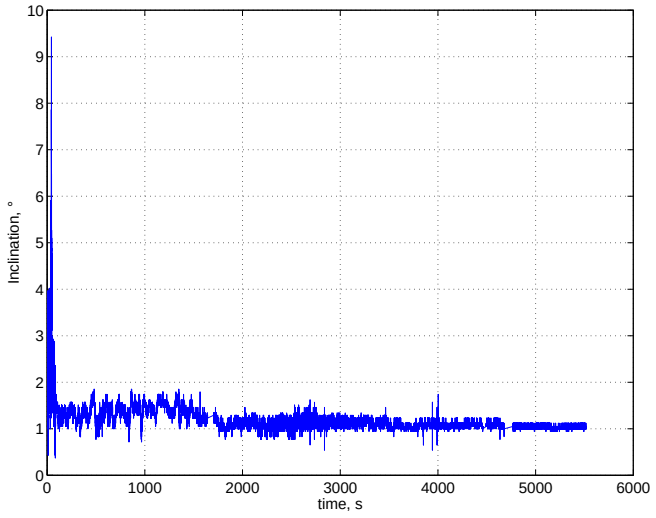

FIGURE 1.21: Inclinometer data, the oscillations caused by launch are visible before 100 seconds.

a quasi-constant inclination of about 2° (figure 1.21), into the optimal band.

During the flight, ARCADE-R2 successfully performed three release operations and two docking procedures. The experiment was launched in the mated configuration, in order to reduce the transient loads that could affect the motors, and was released at 18:20 to perform its programmed procedures. During the first flight test, it was observed that the drogue actuator was not able to capture the probe, due to minimal thermal deformations in ARCADE-R2 (the temperature dropped of about 1.55°C every minute for the first 30 minutes): it was sufficient to increase the previously implemented actuator stroke of 1 mm to allow a better contact between probe and drogue and realize complete docking sequences. Unfortunately, after the link loss, no other procedures were realized, although ARCADE-R2 survived and continued to collect environmental data during the whole flight and after landing.

In conclusion, the mechanism behaved as planned, with only a small difference on the drogue linear actuator stroke control. Results demonstrated the mechanism intrinsic robustness and confirmed the design process; future works may improve the docking interfaces to reduce the mass utilization and the power budget, evaluating the implementation of passive hard docking latches.

1.4 Research motivations

In the European space technology strategy, research and development represent key issues. If the realization of large projects is possible only with international collaborations (e.g. Cassini-Huygens, EXOMARS), the technology exchange is actually subjected to

national political and economic interests. The objective of European non-dependence from US satellite technology increased after the US congress voted in 1998 for stringent guidelines, moving space-related trades under State Department responsibility and virtually subjecting commercial agreements to the International Traffic in Arms Regulation [39], despite in 2013 such limitations were removed. The development of skills and enabling technologies for unmanned exploration missions is therefore important in ESA plans, as remarked in AURORA program [40] for planetary robotic exploration, as much as the advancement in orbital assembly capabilities. Joining technologies are vital in the future of the space exploration and exploitation. Both capture and mating systems can improve spacecraft abilities, reduce costs and allow more flexible operations.
Main fields that would benefit from further studies (figure 1.22) involve scientific (e.g.: exploration and sample-return missions [1]), industrial (e.g.: spacecraft refuelling / repairing [3] [4], resources extraction [41], in-space assembled structures) and safety (e.g.: ADR - Active Debris Removal) applications: joining systems are crucial for many space tasks from interplanetary to Earth orbit missions. Unlike manned spacecraft and large resupply vehicles (e.g.: ATV, Cygnus, Dragon), usually employing standardized docking interfaces, small spacecraft do not present standard mating interfaces; about capture systems, at today there is no space technology with demonstrated Technology Readiness Level above 5.
On these preliminary considerations, next sections will introduce the motivations to research on both capture mechanisms and docking interfaces for small satellites, and the advantages that could be reached developing such devices.

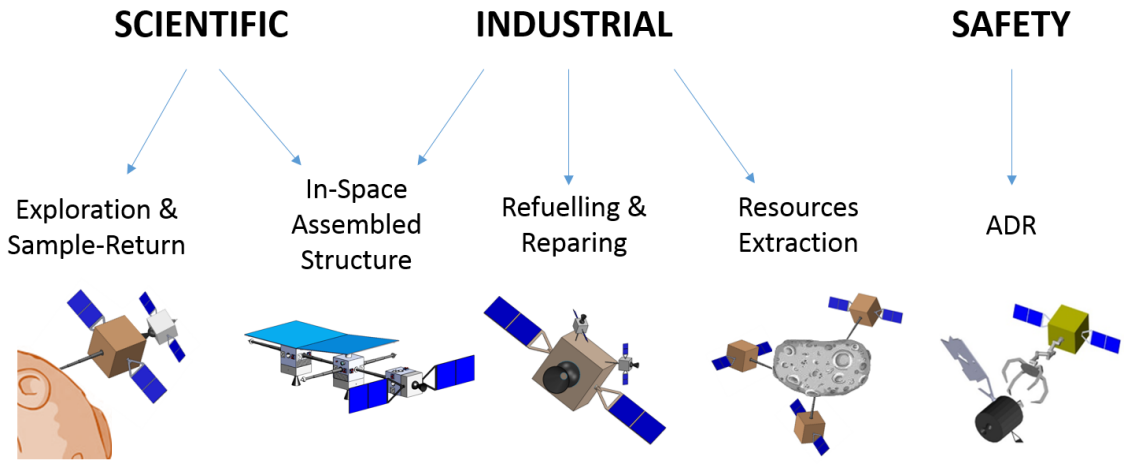

FIGURE 1.22: Fields benefiting from joining technologies

1.4.1 Capture systems

The number of uncontrolled artificial objects orbiting around Earth has constantly increased over the years and the collision threat for operative satellites is today a serious issue that endangers the future exploitation of space, so disposing of old spacecraft is a first task for the international community, as demonstrated by initiatives like ESA's CleanSpace. ADR is therefore indicated to be one of the only means to effectively preserve Earth orbits from space debris growing, but difficulties primarily related to uncooperative objects capture are still constraining the technical feasibility of such operations. However, the capture of uncontrolled objects in space has never been accomplished so far. Non-operative satellites with no active attitude control might in fact be characterized by random tumbling motion and orbital debris originated by collisions of satellites could have unknown and irregular shape, thus making their location and capture very challenging tasks. Furthermore, debris are usually not provided with any features that can facilitate approach and grasping by the servicing vehicle, such as optical markers, retro-reflectors and handles.
In parallel, capture technologies could also be employed for refuelling/repairing missions to old operative spacecraft (i.e. with no grasping features). Usually, manufacturing and launch costs are some orders of magnitude higher than orbit operation expanses. Most of the payload sent in space is constituted by the fuel needed for orbit insertion and station keeping, narrowly constraining the life duration to cost evaluations. For example, at today GEO telecommunication satellites life mostly depends from their station-keeping fuel consumption: the development of a float of servicing spacecraft, each one able to approach, capture and refuel different units, may avoid to replace perfectly working high-value satellites because out of fuel. The convenience behind such operations is however not merely economic: delaying spacecraft end of life lowers the number of required launches to substitute them and improves the possibility to develop and realize disposing operations before losing the vehicles, mitigating the risk of increasing the debris population.

1.4.2 Nanosatellites and CubeSat docking

In recent years there has been a continuously growing interest in space missions conducted with small spacecraft, down the nano and picosatellite class (respectively < 10 kg and < 1 kg). In such a framework, CubeSats were proposed in 2003 as small-scale modules to offer students and young engineers valuable educational experiences with real flight programs. In less than ten years, the CubeSat standard became rapidly a reference in nano and picosatellites design with more than 100 modules placed into orbit as of

October 2012 [42] [43], and now a vital miniature spacecraft community exists including participants from universities, industries and national space agencies. The reasons behind this success are related to the several perspectives provided by the use of this type of spacecraft, e.g. (1) enable fast, low-cost, low-risk technology development programs, (2) employ components and technologies coming from outside the traditional space industry and (3) make use of hosted payload opportunities on institutional launches, resulting in a consequent drastic cut of the costs to access space (down to 100,000 € for 1U or less). However, the same nanosatellites advantages that allow universities, corporations and small companies to easily access space are counterbalanced by important technical limitations, which make miniature spacecraft unattractive for complex and high performance missions. Such limitations are mainly related to the short life (usually less than one year), the small payload size and mass, and the minimal resources available on board in terms of power, attitude control and telecommunication. To date, it has been proposed to partially cope with this nanosatellites weakness by distributing mission operations on several miniature spacecraft forming a constellation and/or flying in tight formation [44] [45] [46] [47] [48] [49]. Even though such approach appears to be promising in some special cases where distributed sensing is required, it does not provide a conclusive solution to the problem, since the system resources available in each spacecraft remain inadequate to the vast majority of missions.

In this context, nanosatellites projects have been recently promoted by ESA and NASA, with the objective of supporting the development of new technologies to enhance or expand the capabilities of small spacecraft. A particular mention is due to the NASA's Small Spacecraft Technology Program: in that framework three multi-million contracts have been recently awarded to US universities and small industrial partners to develop specific nanosatellites technologies in the fields of telecommunications, formation flight and orbital docking [50]. This clearly proves NASA's growing interest on nanosatellite missions and their possible applications in the future. Among all, perspective applications are foreseen in the field of optical communications, imaging and Earth observation, biological research and astrobiology, distributed scientific instruments, space weather studies and astronomical observation like exo-planets transits detection.

In conclusion, the realization of a standard docking system for nanosatellites would provide such vehicles with the capability to aggregate in orbit to form larger structures. This would enable scenarios where small spacecraft can join together to generate multi-part systems with the possibility to rearrange, be repaired or updated, dramatically extending the spacecraft lifetime, producing more profitable missions and reducing the number of launched platforms required to maintain satellite constellations [51] [52] [53]. Lowering the number of launches would also mitigate the risk of space debris creation, underlining ulterior long-term advantages to on-orbit assembly. Moreover, rearranging and updating modular structures will improve their flexibility and fault tolerance. Most

noticeably, this improvement is a crucial step in the direction of making nanosatellite platforms competitive compared to traditional space vehicles.

1.5 Work logic & structure

At the end of this introductive chapter, the study logic of this work is presented. The docking mechanism design process followed a logical flow, were every step was the basis of the sequent work: figure 1.23 shows inch by inch the processing path.

The different colours of the packages are related to the chapter division of this document,

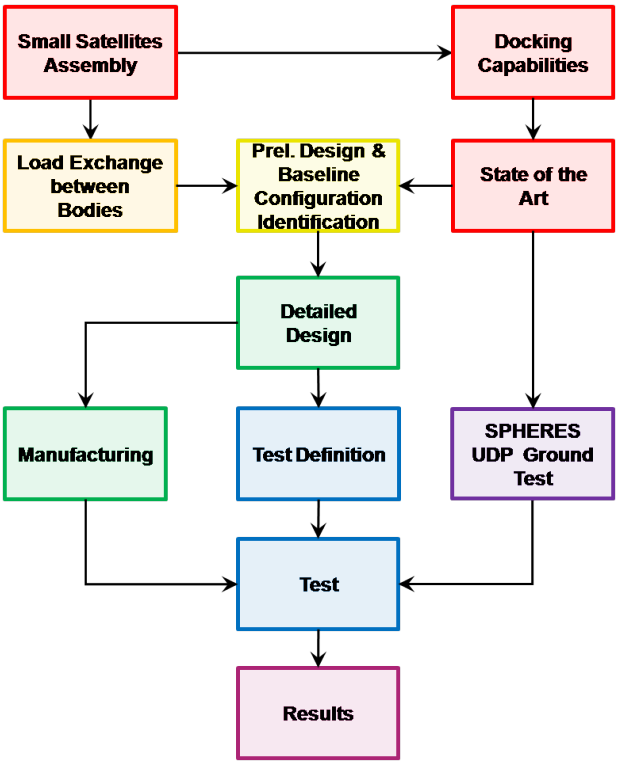

FIGURE 1.23: Study logic flux diagram

as visible in the Work Structure (figure 1.24). The preliminary work (red) consisted in the analysis of the small satellites assembly aspect and in the definition of the state of the art of small spacecraft docking mechanism, as introduced in this chapter; this preliminary investigation was followed by a simplified analysis of the loads a mating system should withstand (orange) in joint configuration. Preliminary design followed by a trade-off between different solutions, based on requirements and constraint definitions, led to a baseline configuration (yellow) that was analysed, simulated and manufactured, obtaining a new-concept docking interface (green). Test-bed design and the successive test campaign (blue) allowed to obtain important data in order to identify the mechanism response to nominal and non-nominal rendezvous (purple) and compare it with the

simulations. In parallel to the work, a visiting period at MIT Space System Laboratories was capitalized to become familiar with 2-D low friction test facilities and the SPHERES Universal Docking Port program. The possibility to learn the methodology behind the UDP development and management helped in the organization of the investigation and allowed to compare the collected results with the outcomes from a similar research program.

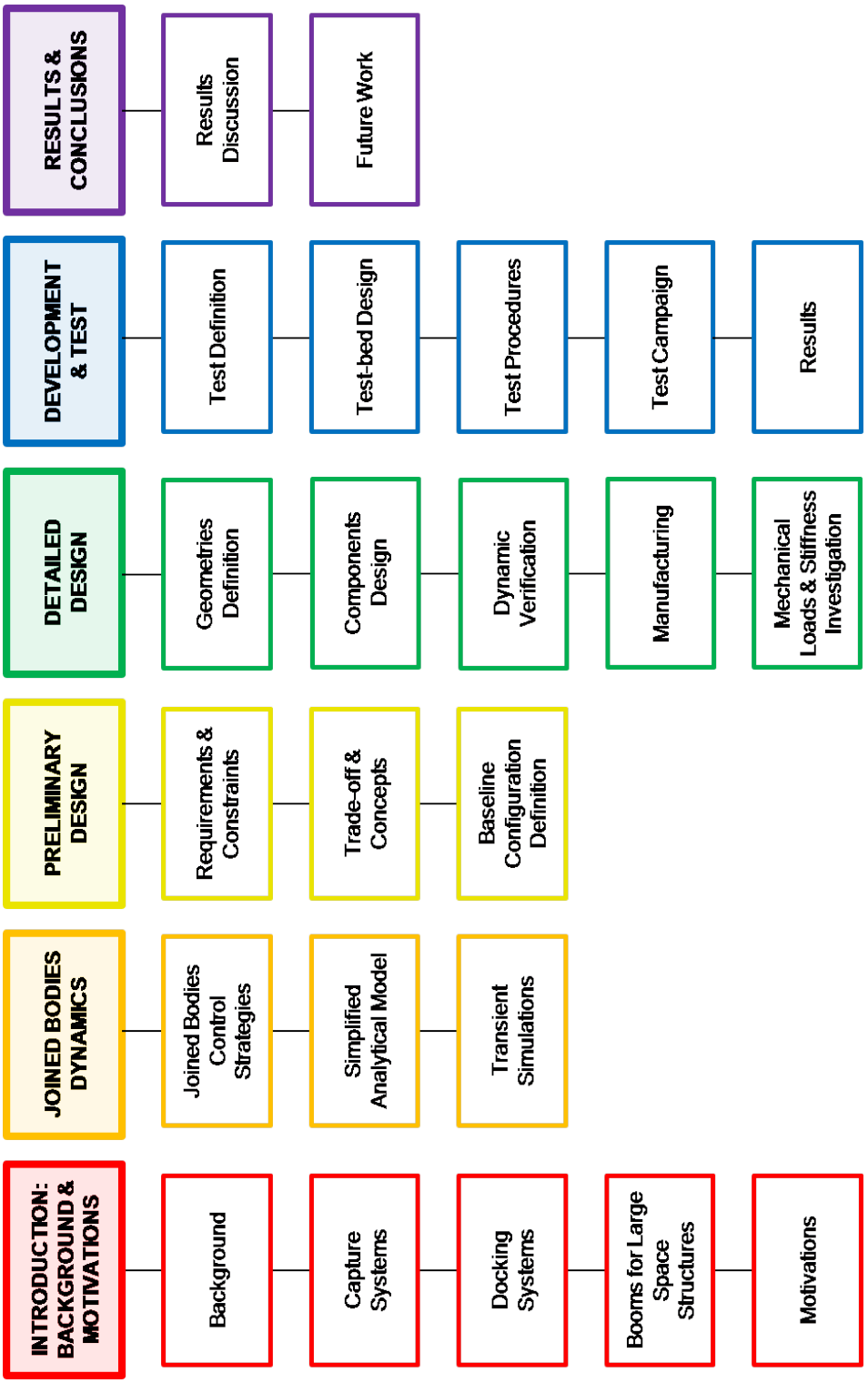

FIGURE 1.24: Work Structure

Chapter 2

JOINED BODIES DYNAMICS

The goal of this second chapter is the definition of a series of mechanical constraints that characterize the docking interface, through the evaluation of some possible configurations of the control strategy of the assembled body. A simple analytical model allowed to define the docking joint required mechanical resistance in function of estimated disturbances, parametrized on the satellites mass: for example, two 20 kg spacecraft would require an axial resistance of 1 N and torsional and flexional resistances of about 0.1 Nm due to the disturbances and the loads acting on a 650 km high orbit. As regards the stiffness, it was shown its dependence with the assembled structure requirements in terms of relative alignment and position of the composing vehicles: in case of optical payloads without dedicated pointing systems, such values would be around 10^{-7} m, hardly satisfiable for satellites larger than CubeSats. More complex simulations determined that damping ratios higher of 0.001 help to reduce transmitted vibrations of about 50% respect to configurations with ratios under 10^{-4}.

2.1 Definition of mechanical constraints

The docking joint acts as a mechanical connection between two spacecraft, and it should be able to transmit loads without failure or separation, possibly reducing vibrations that could affect the mated configuration; in parallel, it should be able to avoid excessive misalignments between the two bodies, maintaining deformations in a well-defined range. The objective of this chapter is to numerically define such constraints, evaluating the required joint stiffness, resistance and dumping, relating them to some satellites key parameters, in the directions of flexion, torsion and x-axis visible in figure 2.1.

Two potential failure modes of the docking mechanism were considered, the damage of the interface structure due to material resistance limit and the presence of loads higher

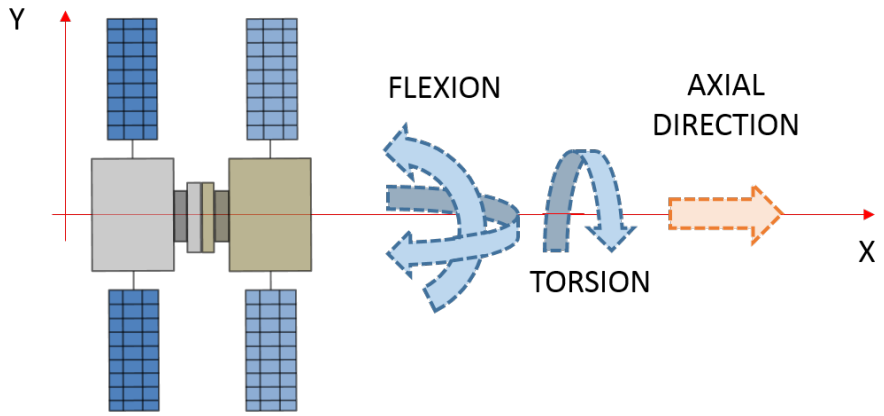

FIGURE 2.1: Flexion, torsion and x-axis directions in the joint configuration

to the mechanism actuator holding capabilities. In both of the cases, the first mechanical constraints to be analysed and defined were axial resistance (R_A) to forces and torsional and flexional resistance (R_T and R_F) to torques and non-axial forces, considering the external loads and disturbances acting on the satellites.
In parallel, the stiffness requirements were defined evaluating the deformations that the mechanism could reach under the effect of the same external loads. In this case, allowed misalignments range is strictly related to the assembly mission objective: if a servicing module could sustain a certain amount of deformation compatible to the operations it should perform, more complex structures as multi-body telescopes and antennas must reduce the relative misalignments between mirrors to well-defined values; for example, in case of optical telescopes, a good value for deformations and displacements can be fixed from the investigated wavelength at $\lambda/10$, that is 10^{-7} m for near infra-red optics [54]. The result of an analytical analysis allowed to define the trend of maximal misalignments in function of the joint axial, torsional and flexional stiffness (K_A, K_T and K_F)
Last, dynamical simulation allowed to define the effect of different damping in the reduction of peak loads and transmitted vibrations.

2.2 Joined bodies control strategies

In the simplest joined configuration, two satellites connected by a docking mechanism, three different strategies can be applied to the whole body to control its position and attitude (see figure 2.2): the spacecraft can be (1) totally autonomous, with complete control capabilities, (2) cooperative, sharing part of the external loads through the docking link, to control them, and (3) strictly dependant, with only one module dedicated

to the position and attitude control, and the other one dedicated to other tasks.

In the first case, the autonomous satellites are designed to bear the full loads and

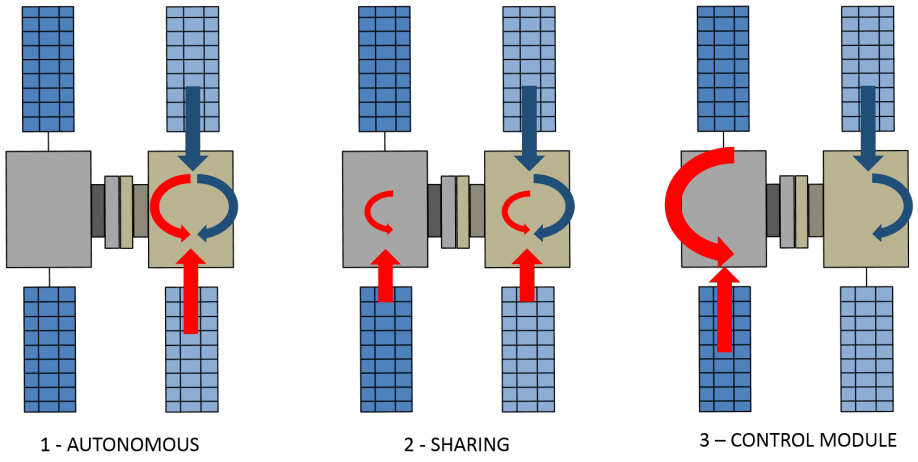

FIGURE 2.2: Comparison between the three different control strategies of a two-bodies assembled structure, from left to right, (1) totally autonomous satellites, in which every one controls its disturbances, (2) vehicles sharing part of the loads, and (3) only one spacecraft has a complete control subsystem bearing the full disturbances; external loads are reported in blue, control forces and torques in red.

disturbances, controlling them without transmitting to the other spacecraft any residual vibration or misalignment; this configuration requires high control capabilities and a continuous communication with the other satellite, to avoid any residual misalignment, but does not establish any constraint on the docking link, that could be a simple tether or even can non exist, reducing this configuration to the case of close formation flight.

The second one could be really interesting, due to the potentiality to reduce the required control authorities of every single satellite thanks to sharing capabilities: with the goal to reduce costs and complexity, the possibility to limit on board actuations could be an interesting research topic. As regards the docking mechanism, stiffness and resistance constraints would depend on the dimension of the assembled structures and on the level of cooperation.

Last, the utilization of only one control module is the most critical configuration for both the control system and the docking joint. In this latter case, loads acting on the other vehicle are transmitted to the first one, increasing the constraints in terms of transmitted loads and desired actuation. On these considerations, this configuration was chosen for further investigation, to define the required resistance and stiffness in function of vehicle masses and joining link geometry.

2.3 Analytical model

A simplified analytical model was realized to determine the resistance and stiffness constraints that a docking system should present to be able to bear loads transmitted between two satellites, with only one deputed to control the assembled structure. The most critical configurations were determined, considering the different disturbances affecting the two bodies; to apply the results to a wide range of different situations, a simplified parametrization of the spacecraft and of the affecting loads was realized, introducing a direct dependence to the vehicles mass and the distance between the two satellites centres of mass. In first approximation, the two spacecraft were considered similar in mass and with cubic shape, with the uncontrolled one having a large solar panel. The satellites dimensions were directly correlated to the mass, considering a mean density of 1000 kg/m^3, defining the edge L as:

$$L = \sqrt[3]{\frac{m}{\rho}} \tag{2.1}$$

With this relation, the satellites dimensions varied form 10 cm (CubeSats) for 1 kg bodies to about half a meter for 100 kg (small-size) spacecraft. On this definition, the single vehicle inertia I is equal for every principal axis, and was calculated as:

$$I = \frac{m \cdot L^2}{6} = \frac{m^2}{6000} \tag{2.2}$$

A spacecraft solar panel was supposed to be $2 \cdot L$ long and L wide, causing an estimated variation of the inertia ΔI on the involved axis of $0.1 \cdot I$.

2.3.1 Loads definition

The satellites were considered in a circular orbit around the Earth, with an height of about 650 km. The main disturbances acting on them were related to the gravity gradient, the magnetic interaction and the effect of solar pressure. The gravity gradient resulting torque T_G was calculated as:

$$T_G = \frac{3}{2} \cdot \frac{\mu}{R^3} \cdot |I_z - I_y| \cdot \sin(2\theta) \tag{2.3}$$

with R the distance from Earth centre (defined in the spacecraft's reference frame), μ the Earth standard gravitational parameter I_z and I_y the values of inertia in the principal axes and θ the maximum deviation of z-axis from the local vertical [55]. Inserting the aforementioned mass parametrization, the chosen orbit, and considering the worst case

of $\sin(2\theta) = 1$ the equation was rewritten as:

$$T_G = \frac{3}{2} \cdot \frac{\mu}{R^3} \cdot 0.1 \cdot I = 0.15 \cdot \frac{\mu}{R^3} \cdot \frac{m^2}{6000} \simeq 2 \cdot 10^{-7} \cdot m^2 \text{ Nm} \tag{2.4}$$

The magnetic field torque is the resultant of the interaction of the spacecraft residual dipole and the Earth magnetic field. As defined by Larson and Wertz [55], the satellite residual dipole D lies in the range 0.1 - 20 A·m^2; it was estimated that for small satellites it could lie in the range 0.1 - 1 A·m^2, and a relation with the vehicles mass was derived as $D = 0.1 \cdot \sqrt{m}$. The magnetic field varies with the orbit height and inclination, but for the chosen parameters the maximum values was calculated from the simplified Earth dipole M as:

$$B_{max} = 2 \cdot \frac{M_{max}}{R^3} \simeq 4.6 \cdot 10^{-5} \text{ T} \tag{2.5}$$

The magnetic torque was then derived as:

$$T_M = D \cdot B_{max} \simeq 4.6 \cdot 10^{-5} \cdot m \text{ Nm} \tag{2.6}$$

As regards the solar pressure, the force acting on the exposed surfaces was calculated considering the solar constant F_S, the speed of light c and a surface reflectance q of 0.6 for a solar panel of area A_S [55]. Inserting the mass and size parametrization and considering a panel with the aforementioned dimensions, and with a perpendicular incident radiation, the solar pressure force acting on the panel centre of pressure was calculated as:

$$F_{SP} = \frac{F_S}{c} \cdot A_S \cdot (1+q) = \frac{F_S}{c} \cdot (2 \cdot L^2) \cdot (1+q) = \frac{F_S}{c} \cdot (2 \cdot \frac{m}{1000}) \cdot (1+q) \simeq 1.5 \cdot 10^{-8} \cdot m \text{ N} \tag{2.7}$$

Last, forces and torques caused by satellites propulsion systems were also evaluated. Larson and Wertz [55] defined cold gas actuators and small liquid mono-propellant motors thrust range between 0.05 and 5 N, so another simplified parametrization allowed to define the propulsive thrust as:

$$F_{Prop} = 0.05 \cdot m \text{ N} \tag{2.8}$$

Considering a maximal misalignment $\Delta\theta$ of about 5 degrees between the motor and the satellite centre of mass, the torque generated by the propulsive thrust was calculated as:

$$T_{Prop} = F_{Prop} \cdot \frac{L}{2} = \frac{F_{Prop}}{2} \cdot \sqrt{\frac{m}{1000}} \simeq 8.3 \cdot 10^{-5} \cdot \sqrt{m^3} \text{ Nm} \tag{2.9}$$

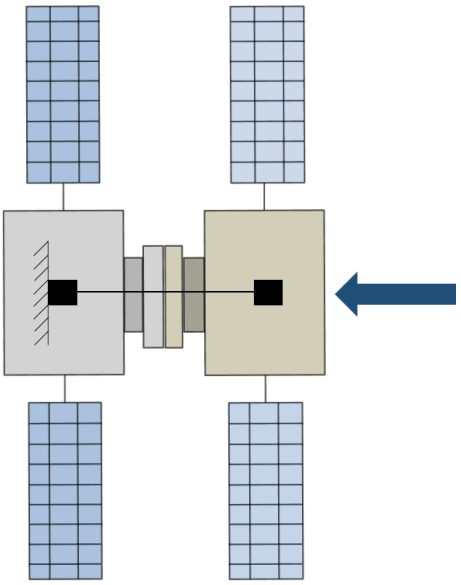

FIGURE 2.3: Load configuration for case 1: the propulsive loads acts on the uncontrolled satellite and is transmitted to the other spacecraft through the docking link.

2.3.2 Loads envelope and critical cases

The aforementioned loads were applied to a simplified static model, in order to analytically determine the characteristics of the joint. The three most critical cases were defined, imposing the worst possible loads for axial, flexional and torsional configurations.

2.3.2.1 Case 1: axial loads

In the first case, the highest axial load is caused by the propulsion system, that was foreseen to act in the direction of the docking joint. In this case, for every possible satellite mass, the solar pressure force is several orders of magnitude lower than the propulsive one. The configuration is visible in figure 2.3. In this case, the resistance was easily evaluable as the capacity to bear the propulsive force in the highly conservative case of considering one spacecraft as fixed. The resulting resistance constraint respect to satellite mass is visible in figure 2.4, on the left, with a value of 1 N for a 20 kg satellite. Stiffness directly influenced the maximal deformation at the limit axial force value: on the right of figure 2.4 it is possible to see that with such values most of the evaluated configurations presented deformations larger than the 10^{-7} m value choose from telescope imaging requirements, but it must be considered that, when orbital manoeuvres are performed, usually the scientific operations are suspended, so higher deformations could be still acceptable.

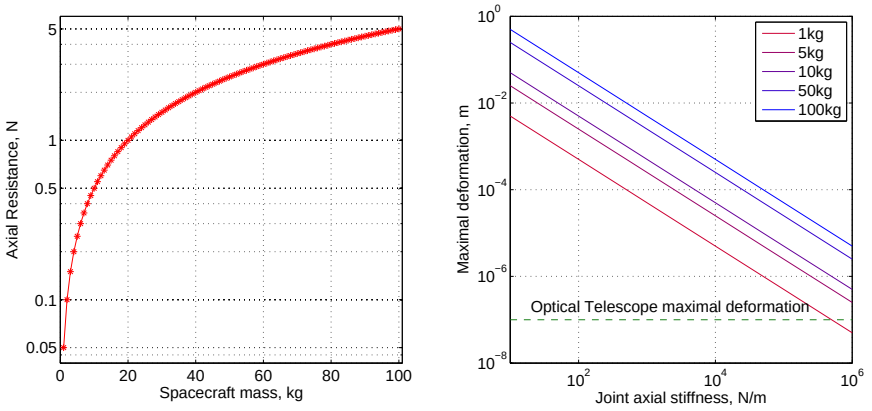

FIGURE 2.4: Resistance constraint (left) and deformation-stiffness curves at different spacecraft masses (right) for the axial loads configuration.

2.3.2.2 Case 2: torsional loads

In this second case, the most critical load configuration is caused by the sum of gravity gradient, magnetic, propulsive and solar pressure torque, the last one considered as the product of solar pressure force for the length of the lever arm L_S (i.e.: the distance between the solar panel centre of pressure and the spacecraft centre of mass). The resulting configuration is visible in figure 2.5.

Here again the resistance of the docking link was calculated as reported in figure 2.6,

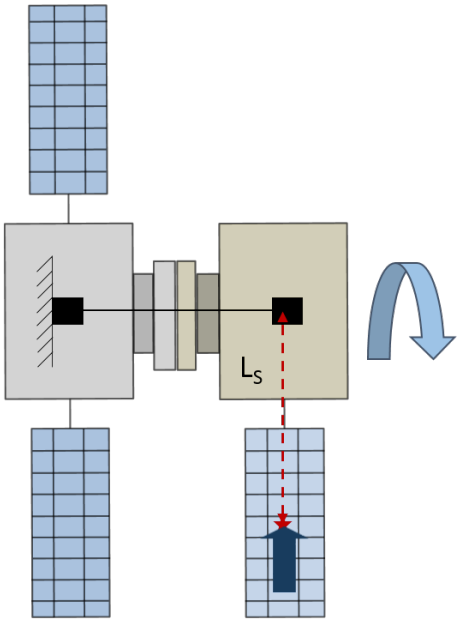

FIGURE 2.5: Load configuration for case 2: torques from gravity gradient, magnetic interaction, thruster misalignments and solar pressure act on the uncontrolled satellite and are transmitted to the other spacecraft through the docking link.

on the left, as well as the joint stiffness at different masses (on the right). In this case, resistance constraint for a 20 kg satellites resulted to be of about 0.01 Nm, and for a joint stiffness larger than 10^3 Nm the maximal deformation was well under 0.01 degrees.

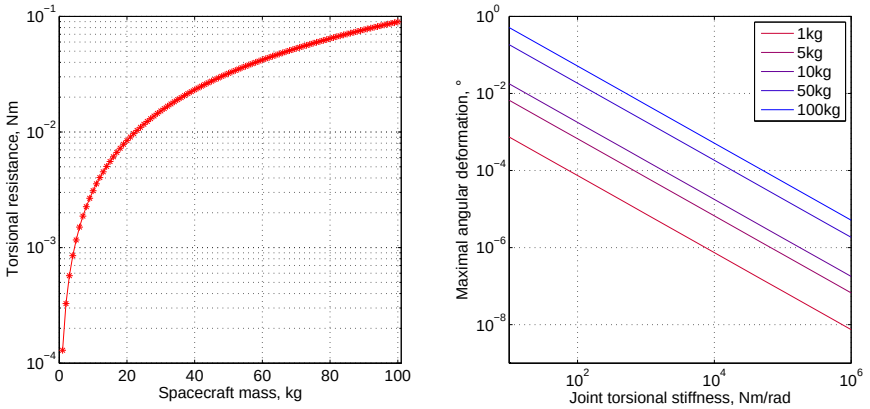

FIGURE 2.6: Resistance constraint (left) and deformation-stiffness curves at different spacecraft masses (right) for the torsional loads configuration.

2.3.2.3 Case 3: flexional loads

Last configuration analysed the flexional loads, under the effect of gravity gradient, magnetic and propulsion torques and solar pressure force, the latter creating a larger torque in this case, due to its longer arm, as visible in figure 2.7.
The influence of the solar pressure torque was however negligible (less than 0.01 percent of the other torques) considering docking link lengths L^* up to 10 times the size of the spacecraft.
The docking link flexional resistance was then calculated for different spacecraft masses, as reported in figure 2.8, on the left; due to the similar loads, the trend is comparable to the previous one, with a value of about 0.01 Nm for 20 kg satellites assembly. On the right, the angular misalignment between the two spacecraft are reported, at different values of the joint stiffness; on these considerations, it was also possible to determine the maximal deflection of the docking joint, in function of the joint parametrized length L^*. In a simplified condition, defining the flexional stiffness K_F of a beam as function of its equivalent Young Module E, section area A and length L with the relation:

$$K_F = \frac{T}{\theta_{max}} = \frac{E \cdot A}{L} \tag{2.10}$$

the maximal deflection was calculated as:

$$d_{max} = \frac{1}{2}\frac{T \cdot L^2}{E \cdot A} = \frac{L}{2}\frac{T}{K_F} \tag{2.11}$$

In figure 2.9 the results obtained for satellites of respectively 1 kg (left) and 20 kg (right) are reported. It is visible that for CubesSat-sized satellites docking joints having high stiffnesses are still allowing to satisfy optical telescopes alignment requirements for the

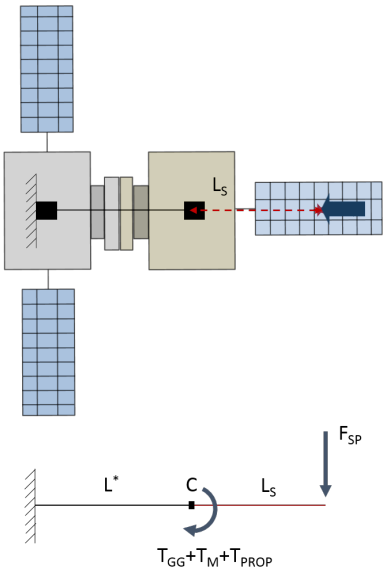

FIGURE 2.7: Load configuration for case 3: torques from gravity gradient, magnetic interaction, thruster misalignments and solar pressure act on the uncontrolled satellite and are transmitted to the other spacecraft through the docking link (up); the applied mechanical simplification shows the position of the solar pressure force F_{PS} and its arm $L_S + L^*$.

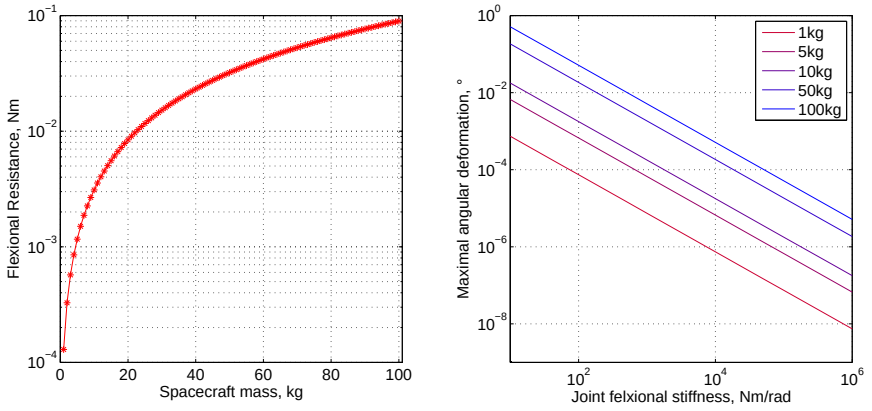

FIGURE 2.8: Resistance constraint (left) and deformation-stiffness curves at different spacecraft masses (right) for the flexional loads configuration.

different length of the docking joint, but for larger spacecraft the misalignment is in every case over the 10^{-7} m limit.

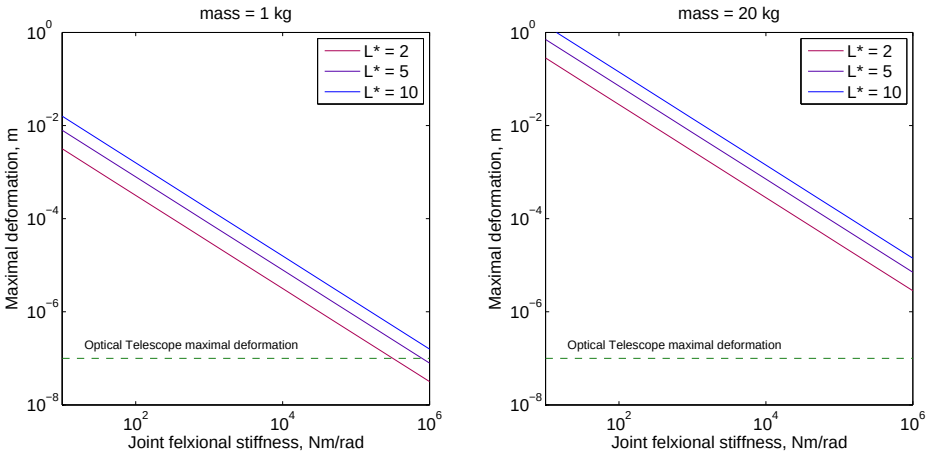

FIGURE 2.9: Maximal deformation in function of the joint stiffness, for 1 kg (left) and 20 kg (right) spacecraft

2.3.2.4 Results summary

The analytical model allowed to determine the values of the required docking link resistances for different load conditions, as reported in table 2.1. About the stiffness, results were strictly related to the level of allowable deformations that the assembled structure payload requires. In case of multi-body optical telescopes, it was calculated that, considering the limitations of this simplified model, external loads can create misalignments well over the imposed range; only CubeSat-size vehicles are able to limit deformation to the desired values, but only in case of high stiffness. Such limitations could be overcome using a separate high-precision alignment system for the telescope elements, but this application was not analysed in this contest, being out of topic respect to the goals of this research.
On these considerations, it was not imposed a series of parametrized values for the docking system stiffness.

TABLE 2.1: Resistance constraints for different mass spacecraft assemblies

Resistance	**1 kg**	**20 kg**	**100 kg**
Axial	0.05 N	1 N	5 N
Torsional	$1.2 \cdot 10{-}4$ Nm	$8.4 \cdot 10{-}3$ Nm	$9.0 \cdot 10{-}2$ Nm
Flexional	$1.2 \cdot 10{-}4$ Nm	$8.4 \cdot 10{-}3$ Nm	$9.0 \cdot 10{-}2$ Nm

2.4 Transient simulations

A numerical model was realized to complete the evaluation of the loads transmission between the mated spacecraft, considering the previous disturbances, that could vary during the orbit or at different heights, and the vibration environment caused by the satellites control system. The analytical model main limitations were to consider (1) the control spacecraft fixed instead of an active body acting with time-dependant control laws and (2) the load transmitted in a static case; the goal of these simulations was to determine the effect of damping on the joined dynamics, still maintaining the previous results in terms of resistance constraints. Matlab® programming tools were utilized to develop this model, simulate it and monitor its behaviour in time-dependant analysis, calculating the external torques magnitude with a reasonable approximation and using a simple control algorithm to simulate the satellite ADCS.
Results showed that the presence of damping joints behind the docking interfaces can be a good way to reduce transient forces and keep transmitted loads during navigation under the resistance limits defined by the analytical model.

2.4.1 Loads and disturbances

This subsection briefly describes the loads acting on the spacecraft and their reduction to simple models, better defines the disturbances introduced in the analytical model. The main loads were divided in two main classes: “external”, caused by the interaction of the satellite with space environment, and “internal”, related to the spacecraft subsystems (i.e. the ADCS actuations) [56]. External disturbances were further classified in gravitational, magnetic, drag-related and solar-pressure forces and torques, all acting at low frequencies, in the order of the orbital rate. Disturbing forces effects are usually considered negligible in simplified models like the previous one, but the resulting torques acting on the spacecraft can produce attitude errors, activating the ADCS. On the other hand, the attitude control usually lies in a wide spectrum of frequencies and can interact with satellite vibration modes.

2.4.1.1 Gravity gradient force and torque

On a distributed mass, the Earth gravitational field is not uniform and can act a gravity gradient. Considering, as a simplified hypothesis, the Earth field as ideal (i.e. generated by a homogeneous perfect sphere), the force acting on a spacecraft’s infinitesimal

element of mass dm was calculated as:

$$d\mathbf{F} = -\mu \frac{dm}{|\mathbf{r}|^3}\mathbf{r} \tag{2.12}$$

with $\mathbf{r}$ the distance from Earth centre (defined in the spacecraft reference frame), and μ the Earth standard gravitational parameter.
Defining $\mathbf{r}_{CM}$ the distance between the spacecraft centre of mass and the element, the resultant torque acting on the satellite was defined as:

$$\mathbf{T_g} = \int_{SP} -\mu \frac{dm}{|\mathbf{r}|^3}(\mathbf{r}_{CM} \times \mathbf{r}) \tag{2.13}$$

Introducing Euler angles notation for the spacecraft attitude (with the 3-2-1 configuration) and solving the integral, the gravity gradient torque was written as visible in equation 2.14:

$$\mathbf{T_g} = \frac{3}{2} \cdot \frac{\mu}{|\mathbf{r}|^3} \begin{pmatrix} (I_z - I_y)\sin 2\phi \cos^2\theta \\ (I_x - I_z)\sin 2\phi \cos\theta \\ (I_y - I_x)\sin 2\phi \sin\theta \end{pmatrix} \tag{2.14}$$

In addition, the gravitational force acting on the spacecraft centre of mass was defined in the spacecraft's reference frame as:

$$\mathbf{F_g} = -\mu \frac{m_{SP}}{|\mathbf{r}|^3}\mathbf{r} = -\mu \frac{m_{SP}}{|\mathbf{r}|^3} \left([R_{3,2,1}]^T \cdot \begin{pmatrix} 0 \\ 0 \\ |\mathbf{r}| \end{pmatrix} \right) \tag{2.15}$$

with $R_{3,2,1}$ the attitude Euler's rotation matrix. The main advantage of this notation was the expression of the orbit radius r only with scalar terms.

2.4.1.2 Magnetic field effects

Earth magnetic field $\mathbf{B}$ can interact with the spacecraft residual magnetic dipole $\mathbf{D}$, creating a non-negligible torque. The simple dipole model of Earth's field previously employed in the analytical model was used, and the resultant torque was defined in the spacecraft's reference frame as:

$$\mathbf{T_B} = \mathbf{D} \times ([R_{3,2,1}]^T \cdot \mathbf{B}) \tag{2.16}$$

2.4.1.3 Drag Force and Torque

The drag-related force was defined in the spacecraft reference frame as:

$$\mathbf{F_D} = \frac{1}{2}\rho \cdot C_D \cdot A \cdot |\mathbf{v}|^2 \cdot \hat{v} \tag{2.17}$$

with **A** the incident area and C_D the drag coefficient (in this case, $C_D = 2$). The atmosphere density value ρ was calculated with linear interpolation form COSPAR International Reference Atmosphere (CIRA-2012) [57] tabular data for medium solar activities. Defining **b** as the vector joining the spacecraft centre of mass and centre of pressure, the resultant torque was defined as:

$$\mathbf{T_D} = \mathbf{b} \times \mathbf{F_D} \tag{2.18}$$

2.4.1.4 Solar Pressure

Considering the calculations form the analytical model, in first approximation the solar pressure was considered negligible on a small-class satellite, thanks to its limited surface.

2.4.1.5 Control Algorithm

The ADCS system was modelized with a simple PD control using the attitude information (Euler rotation matrix) and the rotation rates to calculate the angle and velocity errors $\mathbf{e_a}$ and $\mathbf{e_w}$. The control torque was written as:

$$\mathbf{T_C} = K_P \cdot \mathbf{e_a} + K_D \cdot \mathbf{e_w} \tag{2.19}$$

The proportional gain K_P was calculated from the relation with the controller frequency domain $\omega_n \approx \sqrt{K_{P_i}/I_i}$; the proportional gain value was then calculated as $K_P = cost \cdot I$. The calibration of the constant led to a performing control. The derivative gain was manually tuned to acceptable values. Last, a maximum control torque was chosen to simulate limited ADCS resources, defined in function of the satellites mass.

2.4.2 Model Description

The dynamical model considered the two spacecraft as separate bodies and the docking link as a joint capable of forces and torques transmission; this was realized using the two-nodes model showed in figure 2.10. In the simulations, the external forces and torques acted on the bodies centres of mass, modifying their attitude and position. The main issue of this approach was related to the management of the gravitational forces

applied to the two satellites: the simulations were designed to work in a relative reference frame, centred on the assembly common centre of mass, and the orbital dynamics was implemented only for the attitude evolution. The selected solution was to calculate the gravitational force F_{CM} in the common centre of mass CM, as the sum of two components:

$$F_{CM} = -\mu \frac{m_1 + m_2}{{R_{CM}}^2} = -\mu \frac{m_1}{{R_{CM}}^2} + -\mu \frac{m_2}{{R_{CM}}^2} = F_{CM,m_1} + F_{CM,m_2} \tag{2.20}$$

In this way, it was possible to apply on the two satellites centres of mass only the force difference $\mathbf{\Delta F_{G,i}} = \mathbf{F_{G,i}} - \mathbf{F_{CM,m_i}}$ and calculate from it the exchanged torques and the forces, reducing the computational cost of the operation.
The docking joint acted as a spring-damper link, and every time-step the differences in relative attitude and position were used to calculate the forces and torques caused by misalignment respect to the unloaded state.

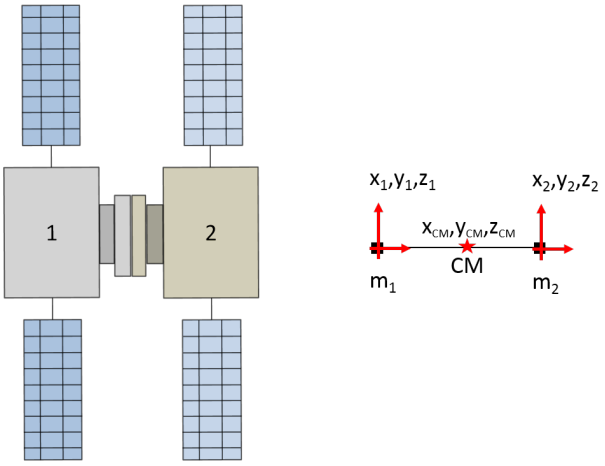

FIGURE 2.10: Two-nodes model of the assembled spacecraft with reference frames

2.4.3 Simulations results

The simulation campaign has given a wide range of results; the ones presented in this section are related to two mated satellites both of 20 kg in a circular orbit of 700 km, but are still representative of the whole campaign that was performed for different masses and altitudes. The external disturbances, having low frequencies ($<<$ 1 Hz), could be treated as semi-steady loads due to the difference with the control pass band; on the contrary, the joint behaviour was more intriguing, showing higher frequencies response, and during manoeuvres it could cause a long transient phase, transmitting vibrations at various frequencies related to its stiffness in the different directions. For a simple rotation of the assembly of 1 degree around its docking link, the presence of damping helped both to reduce the amplitude and the duration of such vibrations, as visible in

figure 2.11.

On these results, some considerations were stated. The effect of the damping ratio had

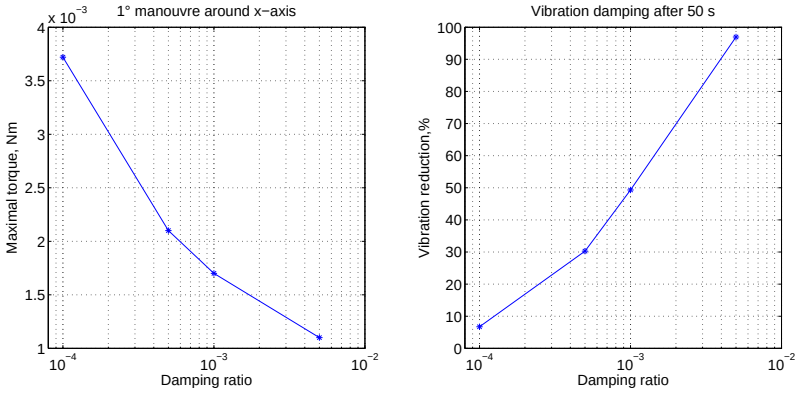

FIGURE 2.11: Peak load due to 1° manoeuvre (on the left) and effect of different damping ratios on vibrations reduction (on the right).

to be considered, in order to reduce the induced vibrations. An easy way to implement this solution would be to mount an independent damping joint behind the docking port, as visible in figure 2.12. Another evaluated solution was to use deployable booms to maintain the desired distance between the two spacecraft. In this configuration, the booms would be mounted behind the docking ports, and deployed before or after the mating; their intrinsic damping, caused by internal mechanisms frictions, could reduce the vibrations as desired. A small analysis of deployable booms state of the art is presented in Appendix A. In every case, simulations suggested that a value of at leas 0.001 for the damping ratio should be chosen to reduce vibrations of about 50% respect to cases involving damping ratios less than 10^{-4}.

2.5 Final considerations

The developed tool introduced in this chapter was used to simply simulate the proposed port behaviour under environmental disturbances; on the defined set of results, it was possible to start the preliminary design of the docking mechanism. Resistance constraints were determined, as visible in table 2.1, as function of the spacecraft mass, and discussions on the link stiffness introduced its dependence to the spacecraft payload requirements in terms of relative position and alignment. Results exposed in this chapter were based on the simple problem of only two joined bodies. Larger structures could be analysed, considering that for example space telescopes could be composed of tens of small mirrors [58] and studies are being performed to create long assemblies of modular spacecraft for telecommunication antennas arrays [59]. In these cases, the

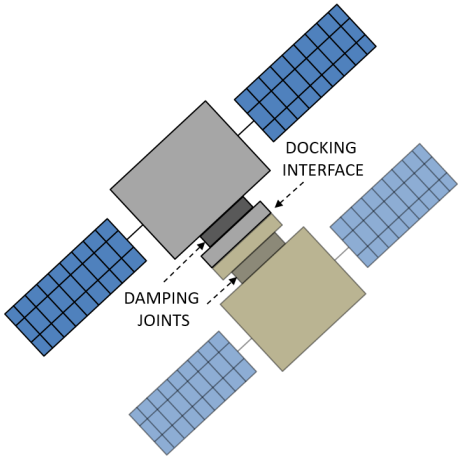

FIGURE 2.12: Docking system possible configuration

problem acquires a great complexity, due to the presence of many different bodies subjected to the disturbances environment, and various vibration mode can be activated. In a preliminary evaluation, a simplified square structure composed by 100 satellites was simulated, considering them connected by a rigid docking link: giving to the central satellites a disturbance comparable with space environment and monitoring the oscillations of the whole structure, it was possible to evaluate the deviation from planarity, as reported in figure 2.13, for free different satellites masses. Comparing with the optical mirrors requirements, it is possible to see that CubeSats and in general lighter spacecraft may employ less stiff docking joint still performing the needed alignments; further investigation should be performed to obtain more complete outcomes.

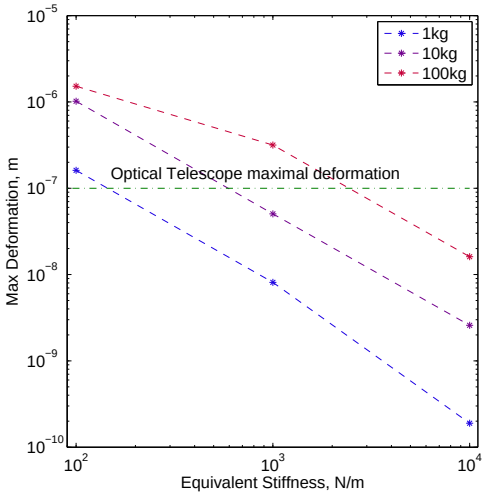

FIGURE 2.13: Maximal deviation from planarity of a 100 x 100 satellites assembly, evaluated at different satellite mass varying joint stiffness.

Chapter 3

PRELIMINARY DESIGN

This chapter describes the preliminary design of some new concept docking mechanisms. The knowledge and capabilities acquired during ARCADE-R2 experience allowed starting a new design process, based on State of the Art analysis, practical considerations and requirements and constraints definition. The description of the main requirements led to the definition of different level conflicts between them. The hardest conflicts were related androgyny, rotational symmetry and simplicity (in terms of number of components and actuators); information from the conflict analysis helped to define relaxing requirements and the effect of different design solutions on the docking subsystem characteristics. At the same time, small spacecraft have restricted on-board resources, limiting the possible payload mass, volume and electrical power, that shall be taken in account in the design process. In order to establish a good compromise solution, three different classes of requirements were defined, weighting the influence of the three mentioned features of androgyny, rotational symmetry and simplicity; on these basis, a conceptual solution was developed for each class, analysing and comparing its strength characteristics and weaknesses. The first one was directly inspired to the Androgynous Peripheral Attach System series and presents a three petals structure with an external soft docking ring. It consequently benefits from consolidated design aspects but also presents some minor disadvantages of high power consumption and mass budget. The second concept has axis-symmetric interfaces with a "probe and drogue" logic with new-concept totally passive latches: the capture mechanism is designed to perform docking manoeuvre demanding only a well-defined chaser approach velocity and to separate using only propulsion abilities. The mechanism main feature, the capability to do not consume electric power, may be the source of its main drawback: well-defined approach velocities and propulsion capabilities can be too stringent for spacecraft and may cause high impact forces and transmitted loads. The third solution was designed to combine the advantages of an androgynous system with the simplicity of a gender mating mechanism,

using a shape-shifting structure. Far from the existing interfaces, the presented solution does not employ active latches for hard docking and uses only one electric motor for activation and docking: the internal stiffness and pre-load in the docked configuration creates the solid joint. A comparison between the three concept and the requirements and constraints suggested that the third solution was a good compromise and it was therefore selected for further developments. A smart technology, consisting in an application of electroactive polymers, was proposed for the port actuation; this solution was for the moment postponed, preferring the utilization of simpler COTS motors for this first investigation.

3.1 Requirements and constraints

The work on ARCADE-R2 returned a good experience on the development of a small docking system; the issues showed by the experiment were the result of a novel technology development, carried out in short time, with few background experience. The acquired knowledge and capabilities allowed starting a new design process, based on State of the Art analysis, practical considerations and requirements and constraints definition. The design of the mating interfaces is subject to a number of different factors, from the dynamics to the mission objectives to the mechanism complexity. The State of the Art and the History can give some of these preliminary indications: the main qualitative requirements are listed in table 3.1. Before an appropriate analysis of these drivers, it is noteworthy that some requirements may conflict with each other. For example, the requirement of androgyny can be achieved only with simply non-rotational symmetric mechanism or with more complicated symmetric interfaces; at the end of this section a brief paragraph will discuss this issue. The definition of the possible relaxing requirements is an important stage of the conceptual design.

3.1.1 System requirements

3.1.1.1 Androgyny

Docking subsystems can adopt androgynous or "gender-mate" configurations. The main difference is that in androgynous interfaces each side can be active or passive and a spacecraft with this port can mate with any other similar docking interfaces. Since Syromyatnikov designed the first androgynous docking mechanism for Apollo – Soyuz Test Project (1975), "gender-mate" ports has been used only for automatic missions and the Russian Soyuz.

As visible in figure 3.1, non-androgynous interfaces are really simple to outline: a

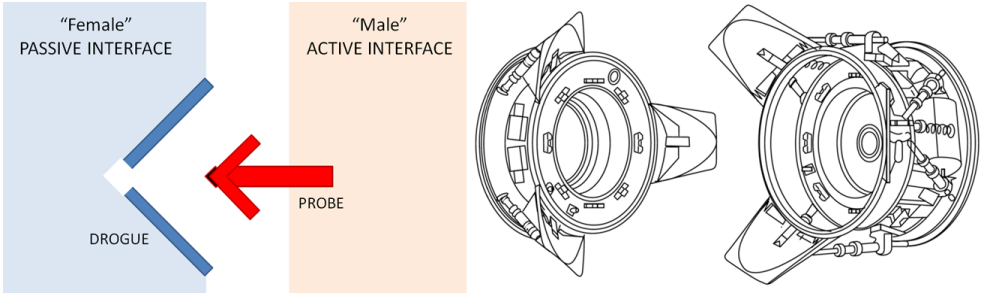

FIGURE 3.1: "gender-mate" configuration (left) vs. androgynous interfaces (right: APAS-75, courtesy by NASA)

TABLE 3.1: Qualitative requirements list

N.	Requirement	Explanation
01	Androgyny	Each interface should be able to be both active or passive so a spacecraft with androgynous mechanism could mate with any other port.
02	Rotational Symmetry	The docking port should be symmetric with respect to a central axis, so spacecraft could dock with a free DOF (rotation respect to the axis).
03	Simplicity	The interface should not involve complex mechanism and uses simple and reliable mechanisms.
04	Mechanical Transmission	The mechanical connection should be able to transfer loads, allowing separate attitude control and propulsion to operate on the entire modular structure.
05	Electrical Connection	The two spacecraft should provide electrical connections in order to share and distribute power.
06	Fluid Exchange	The two spacecraft should provide fluid exchange, allowing refueling procedures or thermal fluid exchanges.
07	Communication	The two spacecraft should provide continuous (wired or wireless) communication for data transfer and docking/undocking/ranging control.
08	Tolerance to Misalignment	The docking mechanism should work under a certain misalignment between the two interfaces.
09	Soft Docking	The docking procedure should be independent from the relative velocity.
10	Thermal Compatibility	The two interfaces should maintain the docking capability in a well-defined range of temperature.
11	Undocking Protection	In the separation of the chaser from target, the docking interfaces and other expose surfaces should be protected from the chaser propulsion subsystem.
12	Protection from Space Environment	The docking ports and mechanisms should survive to a long exposure to the space environment.

probe fits the "female" interface (drogue) and a simple locking mechanism creates the mechanical junction.
The extreme simplicity of probe-drogue systems is counterbalanced by the positive features of androgynous ports: spacecraft with "gender-mate" interfaces can dock only with other gender ports, reducing mission reconfiguration and flexibility options.

3.1.1.2 Rotational symmetry

The attitude determination and control in approaching and docking phases are really stringent, depending on the docking mechanism and vehicle characteristics; for large satellites, the maximal angular misalignment shall be less than 5° [7]. If the docking ports present an axial symmetry respect their longitudinal axis, the DOF of rotation around this direction is free, relaxing the alignment requirements to perform the joining procedure. Examples of a partial rotational symmetry are visible in most of the docking interfaces. The main issue is about the position of umbilical connections (e.g. electric transmission or fluid transfer): as visible in figure 3.2, the Soyuz shows a symmetric mechanical configuration, but the presence of the electrical connectors (four rectangles on the external ring) makes docking possible only with the right orientation.

FIGURE 3.2: Soyuz docking port from ISS: note the four electrical connector on the external ring (courtesy by NASA)

3.1.1.3 Simplicity

Leonardo da Vinci once said: "Simplicity is the ultimate sophistication". The principle of mechanical simplicity can be summarized with that sentence, because the only certain way to avoid components or mechanisms failures is to avoid their installation. Since the production of the celebrated FORD Model T (1908 - 1927), simplicity is often associated to a lack of technology, but it is the best way to avoid failures and ensure low costs and long lifespan. It is not easy to design simple, adding components and complex mechanisms is often a short cut to requirements satisfaction: simplicity means complete redesign and new solutions development. The docking system should be as easy as possible and implement simple and reliable mechanisms, but this requirement could conflict with the other design constraints.
In order to give a more tangible sense to the simplicity requirement, it can be established that the docking mechanism should have the least possible number of active elements and actuators. Usually, a standard mating mechanism employs actuators to perform the soft docking and active latches to create the solid joint between the interfaces.

3.1.1.4 Mechanical transmission

During mating, the docking ports are subjected to the loads of both spacecraft. If the target (or the chaser) attitude needs corrections, the actuators loads are distributed to the other craft through the contact surfaces. Docking subsystems should be able to transfer such loads without interrupting the mechanical and electrical contact, allowing separate attitude control and propulsion to operate on the entire modular structure. Tidal forces can create other loads on the interfaces, but in first approximation they are negligible respect to attitude control forces and torques. The magnitude of the transferred loads can be approximated with a simplified model visible in figure 3.3, but a more accurate investigation of the mechanical characteristics of two mated bodies was introduced in chapter 2.

To simplify the problem, the docking port is considered on the line between the two

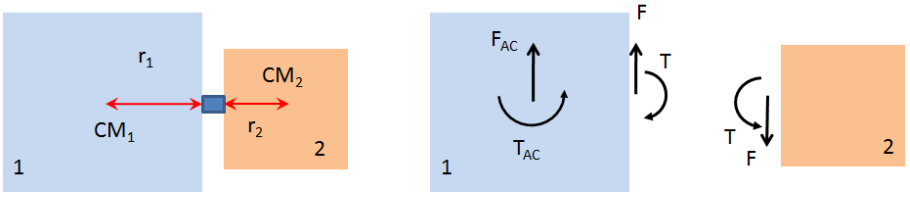

FIGURE 3.3: Load transfer model: docked spacecrafts geometry (left) and loads on the docking ports (right)

satellites centres of mass. If spacecraft n° 1 delivers the control torque and the control

force , the dynamics equations for body 1 can be written as:

$$\begin{aligned} m_1\ddot{x}_1 &= F_{AC} - F \\ I_1\dot{\omega}_1 &= T_{AC} - T \end{aligned} \tag{3.1}$$

Body 2 can be represented by equations:

$$\begin{aligned} m_2\ddot{x}_2 &= F \\ I_2\dot{\omega}_2 &= T \end{aligned} \tag{3.2}$$

If the two spacecraft are mated, they work as a single body and the accelerations of the centres of mass is the same. In first approximation it is, therefore, possible to calculate the maximal loads the docking subsystem is subjected to:

$$\begin{aligned} F &= F_{AC} \cdot \tfrac{m_2}{m_1+m_2} \\ T &= T_{AC} \cdot \tfrac{I_2}{I_1+I_2} \end{aligned} \tag{3.3}$$

3.1.1.5 Electrical connection

The docking ports should provide an electrical connection between the spacecraft in order to share and distribute power. Usually multi-pin connectors are applied on the docking rings (see Soyuz docking port, previous picture), allowing a high number of different connections; the main issue of this solution is the usual lack of central symmetry, using peripheral connectors.

3.1.1.6 Fluid exchange

One of the most important requirements of a new standard docking system is the capability to transfer fluids between the two spacecraft. The interfaces should allow the exchange of propellant or thermal control fluids without significant leakages.

3.1.1.7 Communication

Docking and undocking procedures require continuous communication between the two spacecraft; chaser ranging also would need feedback from the target during close rendezvous phase. Data transfer would also be important during scientific missions. The docking interfaces could use different strategies for each of the previous activities or implement a simple wireless system.

3.1.1.8 Tolerance to misalignment

Due to the dynamical behaviour of the spacecraft, possible little errors in terms of position, direction, inclination and speed can influence mating procedures. In state of the art of large satellites joining systems, allowed lateral and angular misalignments are in the range of $0.05 - 0.2$ m and $1 - 5°$, while approach and lateral velocity and angular rate shall be respectively less than 0.3 m/s, 0.05 m/s and 0.25°/s [7]. The docking mechanism should be able to work under a certain misalignment between the two interfaces, usually employing shock attenuation devices. Considering the size of small-class spacecraft, a preliminary value of tolerable misalignments can be stated of $5 - 10$ mm and $1 - 5°$.

3.1.1.9 Soft docking

The development of new concept docking mechanisms (e.g. NASA Docking System – NDS [25]) considers soft docking an important requirement. Usually, during passive docking the interfaces need a minimum relative velocity to activate passive spring latches, but this procedure also involves various impacts. New applications can present different solutions like electromagnetic surfaces: only the proximity or the soft contact of the two ports would activate the passive mating, without position or velocity requirements and limiting the contact loads.

3.1.1.10 Thermal compatibility

The wide range of temperature the interfaces can reach passing from sunlight to shadow could modify the docking interfaces geometry and deform its dimensions. The two ports should maintain their mating capability between two predefined temperatures.

3.1.1.11 Undocking protection

After the opening of the mechanical joints between the satellites, the chaser could apply an impulse to separate from the target, with potentially dangerous effects on the target expose surfaces from the chaser propulsion subsystem. The implementation of passive release devices as pre-charged springs could satisfy this requirement.

TABLE 3.2: Requirements conflicts table

N.		02	03	04	05	06	07	08	09	10	11	12	13
01	Androg.	H	H	M	M	M	M	L	L	L	L	M	L
02	Rot. Symm.		M	M	L	L	L	L	L	L	M	M	L
03	Simplicity			M	M	H	M	L	H	L	H	M	H
04	Mech. Transmission				L	L	L	M	M	L	M	M	M
05	Electrical Connection					L	L	M	M	L	L	L	M
06	Fluid Exchange						L	M	M	M	L	L	L
07	Communication							L	L	L	L	M	L
08	Tolerance to Misalignment								M	M	M	L	L
09	Soft Docking									M	M	M	L
10	Thermal Compatibility										M	L	L
11	Undocking Protection											M	L
12	Protection from Space Environment												L
13	Mission Flexibility												

3.1.1.12 Protection from space environment

The docking interfaces are exposed to space environment and materials, mechanisms and electronics should be protected and qualified to survive until the end of the mission.

3.1.2 Requirements conflicts and mission flexibility

As briefly introduced, there are particular conflicts between most of the described requirements. Table 3.2 presents a list of these frictions with a colour codex to emphasize the conflict level (H-red: Hard, conflict; M-yellow: Medium, potential conflict; L-green: Low, potential cooperation). In addition, a 13^{th} requirement is added to the table, defining the mission flexibility: the docking system would not influence seriously the satellite capability to adapt to different operation conditions. This requirement is deeply correlated to androgyny, because spacecraft with "gender-mate" ports can dock only with other gender interfaces, reducing mission reconfiguration options. The hardest conflicts are related to the first three requirements, (androgyny, rotational symmetry and simplicity): for example, it is difficult to design simple androgynous systems with rotational symmetry, as much as creating simple mechanisms with soft docking or fluid exchange capabilities.

Information from the conflict table helps to define the relaxing requirements and the effect of different design solutions on the docking subsystem characteristics. It is also important to underline that hard conflicts between requirements do not imply unfeasibility; it only means more complicated conceptual or design solutions that can influence the mechanism working principle and its response to other requirements. The design phase needs to consider these aspects, in order to establish good compromise solutions.

3.1.3 Constraints

The design of a novel docking system for small satellites can be constrained by the field of application. Small spacecraft, and particularly CubeSats, have restricted on-board resources, limiting the possible payload mass, volume and electrical power. About the mass constraint, lightweight systems can be engineered using smart and thin structure and employing composite or plastic materials. These solutions can considerably reduce the required mass but often influence the components cost, manufacturing and integration techniques. Bulk constraints usually limit the subsystems design to the spacecraft structure volume. On CubeSats, all the components should be adapted to a 10 cm x 10 cm frame, limiting the possible configurations for internal component; external deployable structures sometimes can overcome this problem (e.g.: solar panels or large antennas). For small spacecraft available on board power is often related to the satellite size; at today, all the cited docking mechanisms depend on conventional moving parts, such as mechanical latches and retractable probes, actuated by electric motors or other active devices (e.g. electromagnets and solenoids) with elevated power requirements. Power consumption is therefore an influential constraint and, with mass and geometry restriction, can influence the mating interfaces definition and trade-off. Last, docking procedures involve contact between different bodies that can create high impulsive forces. This could influence both the satellite attitude (through transmitted loads) and the employed technologies and materials, affecting mass and volume constraints.

3.2 Requirements trade-off and concepts

As reported in section 3.1.2, table 3.2 shows that the hardest conflicts are related to the first three requirements of androgyny, rotational symmetry and simplicity.
In order to establish a good compromise solution, three different classes of requirements were defined, weighting the influence of these three features; on these basis, for each class a conceptual solution has been developed, analysing and comparing characteristics and weaknesses.

3.2.1 First class: androgyny

The first requirements class considers the androgyny as essential for the docking mechanism; this would allow a satellite to dock with every interface equipped with an identical port, with no order or preference between target and chaser. Looking at the state of the art, androgynous solutions are often realized with petals structures that in part limit the rotational symmetry. Another limiting design solution is however related to the form

and position of electrical and fluid exchange connectors, that should be androgynous themselves and can influence simplicity and symmetry. At today, these kind of ports uses simple electromagnets to soft dock and heavier electromechanical latches to create the solid joint, transmit loads and preload undocking spring actuators. To summarize, in table 3.3 the requirements conflict levels with androgyny are listed, with the same previous colour codex to emphasize the conflict level (H-red: Hard, conflict; M-yellow: Medium; L-green: Low).

TABLE 3.3: Androgyny requirements conflict

Requirement	Conflict
Rotational Symmetry	H
Simplicity	H
Mechanical Transmission	M
Electrical Connection	M
Fluid Exchange	M
Communication	M
Tolerance to Misalignment	L
Soft Docking	L
Thermal Compatibility	L
Undocking Protection	L
Protection from S. E.	M
Mission Flexibility	L

3.2.2 Second class: rotational symmetry

As previously introduced, symmetric interfaces reduce the navigation requirements between target and chaser but are normally related to non-androgynous mechanism; this reduce the docking opportunities only to other gender ports but simplify the satellite attitude control requests (Table 3.4).

3.2.3 Third class: simplicity

Simplicity requirement is the most difficult to relate with androgyny (complex interfaces), fluid exchange (complex mechanism with gaskets and valves), soft docking and undocking protections (complex preload and release mechanisms).

However, simple mechanisms with reliable components should be preferred to avoid failures and ensure low costs and long lifespan. For this reason, despite the high conflict levels visible in table 3.5, this class of requirements was not rejected and a related concept solution was developed.

TABLE 3.4: Rotational symmetry requirements conflict

Requirement	Conflict
Androgyny	H
Simplicity	M
Mechanical Transmission	M
Electrical Connection	L
Fluid Exchange	L
Communication	L
Tolerance to Misalignment	L
Soft Docking	L
Thermal Compatibility	L
Undocking Protection	M
Protection from S. E.	M
Mission Flexibility	L

TABLE 3.5: Simplicity requirements conflict

Requirement	Conflict
Androgyny	H
Rotational symmetry	M
Mechanical Transmission	M
Electrical Connection	M
Fluid Exchange	H
Communication	M
Tolerance to Misalignment	L
Soft Docking	H
Thermal Compatibility	L
Undocking Protection	H
Protection from S. E.	M
Mission Flexibility	H

3.3 Alternative solutions definition & trade-off

In this section the requirement analysis evolved in three baseline configurations. For each one a preliminary design is presented; between them, only one solution was selected for development, manufacturing and test.

3.3.1 First class solution

This mechanism was directly inspired to Syromyatnikov's APAS series [24] and presents a three petals structure with an external soft docking ring, as visible in figure 3.4. The petals shape was designed to reduce the contact forces and to self-align the interfaces during docking. The external ring was provided of electromagnets to create an attractive force and realize the soft docking active joint. A cam, black in figure, actuated by an

electrical motor, was designed to rotate after soft docking to fill the grooves into petals base and lock the mechanism. Last, a central body acted as docking interface, that could be designed for refuelling and power transmission. There was no novelty in the concept, that involved standard and proved technologies to small-scale systems.

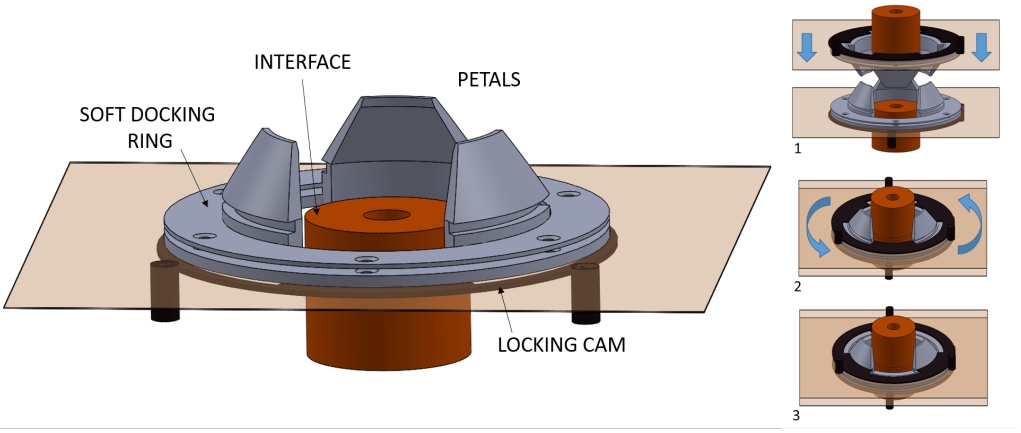

FIGURE 3.4: Androgynous port concept with main components (left) and working principle (right): after soft docking, the locking cams rotates to fit into the other port petals grooves and create the hard lock.

3.3.1.1 Petals concept

A preliminary structural analysis was executed to analyse the petals geometry and chose the material. As visible in figure 3.5, this part is a monolithic structure composed by a mounting ring and the three petals with the locking groove at their basis. This shape allows simpler mounting procedures, reducing the mechanism number of elements. PTFE was firstly chosen as manufacturing material, thanks to its friction reduction properties, and simple static analysis were performed to study its response to the expected loads.

The petals are subjected to three different loads: contact forces, hard docking stresses and thermal deformation conditions. The contact forces (figure 3.6, left) act at the top of the elements and can reach high values for large misalignments (up to 100 N and over, from simulations); on the other hand, the hard docking is created through the loads transmitted to the grooves at the petals basis (figure 3.6, right). Results (figure 3.7) showed that in the first case the equivalent von Mises Stress reaches 70 MPa, far over the PTFE yeld stress (24 Mpa) and in the second case the worst value was of about 21 MPa.

These preliminary results demonstrated that, considering the simplified static simulation settings and an elastic behaviour for the material, the PTFE cannot be used for this application. The thermal analysis (figure 3.8) confirmed that, showing deformations up to 0.5 mm for temperature gradients of 70 K: this could led to interfaces jamming and

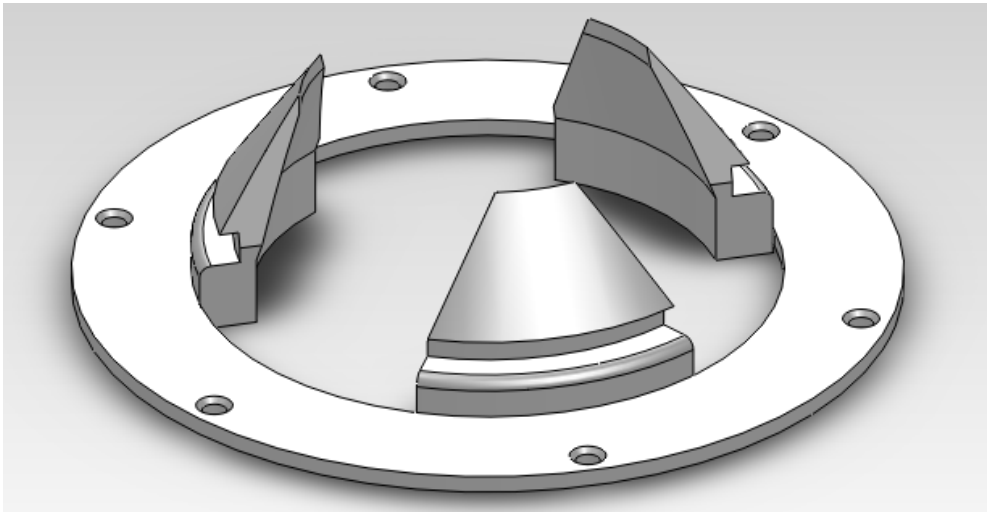

FIGURE 3.5: Petals geometry

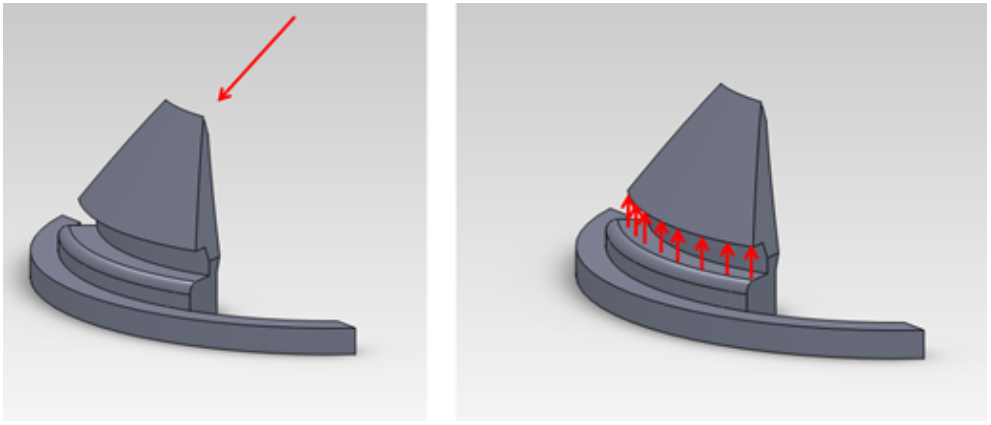

FIGURE 3.6: Contact forces (left) and docking stress (right) acting on the petals

thermal incompatibility during docking.

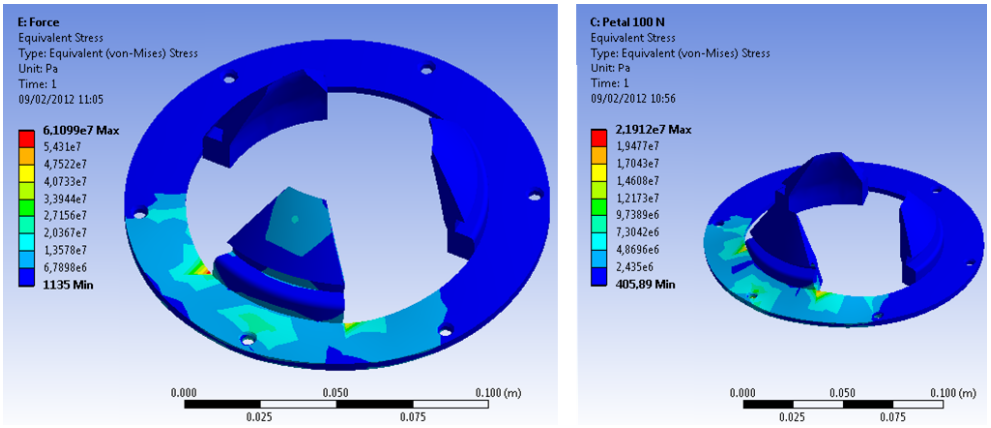

FIGURE 3.7: PTFE: structural analysis results for contact (left) and docking (right)

Repeating the analysis with aluminium petals the results were more interesting, with thermal deformations under 0.1 mm and acceptable stresses.

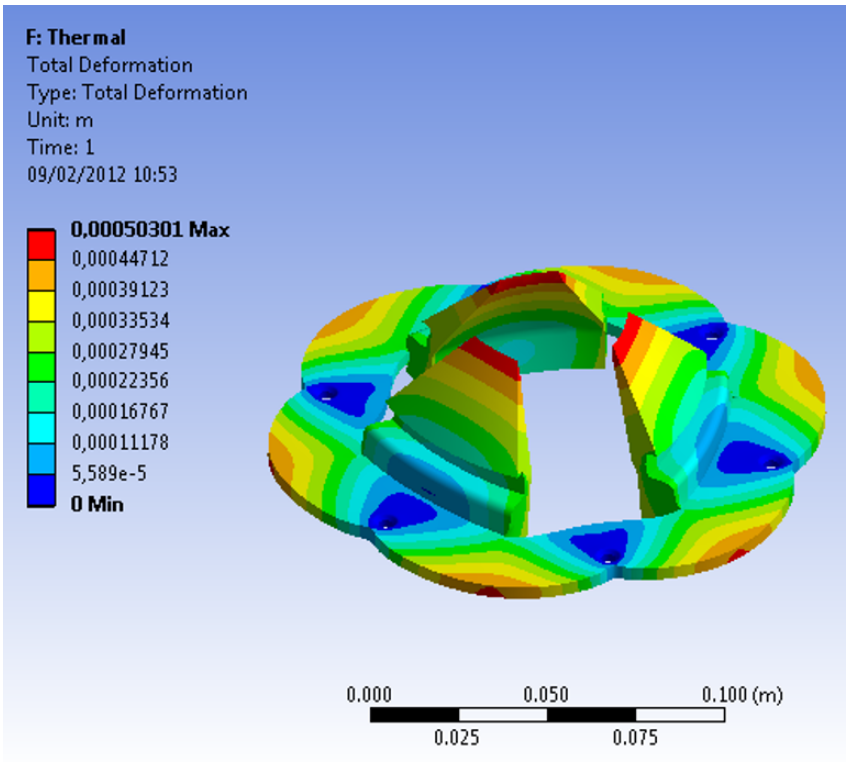

FIGURE 3.8: PTFE: thermal analysis deformations results

3.3.1.2 Concept evaluation

The proposed androgynous mechanism was based on consolidated solutions and it was strictly related to larger interfaces like APAS series. This solution could consequently benefit from the consolidated design aspects reported in documents such the IDSS [2] but also presented some minor disadvantages. First, the interfaces needed electrical power to activate the soft docking electromagnets and the hard docking electric motor, with non-negligible consumption compared to small satellites power budget. Furthermore, the petals could be subjected to high impulsive forces during approach and great stresses at docking, requiring heavy structures, strong materials and damping components, increasing the mechanism mass. A minimum three-axis attitude and navigation control was also required, in order to align the interfaces and reduce the impact-generated forces. In conclusion, for the androgynous interfaces high power consumption and mass budget were the main constraints that limited the design opportunities.

3.3.2 Second class solution

The proposed system [36] had axis-symmetric interfaces with a probe-drogue logic; the target mating interface (drogue) used five identical latches to capture the chaser probe (figure 3.9). The capture mechanism was designed to perform docking manoeuvre demanding only a well-defined chaser approach velocity and to separate using only propulsion abilities. To satisfy this condition, the new-concept latches were totally passive: the energy exchange between the target and the chaser activated and deactivated the locking mechanism, allowing the probe to mate or separate.

The design of the mating interfaces was subject to a number of different factors, from

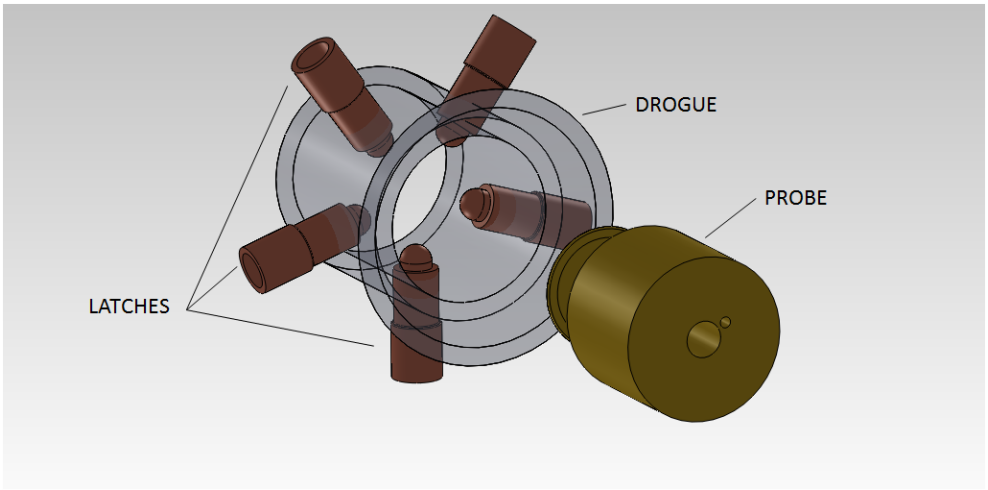

FIGURE 3.9: Axis-symmetric concept with probe-drogue configuration

the dynamics to the mission objectives to the mechanism complexity. In order to simplify the design and to allow the spacecraft to dock with a free DOF (rotation around the probe-drogue axis), the interfaces were not androgynous but presented an axis symmetry. Far from the existing mechanisms, the presented solution did not show powered latches: only propulsion capabilities were needed to perform joining maneuvers. In fact, the locks had bistable behaviour, they could rest in either of two states: "engaged", when they secured the docking ports thanks to a system of five pins, and "off", with pins retracted, not mated interfaces and the probe free to move in the x direction. The probe shape was designed to activate and disengage the latches respectively during docking and separation. The working principle is better explained in figure 3.10: during docking, the chaser probe (red) engages the latches (1) (in blue, only one of five), and the kinetic energy is stored as elastic energy (2) in the locking mechanism springs. When the probe approach velocity goes to zero, the springs lock the chaser in mating condition (3). To undock, an impulse from the chaser propulsion system pushes the latches disengaging the mechanism (4) (5), allowing the probe to slide away (6). After

separation, the mechanism is ready for another docking manoeuvre. It was also considered the issue of unwanted separation due to unexpected external or operative loads, that could deactivate the latches: in the analysis of the mechanism dynamics such topic was better investigated in next sections.

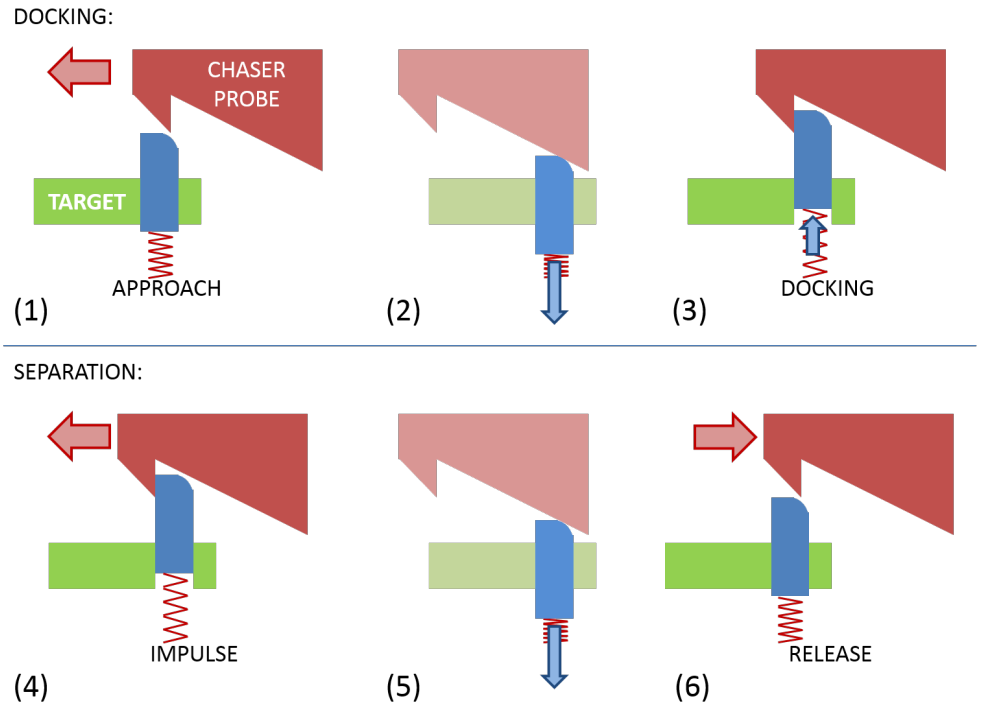

FIGURE 3.10: Mechanism working principle

3.3.2.1 Geometry model & kinematics

The capture system presented a new concept mechanism composed by five latches mounted on the drogue and a groove on the probe. The particular behaviour of the five latches consisted in the capability to remain in one state (active o off) unless actuated by pushing the top up to the activation level. The mechanism was totally passive and used only the movement caused by the probe sliding to block or unlock the target to the chaser. In figure 3.11 the latches geometry model is shown with the mechanism main components: the spring accumulates the energy transmitted from the probe to the sliding element, which is moving into the external shell (ES); the activation and the blockage of the lock are controlled by the different grooves on the ES, the blocking component (BC) and the active cylinder (AC).

The ES (figure 3.12, left) has eight thick prominent grooves (dark blue); the eight spaces between them alternate four thin grooves (light blue) and four empty sectors (white). The AC (right) has eight thin grooves that are able to slide into both the four empty sectors and the four thin grooves of the external shell, forcing the motion only in the

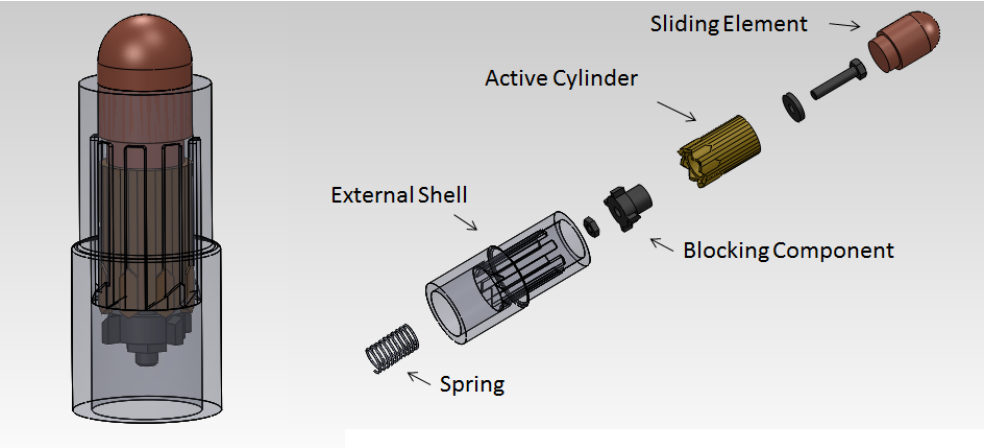

FIGURE 3.11: Latch geometry and components

axial direction. The BC has four thick teeth, allowing sliding only in the empty spaces

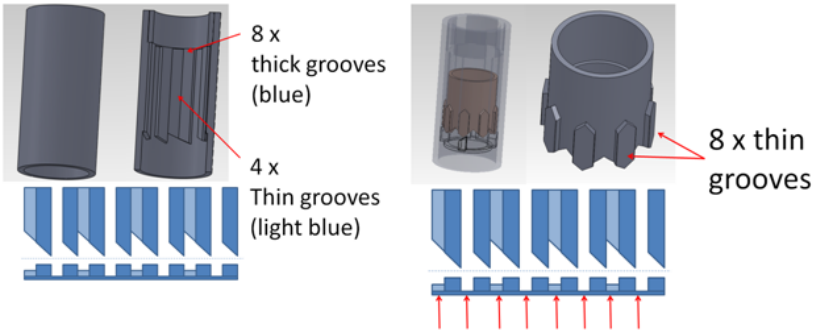

FIGURE 3.12: External Shell (left) and Active Cylinder (right) section and grooves net. In dark blue, thick grooves, in light blue, thin grooves

between the ES grooves. The shape of the upper part of the teeth and the presence of the spring behind the BC force it to contact with both SC and ES: the orientation of BC engages or locks the mechanism. In figure 3.14, the latch working principle is better

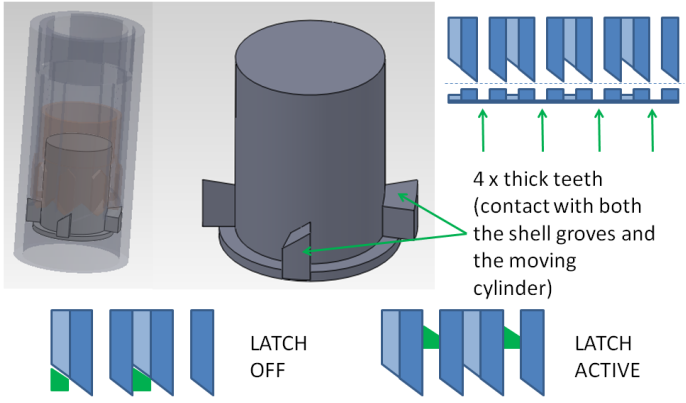

FIGURE 3.13: Blocking Component geometry and possible sliding grooves

shown. When the mechanism is off (A) the spring force acts on the BC (green) but there

is no motion because of the contact with the ES (light blue - thin grooves). The probe contact and sliding causes the AC to move downward (B) pushing the BC until it snap over the thick groove (C). When the probe contact force lowers, the spring force moves up BC and AC to the locking condition (D). The deactivation is similar: the contact

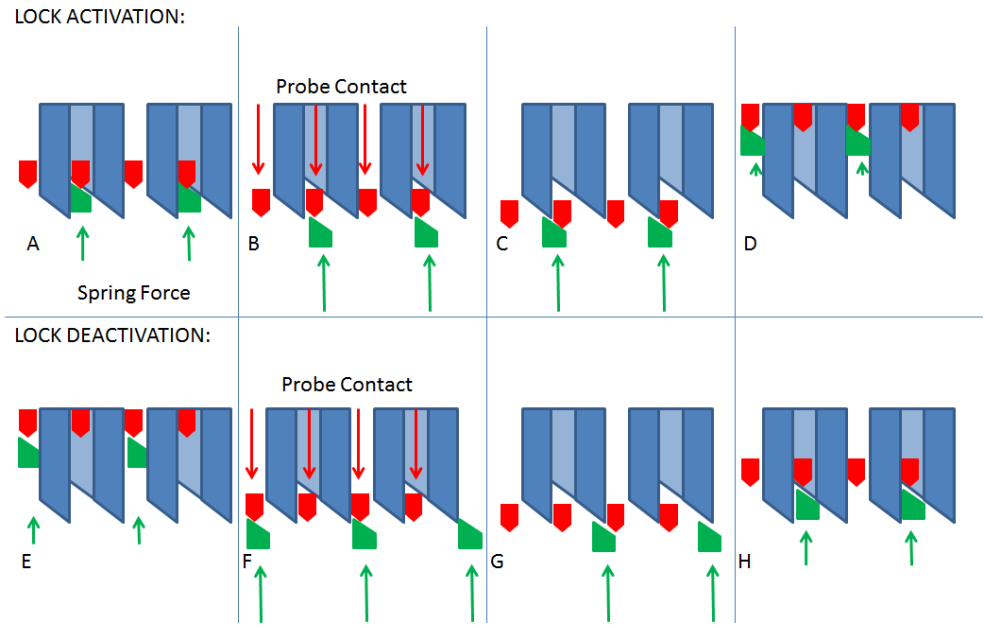

FIGURE 3.14: Latch working principle, in blue ES internal grooves net, in red SC grooves, in green BC teeth. Red arrows represent probe contact force (acting on AC), in green spring reaction (on BC)

force pushes down the AC and the BC until the BC snaps over the ES prominent groove; at the end, the mechanism returns in the initial condition.

3.3.2.2 Analytic model

A simple analytic model (Fig.3.15) was realized to study the energy transmission between probe and mechanism and to define the relations between the latches spring constants and the chaser approach velocity and required propulsion capabilities. As simplifying hypothesis the latches mass is assumed negligible with respect to the chaser mass, and the total energy is assumed constant. The energy equation for docking procedure can be written considering the instants before the first impact (latches off in figure), with the chaser approach velocity v_1, and just after the latches activation (probe velocity equal to zero):

$$\frac{1}{2}mv_1^2 + \frac{1}{2}(5k)\cdot\Delta x_1^2 = \frac{1}{2}(5k)\cdot\Delta x_2^2 \tag{3.4}$$

Another equation can represent the equivalent kinetic energy required to perform separation, that is the energy to reach mechanism maximal deformation and deactivate the

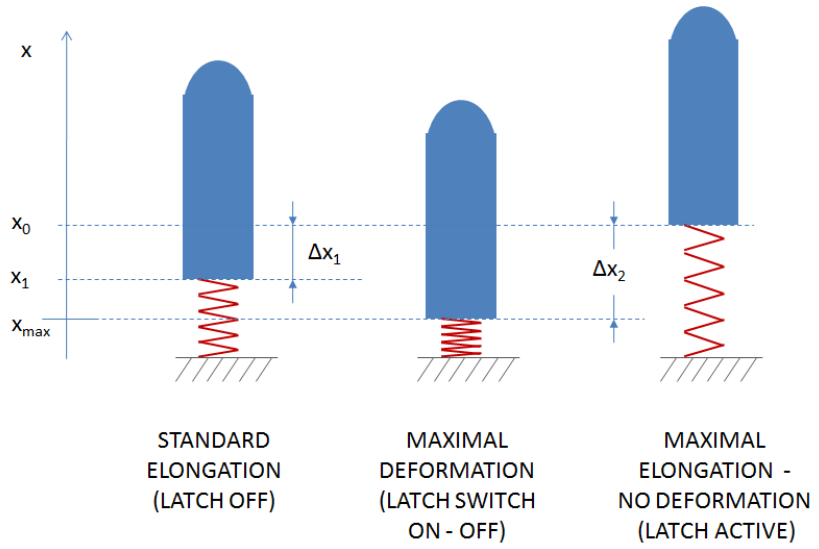

FIGURE 3.15: Latch spring deformation

latches:

$$\frac{1}{2}(5k) \cdot \Delta x_2^2 = \frac{1}{2} m \cdot \Delta v_2^2 \tag{3.5}$$

where Δv_2 is the equivalent change in velocity to undock. Knowing that form the momentum equation the impulse of a force is:

$$I = F \cdot \Delta t = m \cdot \Delta v \tag{3.6}$$

it is possible to calculate the relations between the approach velocity v_1, the spring constant k and the separation impulse I. For a chaser of 50 kg (small satellite-class) and precise values of Δx_1 and Δx_2 (10^{-2} and $1.7 \cdot 10^{-2}$ m, from latches geometry), the results are shown in figure 3.16. In order to maintain the approach velocity under 1 dm/s, a value of 500 N/m for spring constant was chosen. Looking to off-the-shelf components, in terms of geometry and characteristics the most fitting solution is a 410 N/m spring, reporting an approach velocity of 0.09 m/s and a separation impulse of 5.6 Ns. Varying the mass instead of the spring constant, the approach velocity trend can be calculated, showing an inverse proportional relation with the mass (figure 3.17). It must be considered that unpredicted forces with enough magnitude and duration acting in the direction of the docking link could reach the same impulse level, causing an unwanted deactivation of the latches; this could be a great issue to be considered in the mechanism evaluation.

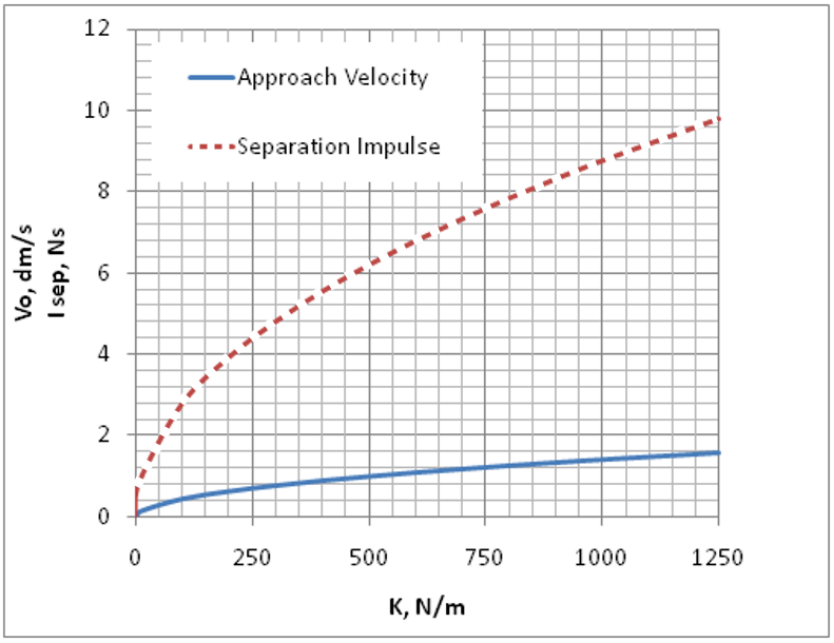

FIGURE 3.16: Analytic model results: approach velocity and separation impulse in function of latch spring stiffness k

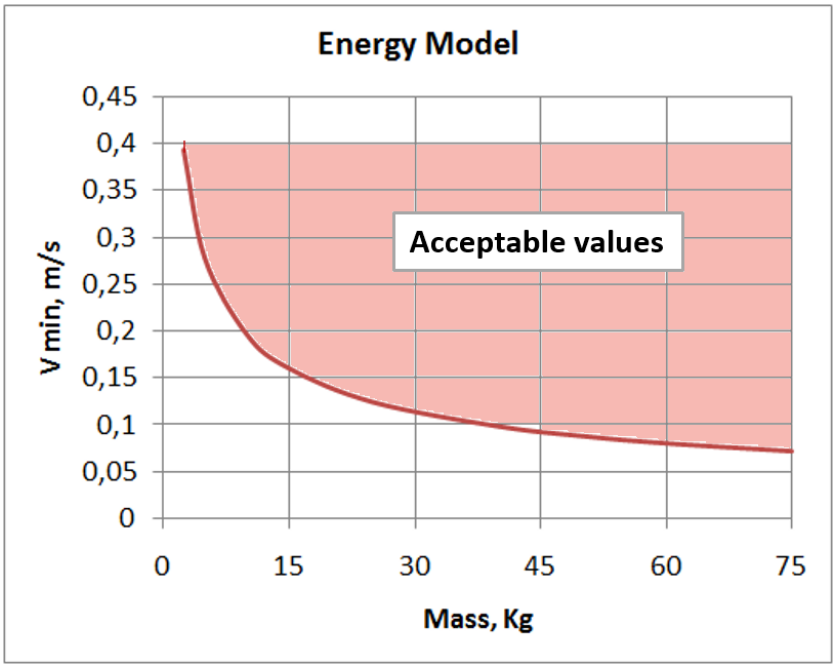

FIGURE 3.17: Energy model: chaser mass and required approach velocity

3.3.2.3 Dynamical model

Preparing and testing different models is an expensive approach during design phase; performing dynamic simulations with engineering software like ADAMS® can reduce development cost and dedicated resources. ADAMS® allows to simulate complex mechanisms and multi-body motion, calculating kinematics and dynamics. The first model consisted in 5 latches mounted on a drogue and in a probe impacting on it; considering the presence of at least five parts per each latch, there would be 27 solids involved in the simulation, with different contacts and constrains. Carrying out long-time numerical simulations on such a great number of components was not useful during this preliminary analysis, so a simplified model was realized to simulate only one latch. As visible

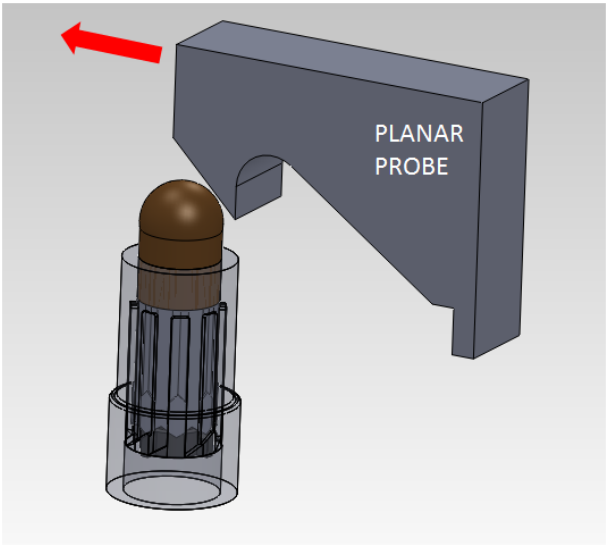

FIGURE 3.18: Simplified planar model with one latch

in figure 3.18, the probe shape was no more conical and the symmetric effect of the other four latches were replaced constraining the probe on a single direction motion. In order to maintain the inertial characteristics of the original model, the chaser mass was reduced to 1/5 of the total. The first simulation analysed the latch (figure 3.19, left) kinematics and compared it with a similar mass-spring model (right) with sliding parts replaced by a cylindrical constraint, to remove all the internal contacts and frictions.
Two identical runs have been processed for the models, to compare the different behaviour of the sliding parts with respect to a monolithic latch: main results are shown in figure 3.20. The initial conditions are 8 kg for chaser mass (equivalent to a total mass of 40 kg) and probe approach velocity of 0.1 m/s.

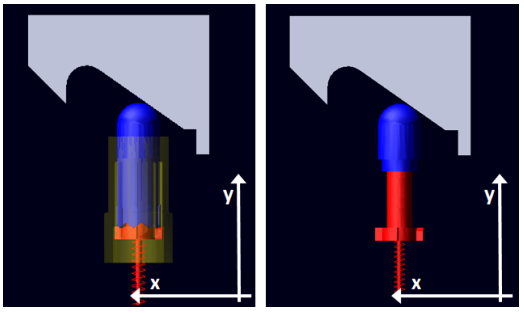

FIGURE 3.19: Simuated latch (left) and simplified mass-spring model (right)

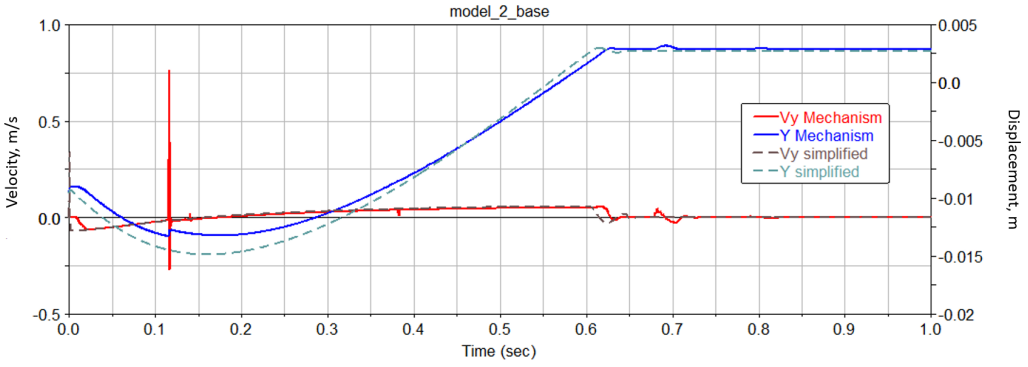

FIGURE 3.20: Single latch and simplified model simulations result

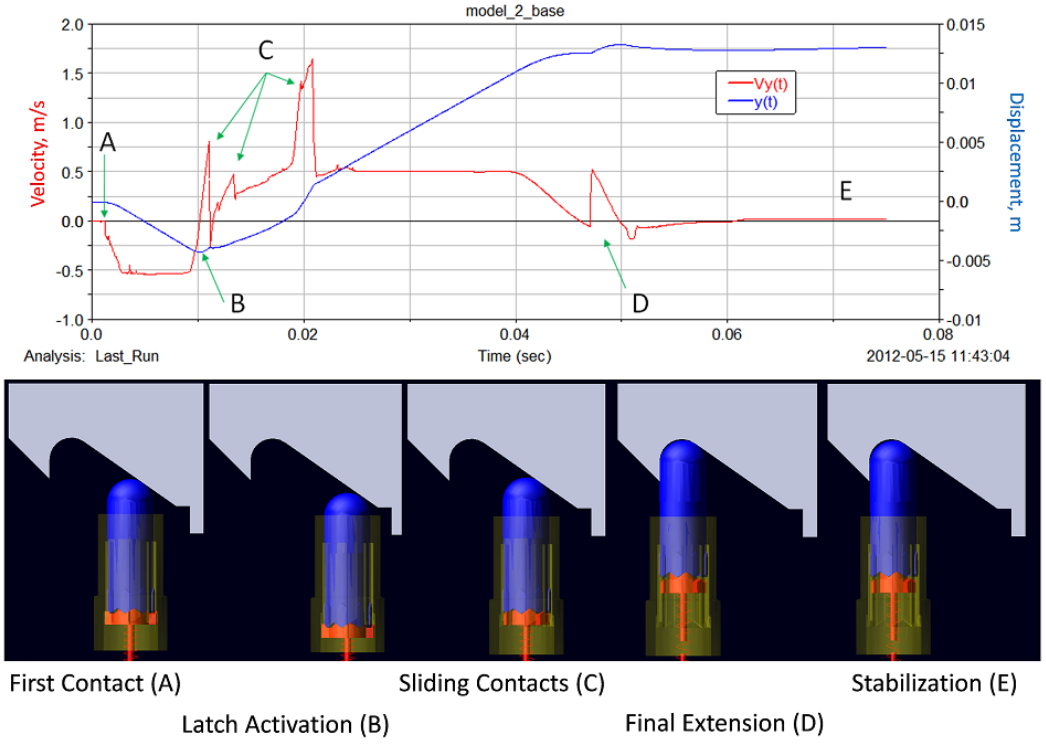

FIGURE 3.21: Impacts effects on latch activation: respect to figure 3.20 the higher energy exchange causes more intense velocity variations

The plot represents the vertical position and speed of the latch respect to an inertial reference frame; the mechanism position curve fits the simplified model really well, the discontinuity at 0.12 s in mechanism data represents only the snap over BC grooves (also visible in the velocities plot – red spike). The plot can be split in three different parts: before 0.15 seconds the latch activation, between 0.15 and 0.6 s the sliding on the probe, and after 0.6 s the stabilization in the locked configuration.
Next simulation analyses the behaviour of the latch mechanism with different initial conditions. In figure 3.21 main results are visible: with an initial velocity of 0.11 m/s, a 10 kg chaser impacts on the mechanism (A) and transfers its kinetic energy to the spring. After latch activation (B), when the probe velocity reaches zero, the spring latch pushes back sliding and bouncing on the probe (C) until it reaches the maximal extension and locks the chaser (D,E). The velocity plot presents some discontinuities directly connected to the contact-impact forces between the probe and the latch. The position data are comparable to previous simulation, and the shape of the velocity graph are similar: due to the higher energy exchange in this second analysis the contact forces cause an higher magnitude of v_y.
Another simulation campaign led to the definition of the minimum approach velocity to activate the latch, varying the chaser mass and the approach directional velocity. The final results have been compared to the analytic energy model (modified for the single latch), as visible in figure 3.22: for mass values higher than 6 kg (equivalent to a chaser of 30 kg) the dynamic model fits very well the energy calculation, with a maximum error of about 15%. Lower masses led to greater errors (up to 40%) probably because of the decays of energy conservation assumption and of hypothesis of negligible latches mass respect to the chaser.

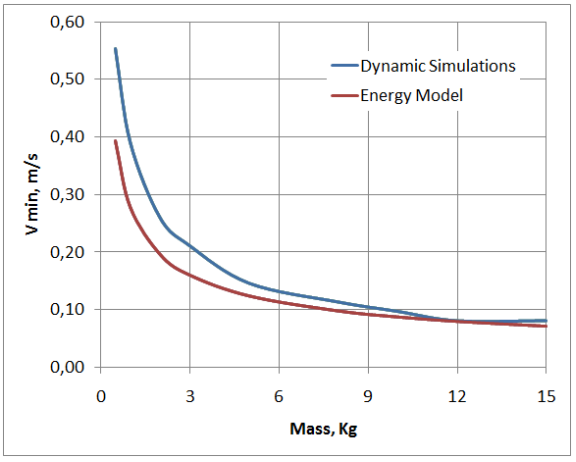

FIGURE 3.22: Comparison between analytic energy model and simulation results

3.3.2.4 Separation dynamics analysis

Separation procedure requires the activation of the chaser propulsion system to create the required impulse. The simplified energy model allows to calculate the value of such impulse, but it does not answer key questions on its magnitude and duration: long impulses would not be able to deactivate the latches due to forces lower than the spring reaction, and would be transmitted to the target. Simulations demonstrates that the impulse length should be shorter than 1 second to avoid this kind of problems.
In figure 3.23 the separation dynamic simulation is presented: results are comparable to the previous docking simulation. Compared to the other plot, velocity gradients are lower, because the probe and the latch are already in contact and slide without separation until the latch reaches its off state; then, the probe can slide away completing the separation phase and the latch is ready for another joining procedure.

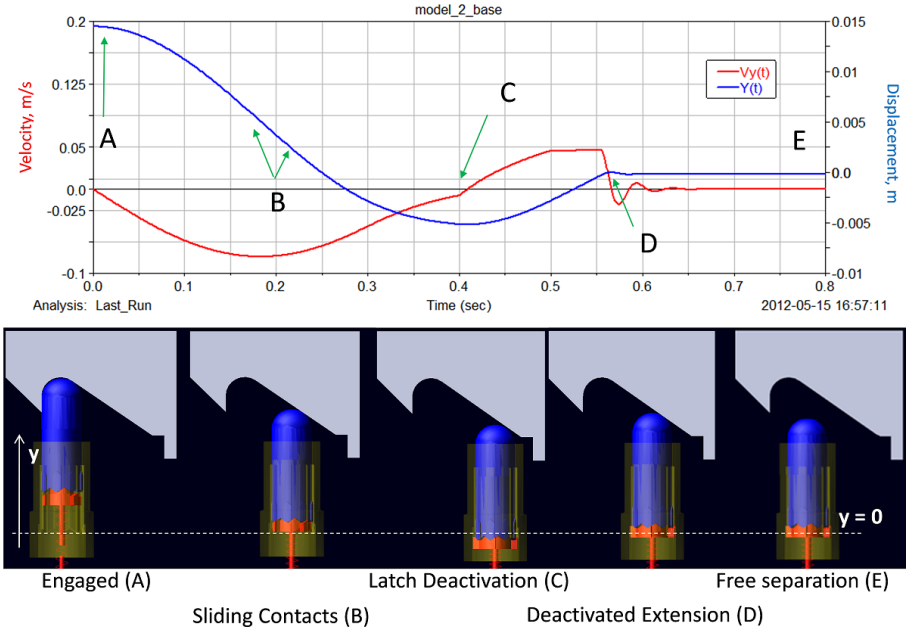

FIGURE 3.23: Separation simulation

3.3.2.5 Interfaces preliminary design and results application

The preliminary design of drogue and probe shape is strictly correlated to the locking mechanism working behavior. To reduce the misalignment between target and chaser and improve locking capabilities, the drogue presents a cylindrical shape with a conical end (next figure). The probe has a conical nose with a deep groove to fit the latches and a cylindrical body to slide into the drogue: in case of translational or angular

misalignments the conical nose would bounce and slip on drogue end, sliding into it and straightening the chaser.
Simulations were carried on to evaluate angular and translation misalignment effects on the mating procedure. The locking mechanism activation requires a chaser axial velocity equal or superior to a well defined threshold value, but bouncing impacts and sliding can reduce the chaser energy and speed. A simple analysis defined the energy loss and estimated the demanded approach velocity to perform mating, straightening the chaser to the target and activating the latches. As visible in table 3.6, small misalignments causes small velocity variations (about 20 % of approach velocity for 2 cm or 5°), but higher values can rise this loss up to the total, with possible damages and docking procedures failure.

All the data collected from the simulations can be applied to find the approach velocities

TABLE 3.6: Velocity losses due to impact

Translation Mis. (cm)	v_{loss}	**Angular Mis. (°)**	v_{loss}
1	9.1	5	23.8
2	21.8	10	88.9
3	40.0		

and impulse required by different mass satellites to activate and deactivate the 5-latches mechanism. For example, a 20 kg satellite would need an approach velocity of about 0.15 m/s, as visible in figure 3.22 (the results were plotted with respect to the single latch mass, so a 4 kg simulation is related to an approaching 20 kg spacecraft), and an impulse of 9.2 Nm; this last value is pretty high for small class satellites, considering that in chapter 2 the propulsion thrust was estimated to be about 1 N for same size satellites, and the separation manoeuvre should be short enough (few seconds or less) to do not transmit excessive loads to the other spacecraft. Another important information is found in figure 3.24, displaying required approach velocities in function of the misalignment between the two spacecraft: small lateral displacements are easily absorbed by the mechanism, but angular misalignments would require high momentum exchange, due to the losses to realign the probe to the drogue that could reach 90 % of the initial velocity for 10 degrees misalignments, due to high impact forces.

3.3.2.6 Concept evaluation

These preliminary analyses indicated the main advantages and drawbacks of a purely passive probe-drogue configuration. The ports are able to dock and separate using only the satellite propulsion capabilities, thanks to a new concept passive latch with no power consumption. The symmetric gender mate configuration allows the satellites to dock with a free DOF (rotation around the probe-drogue axis). Some disadvantages can be

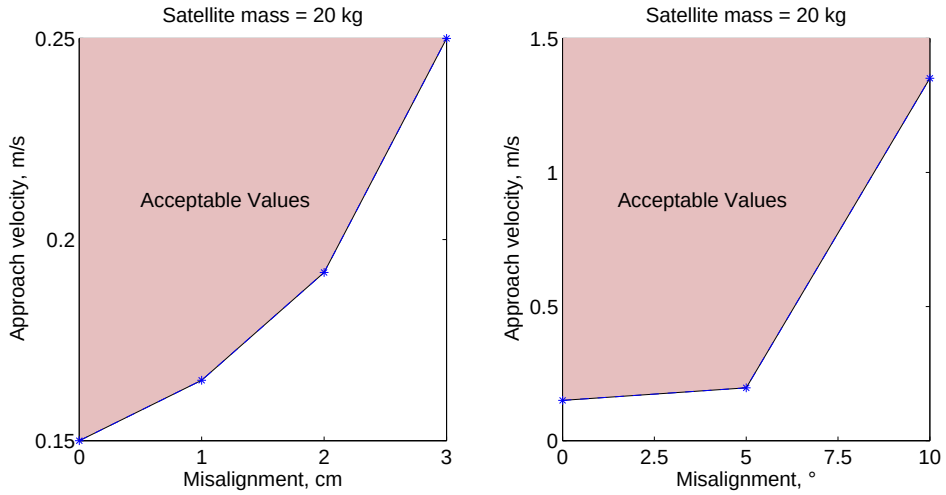

FIGURE 3.24: Required velocities for a misaligned 20 kg approaching satellite: on the left, lateral displacements are easily absorbed by the system, on the right the much more serious effect of angular misalignments

found in the reduced mission flexibility (due to non-androgynous interfaces) and in the complex latches geometry, that may influence the mechanism scalability and reliability. The mechanism main feature, the capability to do not consume electric power, may be the source of its main drawback: well-defined approach velocities and propulsion capabilities can be too stringent for spacecraft and may cause high impact forces and transmitted loads and low misalignment may cause system failures or at least prevent docking.

3.3.3 Third class solution

As introduced in last section, spacecraft with gender-mate interfaces can dock only with other gender ports, reducing mission reconfiguration and flexibility options; differently, androgyny allows mating with every similar interface, increasing the flexibility of the docking system and its possible applications. However, the main advantages of androgynous ports are counterbalanced by the simplicity of probe-drogue configurations both in terms of cost, realization and docking procedures (e.g. misalignment error absorption). Furthermore, another main weakness common to all the cited systems is their dependence on conventional moving parts, such as mechanical latches, electric motors and retractable probes, or other active devices, e.g. electromagnets. The system proposed in this subsection [37] is going to overcome all these limitations by featuring a design which combines the advantages of androgynous mechanisms and the simplicity of the probe-drogue configurations.

3.3.3.1 Docking mechanism concept

The innovative aspect of the solution proposed hereafter is the realization of an androgynous system which does not require any complex mechanism to perform docking. Rather, it employs (1) a special axis-symmetric structure exhibiting a slow-force transition between an undeformed configuration and a buckling state. The transition between the two configurations is made possible by (2) a very simple actuator employing an Electroactive Polymer element. The way these two components are implemented is described in some details in the next sections. This new concept allows several advantages:

- to realize a system universal and symmetrical, that at the same time conjugates the main features of androgynous and probe-drogue architectures;
- to allow docking between any spacecraft provided with this standard interface, regardless of the mechanism orientation about its axis of symmetry, thus increasing the geometries that can be obtained;
- to avoid hard docking active mechanisms such as latches controlled by linear actuators: the security and strength of the joined structure is ensured by its shape and the consequent load on the mating interfaces;
- to ensure low power consumption, low mass and compactness thanks to the EAP actuator;
- to reduce the impulsive loads transmitted upon contact and to lower the mating spacecraft ADCS requirements thanks to the deformable structure intrinsic damping properties;
- finally, the proposed system is easily scalable, and it could be modified for all small-size (micro & nano) satellites, increasing the market opportunities for the product commercialization.

3.3.3.2 Docking mechanism overview

The concept behind the proposed docking mechanism is visible in figure 3.25. The docking interface consists of (1) a cylindrical Central Actuated Body (CAB) with the EAP actuator in its core, supporting the contact plate and (2) a cylindrical passive Grasping and Locking system (GLS) divided in four sectors. The actuation of the CAB results in its translation along the axis of symmetry and allows two configurations for the GLS: "open" during the approach phase, "close" for docking operations and the stowing during the launch. Each petal of the GLS is a special structure that contains a flexible

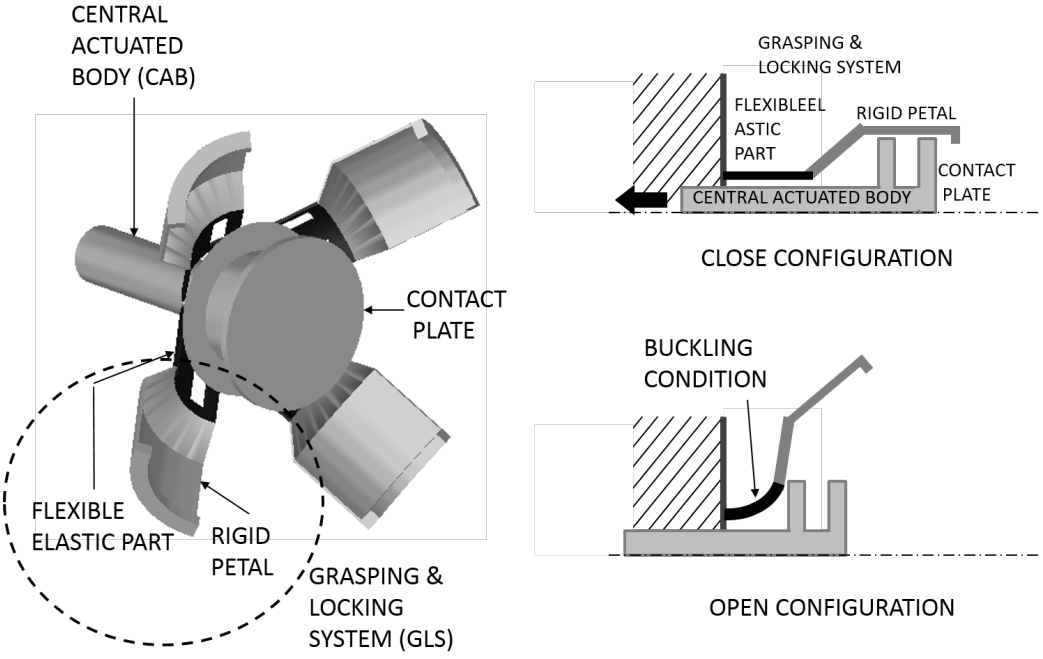

FIGURE 3.25: Docking Port Concept (open configuration, left) and its working principle outline (right)

elastic element (black in Fig. 3.25) to reach high deformation conditions in the open configuration and a stiff part but uses it to lock the ports during docking (light grey in figure).

The high deformation is realized through a snap-through between the undeformed and buckled configuration; the shape of the GLS elastic elements influences the CAB activation force requested for snap-through and the joint stiffness in docked configuration. In close configuration high loads can be transmitted through the port thanks to its working principle: in effect, when the CAB is deactivated, it pushes the other interface contact plate on the rigid petals, engaging them and pre-loading the flexible part (see figure 3.27). In this way, loads are transmitted through the CAB instead of the GLS, and the mechanism can bear loads that otherwise would deform the elastic element. This mechanism therefore allows (1) to change its shape with low actuation forces and (2) to transmit higher loads (up to the actuator limits) in the docked configuration, avoiding unwanted actuations.

3.3.3.3 Docking procedure

As anticipated, the system has two stable configurations, allowing a simple docking and separation procedure. Before mating, the two interfaces are in their stowed condition, as visible in figure 3.26, configuration (1). Once one of the ports CAB is activated, its mechanism starts to open, the GLS reaches the buckling condition (2) and snaps on the

open configuration (3), while the other interface is not actuated and remains in close configuration; when the two ports plates are in contact (4) the first interface CAB is deactivated to close the GLS around the other port contact plate (5). After the grasping phase, the CAB actuator can be switched off, completing the closure around the docked ports. The procedure, as required in modern docking standards, allows to soft dock to another craft and then to create an hard mating. The docking joint present an higher stiffness than the GLS on stowed configuration: thanks to the pushing force the contact plates are creating on each other and on the structure after the CAB deactivation, the GLS is subjected to a tensile stress and is no more able to reach buckling with low load conditions. Separation is similar, with the retraction of the CAB and the return in configuration (3) for another manoeuvre, or in stowed configuration (1). Last, during the whole procedure the axis-symmetry is maintained: the actuated port can close around the other one despite its orientation respect to the docking axis.

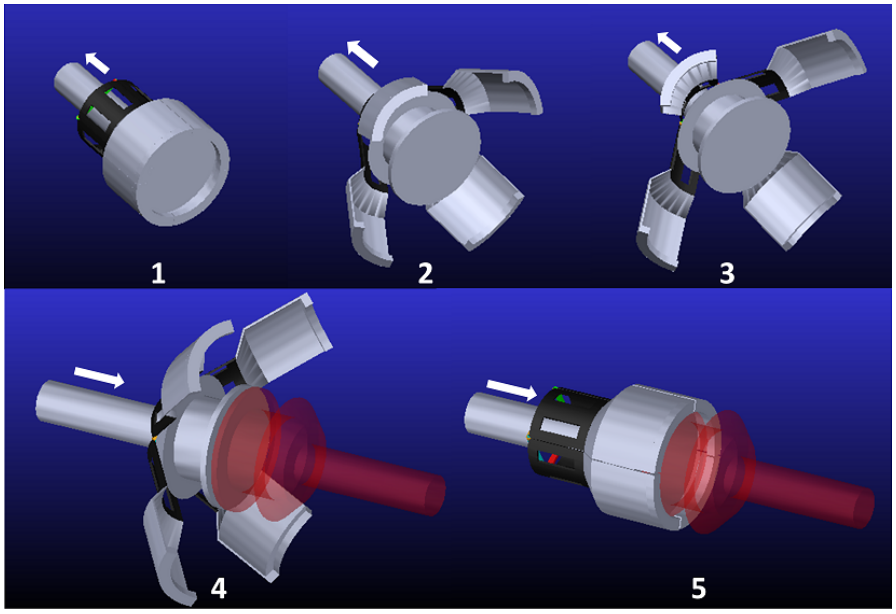

FIGURE 3.26: Docking Procedure with the actuation direction (white arrows)

3.3.3.4 Design and simulations

The docking port is a smart mechanism conjugating new materials and technology solutions with an engineered deformable structure. Actuating and deactivating the CAB makes it possible to change the port shape from a cylindrical object to a contact plate with four petals. The implementation of thin elements leads to high-deformation with small power consumption for the actuation. In this section the mechanism design and preliminary validation through numerical simulations is presented including 3-D modeling, kinematic and dynamic analysis. First, the EAP actuator of the CAB is presented;

then, the port shape shifting capability through the thin elements buckling is reported with the related structural analysis.

Central Actuated Body EAP Actuator As reported, once activated the CAB slides along the axis of symmetry of the docking interface modifying the GLS shape in "open" and "closed" configurations; in stowed configuration, the "closed" shape returns an unloaded state, but during docking the presence of the other port contact plate thickness causes the CAB to have a residual pushing force acting on the GLS, creating a stiffened joint (figure 3.27).

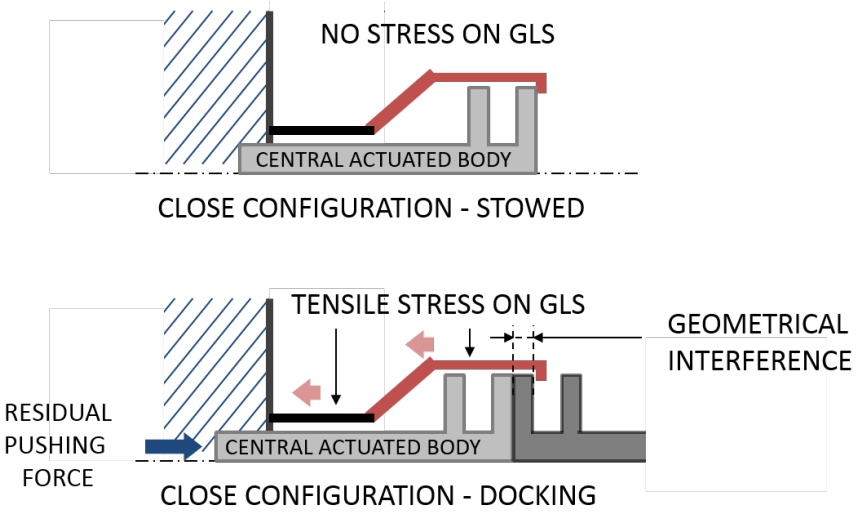

FIGURE 3.27: CAB residual pushing force stiffening the docked configuration: the geometrical interference does not allow the actuator to reach the non-actuated configuration, and a pre-load is created by the equilibrium between the actuator residual force and GLS tensile stress.

The CAB is controlled by an EAP actuator; such technology was chosen because thanks to the structure instability the mechanism actuation requires relatively low forces, that can be provided by electro-active materials. Polymers and composite materials subjected to an electric field can show a change in size or shape: large deformations (up to 300% [60]) can be achieved applying a voltage. EAPs are often referred as artificial muscles and they are widely employed in robotic applications. Active polymers can be classified in two main classes: ionic (driven by ion mobility or diffusion and usually employable only in controlled or wet environments due to out-gassing hazards) and electronic (driven by Coulomb forces). Electronic Active Polymers (EAP) require high activation fields (> 100 V/μm) but can deliver relatively strong mechanical forces with respect to their dimensions and fast displacements without the need of protective coating, allowing an extensive use in hard environments. If an high voltage power supply could be provided, the EAP actuators would gain interest thanks to their small sizes, low consumption and easiness of operation. Linear EAP actuators, realized wrapping polymer layers around

a spring core, have been already studied in various laboratories [61][62], showing forces of about 0.2 N/mm^2 in an experimental set-up, and variable deformations in the range of 10-40% (depending on the actuator length, pre-strain and voltage supply). Thanks to its core spring, switching off the power the actuator returns to its original shape. The implementation of EAPs on the developed port led to a preliminary design of the Central Actuated Body as a single actuator, with its main components acting both as active parts and structural elements. The CAB is composed by two concentric cylinders with the internal one actuated by a roll-spring EAP and able to slide into the external part. The mechanism force can be defined through a careful design of the spring roll element and the cylinders length and diameter.

Grasping and Locking System The Grasping and Locking System (GLS) is composed by four petals (figure 3.25) each one made by one thin elastic element with high deformation capabilities and a rigid part for locking the mechanism in a docking configuration. It can reach large deformations in its open configuration but it has to sustain and transmit the joining state loads; only the utilization of innovative solutions and multiple materials in a special structure can satisfy such design constraints maintaining low masses and power consumption. At today, new concept structures are gaining interest for their advantages in terms of mass and actuation: in space technology they are employed in deployable booms and structures [63][64], thermal louvres [65], solar and drag sails [66]. They can be able to carry mechanical loads, weaken vibration, monitor their status and the environment, or change shape on command, usually thanks to embedded sensors and actuators or smart design and material choices. The GLS design concept is based upon the buckling conditions reached by the thin elastic element under low compression forces, maintaining a relatively high resistance with other load configurations. After the thin elastic element exceeds the critical buckling load, its stiffness dramatically lowers, allowing high deformations without increasing the load. The great advantages of this behaviour are (1) the limitation of the maximal required actuation force and (2) the need of smaller forces to control the return to the undeformed configuration [67]. The design of the GLS followed the logical steps visible in figure 3.28; after the concept definition, a preliminary numerical model of a thin beam was validated with Euler buckling equation, allowing to simulate more complex configurations (thin plates and curved shells) until the definition of the GLS components and their interfacing with the other elements of the docking port.

Euler defined the critical load for a thin beam [68] as:

$$F = \frac{\pi^2 E \cdot I}{(K \cdot L)^2} \tag{3.7}$$

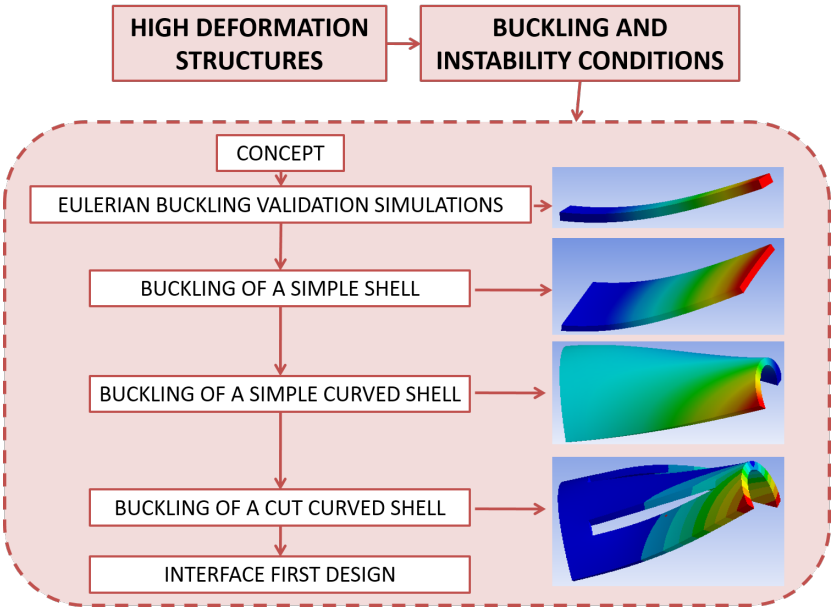

FIGURE 3.28: GLS design logic process

where L is the length of the beam, E the Young modulus and I the minimum momentum of Inertia of the beam section. K represents a coefficient related to the beam support configuration (i.e.: both end fixed, one fixed and one pinned, ...). The comparison between Euler model critical load and the result of the linear buckling numerical simulation in ANSYS® environment pointed out a difference of about 0.5 %. These results validated the method, allowing to use the simulations to calculate more complex geometries (i.e. different form the thin beam) with enough confidence. Varying the model into a square thin plate and then in a curve plate, Euler hypothesis are no more satisfied and the stiffness increase causes the activation of the secondary buckling, usually higher than Euler's on thin beams; knowing the critical load L_p of the planar plate, the buckling force L_c of the equivalent arc configuration can be defined with the equation:

$$L_c = \alpha \cdot L_p \tag{3.8}$$

with α an empirical coefficient related to the different geometry and buckling mechanism, and calculated from the numerical analysis. Results led to the definition of $\alpha = 9.1 \pm 0.1$. The increase of the critical load can be avoided through the reduction of the structure stiffness, without modifying the element arc shape but only with cuttings on the curved shell. With only two small cuttings it is possible to reach values of $\alpha = 6.75$. Main drawback of this method is the stress concentration near the cuts edges, that shall be evaluated to avoid to reach the material yield strength.

At this point, a preliminary element was created and further simulations were realized to develop the geometry (figure 3.29). A new loading condition defined by the presence of a distributed force on the wider face of the inclined part of the model gave a final

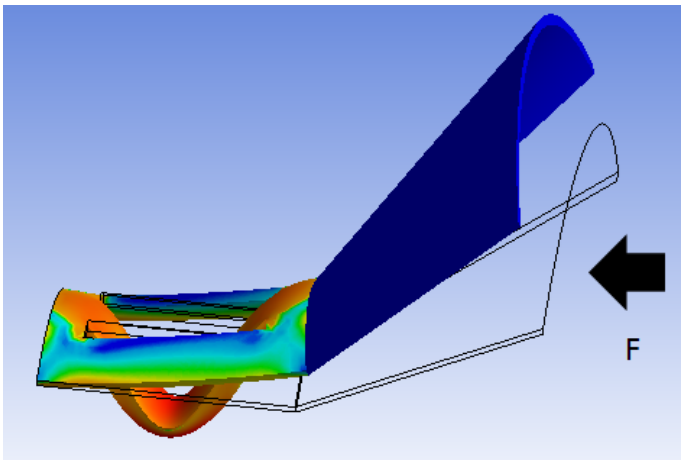

FIGURE 3.29: Elastic element final configuration

value of α=1.13. In figure 3.30 it is visible a comparison between the element linear elastic behaviour and the buckling effect: the critical condition allows a wide range of deformations with a low load. With a simplified simulation, the model showed a critical load of 0.45 N for each element, equivalent to a required actuation load of 1.8 N.

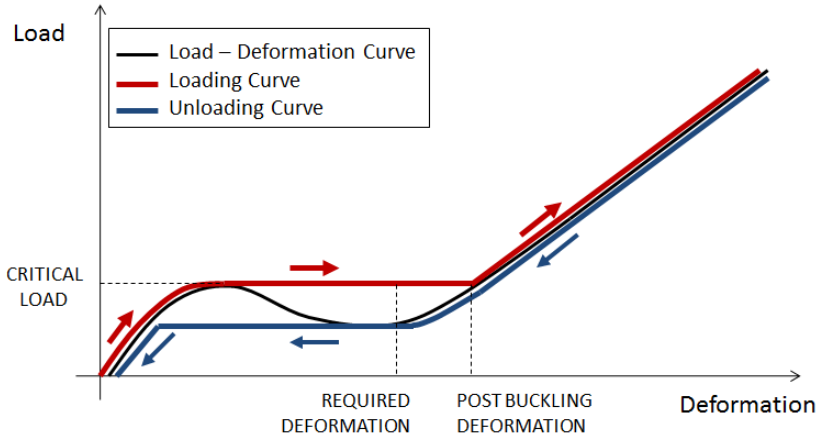

FIGURE 3.30: Force - displacement curves for the linear elastic model and the buckling

3.3.3.5 Concept evaluation

The docking system is designed to combine the advantages of an androgynous system with the simplicity of a gender mating mechanism, using a buckling structure and actuated by a compact ElectroActive Polymer element. Far from the existing interfaces, the presented solution does not employ active latches for hard docking and electric motors for deployment: the internal stiffness and pre-load in the docked configuration creates the solid joint. The proposed docking interfaces show interesting capabilities: this technology could be adopted in different mission profiles: with little or no changes, the

TABLE 3.7: Comparison between the three concepts and requirements conflict; for each solution, Y and N respectively indicate satisfied and non-satisfied requirements

Requirement	Solution 1		Solution 2		Solution 3	
	Conflict	Y/N	Conflict	Y/N	Conflict	Y/N
Androgyny	/	Y	H	N	H	Y
Rotational Symmetry	H	N	/	Y	M	Y
Simplicity	H	N	H	Y	/	Y
Mechanical Transmission	M	Y	M	Y	M	Y
Electrical Connection	M	Y	M	Y	M	Y
Fluid Exchange	M	Y	M	Y	H	Y
Communication	M	Y	M	Y	M	Y
Tolerance to Misalignment	L	Y	L	Y	L	Y
Soft Docking	L	Y	L	N	H	Y
Thermal Compatibility	L	Y	L	Y	L	Y
Undocking Protection	L	Y	L	Y	H	Y
Protection from Space Env.	M	Y	M	Y	M	Y
Mission Flexibility	L	Y	L	N	H	Y

docking system could be scaled and arranged to create modular structures of different sizes.

3.3.4 Solution trade-off

A brief section is dedicated to the comparison between the three concept and to the selection of the most interesting. As visible in table 3.7, at the different conflict levels the three solutions respond with different conditions: if the androgynous concept satisfies all but the two high (in red) requirements and confirms the design process, the symmetric probe-drogue configuration has three non-satisfied cells (one high, two low) and the third mechanism seems to satisfy all the requests.

The constraints table (3.8) also confirms this result: the first concept has great limitations in mass and power consumption and the probe-drogue mechanism shows high impact forces. On the contrary, the third solution can be realized in low weight materials, has a low power consumption and do not imply high impact forces.

In conclusion, solution 3 seems a good compromise between all the requirements and

TABLE 3.8: Constraints table: for each solution, Y and N respectively indicate satisfied and non-satisfied

Constraints	Solution 1	Solution 2	Solution 3
Volume	Y	N	Y
Mass	N	Y	Y
Power Consumption	N	Y	Y
Impacts & Loads	N	N	Y

satisfies all the constraints: the concept was therefore selected as baseline for a complete design, realization and test process.

3.3.4.1 EAP actuator evaluation

As resulted from preliminary analysis, EAP actuators showed relatively low forces with respect to standard components. The considerable realization and application issues related to the EAPs led to choose COTS electric motors, with higher power consumption but less stringent working limits. In case of ulterior investigations, the EAPs actuation (as good as the piezoelectric technology) will be considered, but for the proof of concept of the docking mechanism standard motors were employed. For this reason, the interface preliminary design was modified, to better behave with the actuator.

3.3.5 Selected solution

At the end of this chapter, the solution selected for further investigation is here reported. It is based on the third concept, but employing COTS actuators instead of EAPs. The proposed solution implements an actuating disk able to open and close eight peripheral petals, creating a semi-androgynous port (from now SAM, Semi-Androgynous Mechanism) capable to wrap around a twin one and to capture it. The innovation of the proposed solution is related to its extreme simplicity: the system employs only a linear actuator to perform docking and separation, still conjugating the advantages of an androgynous system with the simplicity of a probe-drogue interface. Chapter 4 will present the detailed design of the docking port, defining the opening-closing mechanism and evaluating its behaviour through numerical simulations.

3.3.5.1 Requirements update for the proof of concept

The requirement table reported in section 3.1 is here presented updated from the outcomes of the previous analysis: table 3.9 list them indicating in the second column if the

TABLE 3.9: Updated requirements table: from left to right, desired requirement name, their state for the proof of concept (Y - yes, to be satisfied, N - no, to be developed/-considered in future) and a quantitative description

Requirement	Y/N	Quantitative description
Androgyny	Y	The mechanism shall always be able to dock with a twin one
Rotational symmetry	Y	The mechanism shall always maintain its rotational symmetry around the docking axis
Simplicity	Y	The mechanism shall use only one actuator
Mechanical transmission	Y	The mechanism shall have the mechanical characteristics defined in chapter 2
Electrical connection	N	Proof of concept - to be developed in future
Fluid exchange	N	Proof of concept - to be developed in future
Communication	N	Proof of concept - to be developed in future
Tolerance to misalignment	Y	Test shall tolerate misalignments of at least 5 degrees and 5 mm
Soft docking	Y	The ports shall be able to realize a complete docking procedure with null residual approach velocity
Thermal compatibility	N	Proof of concept - to be considered in future
Undocking protection	N	Proof of concept - to be considered in future
Protection from space environment	N	Proof of concept - to be considered in future

proof of concept was designed to satisfy them or they were considered for later development and test, and a more quantitative description. Mechanical transmission was related to the constraining values obtained in chapter 2, while the soft docking definition and tolerance to misalignment values were obtained respectively from bibliographic references [25] and from a scaling of tolerate displacements of larger spacecraft mechanisms. The other "frozen" requirements can be divided in "technological" and "environmental", the firsts (mechanical transmission, electrical connection, fluid exchange, communication) that will be satisfy by further technology investigation (and were not considered for the proof of concept), the other three (thermal compatibility, undocking protection, protection from space environment) that are related to the future space application and were partially postponed for the first technology development.

Chapter 4

DETAILED DESIGN

In this chapter, the docking interface detailed design is presented, introducing three different topics: geometric development, dynamic analysis and components manufacturing and procurement.
The proposed solution implements an actuating disk able to open and close eight peripheral petals, creating a semi-androgynous port capable to wrap around a twin one and to capture it. The petals opening mechanism was firstly investigated, comparing two solutions, using respectively a rotational joint and a translational cam; a trade-off between the two solutions indicated that the cam was the more simple and reliable one. On this basis, the whole port is described and its working principle is briefly explained. Dynamical simulations allowed to analyse the port behaviour starting from simple models to evaluate the cams design and adding more complex characteristics to perform more accurate and specific investigations. Results permitted to define the amount of friction acting in the cam mechanisms and its effect on the petals opening and closing process, and then to verify the whole interface actuation, the transmitted loads and, last, a simplified docking procedure.
The calculation of the mechanical characteristics of the mated ports allowed to define the joint stiffness and maximal transmittable loads (i.e. its resistance), and a comparison with simulation results defined the wide safety margins to failure of the mechanism; anyway, a brief analysis of reliability issues, related to the failure of one of the petal cams or of the motor, is introduced and relative actions are described.
Last, most of the interface components were realized with 3D printing, allowing fast prototyping; the linear motors actuating the interfaces were off-the-shelf components, selected for the previous experience acquired on similar actuator employed in ARCADE and ARCADE-R2 docking mechanism.

4.1 Concept evolution

In chapter 3, a preliminary design of the semi-androgynous mechanism (SAM) was proposed, consisting in a four-petals interface able to change its shape in order to open and capture a twin one. The first concept implemented a EAP actuator, that was substituted with a linear motor, considering off-the-shelf components more reliable in this design phase. After this evaluation, some other modifications affected the concept design. First of all, the number of petals had increased from four to eight: some preliminary calculations showed that it easier to close around the non-actuated port with eight petals than with four, thanks to the reduced required opening, as visible in figure 4.1. Calling N the number of petals, and Δ the thickness of the petal normalized by the radius of the petal external circumference, the minimum opening requirement (again normalized by the radius) L is:

$$L = \sqrt{1 - \sin^2 \frac{\pi}{N} \cdot (1 - \Delta)^2} - \cos \frac{\pi}{N} \tag{4.1}$$

With $\Delta = 10\%$ the value of L decreases form 6.4% for 4 petals to 2.7% and 1.5% respectively for six and eight petals.

On these basis, the whole mechanism was redesigned, evaluating different opening actuations instead of the buckling joint. Next section is addressing this issue, in order to introduce the port detailed design.

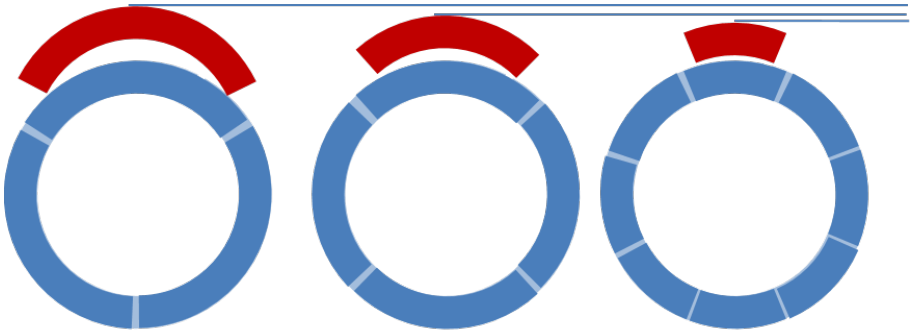

FIGURE 4.1: Petals number and different opening: from left to right, increasing the number of petals the opening actuation is reduced.

4.2 Geometric design

The semi-androgynous port consists in a central body (AD - Actuated Disc), able to slide forward and backward thanks to a linear actuator, opening and closing peripheral petals.

Further investigation was required on the petals opening mechanism: before carry on

with the geometrical design, a comparison between rotative or translational solutions was performed.

4.2.1 Petals opening mechanism trade-off

The docking mechanism petals are actuated by the AD, to open and close as required during the mating manoeuvre. As visible in figure 4.2, the petals-base mechanism could be a rotational joint (allowing the petal to move rotating around a fixed point, left in figure 4.2) or a translational cam (right in figure 4.2), resulting in a pure translation of the petal.

Both the two solutions had their advantages and drawbacks; next sections will address

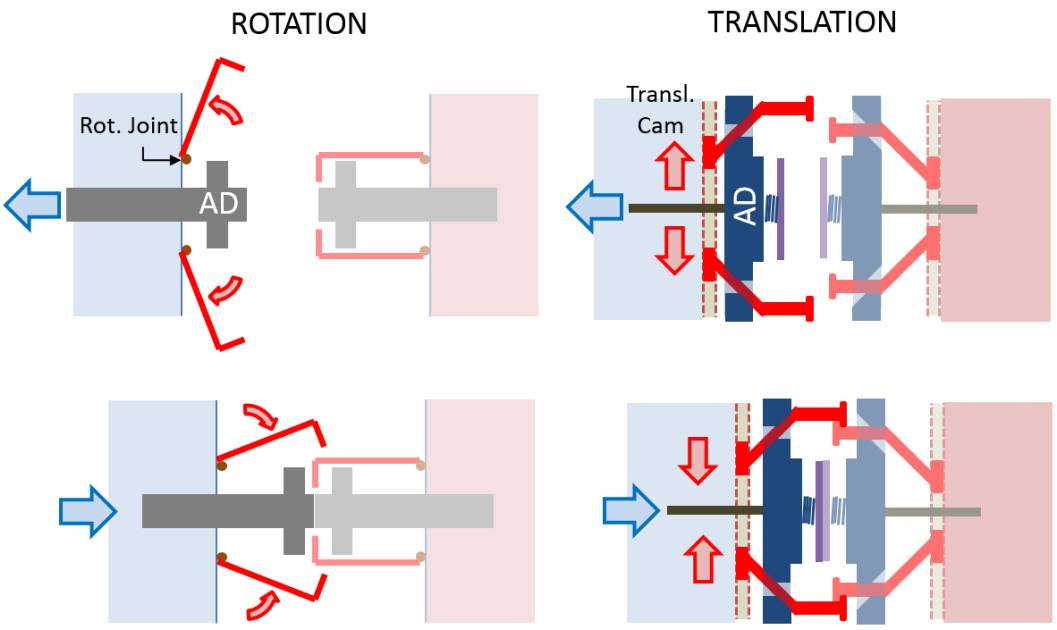

FIGURE 4.2: Comparison between petals opening solutions: both rotational joints (left) or translational cams (right) can be used to allow the actuator (blue arrows) to move the Actuation Disc (AD) to open and close the peripheral petals (red arrows)

them, focusing on technical and manufacturing aspects to determine the best choice.

4.2.1.1 Rotational Joint

In this first case, the petals were designed as visible in figure 4.3, with two hook-shaped parts, in order to wedge into the other interface petals. The preliminary concept was to use a simple rotational joint, on the petal base (orange) to allow the rotation. The opening actuation was given by the AD pushing on the petal internal side, the close one is realized thanks to a rotational spring inserted into the joint.

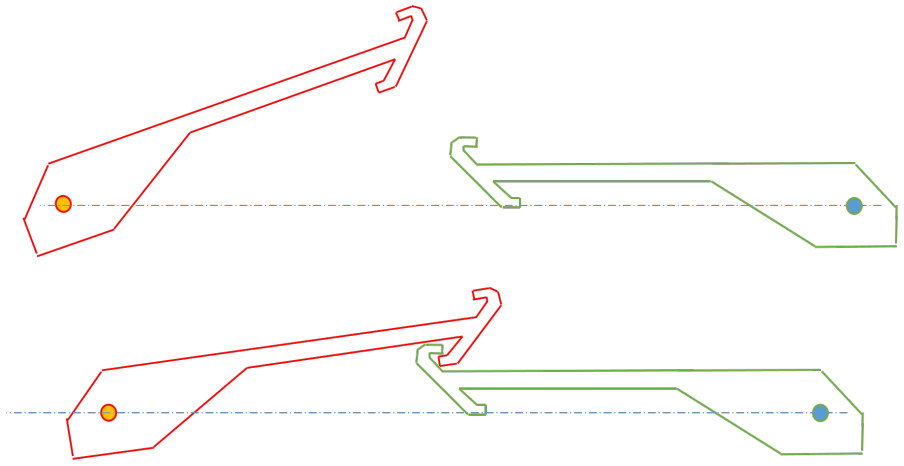

FIGURE 4.3: Petals shape and working principle (first concept): in the open configuration (up) the active interface petal is rotated around a joint, and can wedge into the other interface one (down), thanks to its two-hook shape

This first concept was rejected due to the complexity and vulnerability of a rotational joint; a good compromise was the utilization of an elastic element (EE) connecting the petal to the main structure (4.4), able to deform when pushed by the AD and then to return to its original shape during closure.

The petal shape had to present an optimal sliding shape, with a smooth profile to the

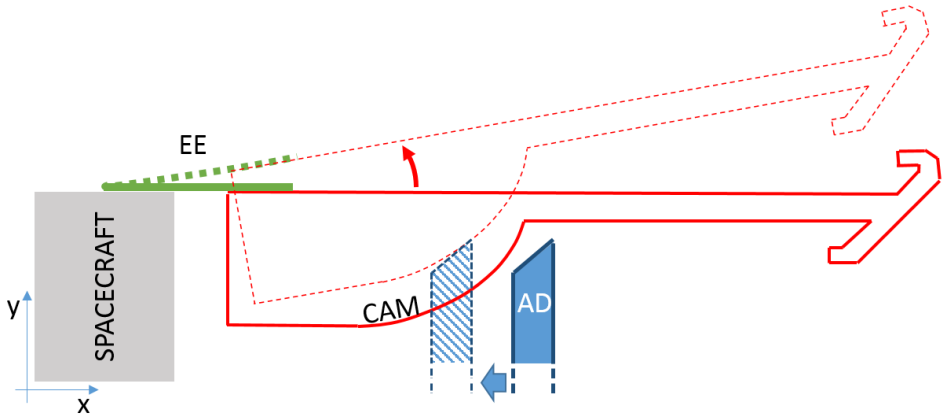

FIGURE 4.4: Petals shape and working principle (second concept): the rotational joint is substituted with an elastic element, deformed by the AD sliding on the petal cam

central actuator (see figure 4.5). The AD was designed in order to slide on the petal with an angle of 45 ° respect to the actuation direction. Starting from this value, the petal cam shape was geometrically calculated as the locus of the points for which during the actuation the tangent is parallel to the AD (i.e. it had the same angle of 45 ° with respect to the actuation direction). The idea was to have the smoothest force profile on the actuator in order to reduce vibrations and possible mechanism damages; this could be reached working on the cam profiles.

The petal shape was then geometrically calculated. As first approximation, the defor-

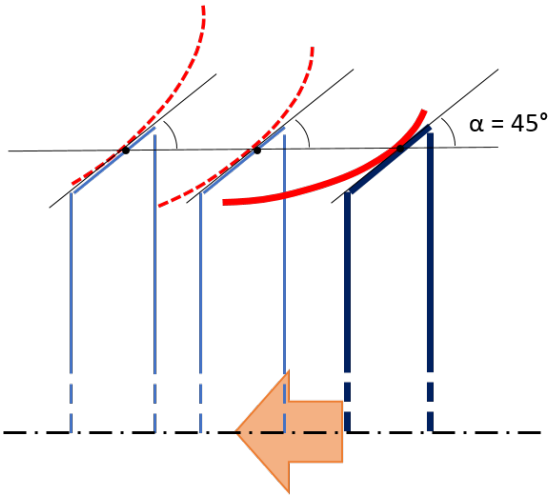

FIGURE 4.5: Cam profile design, the contact point lies on a horizontal line and the contact point angle is always 45 °

mation of the EE followed the theory of thin beams, considering M the bending moment, E the Young modulus and I the beam section moment of inertia (using the reference frame introduced in figure 4.4).

$$M = -E \cdot I \cdot \frac{d^2y}{dx^2} \tag{4.2}$$

Considering that the central actuator created a load on the petal end of the EE, the moment could be rewritten as:

$$M = F \cdot (L - x) \tag{4.3}$$

with L the EE length and x the distance from the EE origin. Solving the differential equation gave the different shapes of the deformed element increasing the load (figure 4.6, left). With large deformations, in first approximation the cubic shape was maintained,

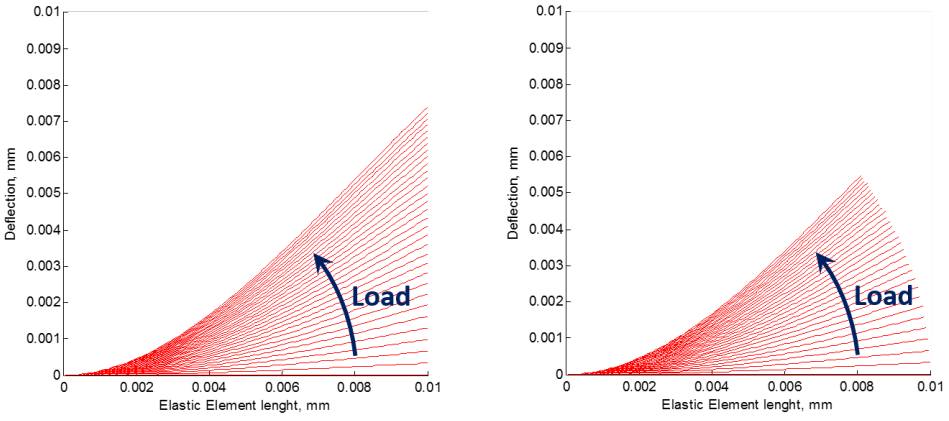

FIGURE 4.6: Deformed EE, classic solution (left) and (right) the same solution with length conservation

but it had to be considered that the length of the EE could not increase, in order to sustain the hypothesis of non-deformability along the x direction; as a good compromise the deformed element length (i.e. the curvilinear) was considered equal to the non-deformed length (figure, right 4.6). The calculation of the different curves was based on the resolution of the original differential equation:

$$\ddot{y}(x) = \frac{\delta^2 y}{\delta x^2} = -\frac{M}{E \cdot I} = -\frac{F}{E \cdot I} \cdot (x_L - x) = const \cdot (x - x_L) \tag{4.4}$$

with x_L the value such that the cubic arc length l was equal to the non-deformed length:

$$l = \int_0^{x_L} \sqrt{1 + (\frac{dy}{dx})^2} dx \equiv L \tag{4.5}$$

The solved equation was in the form:

$$y(x) = \frac{const}{6}(x^3 - 3x^2 x_L) = \frac{F}{6 \cdot E \cdot I}(x^3 - 3x^2 x_L) \tag{4.6}$$

Similar, the deflection orientation of the section x was in the form:

$$\dot{y}(x) = \frac{const}{2}(x^2 - 2x \cdot x_L) = \frac{F}{2 \cdot E \cdot I}(x^2 - 2x \cdot x_L) \tag{4.7}$$

To find the x_L value a numerical integration code was employed, with a "brute-force" small increments evaluation. Over the 500 increments, the relative error integration between lowers to 0.1% for every value of the F/EI ratio, so the solution was considered enough correct (see figure 4.7). Once the deformed shape was defined, the cam was

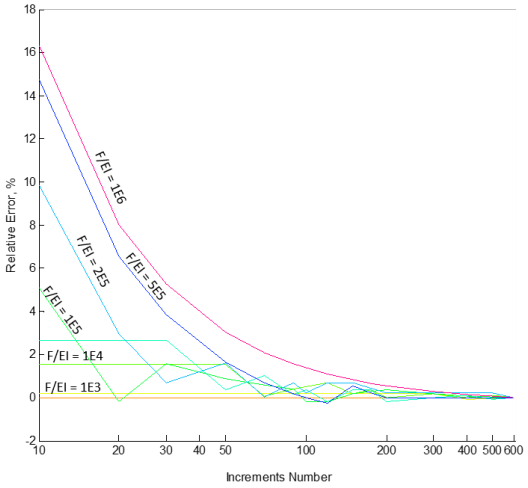

FIGURE 4.7: Integration error reduction at different conditions and increments numbers

designed with the needed characteristics (i.e.: the profile tangent value) and a parametric

curve was extrapolated from the geometry constraints. The equation for each of the contact points in the non-deformed and in the deformed configuration is here reported, considering the geometry entities visible in figure 4.8.

$$\begin{pmatrix} x_{(c,i)} \\ y_{(c,i)} \end{pmatrix} = \begin{pmatrix} x_{(c,i-1)} - d_i \\ [\tan(45\,^\circ - \theta_i) \cdot (x_{(c,i)} - x_{(c,i-1)})] + y_{(c,i)} \end{pmatrix} \tag{4.8}$$

$$\begin{pmatrix} x_{(c_D,i)} \\ y_{(c_D,i)} \end{pmatrix} = \begin{pmatrix} x_{(V,i)} + r_i \cos(\beta_i - \theta_i) \\ y_{(V,i)} + r_i \sin(\beta_i - \theta_i) = h_0 \end{pmatrix} \tag{4.9}$$

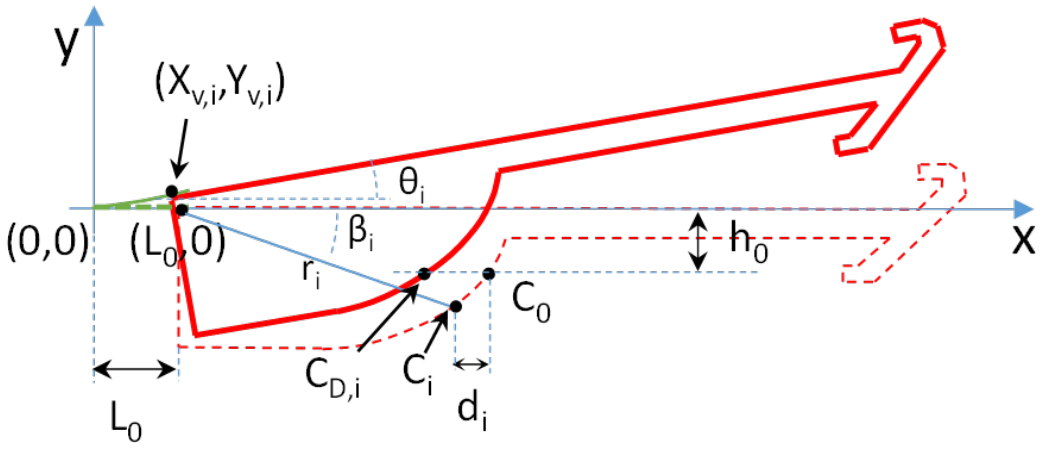

FIGURE 4.8: Geometry entities for the cam points definition

A recursive program calculated the coordinates of the contact points starting from C_0; every step, the calculator hypothesized an increment d_i, calculated the point C coordinates $x_{(c,i)}$ and $y_{(c,i)}$ and evaluates r_i and β_i as they were only function of $x_{(c,i)}$ and $y_{(c,i)}$:

$$\begin{aligned} r_i &= \sqrt{(x_{(c,i)} - L_0)^2 + y_{(c,i)}^2} \\ \beta_i &= \arctan\left(\frac{y_{(c,i)}}{x_{(c,i)} - L_0}\right) \end{aligned} \tag{4.10}$$

Such parameters allowed to calculate the coordinates of the contact point in the deformed configuration $C_{D,i}$: the value of the ordinate $y_{(c_D,i)}$ was compared with h_0, and a new d_i was chosen, repeating the process until the difference $y_{(c_D,i)} - h_0$ was negligible. In table 4.1, the values of the profile contact points were reported; an interpolating curve can be used to create the petal profile, for example a cubic spline, in order to have a profile continuously differentiable to the 2$^{\text{nd}}$ order that should avoid impulsive force transmissions during actuation.

Table 4.1: Calculated profile points

Point Number	X-coordinate	Y-coordinate
C0	0.025000	-0.00400
C1	0.023858	-0.00503
C2	0.022732	-0.00596
C3	0.021626	-0.00677
C4	0.020589	-0.00747
C5	0.019575	-0.00809
C6	0.018632	-0.00861
C7	0.017739	-0.00906
C8	0.016934	-0.00943
C9	0.016184	-0.00974
C10	0.015442	-0.01002
C11	0.014791	-0.01024
C12	0.014187	-0.01043
C13	0.013627	-0.01058
C14	0.013110	-0.01072
C15	0.012632	-0.01083
C16	0.012191	-0.01092
C17	0.011724	-0.01101
C18	0.011349	-0.01107
C19	0.010941	-0.01113
C20	0.010625	-0.01117
C21	0.010269	-0.01121
C22	0.010006	-0.01124
C23	0.009697	-0.01127
C24	0.009410	-0.01129
C25	0.009142	-0.01130
C26	0.008893	-0.01131
C27	0.008663	-0.01132
C28	0.008449	-0.01133
C29	0.008252	-0.01133

4.2.1.2 Translational Cam

The second solution consisted in a linear cam on the petal-base interface, allowing the petal to move radially with respect to the AD actuation direction (figure 4.9); in this case, the opening motion consisted in a perfect translation.

In the preliminary concept, the petal-AD cam presented again a sliding contact at 45 ° respect the actuation direction, and the base-petal cam was orthogonal to it. From this draft, some improvements were implemented, as visible in figure 4.11. The first modification was based on the consideration that in this case the petal did not return to its original position autonomously thanks to an elastic element, so the AD-petal cam had to perform both the opening and closing phases. This could be realized working on the mechanism geometry, in particular on the interface shape, as visible in figure 4.10.

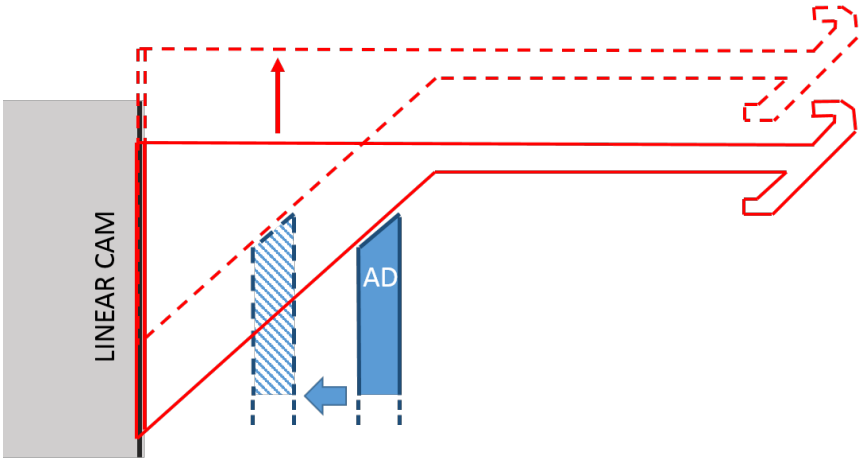

FIGURE 4.9: Linear cam concept

The petal cam section had a rectangular shape (in red) and it was able to slide into the AD, that presented a similar hole; in this way, the AD could push on the petal during every manoeuvre, actuating the structure.

The initial configuration, implementing the two cams respectively at 45 ° and 90 °,

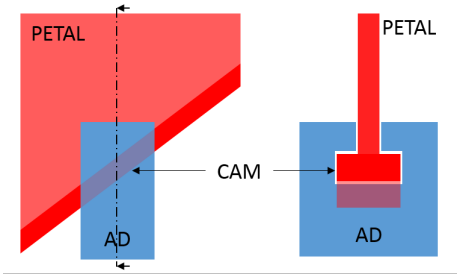

FIGURE 4.10: AD-petal cam particular, lateral view (left) and section (right)

was then modified to reduce the risk of jamming during actuation (figure 4.11, second drawing). In this case, the AD-petal cam showed an inclination of 30 ° respect to the actuation direction, reducing the normal force transmitted to the petal but increasing the actuation length to obtain the same peripheral movement. The base cam was also modified, from an orthogonal direction to 80 °, again to reduce normal forces acting on the petal and improve the sliding. The advantages of this approach were easy to understand: considering the AD acting with a force F on the petal, and defining α and β the aforementioned angles of the AD cam and the base cam, the normal force N_{AD} transmitted to the petal from the AD is:

$$N_{AD} = F \cdot \sin(\alpha) \tag{4.11}$$

and then, the force N_B acting orthogonally on the base cam can be calculated as:

$$N_B = N_{AD} \cdot \sin(\alpha - (90 - \beta)) = F \cdot \sin(\alpha) \cdot \sin(\alpha - (90 - \beta)) \tag{4.12}$$

In the two different configuration, N_B value was respectively $0.5F$ and $0.171F$, with a reduction of about 66 %.

Last modification (figure 4.11, bottom) was the insertion of a flat section on the petal

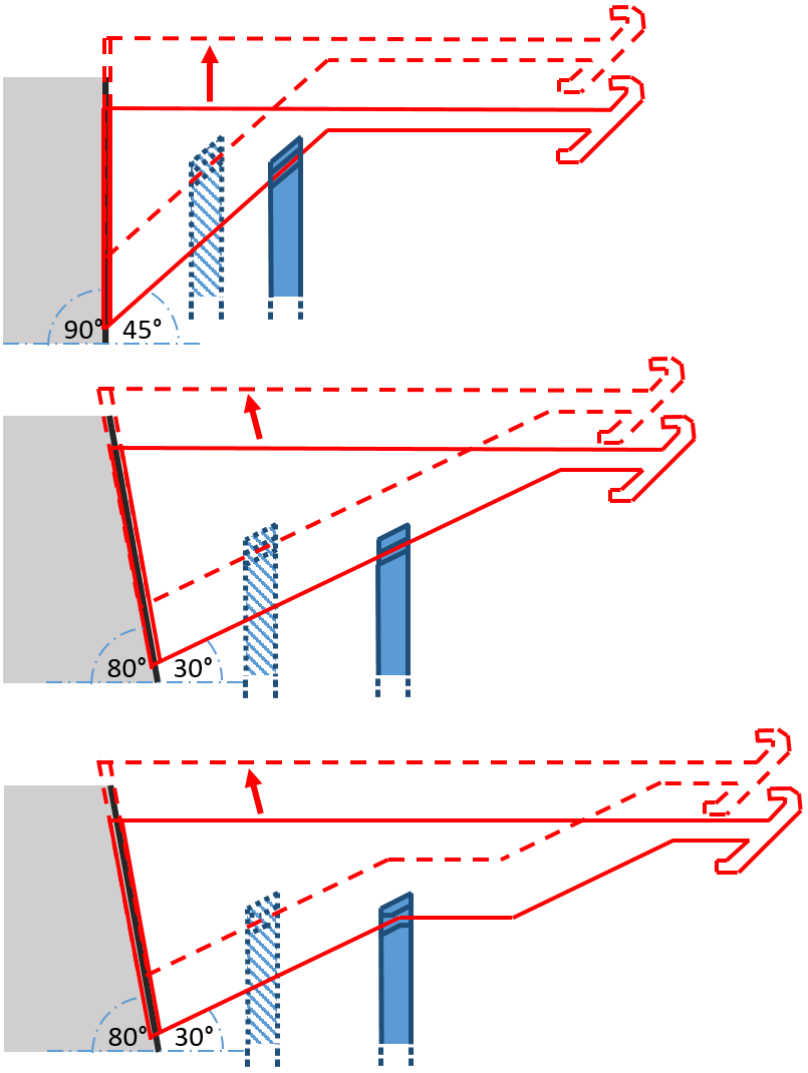

FIGURE 4.11: Concept evolution: from up to down, the simplest petal with the two cams respectively at 45 ° and 90 °, the improvement with inclinations of 30 ° and 80 °, and the final one with the zigzag petal-AD cam

profile, realizing a zigzag cam. In this way, the petal movement could be divided in three different phases: as visible in figure 4.12, the petal moved only when the AD is actuated in the two external sections, and there was no motion as the AD slides in the flat section. This stages actuation could be useful to control the petal closing process, allowing an intermediate stable position in the docking process.

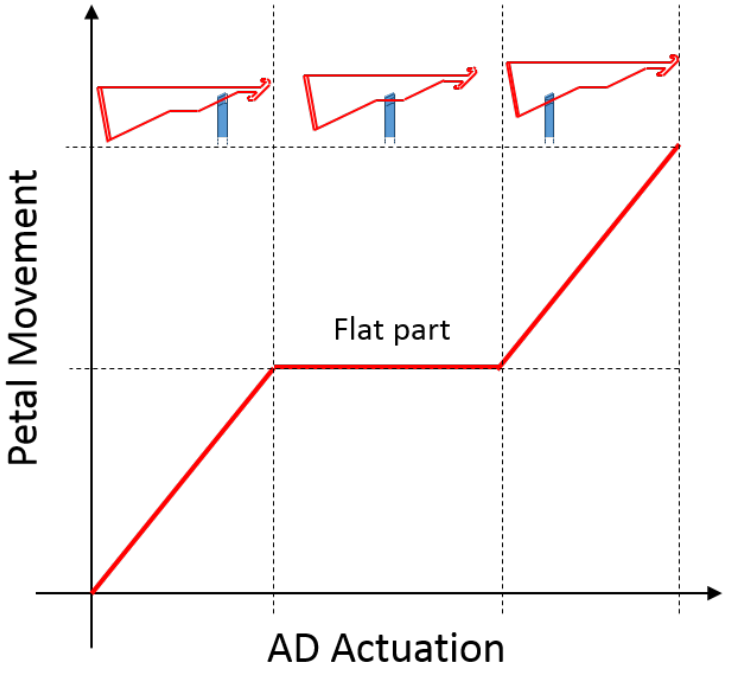

FIGURE 4.12: Different petal movement phases: as the AD moves in the flat section, the petal is not actuated

4.2.1.3 Trade-off

This section compares the two aforementioned solutions, the rotational joint with the elastic element and the base-cam mechanism.

About the first one, the absence of sliding elements on the base interface reduced the friction effects and the jamming risk, with the direct consequence that the required actuation force was directly correlated to the EE stiffness. There were also important drawbacks, first of all the EE design and realization process: the deformable element should have a low bending stiffness to flex when pushed by the AD but at the same time it should be enough rigid to transmit loads in the docking configuration. Another problem was related to the manufacturing of the complex petal profile.

The translational cam avoided all these issues, thanks to an easier geometry and the absence of deformable elements. In this case, the actuation force was correlated only to the friction the two cam mechanisms can create.

In conclusion, the base-cam mechanism seemed to be the easier solution; a brief analysis of its reliability is presented at the end of the chapter.

4.2.2 Final design

After the trade-off between the aforementioned solutions, the base-cam mechanism was chosen and consequentially the whole interface was designed.
The port, visible in figure 4.13, is composed by eight petals, able to open and close to shape-shift the interface between two different configurations. They are mounted on a base structure, where they are able to move radially thanks to a system of linear sliding cams (base cam mechanism); the movement of an actuated disk, which is able to slide back and forth opening and closing the structure, controls their positions (disc cam mechanism).

More accurate mechanical drawings are visible in Appendix C.

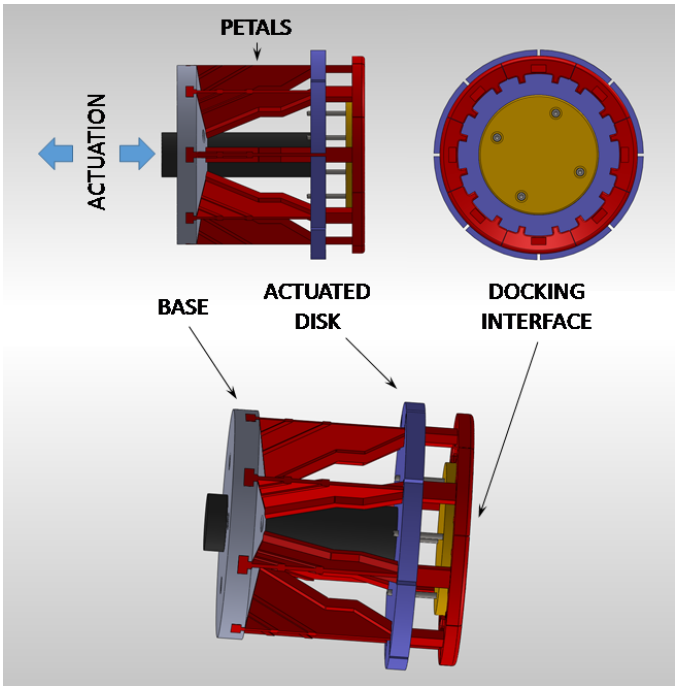

FIGURE 4.13: 3D model of the interface

In figure 4.14 (simplified sketch) it is possible to see the working principle: after the approach phase (A) one of the interfaces shifts its shape to the drogue configuration, in order to receive the other port, through the movement of the blue actuated disk (B). After the opening of the petals (in red) the two mechanisms can move to contact (C) and the movement of the actuated disk closes the left port petals around the right port ones, while the docking interfaces (in yellow) push each other, stiffening the joint with a pre-load (D).

This solution allowed to conjugate the shape shifting and the locking actuations, using only one actuator for both the operations. It is also important to underline that in the docking configuration this interface creates a solid joint depending only by the actuator pushing force: the transmitted loads propagates only in the actuator direction,

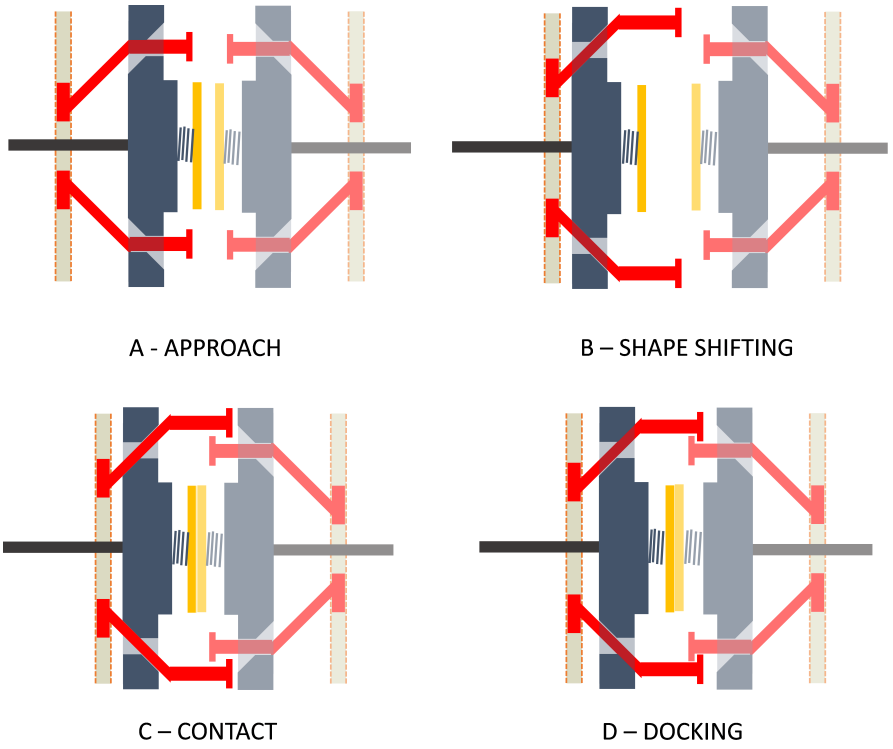

FIGURE 4.14: Simplified model working principle

giving the possibility to use the linear cams instead of elastic components for the shape shifting mechanism. This can be better explained with figure 4.15: axial loads, F_a, are transmitted through the interfaces to the spring system connecting them to the actuated disk and then to the actuator. At the same time, peripheral loads, F_p, are (1) partially transmitted between the interfaces thank to the friction created by the pre-loading and (2) partially unloaded on the petals, and then again through the actuated disk on the actuator.

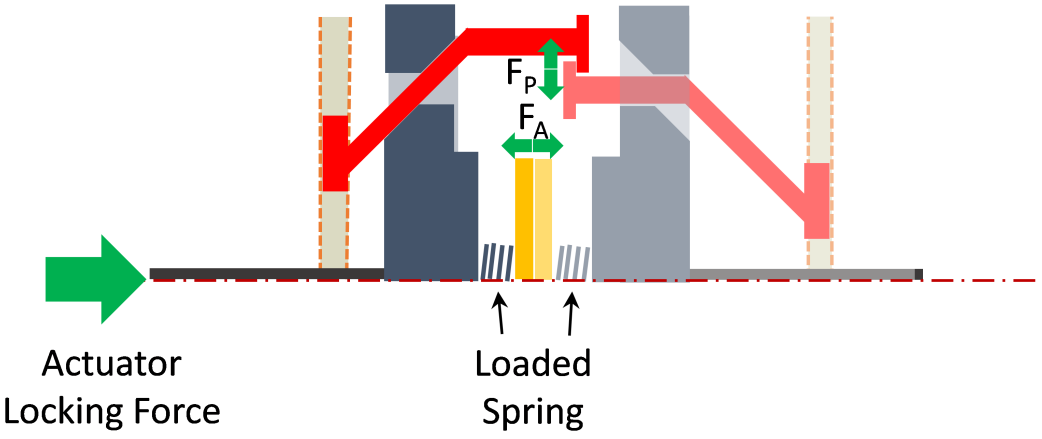

FIGURE 4.15: Axial load transmission stiffens the joint

4.3 Simulations and dynamic verification

This section is dedicated to the docking mechanism dynamical analysis, employing the multi-body dynamics simulation solver ADAMS® by MSC Software Corporation. The study followed a logic path described in figure 4.16, starting from simple models to validate the cams design and adding more complex characteristics to study the interface actuations and, at last, docking procedures. The first model consisted in only $1/8^{th}$ of

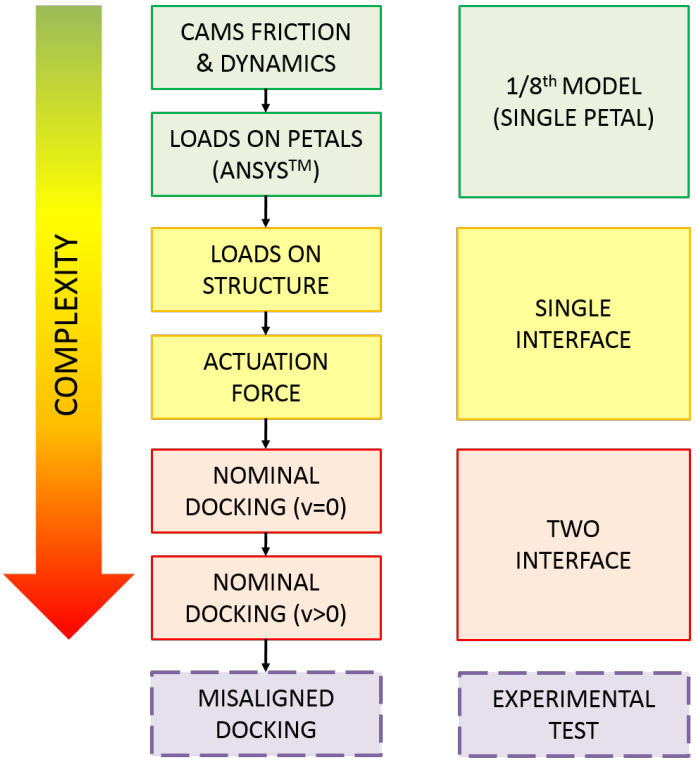

FIGURE 4.16: Logic diagram of the simulations process, starting from a simple model to more complex analysis. The last task, misaligned docking, is performed by test due to its extreme complexity

the whole interface, aiming to monitor the effect of friction on the two cams between the petals and respectively the base and the actuating disk. Data collected was employed to analyse the maximal deformation the petal could be subjected to, and the effect on the shape-shifting performance. A second model studied the whole interface actuation, considering the loads exchange between the port and its mounting structure and the actuation force. The last analysis focused on the simulation of a whole docking procedure in case of nominal alignment between two ports and with two different conditions on the approach velocity. The possibility of simulate the effect of non perfect alignment and the allowable range of angular and lateral misalignments that still allow to successfully perform docking was evaluated; due the model complexity and the necessity to simulate an high number of different misalignment conditions to obtain substantial results, such analysis were directly performed by experimental test.

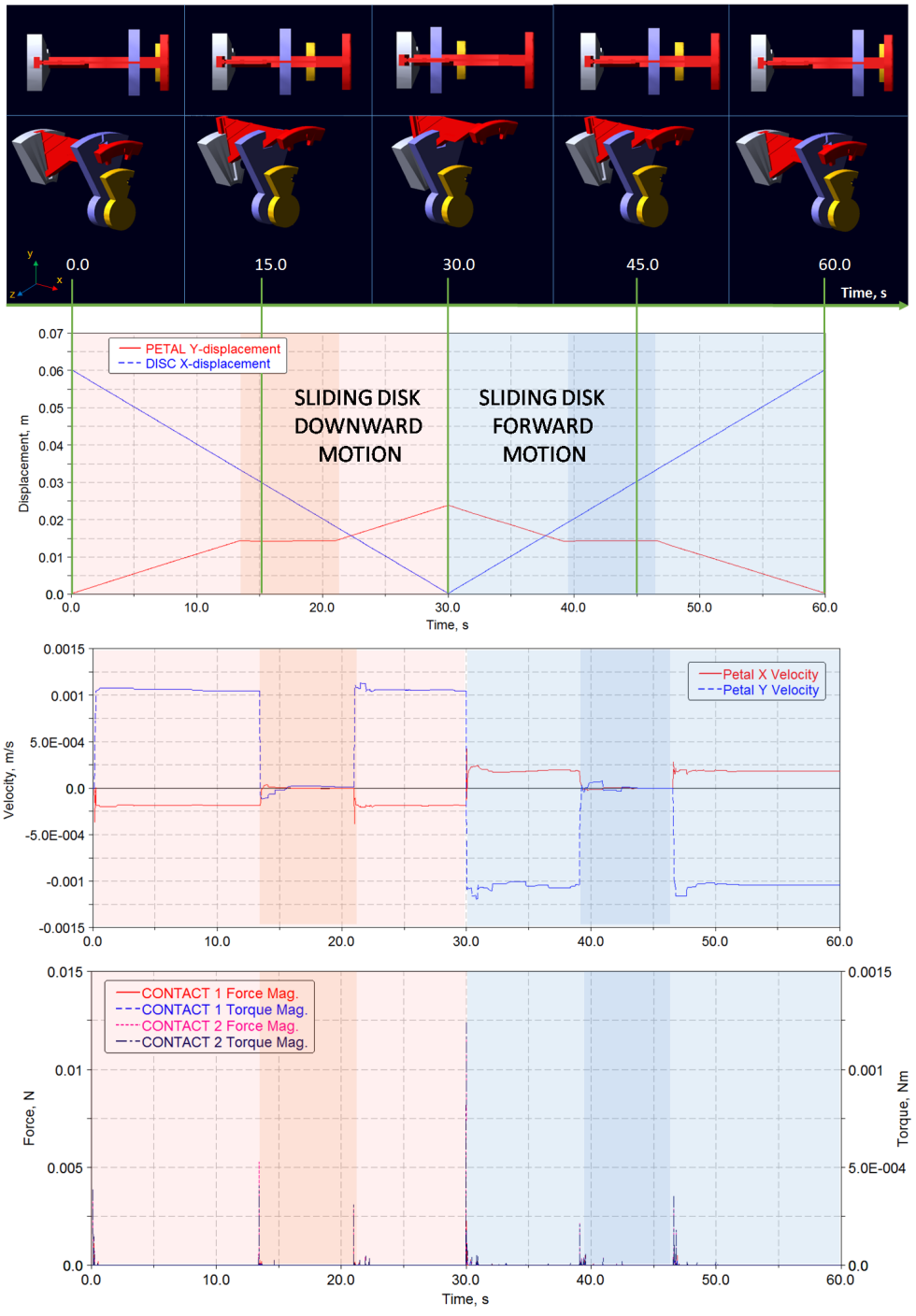

FIGURE 4.18: Analysis results for the cam mechanism: from top to bottom, (1) the representation of the simulated movement, (2) the graph of the imposed disc movement and related petals opening and closing, (3) the velocities plot and (4) the loads graphic. Maximal loads originated by the actuation are located at the same time of major velocities gradients, but are quite negligible in the simulation

4.3.1 Cam mechanism

A preliminary model was implemented with a simplified geometry to study only a wedge of the mechanism as visible in figure 4.17, in order to simplify the preparation and the simulation complexity. The actuated disc was forced at constant speed, opening and closing the petal through the cam mechanism. Two contacts were simulated, between the petal and respectively the disc (actuated disc cam) and the base (base cam), using ADAMS® modified Hertz contact model and static and dynamic friction values respectively of 0.3 and 0.1 for Coulomb friction.

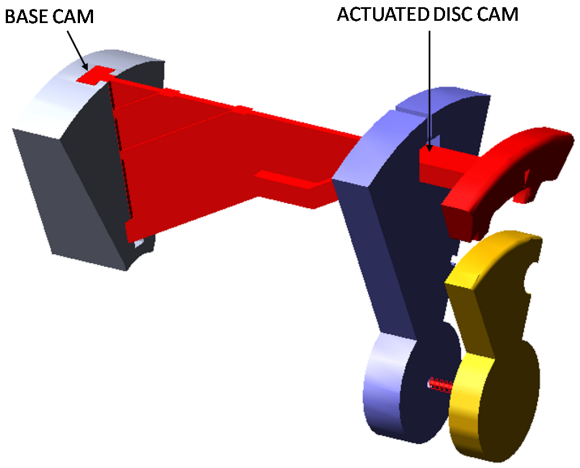

FIGURE 4.17: simplified single-petal model for cam mechanism analysis

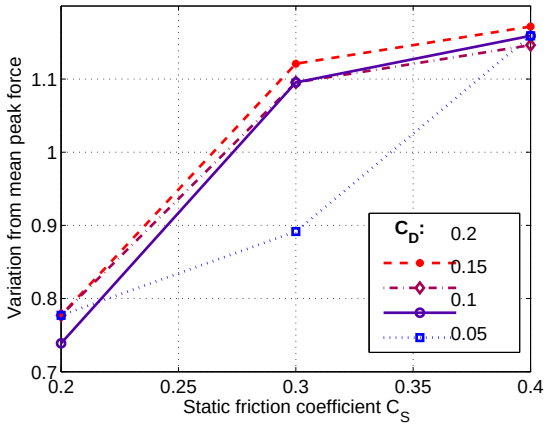

FIGURE 4.19: Effect of friction on simulated peak force: results show the variation respect to peak force due to different friction static and dynamic coefficients C_S (x axis) and C_D (different lines)

The friction values were selected after a simple sensibility analysis, as reported in figure 4.19: a campaign of simulations was performed on the simplified model, applying a constant velocity of 15 mm/s, varying both the dynamic and the static coefficients.

Results were normalized on a mean value, to show the variation of dynamic response due to the different friction. It is visible that small variations of the selected values do not extremely influence the simulation results, with the exception of lower dynamic friction; respect to this particular case, the selected values show an extra-estimation of peak forces of about 15 %.

In figure 4.18, main results are visible: in the first graph the imposed actuated disc

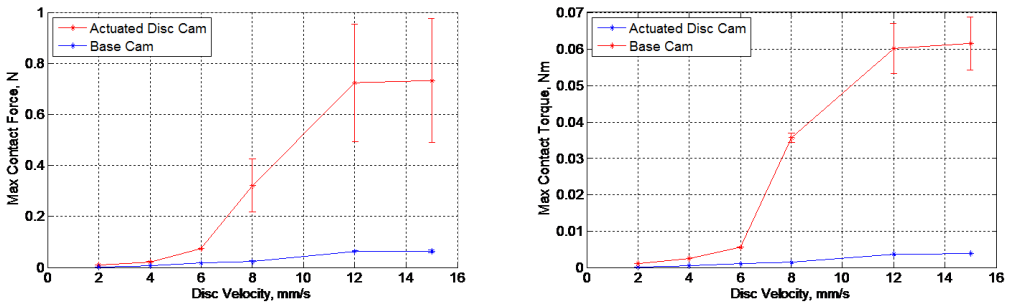

FIGURE 4.20: Maximal contact forces (up) and torques (down) on the disc and the base cams varying actuation velocities. The error band are calculated from the results of multiple simulations, varying the time-steps.

movement is shown, forcing the petals to open and, after 30 seconds, to close, with a constant speed of 2 mm/s. Between 13 and 21 seconds and between 39 and 46 second the petal has an insignificant displacement, due to the disc cam flat part: in the petal velocities graph the X and Y velocity components are negligible in such ranges and the small variations are related to temporary contacts. The base element has a conical shape with an inclination of 10 °, causing the petal to present a X component for the velocity; this solution was chosen in order to reduce possible jamming during the actuation. The maximal loads originated by the actuation are located at the same time of major velocities gradients, but are quite negligible in this simulation; the cams were designed with a play of about 0.1 mm, to reduce every possible slack. In order to better understand the cams dynamics, a campaign of simulations analysed the loads variations at different actuation velocities up to 15 mm/s. Results demonstrated a dependence with the simulations time-steps, with increasing results dispersion for the highest velocities. As visible in figure 4.20, the Base Cam shows the minimum and negligible loads, but for actuation velocities exceeding 10 mm/s the Disc Cam could be subjected to loads up to 0.6 N and 0.05 Nm.

This could significantly influence the petal geometry, causing possible deformations that the simple rigid body simulation cannot consider; in order to avoid jamming, such deformations had to be minor of the cam play. Structural simulations (figure 4.21) of the petal were then performed, with static loads acting on the surfaces of the disc cam, giving a maximal deformation of 0.003 mm with 0.7 N acting at the base of the petal, which was about the 3% of the mechanism play; therefore, it was possible to consider

the petal as a rigid body in all the aforementioned case.

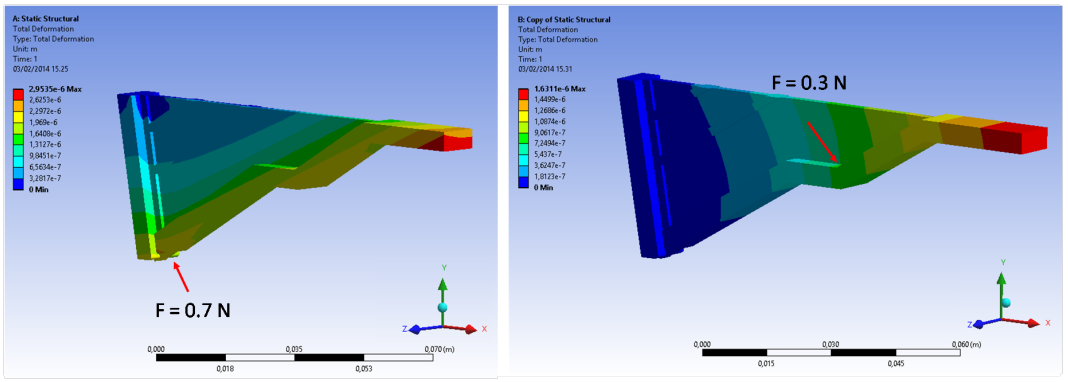

FIGURE 4.21: Petal deformation with the calculated maximal loads acting on the petal-disc cam; the deformations are quite negligible, about the 3% of the designed mechanism play (simulated material: ABS)

4.3.2 Complete mechanism

The simulation was realized to simulate the whole eight-petal mechanism (figure 4.22) and to evaluate the loads transmitted to the structure through the actuation. Considering the base cams as ideal (i.e.: a sliding contact) but applying friction on the central actuated shaft sliding into the base, such loads are usually negligible (less than 10^{-2} N and 10^{-5} Nm), with spikes of about 0.2 N and 2 $\times 10^{-4}$ Nm, as visible in figure 4.23. The

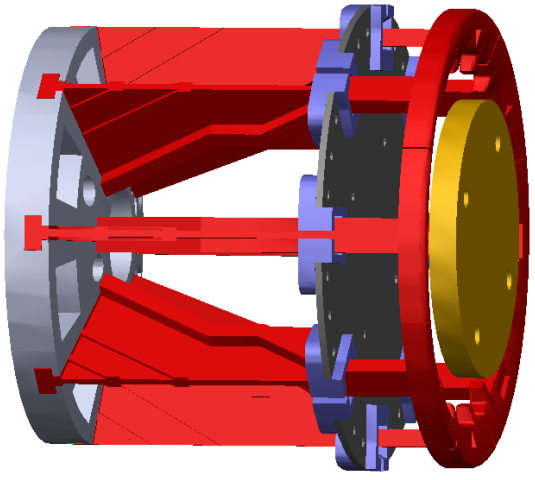

FIGURE 4.22: Complete eight-petals model

results were totally compatible with those collected by the simplified cam mechanism: forces and torques were always quite negligible, with only spikes located at the same time of the major velocities gradients, created by the presence of corners in the petals-disk cams.

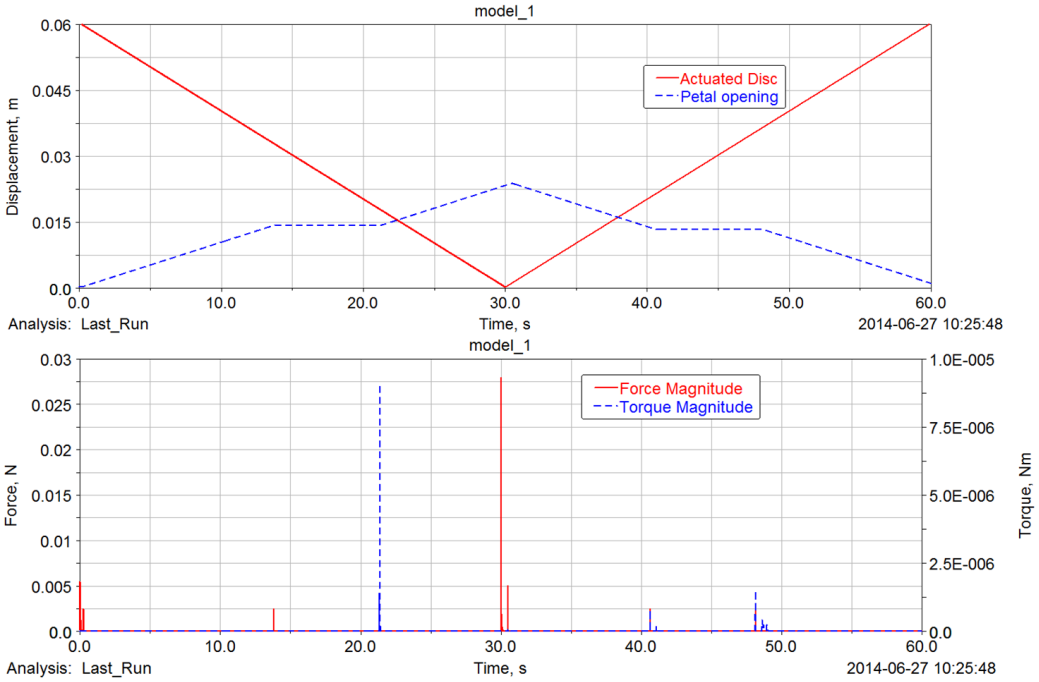

FIGURE 4.23: Analysis results for the whole mechanism: the graph of the imposed disc movement and related petals opening and closing (top), and the loads graphic (bottom). Maximal loads are again located at the same time of major velocities gradients; as for the simplified model, they are quite negligible

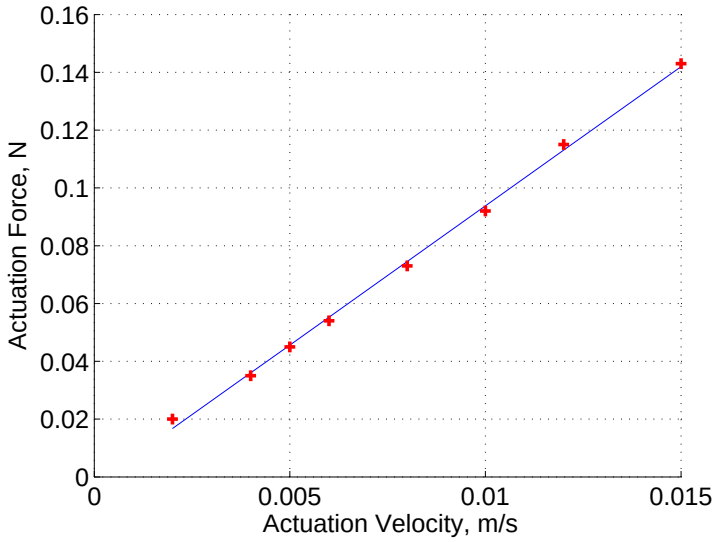

FIGURE 4.24: Required peak actuator force to open and close the complete mechanism

Simulations were performed to define also the maximal force the actuator should generate to open and close the docking interface; such force is directly correlated to cam mechanism friction. Results are visible in figure 4.24: the actuation force, for an opening velocity of 2 mm/s, was about 0.02 N, increasing with a linear trend to 0.1 N at 10 mm/s.

4.3.3 Docking procedure

Last simulation campaign analysed a complete docking procedure, considering the base cam and the actuation ideal (i.e. with negligible friction, as attested by previous simulations). Loads transmitted to the structure were related to the contacts between the two interfaces and show an impulse shape (i.e. duration less than 0.05 s). The docking procedure results are presented in figure 4.25: after the approach phase, the chaser impacted on the target, that closes around it. The target actuation allowed stiffening the joint, loading a spring system up to about 3 N. The preload magnitude depended only from the springs stiffness and the actuator features; future analysis could further investigate on the most performing stiffness to realize an adequate preloading. The simulation was realized with an approach velocity of about 20 mm/s, with a perfect alignment between the two interfaces. Misalignments and different approach velocities simulations would have required further investigation and a long dedicated campaign of simulations; the misalignment conditions were therefore more simply obtained by test.

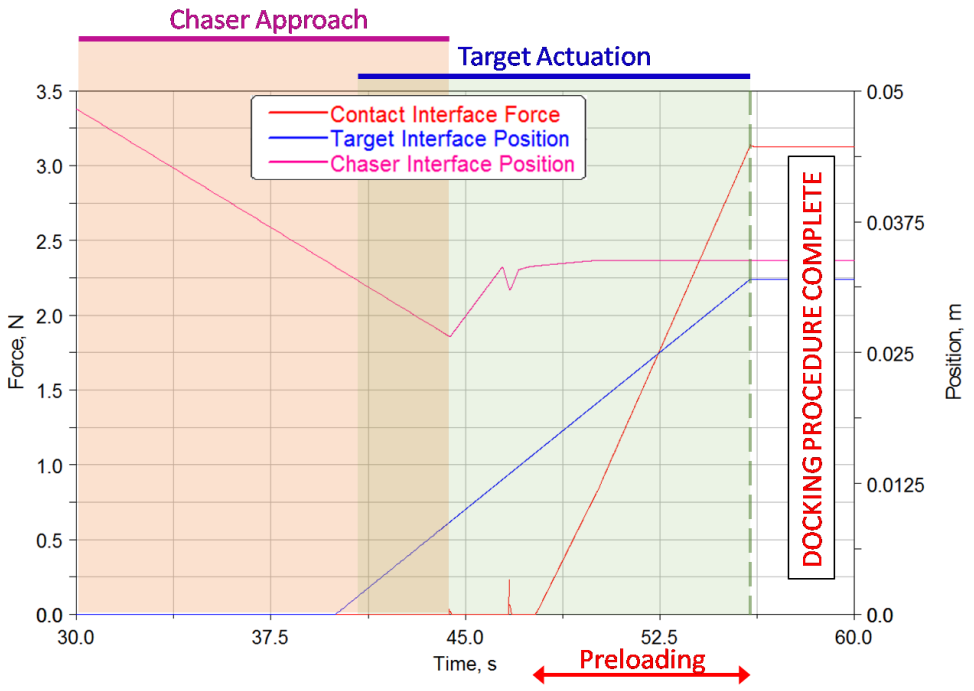

FIGURE 4.25: Docking procedure simulation. The chaser (pink) approaches the target (blue) that is actuated to close around it; after a transient phase (at about the 45th second) the target captures the chaser and creates the solid joint by preloading the spring system.

4.4 Manufacturing and procurement

Most of the components were realized with a Sharebot^{TM} 3D-printer (figure 4.26), through ABS filament extrusion, in order to reduce the machining cost and time maintaining a good surface finish and geometry tolerances. The petals, part of the base and the disk cams were 3D-printed, allowing to produce two interfaces. Different colours were employed (red for the target port and green for the chaser), mostly to improve the identification in case of image analysis.

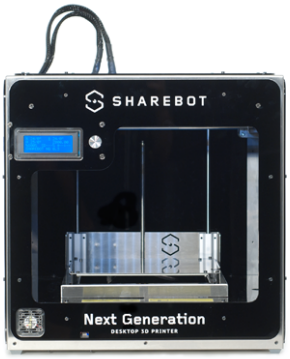

FIGURE 4.26: Sharebot^{TM} 3D-printer

Off-the-shelf linear motors FIRGELLI^{TM} L16-100-63-12-P actuate the interfaces (figure 4.27). They are low-cost accurate actuators, usually employed in biomedicine and robotics; this particular model has a stroke of 100 mm with peak velocity and force respectively of 20 mm/s and 100 N, and position accuracy of 0.4 mm. After a trade-off between different suppliers, FIRGELLI^{TM} was chosen for the cost and the previous experience acquired on a similar actuator employed in ARCADE and ARCADE-R2 docking mechanism.

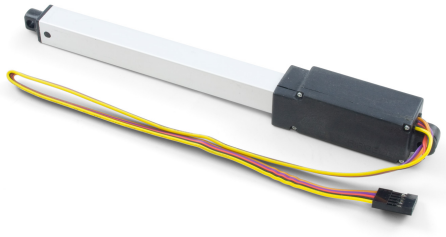

FIGURE 4.27: FIRGELLI^{TM} Actuator

4.5 Joint mechanical characteristics

The definition of the docked mechanism mechanical characteristics is a fundamental information that must satisfy the requirements of mechanical transmission that were defined in the first chapters. Due to the particular geometry of SAM, as visible in 4.15, the resistance and the stiffness of the port are related to both the characteristics of the petals and the docking interface. In the simulations the latter one was considered as a plane plate connected with a spring link to the Actuated Disk, but to determine its behaviour in different load conditions a better description is required.

4.5.1 Docking interface disk spring system

The docking interface disk is connected to the Actuated Disc with four identical spring guides, as visible in figure 4.28, equally spaced respect to the centre of the interface. During the docking procedure, the two plates are in contact, and the petals closing preloads them thanks to a geometrical interference; the amount of such preload is directly proportional to the spring guides stiffness k_S with the relation:

$$F_p = 2 \cdot k_e q \cdot \Delta = 2 \cdot \frac{k_s}{4} \cdot \Delta \tag{4.13}$$

where Δ is the geometrical interference. It is therefore possible to modify the joint mechanical characteristics and this preload, varying the spring guides stiffness; for the simulations and the tests reported in this document, springs with a stiffness of 1300 N/m were employed, with an equivalent stiffness of 650 N/m causing a preload force F_{PR} of 3 N. With this information, the different load case can be introduced.

4.5.2 Case 1: axial compression loads

Axial loads can act as compression or tensile forces: the mechanism response is different due to the preload acting on the docking interfaces. In the first configuration, the force acts against the preload, so two different cases shall be considered. If the compression load is under the preload, the interface stiffness is related to the petals one, as:

$$k_{eq,1} = 2 \cdot \frac{k_{Petal}}{8} \cdot \Delta \tag{4.14}$$

where k_{Petal} is the stiffness of the single petal, calculated as about $6.3 \cdot 10^6$ N/m, and the two numerical coefficients indicate the presence of 8 petals for each interface. In these condition, the structure stiffness $k_{eq,1}$ is about $1.6 \cdot 10^6$ N/m.
Over 3 N loads, the compressive force is able to act on the docking interface springs, so

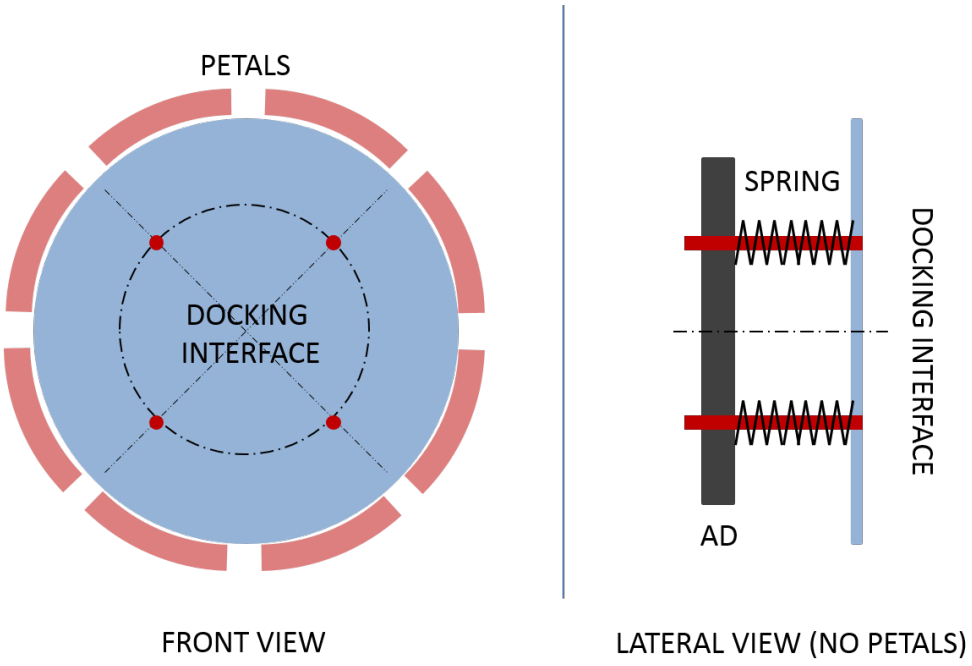

FIGURE 4.28: Docking interface spring guides

the equivalent stiffness is again $k_{eq} = 650$ N/m. About the maximal transmissible loads, for forces up to 10 N the maximal loads acting on the petals is 0.18 % of the ABS yield strength, well under failure limits, as verified through structural analysis; the selected motor is also able to bear this load. It must be underlined that the 10 N value was well over the constraints defined in chapter 2.

4.5.3 Case 2: axial tensile loads

In this case, the force acts in the direction of the preload, so the mechanism stiffness is the petals equivalent stiffness $k_{eq,1} = 1.6 \cdot 10^6$ N/m. Here again the maximal load is well over 10 N.

4.5.4 Case 3: torsional loads

The definition of the maximal torsional torque was more complex: in first approximation it is equivalent to the load required to exceed the friction between the two interfaces realized by the preload force. Considering an infinitesimal area dA of the docking interface disk, with dimensions dr and $r \cdot d\theta$, the static friction force can be calculated as function of the static friction coefficient C_s and pressure $p = \frac{F_{PR}}{A}$:

$$dF_F = C_s \cdot p \cdot dA = C_s \cdot p \cdot rd\theta \cdot dr \tag{4.15}$$

Considering that the torque $dT_F = dF_F \cdot r$, the resultant static friction torque (i.e.: the maximal torsional load) is:

$$T_F = \int_0^R \int_0^{2\pi} r^2 C_s \cdot p \cdot d\theta \cdot dr = 2\pi \cdot C_s \cdot p \int_0^R r^2 dr = 2\pi \cdot C_s \cdot p \cdot \frac{R^3}{3} \tag{4.16}$$

where R is the docking interface radius. Substituting with the preload force F_{PR}:

$$T_F == \frac{2}{3} C_s \cdot F_{PR} \cdot R \tag{4.17}$$

that for a static coefficient C_s of 0.8 for the interfaces realized in PMMA [69], gives a maximal torque of 0.13 Nm.
About the torsional stiffness, no preliminary calculation was performed due to the complexity of any analytical model.

4.5.5 Case 4: flexional loads

Last, the flexional case was considered. Under the condition that the petals stiffness is several orders of magnitude higher than the springs', it is possible to consider the they would remain undeformed and the flexional torque would act only on the docking interface as a couple acting on the springs (see figure 4.29). Only in this configuration the SAM port shows a non symmetrical behaviour, because the docking interface is constrained by the petals of the capturing interface and cannot translate outwards from them, but can move only inward: the rotation θ is visible on the left in figure 4.29. For

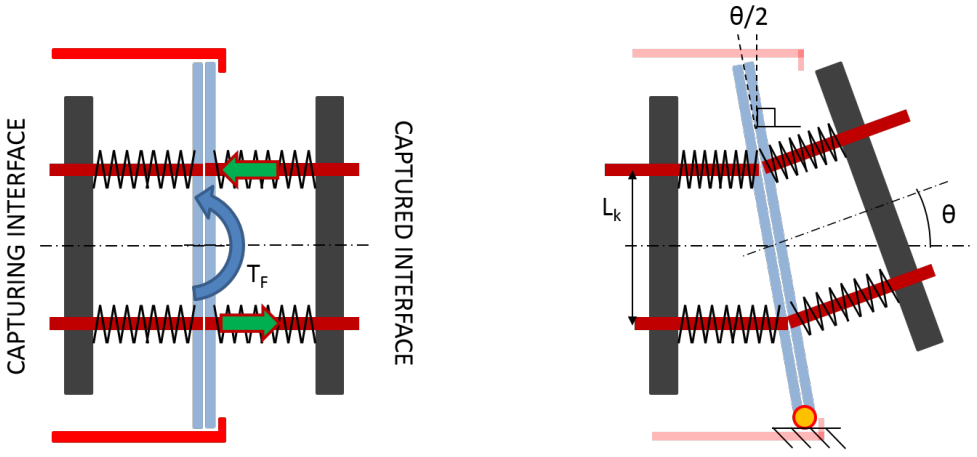

FIGURE 4.29: Schematics of forces and rotations from flexional loads: considering the petals as non deformable, due to their higher stiffness respect to the springs, the docking interface can only rotate respect to the constraining petal (red circle)

couple forces under 3 N, caused by flexional torques under 0.64 Nm , the preload avoids any movement of the interfaces, and the mechanism stiffness is only related to axial

loads acting on the constraining petal. Its value is then related in first approximation from the axial stiffness of the petal k_{Petal}, with this relation considering the effect of the couple caused by the flexional torque:

$$k_F = k_{Petal}/{L_p}^2 = 2.8 \cdot 10^8 \text{ Nm/rad} \tag{4.18}$$

with L_p the distance between two opposite petals (i.e. the diameter of SAM during docking).
In case of higher torques, causing couple forces exceeding the preload, considering L_k the distance between springs reported in figure, a simple calculation evaluates the stiffness $k_F = k_s/{L_k}^2 = 58.5$ Nm/rad.
For the interface resistance, some analysis have been performed: calculating the force couple acting on the petals, and adding the effect of the preload, for a flexional torque of 1 Nm (well over limit values calculated in chapter 2) the maximal stress is 0.07 % of the yield stress of ABS, so the structure would not fail; such loads would also not affect SAM actuator.

4.5.6 Summary

Here the main results presented in last sections are briefly summarized. In table 4.2 the different resistance constraints calculated in chapter 2 are reported (second column) for the different load conditions, and the maximal loads (third column) and equivalent stiffness (fourth column) are introduced; the torsional stiffness was not calculated due to the complexity of any preliminary model.
It is important to note that the SAM has different behaviour depending to the magnitude of the loads acting on the interface, due to the particular shape of the mechanisms, that is able to create a preload stiffening the joint.

In conclusion, the calculation of the mechanical characteristics of the mated ports

TABLE 4.2: Mechanical characteristics of the docking joint

Load	**Resistance Constraint**	**Maximal Load**	**Joint Stiffness**
Axial (Compression)	5 N	>10 N	$1.6 \cdot 10^6$ N/m (F < 3 N) 1300 N/m (F > 3 N)
Axial (Tensile)	5 N	>10 N	$1.6 \cdot 10^6$ N/m
Torsional	0.09 Nm	0.13 Nm	/
Flexional	0.09 Nm	>1 Nm	$2.8 \cdot 10^8$ Nm/rad (T < 0.64 Nm) 58.5 Nm/rad (F > 0.64 Nm)

allowed to define the joint stiffness and maximal transmittable loads (i.e. its resistance);

a comparison with the constraining values calculated in chapter 2 indicates SAM's wide safety margins to mechanical failure. Anyway, for completeness sake a brief analysis of reliability issues is reported in next section.

4.6 Mechanism reliability issues and risk table

One of the key features of the proposed mechanism is the utilization of a single linear motor to simultaneously actuate the eight petals; however, the advantages of simplicity and low mass are counterbalanced by a reliability issue, because the failure of one of the petal cams or of the motor could result in the jamming of the whole mechanism.
On these considerations, a brief risk analysis was performed and some technical solutions to increase the mechanism reliability were analysed, although they were not implemented in the first prototype. Main results are summarised in table 4.3, structured following the guidelines of ESA Risk Management [70], defining a likelihood of occurrence, scoring from A (lower probability) to E (higher probability), and the severity of consequences, from 1 (negligible) to 5 (most severe). The product of likelihood of occurrence and severity gave the risk index, represented with a colour code (green-low, yellow-medium, red-high).

The possible failure causes are listed in the Risk column. First, the petals could

TABLE 4.3: Risk Table

Number	Risk	Risk Index	Action
1	Petals Structure Failure	A5	Material selection & test
2	Actuator Failure	A5	Motor selection & test
3	Jamming in closed configuration	C2	No action, the port acts as probe
4	Jamming in open configuration	C5	Cam separation, 7 petals still working
5	Jamming during operations	A5	Recover to case 4 or 5

have a structural failure, causing the mechanism to jam; mechanical analysis, material selection and load test are the most important foreseen actions. The same issue was considered for the actuator: in case of failure of the linear motor, the whole port would be useless. To avoid such problem, robust and well-tested actuators should be selected. In parallel, for both the first two risks, safe values of allowable loads should be respected, avoiding to reach the petals yield point or the motor limits in terms of holding forces and maximal actuation loads. Jamming in closed configuration was the third risk to be evaluated. In this case, the safest approach is to use the stuck port as probe, thanks to the androgyny of the mechanism, and to actuate the other involved interface to the drogue configuration. On the contrary, the fourth case was the worst, because and open

configuration would be totally useless; the evaluated technical solution was to add to the actuation disk a single shot actuator for every petal, able to separate the jammed petal to the rest of the mechanism, to leave it in the open state. In this case, the other petals would be still able to perform the docking manoeuvre, because for up to three consecutive damaged petals the port is able to capture its twin one and close around it (see figure 4.30). Last risk was related to a failure during the opening-closing operations.

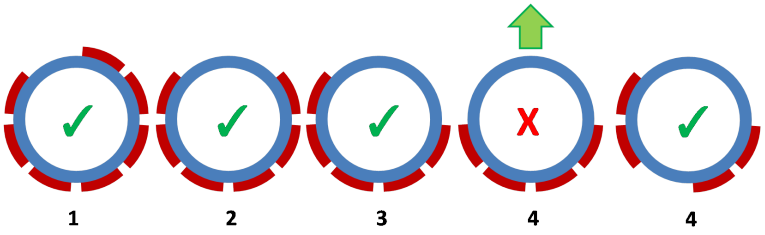

FIGURE 4.30: Petal failures and docking success: for less than four consecutive failed petals, the docking procedure could be successful, as the remaining petals (in red) are still able to close around the other port (in blue)

Due to the low likelihood of occurrence, the proposed action was to try to recover to the open or the close configuration, and then to follow one of the aforementioned solutions.

Chapter 5

DEVELOPMENT AND TEST

This chapter discusses the test campaign performed on the developed prototype, following a logical path correlated with the numerical simulations plan.
The test-bed is a simple open-loop 1-DoF platform, in which the target is fixed on an instrumented structure and the chaser can approach it moving on a rail system. A partial freedom to rotate is also given to the chaser, thanks to suspension strings connecting it to the frame moving on the rail. A preliminary investigation determined both the rail friction coefficient and the effect of frame moving actuation on the measurement system, in terms of vibrations transmitted to the framework.
The experimental verification, in order, aimed to (1) validate the prototype geometry and the opening-closing mechanism through functional tests, (2) determine the loads transmitted to the framework system during nominal docking procedures, and (3) evaluate the working range of the SAM, in terms of maximal allowable linear and angular displacements with respect to the nominal docking operation.
Results demonstrated the mechanism operation, and verified that collected loads were always under 3 N, never affecting the mechanism action. Last, the misalignment test defined the interfaces mechanical ranges in terms of allowed lateral and angular misalignments to perform complete docking procedures.

5.1 Test definition and goals

As visible in the work plan presented in the first chapter, the docking mechanism testing is a fundamental part of this research: the developed prototype shall be tested to better investigate its behaviour and validate its geometries. This phase is planned similarly to the simulation one, as reported in figure 5.1, with every step depending from the previous, with increasing complexity.

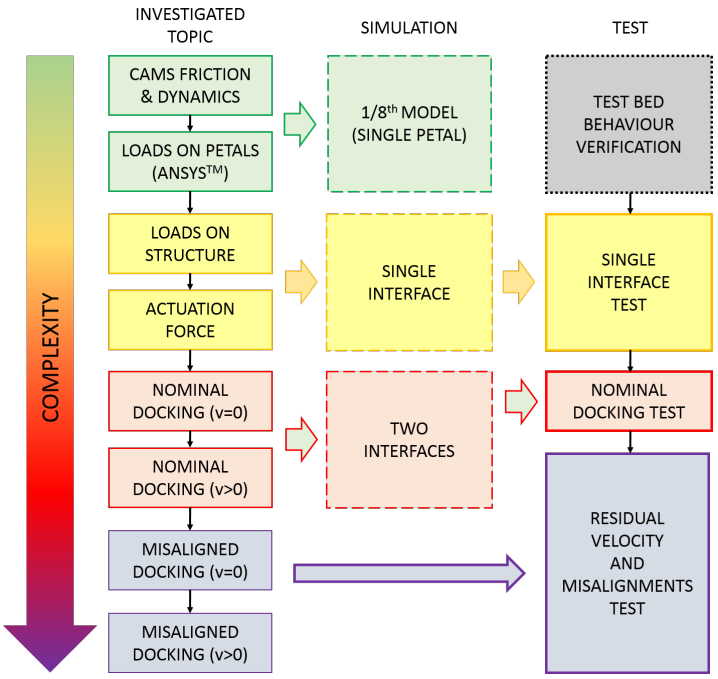

FIGURE 5.1: Logic diagram of the test process, compared to simulations

The testing activity has the first goal to verify the prototype geometry and actuation, validating the dynamical simulations of a single interface and calculating loads acting on the interface base; a second task is related to the evaluation of nominal docking manoeuvres, in which there are no linear or angular misalignments between the interface acting as probe and the drogue one. Last, the working range of the docking interface, in terms of linear and angular displacements respect to the nominal operations that still allow to complete a docking procedure, is evaluated through a dedicated campaign.
The test bed is designed to give to one interface a degree of freedom in the direction of its docking axis thanks to a rail system and the possibility to partially rotate about a vertical axis passing through its centre of mass with the utilization of suspension strings. The test set-up design and preliminary verification is introduced in next section, with a simple test to determine the rail friction coefficient and how this could affect the interface docking.

5.2 Test-bed design

A dedicated and instrumented test bed was designed to test the developed prototype in the laboratory facilities. Different solutions were evaluated, considering the number of free DoF, the availability and the simplicity of realization or access. Next section will briefly introduce the main typologies of test-bed for docking technologies and the

constraints that conditioned the trade-off to the selected one, followed by some simple preliminary test to determine its behaviour.

5.2.1 Test-bed options comparison and concept

Facilities for ground test of navigation, rendezvous and docking of spacecraft have been used from virtually the beginning of the space era, varying from small university test-bed to large government and industries laboratories. The oldest technology is surely related to air-bearing simulators [71], that gives payloads some level of translational or rotational freedom. Some examples are the Stanford Aerospace Robotics Laboratory test-bed for space robotics, consisting in a robotic arm, fixed on a solid base, floating on a low friction table and sustaining two smaller arms able to manipulate target objects [72], and the Tokyo Institute of Technology facility employing two floating robotic arms [73], but at today most of the space research centres are furnished with air-bearing facilities. The utilization of low-friction tables is therefore well investigated and other technologies are employed (such as magnetic suspension), but the state of the art for small satellites test is surely represented by MIT SPHERES ground facility (see Chapter 6); it is composed by a small glass table and one to three independent vehicles mounted on air carriages, giving them one rotational and two translational close-loop controlled DoF.

A completely different approach is based on the utilization of robotic arms to simulate the dynamics of free floating objects, with 3 directional and 3 rotational controlled DoF: the main example is surely DLR's European Proximity Operations Simulator (EPOS) [74], composed by two anthropomorphic industrial manipulators, with the target fixed on the ground and the chaser mounted on a 25 m rail for extra mobility. A similar robotic-arm test-bed has been recently developed by GMV [75].

All the aforementioned facility could give important information on SAM behaviour and the utilization of such advanced test-bed was considered as an important option, but, mainly due to time constraints, it was preferred to utilize a simpler, open-loop system, to perform all the preliminary tests and validate the concept. The developed platform consists in a fixed instrumented base for the target and a rail on which the chaser is mounted with a system of stripes, giving it one free linear and three partially free rotational degrees of freedom. The advantage of this solution was the fast availability respect to the others; the absence of a closed-loop control was counterbalanced by the simplicity of the concept, that allowed a fast collection of experimental information on the SAM behave. In any case, it is planned to perform more accurate tests on more relevant platforms, such as a robotic-arm based simulator [76] and a low-friction-table based vehicle [77], both in development at CISAS.

5.2.2 Test-bed description

The test bed, visible in figure 5.2, is designed to give to one interface a degree of freedom in the direction of its docking axis thanks to a rail system and the possibility to partially rotate about a vertical axis passing through its centre of mass with the utilization of suspension strings.

More specifically, the test-bed holds the target (in red) with its actuation linear motor,

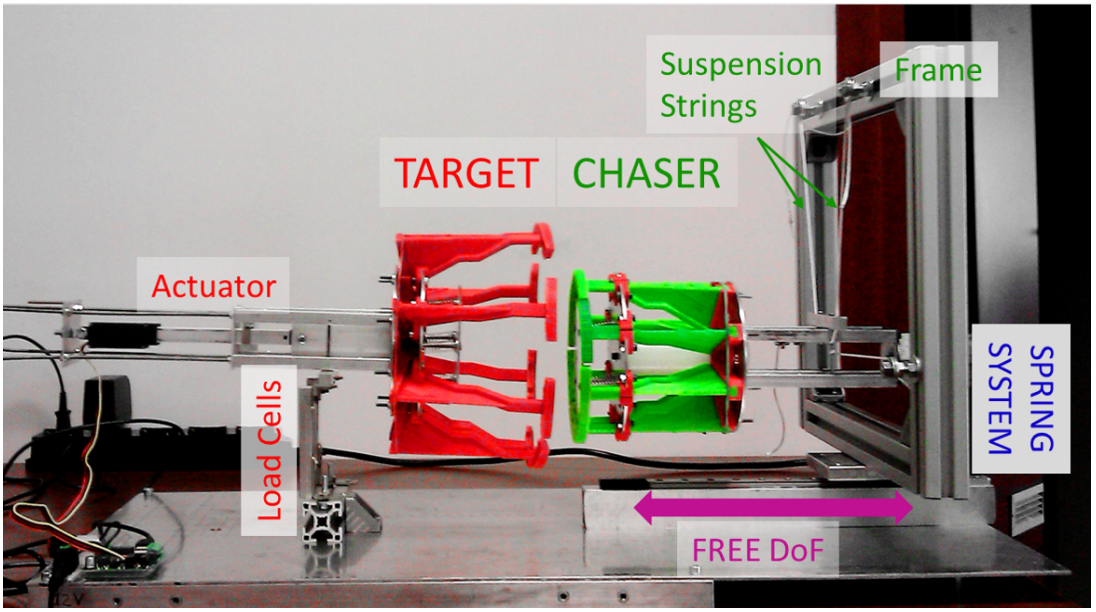

FIGURE 5.2: Test-bed used in the test campaign: the target (red) is fixed and mounted on load cells, the chaser is hung to a frame mounted on a rail and propelled by a spring system

on a rigid structure instrumented with load cells, to measure loads transmitted by the actuation and the docking procedure. The chaser (green) is suspended to a frame, giving it a reduced rotation freedom; the frame is able to move on a rail toward the target. A spring system is mounted behind the chaser and its frame, to give them the required approach velocity.

Both the target orientation and lateral displacement are easily adjustable, in order to test the mechanism in non nominal conditions (i.e.: rotational and translational misalignments.

The load cells are off-the-shelf components, Phidgets RB-Phi-118, working in the range $0 - 5$ kg (figure 5.3); they are directional sensors, based on shear measurement instead of more usual bending detection, with the result of accurate readings regardless of the position of the load respect to the detection area (in red). The cells are mounted symmetrically and with a relative angle of $45\,^{\circ}$ with respect to the port axis, as visible in figure 5.4. From the two measured signals (F_1 and F_2), it is possible to reconstruct the forces acting in the docking axis direction and in the lateral one. Before defining the test

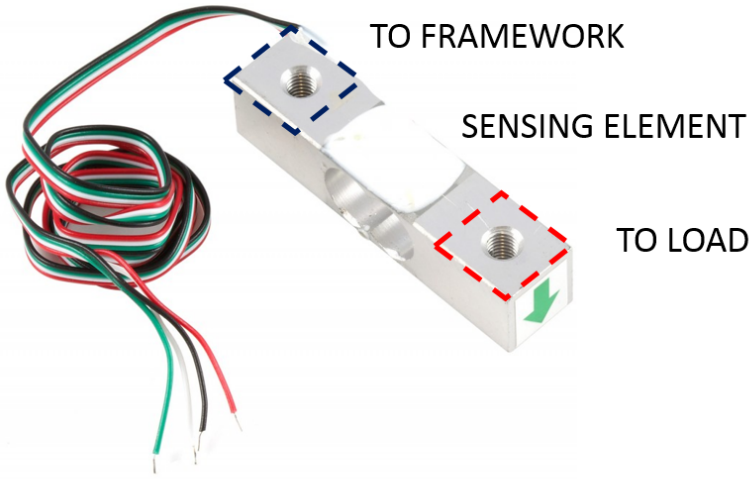

FIGURE 5.3: Selected load cell and mounting instruction

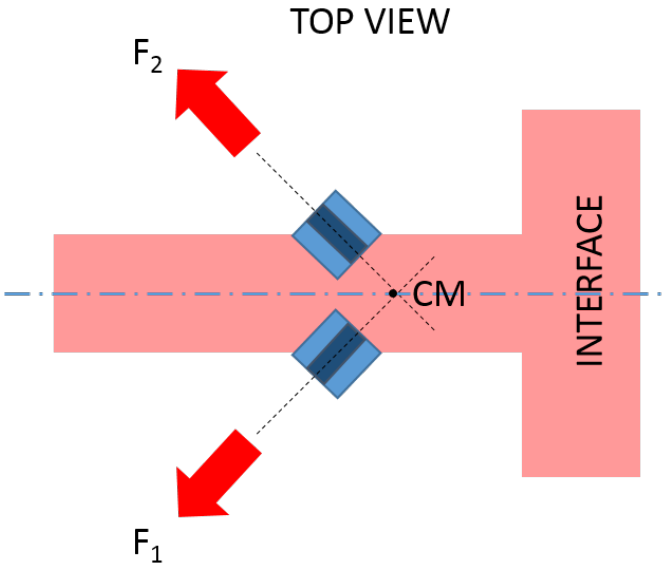

FIGURE 5.4: Load cells mounting geometry, top view: the two cells are mounted with an inclination of 45 ° respect to the docking axis

procedure and perform the test campaign, a preliminary investigation was performed, to determine (1) the friction coefficient of the rail system and its effect on the chaser approach velocity to the target, and (2) the effect of the spring system thrust in terms of vibrations transmitted to the framework and detected as disturbances by the load cells. Last, a group of four fork-led IR sensors were mounted on one side of the rail, to detect the time of frame passage at different fixed position. They have an IR LED and a photodiode calibrated on the same frequency, separated by a slit: the passage of an opaque body between them shades the emitter, with a fast time response (over 1 kHz) and a

precision of detection of 0.002 mm at 25 °C.

5.2.2.1 Friction coefficient determination and rail dynamics investigation

This preliminary test was designed to (1) determine the friction coefficient of the rail-gear system, and (2) evaluate the chaser velocity at the contact with the target.
A simplified sketch of the chaser support is visible in figure 5.5: the spring system is designed to push both the chaser and the frame to an initial velocity v_0, and then they are free to move on the rail. A monodimensional model can be deduced, considering in first approximation only one external force acting on the system, the friction between the rail and the frame. Internal forces are exchanged due to the presence of the support cables acting as a spring; chaser and frame are considered as lumped masses.

If the parallel push avoids oscillations between the frame and the chaser during the

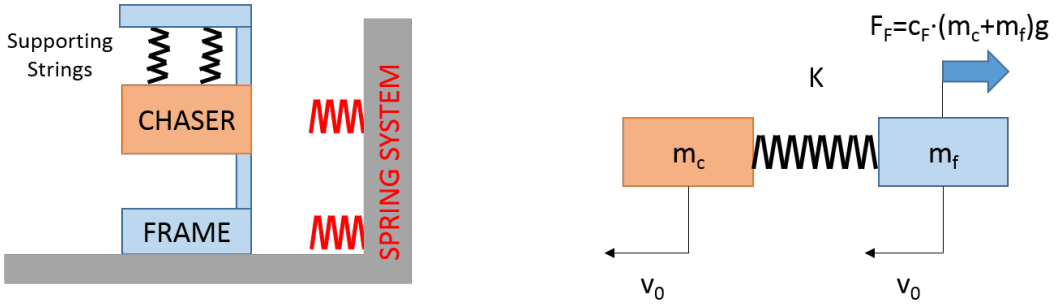

FIGURE 5.5: Simplified sketch (left) and monodimensional model (right): the frame and the chaser are considered lumped masses connected with an elastic element.

initial shifting, when they are free to move the friction slows the frame: this causes the chaser and the frame to exchange forces between the strings, starting an oscillation. A simple numerical model is designed to simulate this behaviour and calculate the chaser and the frame motion solving these differential equations:

$$\begin{aligned} m_c\ddot{x}_c &= -K \cdot (x_c - x_f) \\ m_f\ddot{x}_f &= +K \cdot (x_c - x_f) - F_F \end{aligned} \tag{5.1}$$

where K is the stiffness of the strings and F_F is the friction between frame and rail, function of the friction coefficient c_F:

$$F_F = c_F \cdot (m_c + m_f)g \tag{5.2}$$

Data collected by the IR sensors allowed to measure the frame passage time at different positions, with an estimated time error of 2 ms and a position error of 0.1 mm; this information was compared with the developed model and the values of both the

friction and the chaser approach velocity to the target were calculated, resulting in $c_F = 0.0151 \pm 0.0017$ and $v_c = 0.158 \pm 0.0075$ m/s. Comparison between simulation results and collected data demonstrated the validity of this approach, as visible in figure 5.6.

The results uncertainties were numerically derived from data uncertainty; the pro-

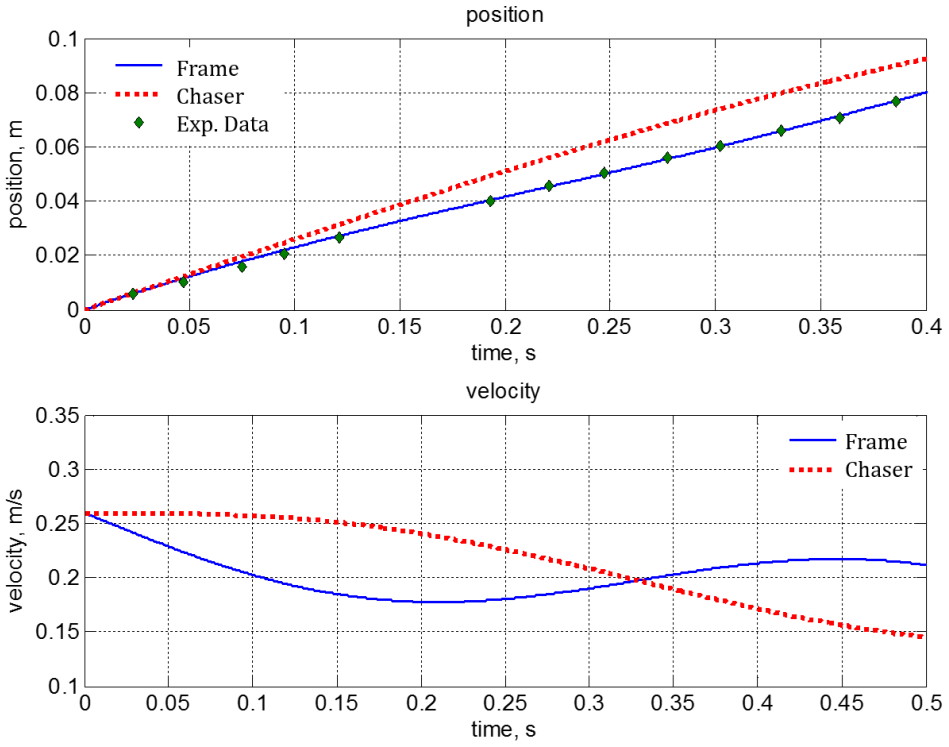

FIGURE 5.6: Comparison between numerical model and collected position information: experimental data is perfectly overlapping the calculated path

cess is here briefly explained. First, a normally random distribution assigned to the experimental data a certain amount of error into the uncertainty limits, and simulations permitted to calculate the desired outcomes. Repeating this process for a large number of times (up to 15000 simulations) permitted to collect a large population of results, on which perform statistical analysis: uncertainties were reported with a confidence of 2σ, assuming a Gaussian statistical distribution. In figure 5.7 the simulation outcomes and their distribution are shown.

5.2.2.2 Disturbances from impulsive loads

The measurement system, consisting in load cells, and the joining elements connecting it to the structure and the interface present a finite stiffness, influencing the data collection with a load effect; to determine such influence and its effect on the measurement, a

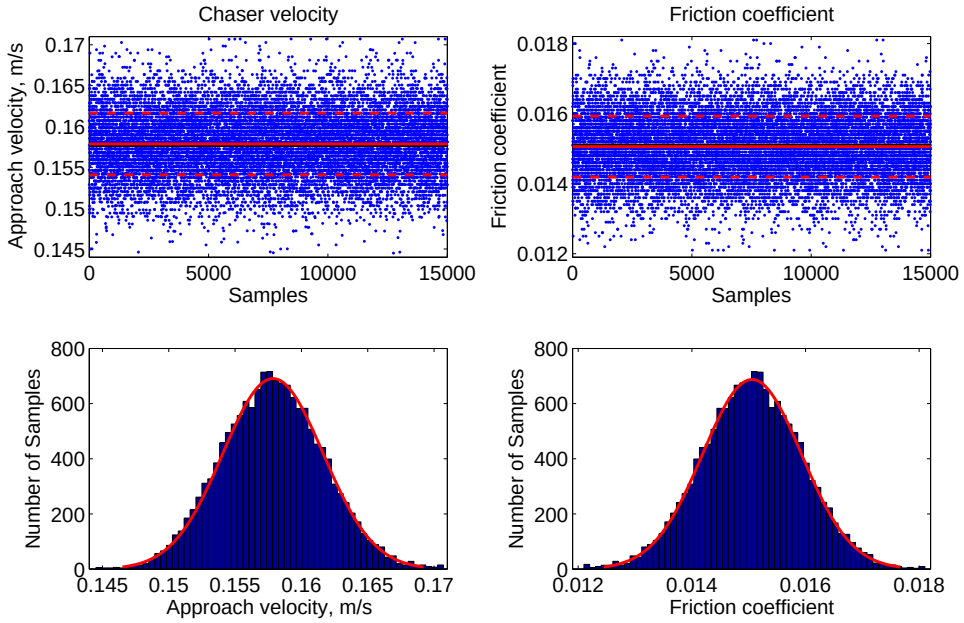

FIGURE 5.7: Simulation outcomes (up) and their distribution (down): on the left, the chaser approach velocity to the target, on the right the friction coefficient, both showing a standard normal distribution

dedicated test was performed, analysing (1) the effects of the chaser push from the spring system and (2) the impact on the target.

Part of the release load is transmitted to the load cells through the framework base, ss visible in figure 5.8: the thrust creates a dumped oscillation, with a peak force of about 3 N and a damping time of about 0.5 s.

At the following impact, no residual oscillation can be found. and the chaser impact on the target is measured at about 1.2 s; the transmitted peak load is of about 1.5 N, with about 0.2 seconds of duration.

The setup measurement system, composed by the two load cells connected to the base

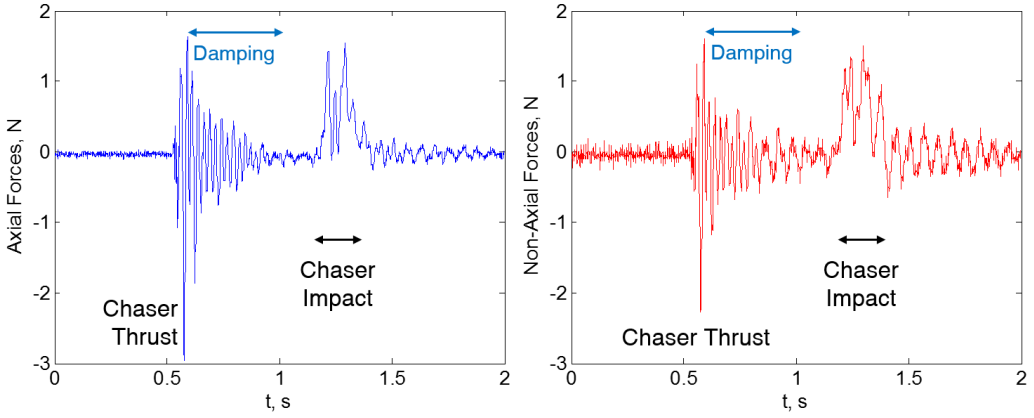

FIGURE 5.8: Data collected in the disturbances test: axial and lateral loads detected from the measurement system due to the spring systems and the chaser-target impact

and the target, has a natural frequency related to cells and joints stiffness and target mass. Analysing the signal in the frequency domain, this first vibration frequency can be easily recognized at 15 Hz. The analysis was realized by Matlab^{TM} Fast Fourier Transform (FFT) algorithm, applied on a sample of the collected signal corresponding to the damping phase (figure 5.9).

This value was utilized to calculate the load effect of the structure joints on the

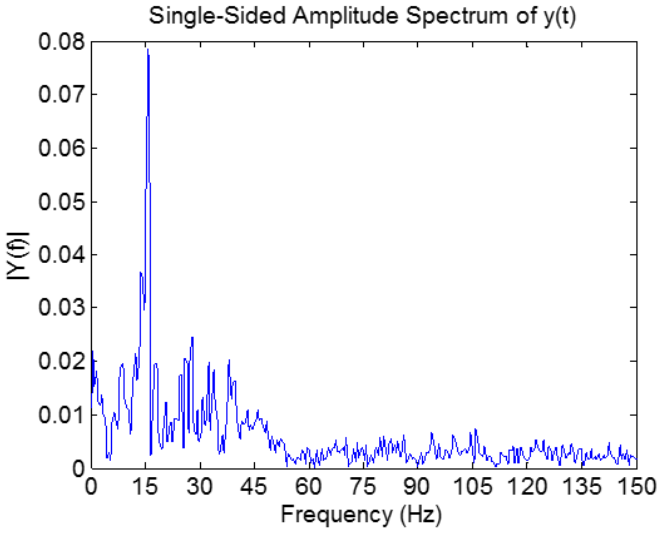

FIGURE 5.9: FFT of the collected data: the 15 Hz natural frequency of the system is easily recognizable

measurements. Respect to the ideal case of a perfectly rigid structure ($K_S = \infty$), in which only the load cells have a finite stiffness K_{LC}, in the real case the measurement error absolute value is:

$$|\varepsilon| = \frac{K_{LC}}{K_S + K_{LC}} \tag{5.3}$$

Both the values were not known (the load cell stiffness value was guiltily missing from datasheet), but K_{LC} was evaluated knowing the load cell material (LY12CZ Aluminium Alloy) and geometry; from the natural frequency m of the system, knowing the mass of the whole structure, it was possible to find the value of the equivalent stiffness:

$$K_{eq} = 4 \cdot \pi^2 \cdot f^2 \cdot m \tag{5.4}$$

and, knowing that the series of two springs can be calculated as:

$$K_{eq} = \frac{K_S \cdot K_{LC}}{K_S + K_{LC}} \tag{5.5}$$

it was possible to calculate the maximal error affecting the measurement system, as reported in equation 5.6

$$|\varepsilon| = 1 - \frac{K_{eq}}{K_{LC}} = 0.11 = 11\% \tag{5.6}$$

5.3 Test organization

The test campaign was organised following a well defined and strictly binding procedure, based on the concepts of repeatability (the variation of experiment results under repetition under the same conditions) and reproducibility (the ability of an entire experiment to be independently reproduced). For this reason, a test table was introduced (see Appendix D), aiming to define the different tests to be performed, to give them a unique and unmistakable name, and to repeat each single test three times.
Three test types were planned, as shown in figure 5.1.

5.3.1 Test 1: single interface test

The first test aimed (1) to verify the port opening-closing actuation and (2) to detect the loads created during the process. Only one interface was involved in this test, the target one, mounted on the load cells and actuated by the linear motor. The test was planned at three different actuation velocities, 2.5 mm/s (opening in 20 s), 10 mm/s (opening in 5 s) and 20 mm/s (opening in 2.5 s).

5.3.2 Test 2: nominal docking test

The second test was dedicated to the determination of the mechanism behaviour in case of a nominal conditions complete docking procedure. In such case, the chaser and the target were in contact with no residual relative speed and perfect alignment; the docking procedure was again tested at the three different actuation velocities of 2, 10 and 20 mm/s. The actuated port was again the target one.

5.3.3 Test 3: misalignments test

For the third test, the objective was to define the mechanism requirements in terms of maximal lateral and angular misalignments.
In this test, the mechanism alignment requirements to perform a complete joining were defined, considering (1) relative velocity equal to 0 and (2) a residual relative velocity of about 0.1 m/s in the axial direction. Complete docking procedures were realized at different alignment conditions, varying both lateral and angular misalignments.

5.4 Test campaign and results

5.4.1 Test 1: single interface test

The first performed test demonstrated the validity of the petals geometry and the whole mechanism design. As described in the last section, three different actuation velocities were tested, respectively 2.5, 10 and 20 mm/s: the axial loads produced by the actuation are reported in figure 5.11. It was expected that peak forces should increase with the actuator speed; at the three different conditions, the measurement system detected respectively 0.15 N at 2.5 mm/s and about 0.3 N at 10 and 20 mm/s in the actuation direction; for the lower actuation velocity, the signal to noise ratio was too low to find significant information except for the first peaks for opening and closure: the other points were localized through geometric evaluations. After the impulsive loads measured by the load cells, damped oscillations can be detected, and are partially recognizable on the 10 mm/s and 20 mm/s plots; a FFT signal analysis shows that the first detected frequency is the previously determined system natural frequency of 15 Hz.
Comparing with the simulations, as visible in figure 5.10, it is possible to define the origin of the peaks in the cam passages at petals corner points. The maximal force is visible at the beginning of the procedure, with a simulated peak of 0.3 N and a collected measurement of 0.2 N. This test also showed that the actuation could cause a vibrating environment, not related to the peak forces collected on the passages in the petals corners, probably due to the motor internal mechanics, that in the experimental set-up was marked by oscillations at the system natural frequency of 15 Hz. Future prototype shall foresee solutions to reduce such possible source of disturbances, evaluating different actuators or dumping mounting joints.

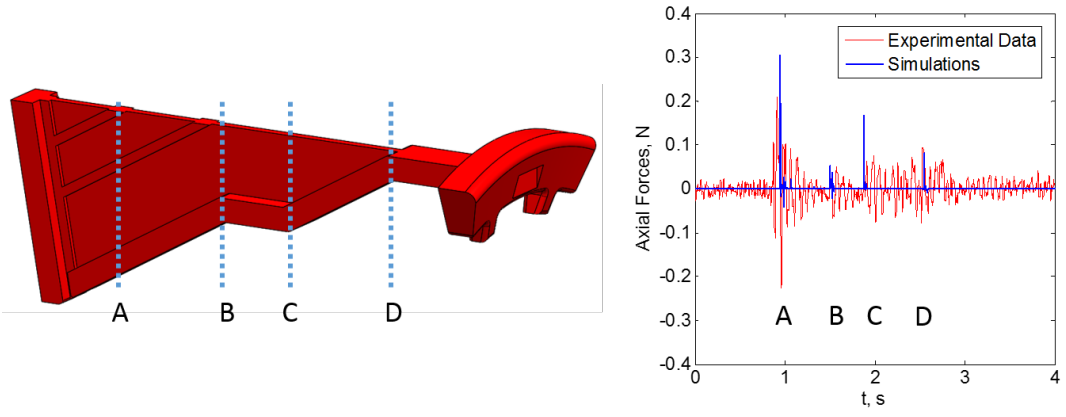

FIGURE 5.10: Axial forces trend in a closing actuation: peaks are directly related to the passages in the petals cams corners

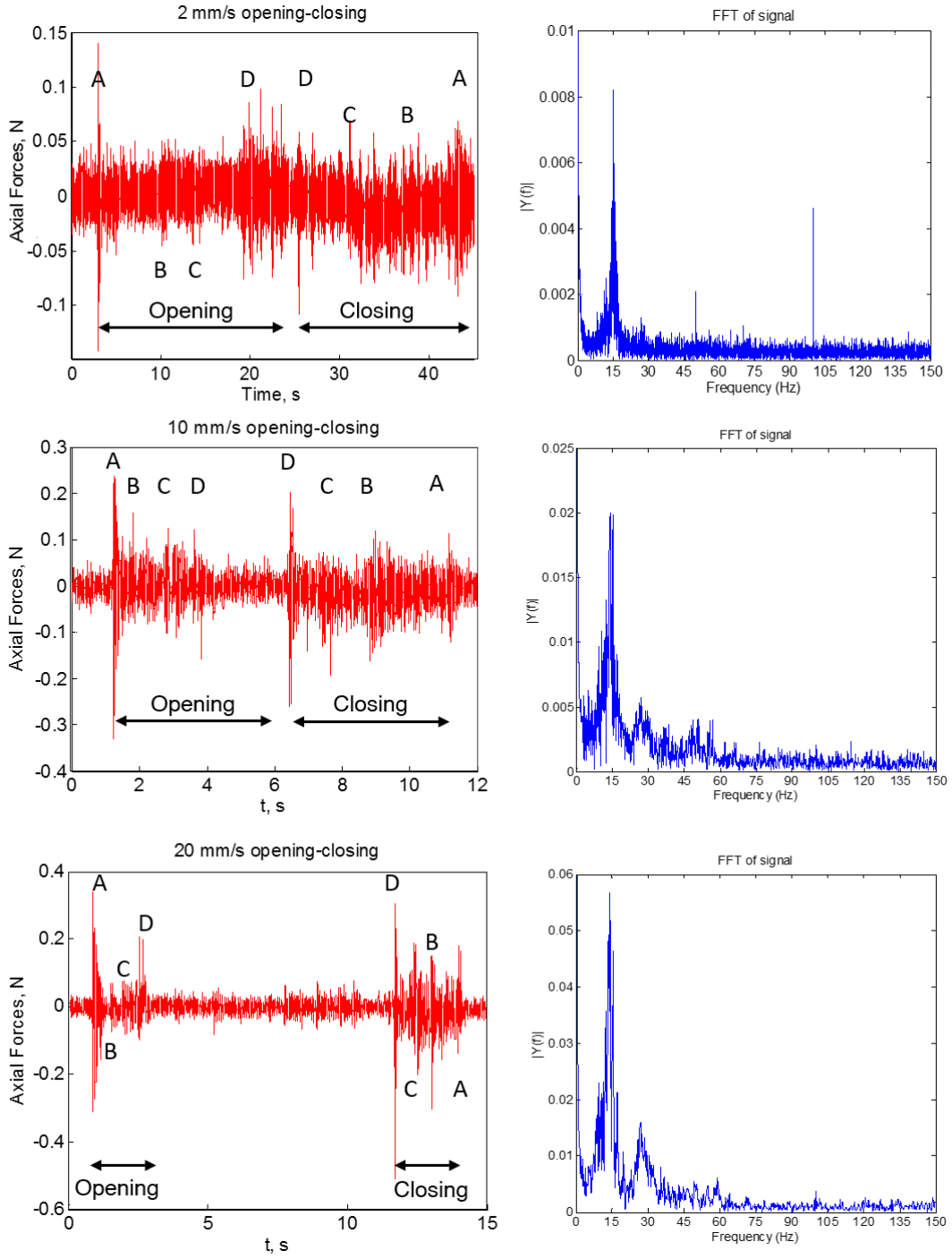

FIGURE 5.11: Measured axial loads during the actuation(left): from top to down, results at 2, 10 and 20 mm/s; for the 2mm/s case, the signal to noise ratio was too low to apply an efficacious filter. On the right, FFT of the collected signal: the 15 Hz natural frequency of the system is again visible.

5.4.2 Test 2: nominal docking test

In the second test, dedicated to the verification of nominal docking, the target captured the chaser closing around it, with again three different actuation velocities (2.5, 10 and 20 mm/s).

Results from the test are visible in figure 5.13: in all the different cases, two phases are easily detectable, the main one being the closing and inside it the capture of the chaser within the target petals. More specifically, three main event can be detected: (1) at the beginning of the closing process a small spike shows the first contact between the chaser and the target; then, (2 - yellow in figure) the actuator pushes back the chaser while closing around it until (3 - light blue in figure) the target petals capture it and create the solid joint. The highest spikes are measured in this phase, when the actuator preloads the mated mechanism stiffening the joint. Axial loads are always below 1.5 N, non axial forces can rise in all the three cases up to about 3 N, with no evident correlation to the actuation velocity.

Collected data shows another interesting outcome in the frequencies analysis: as visible in next figure, the FFTs of the 10 mm/s (left) and 20 mm/s (right) actuation docking procedures show an interesting peak at about 4 Hz, instead of the 15 Hz frequency measured in the previous test. This result is correlated to the increased mass of the joint ports and to the chaser strings supporting system, that constrain the mated mechanism to such lower natural frequency vibration.

The results from this test were compared with the mechanical constraints defined in

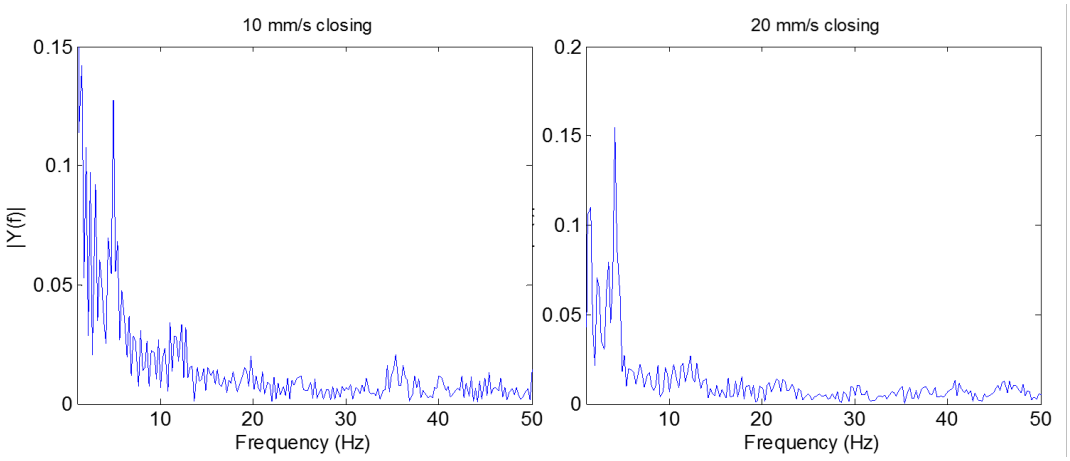

FIGURE 5.12: First natural frequency of the mated system: in both the 10 mm/s (left) and 20 mm/s (right) actuation velocity cases, the mated mechanisms shows a lower natural frequency (4 Hz) respect to the single interface (15 Hz)

chapter 2 (table 2.1) and the mechanical characteristics calculated in chapter 4, section 4.5. The maximal transmitted loads are comparable to the evaluated values: during the docking operation the prototype does not transmit disturbances higher than the external

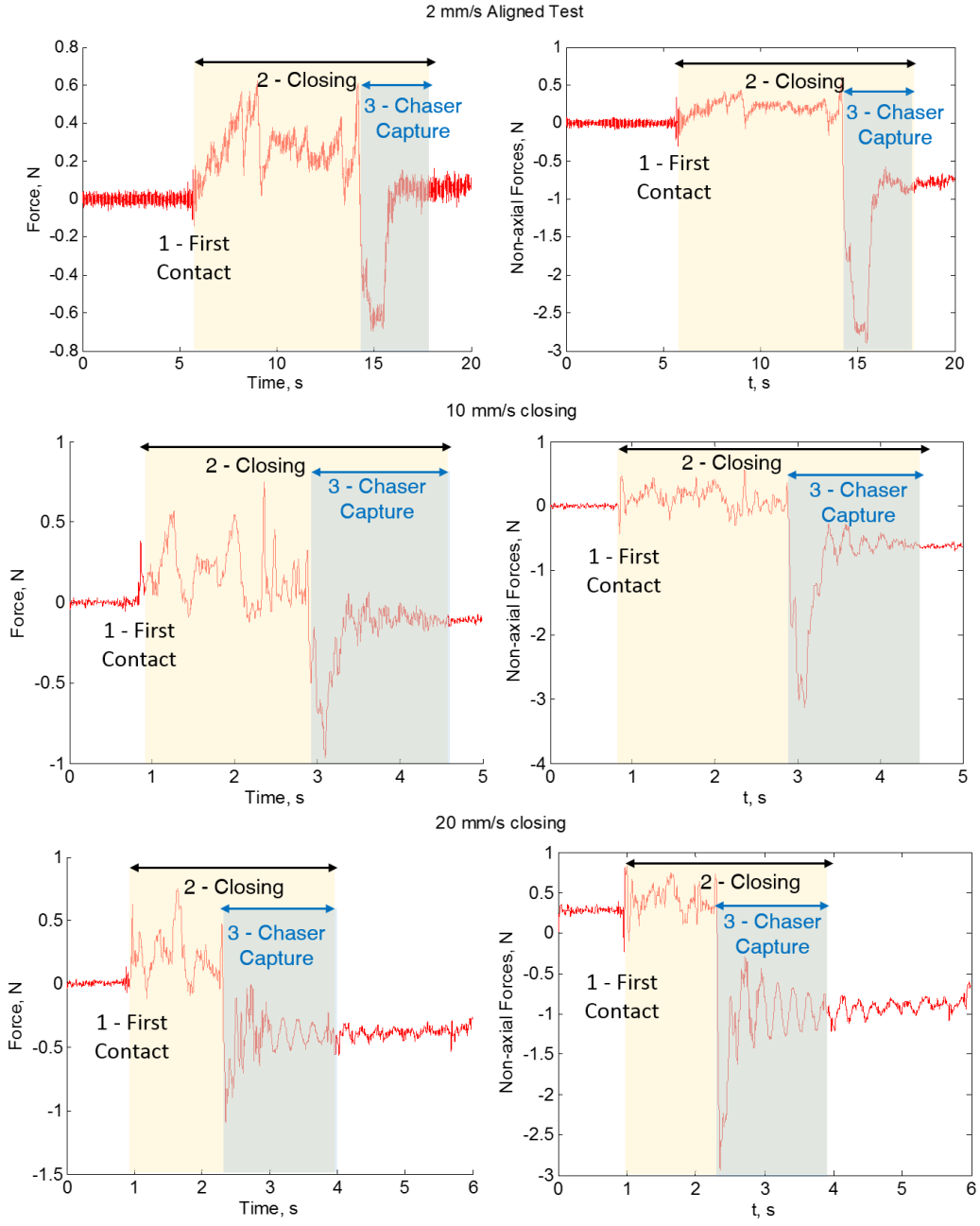

FIGURE 5.13: Measured forces in test 2: from top to down, 2, 10 and 20 mm/s of closing actuation velocity.

ones it should bear (up to 5 N for 100 kg satellites). Future analysis and prototype tests shall evaluate the existence of a relation between the port size and the maximal load: for smaller spacecraft (under 20 kg) the level of transmitted loads must be lowered to 1 N or less.

5.4.3 Test 3: misalignments test

In the last test the mechanical alignment ranges to perform a complete docking procedure were defined, considering (1) a relative velocity equal to 0 and (2) a residual relative velocity of about 0.15 m/s in the axial direction. Complete docking procedures were realized at different alignment conditions, varying both lateral and angular misalignments; figure 5.14 shows collected results. In both the evaluated cases, the maximal admissible lateral misalignment is correlated to the open mechanism dimensions: at 20 mm the chaser petals hit target ones, preventing the docking procedure. It is also interesting to notice that the nominal docking can be performed with maximal misalignment angles of about 5 °, but with higher angles the target interface is similarly able to close and capture the chaser (yellow area), still creating a solid joint but without perfectly aligning the two ports.

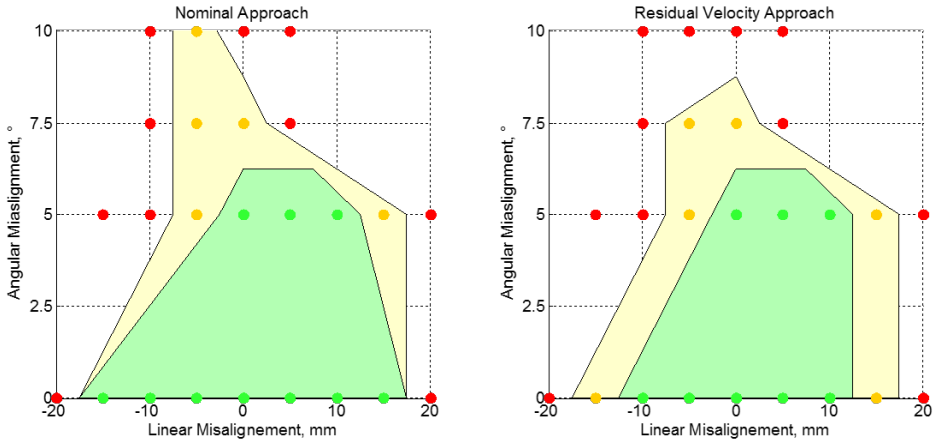

FIGURE 5.14: Alignment ranges to perform a complete docking procedure with null relative velocity (left) and residual relative velocity (right) in the axial direction between chaser and target. Dots indicate performed tests, coloured areas the interpolated results. In green, performed tests lead to nominal docking; yellow areas indicate the creation of a solid joint but with residual misalignments and non-perfect interface mating.

5.5 Comments

The laboratory test campaign demonstrated the proposed docking mechanism working principle and validated the design process. Comparing with simulations, collected data demonstrate that the axial loads acting on the mechanism were well defined; about lateral loads, higher spikes are always under 3 N and do not affect the interfaces action. Last, misalignment test gives important information on the ports working ranges, indicating that further investigation could be afforded to improve the interfaces performance and broaden the current allowed limits.

Chapter 6

SPHERES UDP Ground test

At the MIT Space Systems Laboratories, in the framework of the SPHERES programme, the Universal Docking Port (UDP) is in development, consisting of a new androgynous interface compatible with the test platforms and planned to fly on ISS in 2015. The SPHERES ground test bed consists in a low friction glass table, on which it is easy to test the developed hardware and control software to verify it before in-space experimental validation.
A visiting period of about two months allowed to understand the methodology behind the UDP development and management and more generally the advantages to use a fast-available test bed for the continuous comparison between developed numerical investigation and its verification. In this period, some control codes for the SPHERES were developed, to test the rendezvous and docking on the low friction facility. Simulations demonstrated the goodness of the proposed manoeuvres and the reliability of both collision avoidance and close rendezvous controllers; unfortunately, some issues related to the SPHERES state determination affected the system during the test campaign, preventing the complete verification of the developed code.
Last, a comparison between the UDP and the semi-androgynous port demonstrates that the latter has a larger working range in terms of accepted angular and lateral misalignments at docking.

6.1 SPHERES, the UDP and the Guest Scientist Program

SPHERES (Synchronized Position Hold Engage and Reorient Experimental Satellite) system consists is a safe and reusable zero-g platform, to test a wide number of technologies related to relative navigation and space rendezvous on board the International

Space Station (figure 6.1). The program is developed by the MIT Space Systems Laboratory in collaboration with NASA, DARPA and Aurora Flight Sciences, and at today more than 60 experiments were carried on the ISS, thanks to the three SPHERES on board since 2006 and other components added in the next years.

Typically, space-operating test platforms are directly exposed to the harsh space en-

FIGURE 6.1: SPHERES on board the ISS (courtesy by NASA)

vironment, risking unrecoverable failures and not allowing a continuous monitoring and maintenance. By operating inside the ISS, SPHERES merges the advantages of space microgravity with safer test conditions. In this way, SPHERES can perform test unsuitable for autonomous spacecraft, from simulating GN&C failures that otherwise would be too risky to represent, to test algorithms up to their physical limits in relevant conditions with live monitoring. Last, the possibility to set tests in a relatively short time makes SPHERES a cost-effective platform for microgravity testing.

In parallel, on ground, other facilities (i.e. parabolic flight planes and low friction tables) are used for the preliminary verification of the experiments developed in the framework of the SPHERES program. In MIT laboratories a small glass table (about 2 m x 1.4 m) is available for test; one or more SPHERES are mounted on air carriages, giving them one rotational and two translational degrees of freedom. The facility can work both with a simplified software or with the same GUI used by astronauts on ISS, allowing scientist not only to get preliminary experimental data, but also to evaluate and improve the test procedures in order to fully define every detail and optimize the utilization of the space facility.

6.1.1 SPHERES platform description

Each SPHERES is an autonomous spacecraft with propulsion capabilities, absolute and relative navigation sensors and telecommunication links (figure 6.2) [78][79]. Position and Attitude control is allowed by twelve cold gas actuators, delivering a thrust of about 0.01 N. The propellant, carbon dioxide, is stored in a tank at about 60 bar, and then it is distributed through a low-pressure circuit (at about 2.5 bar). Being the thrusters not throttle-able nor adjustable, they are commanded in pulse-width modulation (PWM), allowing to control the SPHERES in all the degrees of freedom. Satellites position and attitude are determined both with internal sensors (accelerometers and gyroscopes) and 24 microphones detecting the ultrasound emission from up to nine external fixed beacons. Power is provided by 16 rechargeable AA batteries, giving SPHERES the autonomy of usually more than one hour. Communication is performed through two channels respectively of 916.5 and 868.35 MHz, allowing downlink and uplink with a standard laptop and relative communication between SPHERES.

To perform preliminary rendezvous and docking tests, SPHERES were furnished with

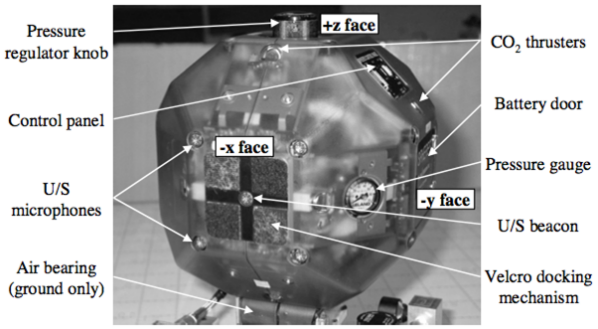

FIGURE 6.2: SPHERES main components and parts (courtesy by MIT SSL)

a Velcro interface, giving them the capacity to perform mating operations, but still requiring external intervention to separate.

6.1.2 SPHERES projects and expansion

Since the first tests on board the ISS, the SPHERES program continued to grow, exploring new technologies in the fields of relative navigation, servicing and flight formation. Among all, the most important projects developed in these years are RINGS, aiming to demonstrate electromagnet relative navigation [80], SIMO, studying precision spacecraft formations for telescope systems [81], SWARM, investigating the use of reconfigurable modular satellites [29][82], VERTIGO, developing computer vision based navigation and non-cooperative target detection [83], Halo, consisting in an expansion of the SPHERES

single port allowing to connect and monitor up to six different elements, and INSPECT, conjugating thermal cameras, optical range finder and control moment gyroscopes to improve SPHERES capabilities and as first step to realize satellites able to work outside the ISS [84].
In this framework, the Universal Docking Port is in development, in order to substitute the original Velcro interface with a more reliable mechanism that would not need the assistance of an astronaut to separate.

6.1.2.1 The Universal Docking Port

As introduced in section 1.3.2, each Universal Docking Port [85] (figure 6.3) is an androgynous non-symmetric interface, composed by a lance acting as a probe and a cavity behaving as drogue during the joining procedure. As the mating is accomplished and the lances enter the other port opening, a photosensor sense their presence and activate a linear motor, closing two metal cams around each lance and creating a rigid joint.

On UDP side, a small camera is mounted to allow vision guidance (right in figure,

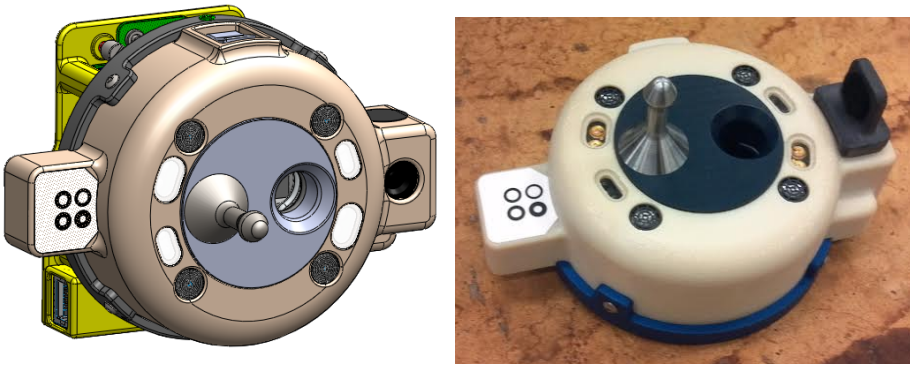

FIGURE 6.3: SPHERES Universal Docking Port, geometric draws on the left and flight model on the right (courtesy by MIT SSL)

covered by a protective black cap). Algorithms are in development, to use the marks present on the ports (left in figure, the four circles) to autonomously determine the relative distance and attitude during the rendezvous and docking operations.
The UDP should be sent on board the ISS in spring 2015, to be assembled to SPHERES an to be subjected to test, evaluating its behaviour and the developed navigation, rendezvous and docking algorithms. As part of its development, pre-launch tests on both the camera and the docking mechanism are scheduled on ground facilities. A first mating manoeuvre was tested on the MIT SSL glass table, with a chaser SPHERES able to reach the target and dock with it; in this simplified case, this target was fixed, and the chaser did use absolute navigation sensors instead of relative measurements.

6.1.3 SPHERES GN&C algorithms for rendezvous and docking

Algorithms for Guidance, Navigation and Control for rendezvous and docking have been developed since the first years of space exploration: as a good example, back in 1963 Buzz Aldrin's PhD thesis [86] dealt with manual line-of-sight guidance. As the space technology advanced, all GN&C changed and evolved, both implementing solutions from other engineering branches and developing brand new architectures.
As reviewed by Nolet [78], rendezvous and docking algorithms can be classified in four main groups: estimation, control, path planning and FDIR (Failure Detection, Isolation and Recovery). Estimators uses raw data from all the sensors to define the absolute and/or relative position of the spacecraft; on SPHERES, a Kalman estimator propagates the vehicle state associating sensors data when available. The advantages of such solution are a good time of convergence and its ease of implementation, but in case of non linear systems the Kalman estimator did not behave as desired and could diverge. About control, the available hardware on board of SPHERES (twelve thrusters) limits the suitable algorithms to Phase Plane, Linear Quadratic Regulator or PID/PWM (Proportional, Integrative, Derivative and Pulse Wave Modulation). The first one is only a sort of look-up table defining different commands at several initial conditions, while the second is a minimum cost function (optimizing, for example, propellant consumption). The latter one is implemented on SPHERES: PID/PWM is both the simplest solution and the more stable, but in terms of fuel consumption, it remains the most expensive. Path planning usually requires many computational resources to provide trajectories for satellite position and attitude: often it involves the solution of optimization problems. For this reason, often on SPHERES path planning cannot be used for real-time navigation: trajectories shall be evaluated off-line and then uploaded for test. One of the few exception is the glide-slope algorithm, commonly used on Apollo and Shuttle docking manoeuvres as a straight line approach is available: it prescribes a velocity pattern the chaser shall follow, using a pre-determined number of thruster pulse and reaching the target with zero relative velocity [87].
Last, at today FDIR algorithm for rendezvous and docking are still in development for implementation on board of SPHERES; usually they have high requirements in terms of computational resources or many different failure options, making them not always reliable for docking procedures, in which many non-linear events may happen (e.g.: contact/impact dynamics).

6.1.4 The Guest Scientist Program

The Guest Scientist Program (GSP) allows researchers from the whole world to develop their own projects in the framework of the SPHERES programme [88]. This is possible

thanks to a software interface that can be provided from the MIT, that gives the access to a complete simulation suite and to all the standard library functions for direct access to SPHERES sensors and actuators.

As visible in the logic diagram in figure 6.4, the Guest Scientist can develop its own

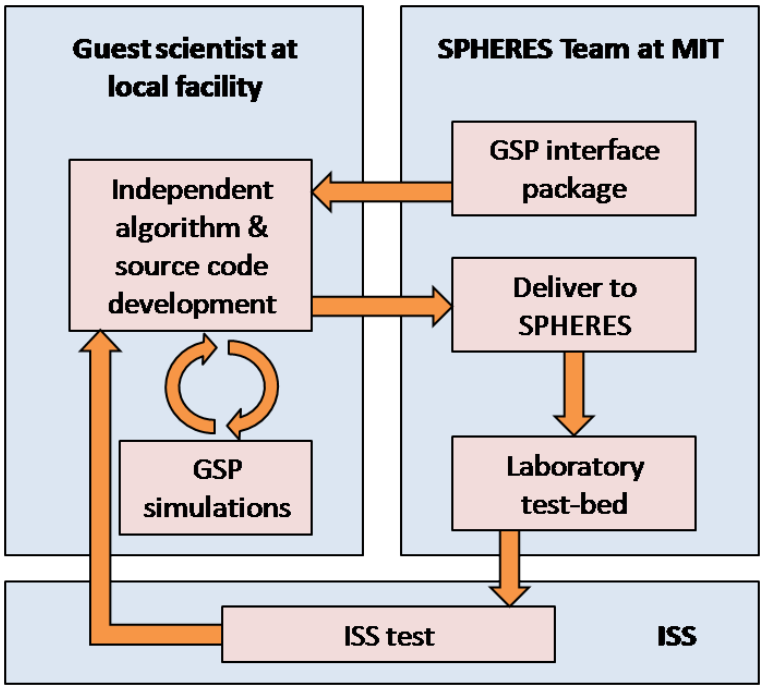

FIGURE 6.4: Guest Scientist Program logic: the code developed by the guest scientist is evaluated on SPHERES ground facility and then sent to ISS for test

project and simulate it without leaving its local facility. Pre-flight test can be performed by SPHERES team at MIT, on the low friction glass table at the Space Systems Laboratory. Last, test on board the ISS will close the loop, with the experimental results delivered to the investigator.

The GSP software provides real-time simulations, and, thanks to a graphic interface developed in Matlab® Simulink® environment, it can show geometric models of the SPHERES as they behave in real environment. This simulation engine can be used to evaluate the developed code in both the ground and microgravity conditions.

From the user point of view, the main element of the GSP software is a single file (gsp.c) in which the Guest Scientist can develop its code in C++ language. This file contains all the headers to access the SPHERES libraries (called SPHERES Core) and it is used both in the simulations and in the laboratory test, to be compiled and become part of on-board SPHERES software. In this way, the investigator is able to start to program and to develop its own research without advanced learning of SPHERES core and working principle, allowing to access the test phase as soon as the code is working in simulations. At the same time, many basic and advanced thrusters control, attitude and

position determination, navigation and telecommunication libraries are already available in the GSP software and the user can implement them as well as develop new ones.

6.2 Motivation and objectives

The possibility to collaborate with MIT Space Systems Laboratory was evoked from the beginning of this work, being the unique institute with a well developed investigation on docking technologies for small spacecraft. Unfortunately, only in the second half of the last year this opportunity realized in a two-months visiting period.
The research exposed in this document presented in some ways the same path that the UDP development has followed: for both the studies preliminary studies led to the definition of a first concept (for UDP as part of the SWARM project) and further progress allowed to realize a working prototype to be tested in a simplified laboratory facility. In this visiting period, I had the possibility to understand and observe the next steps in such development, from the realization and the assembly of flight-approved components, to their preliminary test to assess the interfaces behaviour in a controlled environment. Learning the methodology and the process behind the SPHERES management will be useful in the further development of the semiandrogynous docking port.

Tests performed in CISAS laboratories were able to furnish important data on the

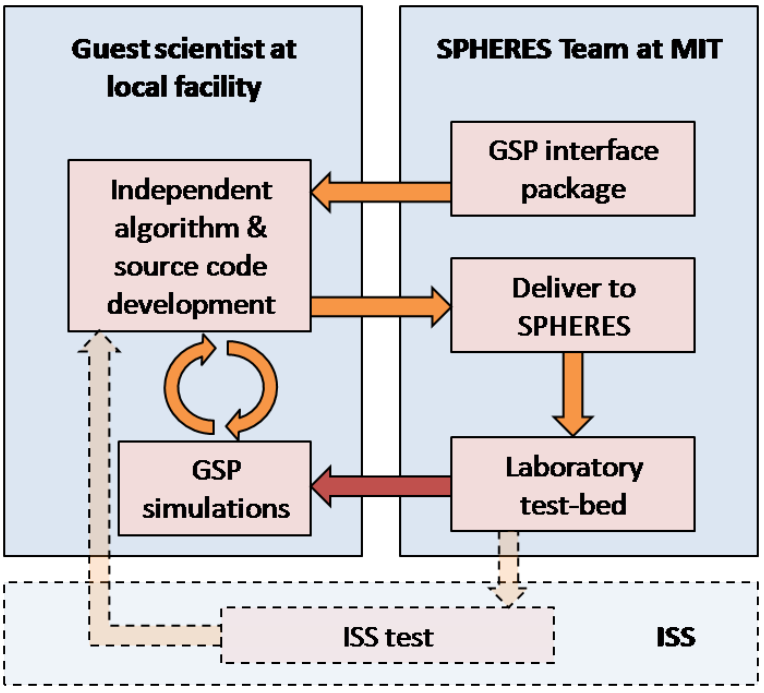

FIGURE 6.5: Modification respect to a standard GSP activity (see figure 6.4): the test loop is closed on data collected on the ground test bed

ports mechanisms behaviour, but at the same time their validity was limited due to the

reduced DoF of the test bed. Another drawback was that the interfaces were tested in open-loop, due to the absence of docking sensors and actuation on the test-bed. In reverse testing the UDP on SPHERES allows to work in a (2+1)-D close loop environment, with the possibility to program them as needed and collect experimental data as soon as the simulations are developed, reducing the delays usually correlated with test implementation.
This methodology also allows to organize the work on engineering process cycles, with a continuous feedback between theory and experimental data. Developed research can be tested as soon as the facility is available, and results can clarify and direct investigation to a continuous optimization.
Due to the limited amount of time spent collaborating with MIT, the GSP study logic presented in figure 6.4 was excessive, so a simplified work was developed, as shown in figure 6.5.

6.3 First code: close-loop navigation and rendezvous algorithm

The developed algorithm is based on previous models tested both on 2-D facilities and the International Space Station. The main script consist in a series of functions recursively called, commanding both chaser and target SPHERES, defining these manoeuvres:

1. estimator initialization: chaser and target determine their absolute position in the operative space;
2. far-rendezvous: chaser navigates to a way-point positioned in front of the target port;
3. alignment: chaser rotates to align its port with target's, maintaining the position;
4. approach: chaser gets closer to target, until the two interfaces are in contact;
5. docking: the two ports are actuated, creating a solid joint between spacecraft.

Respect to the first 2-D test, the main innovations presented are (1) the implementation of real-time communication to estimate the target position, (2) the utilization of a simple collision avoidance algorithm during the rendezvous phase and (3) the development of an extremely simple control law based on the glide-slope concept for the approach.

6.3.1 Real time communication

The utilization of the communication link between target and chaser allows to create a close-loop navigation algorithm. Before far-rendezvous (phase 2) the target communicates its position to the chaser, allowing to implement the collision avoidance manoeuvre in case of necessity. From phase 3 to 5 the target state is communicated once a second to chaser, allowing all the proximity operations.

6.3.2 Simplified collision avoidance algorithm

During the far-rendezvous, the chaser knows both position and attitude of the other vehicle, and it has to calculate the trajectory to reach the way-point in front of target port. The fastest trajectory consist in a straight line from chaser position to way-point, but it can happen that the calculated path could cross the other SPHERES volume. In this case, a simple collision avoidance algorithm calculates intermediate way-points until the straight-line approach becomes allowable.
In more details (see figure 6.6), the chaser, located in point $1(x_1, y_1)$ first of all calculates the straight-line approach to way-point $W(x_w, y_w)$. Defining $a_1 = y_w - y_1$ and $b_1 = x_w - x_1$, the line connecting point 1 and W can be described as:

$$\mathbf{1W}: \ a_1(x - x_1) + b_1(y - y_1) = 0 \tag{6.1}$$

The target position $0(x_0, y_0)$ is used to define the line connecting target and way-point W:

$$\mathbf{0W}: \ a_0(x - x_0) + b_0(y - y_0) = 0 \tag{6.2}$$

where $a_0 = y_w - y_0$ and $b_0 = x_w - x_0$. First, the chaser shall define if it is located in the part of $X - Y$ plane in front of target docking port (in white in figure 6.6), that can be calculated as:

$$b_0(x_1 - x_0) - a_0(y_1 - y_0) > 0 \tag{6.3}$$

being $b_0(x - x_0) - a_0(y - y_0) = 0$ the line orthogonal to **0W**.

In case the chaser is not in the safe zone (blank in figure 6.6), it is defined a circular exclusion area around the target that cannot be crossed (figure 6.7). Defining ρ the radius of such area, it can be compared with the minimum distance d between the approach line and target centre (x_0, y_0):

$$d = \frac{(a_1(x_0 - x_1) + b_1(y_0 - y_1))}{\sqrt{(a^2 + b^2)}} \tag{6.4}$$

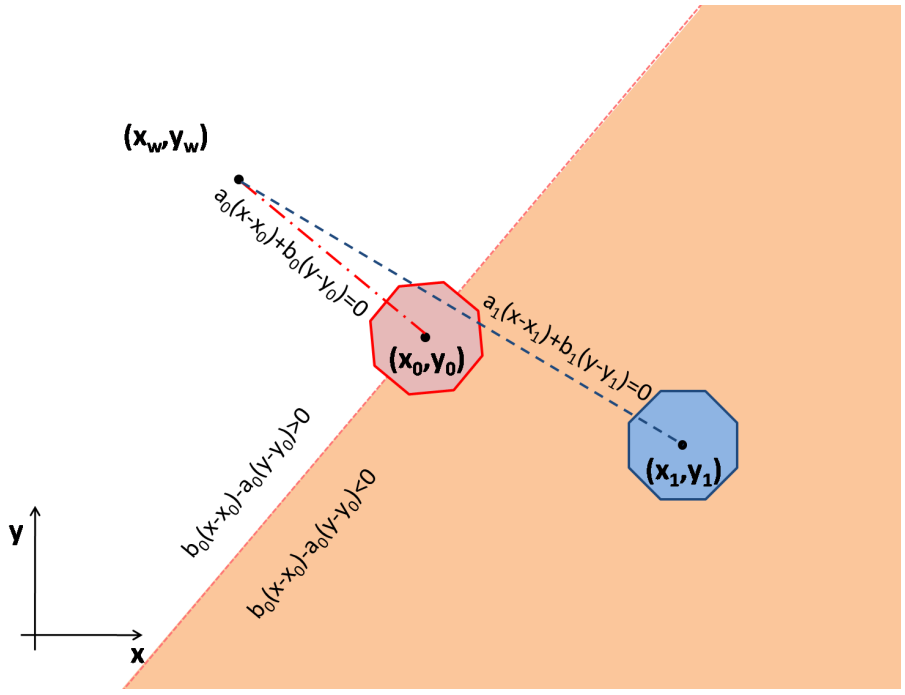

FIGURE 6.6: Geometry references and main lines

To simplify computation avoiding square roots, the comparison is calculated between the squares of d and ρ:

$$[a_1(x_0 - x_1) + b_1(y_0 - y_1)]^2 > \rho^2 \cdot (a^2 + b^2) \tag{6.5}$$

If this condition is not fulfilled, a safe way-point W_1 is calculated. The W_1 way-point lies on a line orthogonal to **1W** and passing in target centre. The distance between the target centre and point W_1 is $1.5 \cdot \rho$, the safe zone radius, if the chaser is far from target, and increases as chaser is getting close, avoiding possible intersections with the exception area. This is made possible calculating the square of the distance between target and chaser L_{01} and defining a gain factor (tuned by simulations):

$$L_{01} = (x_0 - x_1)^2 + (y_0 - y_1)^2 \tag{6.6}$$

$$gain = 1.5 + \frac{0.03}{\rho \cdot L_{01} - \rho^3} \tag{6.7}$$

With this informations, it is possible to calculate the way-point W_1 coordinates:

$$y_{W1} = \pm \frac{b_1 \cdot \rho \cdot gain}{\sqrt{(a_1^2 + b_1^2)}} + y_0; \tag{6.8}$$

$$x_{W1} = -\frac{a1}{b1} \cdot (y_{W1} - y_0) + x_0; \tag{6.9}$$

The equations return two possible solutions, representing two points on each side of the

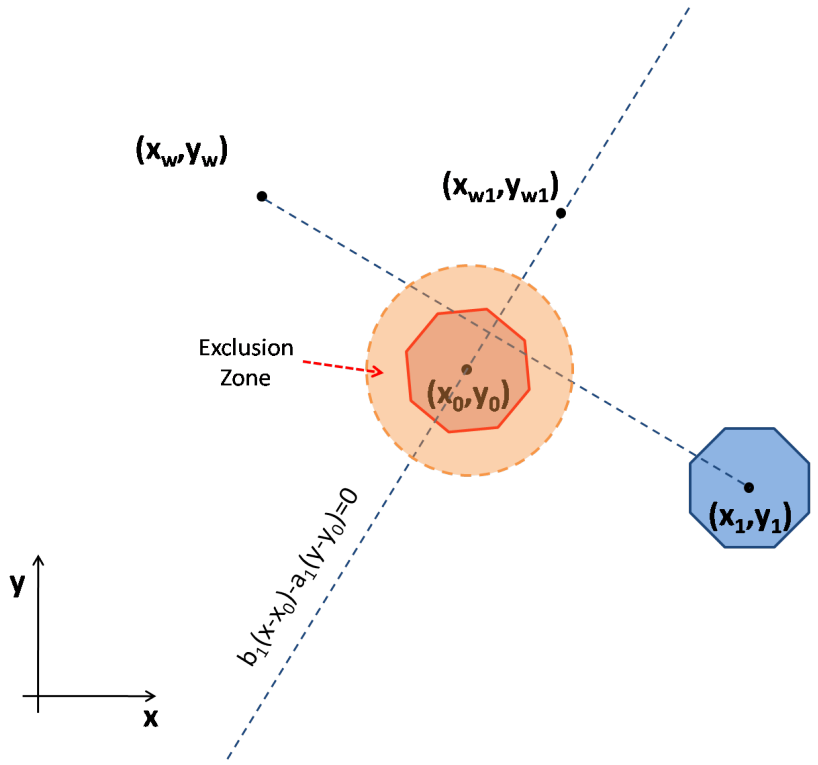

FIGURE 6.7: Exclusion area definition: way-point W_1 is calculated if the straight-line path between chaser and way-point W is not allowed

target centre, so a simple comparison leads to the definition of W_1 as the nearest to the chaser.

This whole procedure is executed every one second, recalculating the way-point respect to the chaser updated position, until the straight-line approach becomes allowable. The algorithm is simple and fast, consisting in only elementary operations like sums and products. The only square root, present in the way point calculation, is solved by a recursive sub-algorithm, further reducing the computation time.

Before implementing in SPHERES simulation tool, the algorithm has been widely tested through Matlab simulations. As visible in figure 6.8, the chaser calculates intermediate way-points W_1 at every simulated step, avoiding the target exclusion zone until it can reach by a straight-line trajectory the way point W. Simulations also demonstrate that for small target movements (e.g. velocities less than one tenth of chaser maximal velocity) the algorithm is able to avoid collisions.

6.3.3 Approach control law

At today, most of path-planning and navigation algorithms for target approach are based on the glide-slope concept, that is both a velocity control and a trajectory planner. The idea is to approach to the target with velocity decreasing with distance. Defining ρ the

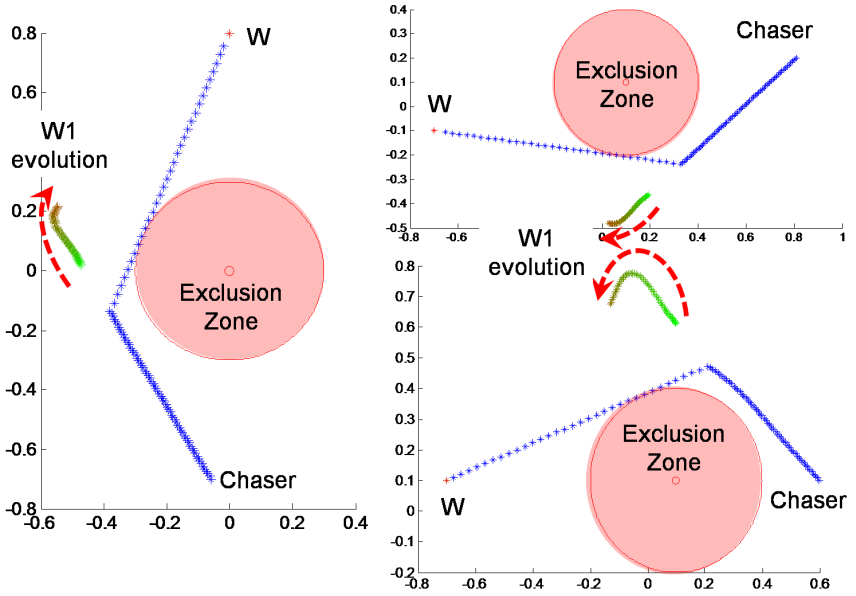

FIGURE 6.8: Chaser elaboration of intermediate way-point W_1 (green to brown) during the collision avoidance manoeuvre (blue), three different examples

distance between target and chaser and ρ' the chaser velocity, the glide-slope equation can be defined as:

$$\rho' = a \cdot \rho + \rho'_T \tag{6.10}$$

where ρ'_T is the target speed and $a < 0$ is the glide-slope. In the simple 2-D test, ρ'_T can be considered negligible, so the equation can be rewritten as:

$$\rho' = a \cdot \rho \tag{6.11}$$

and, considering ρ'_0 and ρ_0 the manoeuvre starting condition, the glideslope can be defined as

$$a = -\frac{\rho'_0}{\rho_0} \tag{6.12}$$

The approach manoeuvre is then defined in three different stages:

1. the approach velocity is commanded to a value v_0 for the first 10 seconds;
2. the system evaluates both the real values of ρ'_0 and ρ_0, allowing to calculate the glide-slope a;
3. the velocity is commanded with the glide-slope law $\rho' = a \cdot \rho$.

The utilization of this kind of control allows the chaser to approach with a decreasing velocity and at the closest ranges reduces the thrusters plumes respect to other control

laws. Simultaneously a derivative control is implemented to avoid lateral misalignment due to the non ideal thrusters behaviour and numerical errors. In this case, a velocity control acts in the direction of the misalignment. The port axis is defined by its rotation ψ respect to the inertial frame, so the axis equation is:

$$r: \ (x - x_0)\sin\psi - (y - y_0)\cos\psi = 0 \tag{6.13}$$

with (x_0, y_0) the target coordinates; $\sin\psi$ and $-\cos\psi$ are respectively the two coefficients a and b in the implicit line equation $ax + by + c = 0$. First, d is defined as the distance between the port axis and the chaser, located in (x_1, y_1):

$$d = \frac{r(x_1, y_1)}{\sqrt{a^2 + b^2}} = \frac{(x_1 - x_0)\sin\psi - (y_1 - y_0)\cos\psi}{\sqrt{\sin^2\psi + \cos^2\psi}} \tag{6.14}$$

$$= (x_1 - x_0)\sin\psi - (y_1 - y_0)\cos\psi \tag{6.15}$$

The main advantage of this formulation is that the sign of d can determine the position of the chaser respect of the docking port axis. The control is again applied to the velocities, in this case in the direction normal to the axis, defining:

$$v_c = -d \cdot gain \tag{6.16}$$

$$v_{cx} = v_c \cdot (-\sin\psi) \tag{6.17}$$

$$v_{cy} = v_c \cdot (\cos\psi) \tag{6.18}$$

with a gain tuned to avoid excessive oscillations around the axis.

6.3.4 Simulations and test

During the simulation campaign, the developed code was tested to study its behaviour at different initial condition. The simulation tool allowed a real-time observation of SPHERES virtual environment, permitting rapid tuning and fast modifications.

In figure 6.9 is visible the output of one complete simulation, in terms of attitude and position. For both the SPHERES, the z coordinate is constant at about 0.8 m (being all the developed code designed for verification on the low-friction table) as well as the pitch and roll angles values, with negligible oscillations caused by sensors noise; being the target not moving, all of its coordinates are fixed. To better explain the chaser movements, it is useful to plot its position in a Cartesian reference, as reported in figure 6.12: here the chaser position is plotted with a chromatic scale (from blue to yellow to red) to indicate time advancement. The position estimation (number 1 in figure) process last 10 seconds and initialize in both the SPHERES the attitude and position

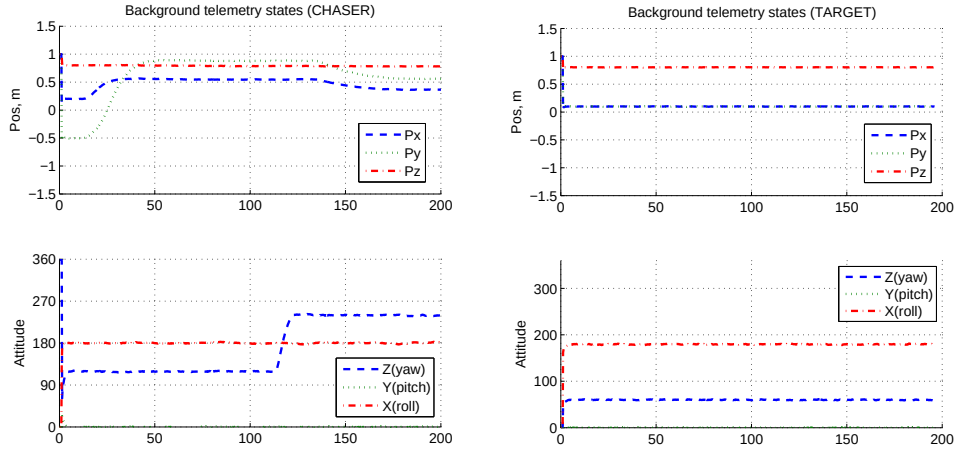

FIGURE 6.9: Complete approach manoeuvre simulation: the chaser (position and attitude data on the left) is commanded to avoid the fixed target (right), perform far rendezvous, and then dock to target

estimation algorithm; after that, the chaser is ready to receive target state information and move to the far rendezvous way-point (manoeuvre 2), in this case calculating the collision avoid path beforehand introduced. The third phase consists in the alignment of the chaser docking port with target's (visible in figure 6.9 between 110 and 120 s as a rotation around the Z axis); in the end, the glide-slope approach (4) permits to reach the docking position (5).

Manoeuvre 4 is shown in figure 6.11: the relative distance trend shows, as expected from the glide-slope, an exponential evolution, resulting in a safer close approach; the oscillations visible in the velocity plot are related not only to the thrusters modulation, but also to the lateral misalignment control law.

Another simulation analyses a simpler case, without the need of the collision avoidance manoeuvre (figure 6.12). Here again the target is fixed, and the chaser follows the five-phases rendezvous and docking. This case was chosen for the first test on the low friction table.

Figure 6.13 shows results from the test (solid line) and compare them to the previous simulation (dotted line). As visible, the test was not successful, with the target not able to reach the required position nor to align with the other docking port. More remarkable, the target coordinates values showed an excessive oscillation, probably caused by an hardware bug to be fixed.

In conclusion, results from both simulations and test demonstrated that the algorithm is working under standard conditions (e.g. reduced noise) but did not allow to perform a complete docking manoeuvre on the low friction table. On these basis, a novel algorithm was defined, as visible in next section, implementing a longer initialization time, deleting the collision avoidance manoeuvre (as useless in simple tests), and last defining a docking

failure detection, to determine if the two SPHERES have excessive misalignment and, in case, reinitialize the docking procedure without restarting the whole test. Further simulations and test were also planned as well as an investigation of the SPHERES navigation hardware.

6.4 Second code: simplified approach and failure detection

On the results form the first test, a second algorithm has been developed to afford the detected issues; the proposed code consist in 5 manoeuvres:

- estimator initialization.
- far rendezvous: the chaser aligns orientates the docking port to target.
- approach: the chaser reaches the docking position.
- holding: the chaser maintains its docked position for a fixed time.
- separation: the chaser returns to the far rendezvous way-point.

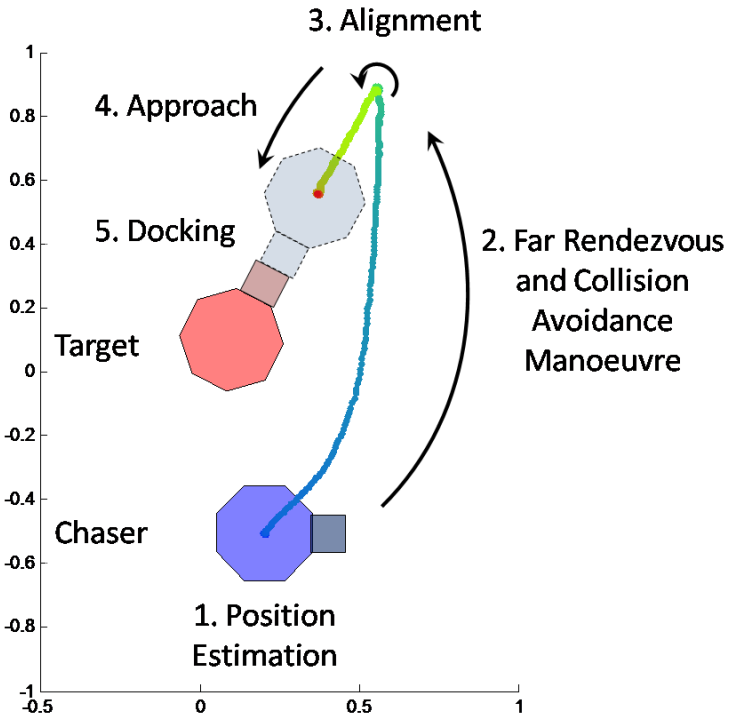

FIGURE 6.10: 2-D representation of previous manoeuvre: after estimator convergence (1) the chaser is commanded to reach the far rendezvous way-point avoiding collision with the target(2); docking ports alignment follows (3) to allow final approach (4) and docking (5)

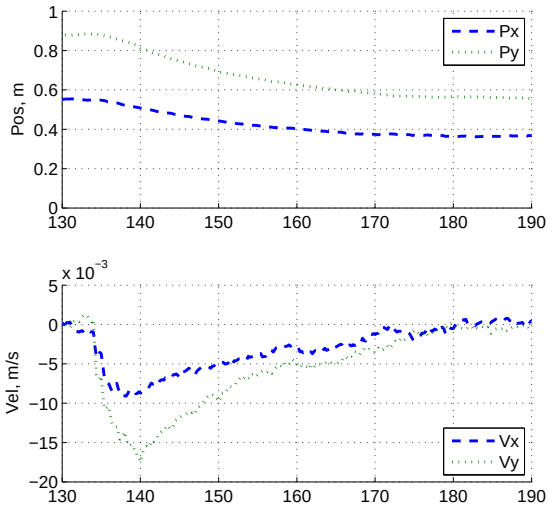

FIGURE 6.11: Chaser-target relative position and velocity: in manoeuvre 4 the chaser approaches the target with velocity decreasing with the distance

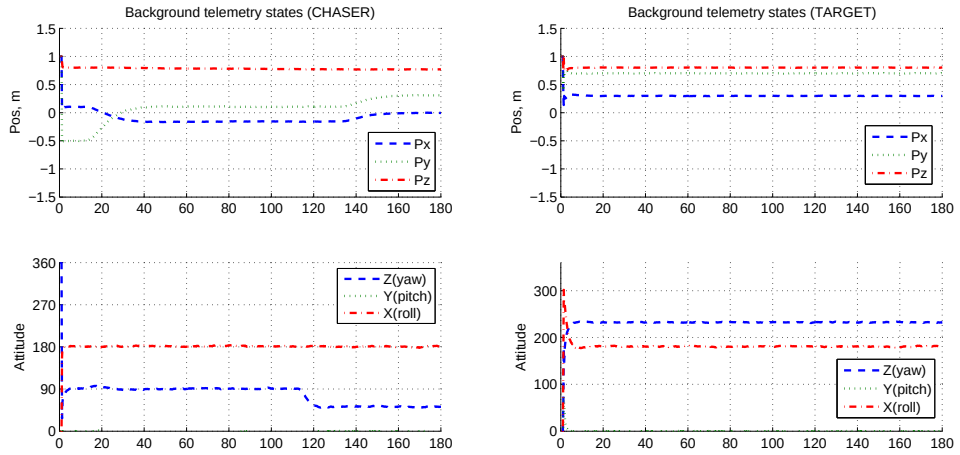

FIGURE 6.12: Simple approach manoeuvre simulation: in this case, the chaser does not need collision avoidance manoeuvres to perform the far rendezvous

Considering that the docking port is not symmetric, the docking approach does not follow the docking axis but presents a misalignment of about 4 ° opposite to the port lance, as visible in figure 6.14.

6.4.1 Docking failure avoidance

In parallel to the main algorithm, a simple code controls the docking phase, monitoring excessive misalignments between the two ports: if the chaser moves out of the approach cone (the triangle visible in figure 6.14), it returns to the far rendezvous way-point and

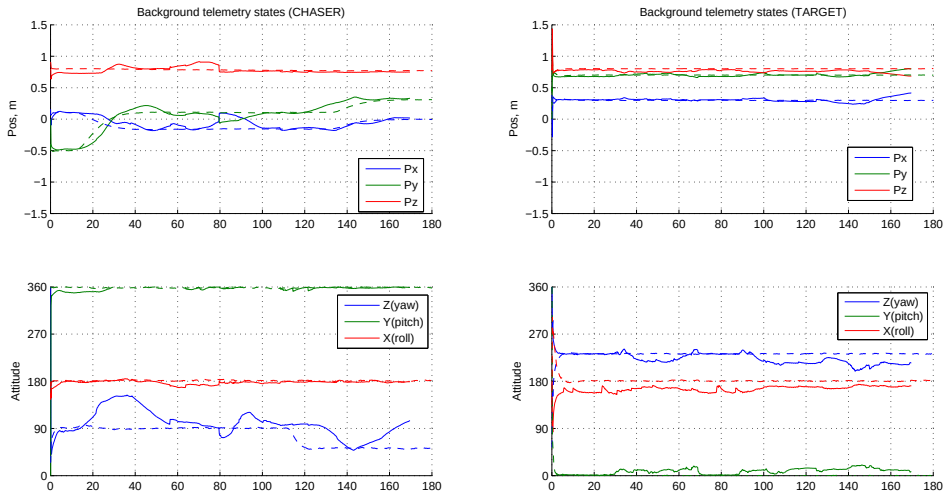

FIGURE 6.13: Comparison between simulation and test results: the position and attitude signal presents much more noise than expected, comporting in the failure of docking procedure

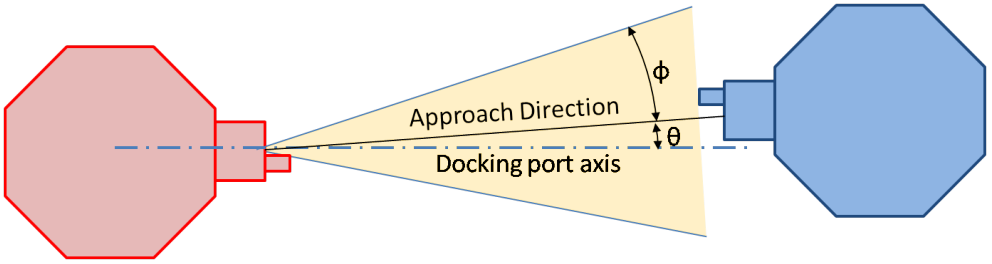

FIGURE 6.14: Geometry of approach line respect to docking axis

retries the approach for at most two times, before aborting. The safe zone is in the range of $\pm 11.5\,^{\circ}$ from the approach line, and it is defined as follows. Defining (x_1, y_1) and (x_2, y_2) the position of chaser and target centres of mass, R the distance between the centre of mass and the port, and α_1 and α_2 their attitude respect the X axis, the docking port centre coordinates can be defined respectively:

$$P_1 = (x_1 + R \cdot \cos\alpha_1;\ y1 + R \cdot \sin\alpha_1) \tag{6.19}$$

$$P_2 = (x_2 + R \cdot \cos\alpha_2;\ y2 + R \cdot \sin\alpha_2) \tag{6.20}$$

and the target docking port axis as:

$$r:\ (x - P_{2x}) \sin\alpha_2 - (y - P_{2y}) \cos\alpha_2 \tag{6.21}$$

The approach direction line passes for P_2, but it has an angular misalignment of $+\theta$, so its equation can be written as:

$$r_1 : \ (x - P_{2x}) \sin \alpha_2 + \theta - (y - P_{2y}) \cos \alpha_2 + \theta \tag{6.22}$$

with θ close enough to zero, such simplifications can be accepted:

$$\cos \theta = 1 \tag{6.23}$$

$$\sin \theta = 1 \tag{6.24}$$

and then:

$$r_1 : \ (x - P_{2x}) \cdot (\sin \alpha_2 + \theta \cdot \cos \alpha_2) - (y - P_{2y}) \cdot (\cos \alpha_2 - \theta \cdot \sin \alpha_2) \tag{6.25}$$

Now, defining d as the distance between r_1 and P_1 and L as the distance between P_1 and P_2, it can be defined:

$$\tan \phi = \frac{d}{L} \tag{6.26}$$

and if ϕ is in the range $[-11.5\,^\circ; +11.5\,^\circ]$, the point P_1 is in the safe area.

6.4.2 Simulation and test

Before testing the developed algorithm, some minor modifications on both the attitude/position determination code and SPHERES hardware were performed, allowing to improve the signal as visible in figure 6.15. The position coordinates oscillation is reduced to about 1 cm, into the SPHERES design limits; about attitude, the oscillation amplitude is again well reduced, but collected data are still too noisy respect the expected values, that should bye less than 1 degree.

Nevertheless, thanks to these improvements, some test were performed to validate the new code. In figure 6.17 a comparison with simulation data and results collected from laboratory test is visible. Again, the numerical evaluation demonstrated the algorithm robustness, but the experimental verification was not similarly satisfying: the trajectory shows continuous oscillations and the chaser was not able to dock with the target. Furthermore, the z coordinate (red in figure), that should be constant during the whole test, shows an unexpected change during the test, indicating an error in the position estimation; a similar behaviour is visible in the attitude data, as the roll angle variation indicates.

In conclusion, results confirmed that some issues, probably related to the SPHERES hardware or the state estimator, are affecting the facility; further investigation should be dedicated to solve such problems. Due to the conclusion of the visiting period, the

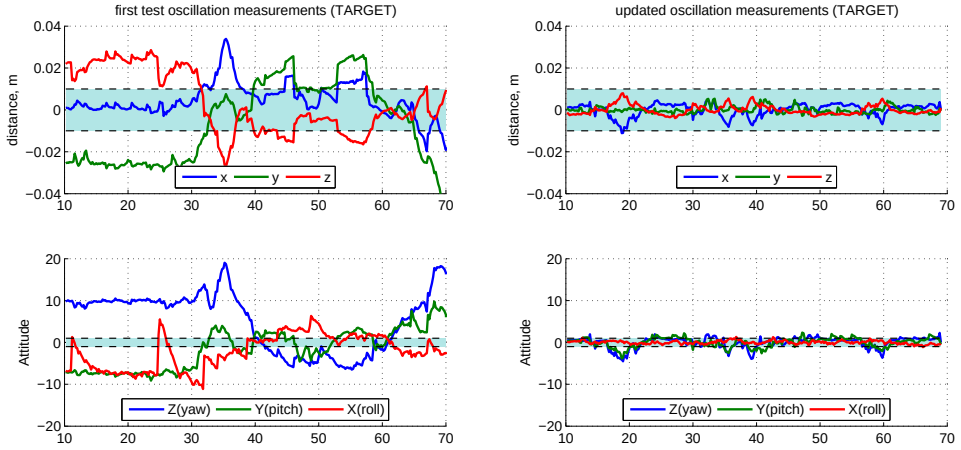

FIGURE 6.15: Variation on data oscillation between first test and updated set-up: working on both the code and the SPHERES hardware, the position coordinates oscillation is reduced to the expected level, although results are still not satisfactory for the attitude

experimental activity ended with this test; the UDP ground test was postponed to the first months of 2015.

6.5 Results discussion

The visiting period, although only two months long, gave the unique opportunity to work in collaboration with a research group investigating rendezvous and docking technologies, allowing to understand the methodology behind SPHERES development and management. The fast availability of SPHERES test bed is surely a great advantage in the organization and evolution of a research project, allowing accurate comparison between simulations and test during the whole design and development. Unfortunately some issues related to the SPHERES state determination affected the system during the test campaign, preventing the complete verification of the developed code.

A brief comparison between the UDP and the semi-androgynous docking port can be introduced, to better comprehend the different design logic that led to the two solutions. The UDP was developed to work on SPHERES, so it presents both the mechanical interface and the required electronics and sensors to be integrated on such support. On the contrary, the semi-androgynous interface was tested on a simpler test-bed, and did not employ any navigation or docking sensor; in the conclusive chapter this topic will be better introduced.

Another feature of the UDP, directly correlated to the SPHERES characteristics in terms

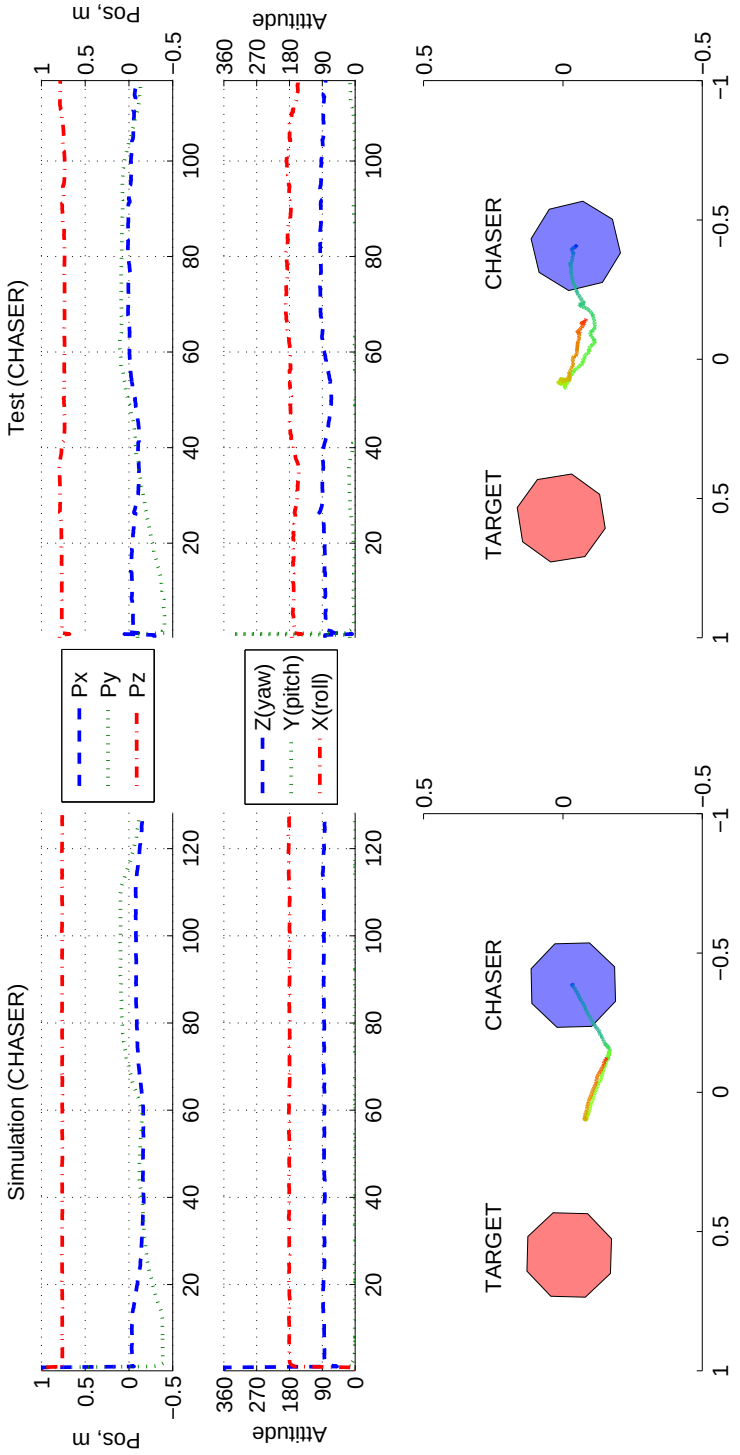

FIGURE 6.17: Comparison between simulation (left) and test results (right): experimental data shows higher noise, affecting the manoeuvres. From top to down: position, attitude, and 2-D trajectory reconstruction

of navigation precision, is its reduced tolerance to misalignment: the solid joint between two ports is created through the mutual capture of the long lance penetrating a hole acting as drogue, required a precise alignment. There are no indications on UDP documents on the allowed misalignment range, so a first estimation was performed comparing the geometrical shape of lance and hole. First of all, the axial limit was evaluated as the external diameter of the hole countersink, considering that the hole shape could act as redirecting drogue; later, during some test on the glass table it was noted that the probe bounced off instead of realign, probably due to the inclination of the countersink. On this consideration, it was evaluated that the maximal allowable misalignment for the lance is equivalent to the hole diameter, minus the radius of the curved part on the lance nose tip, resulting on about 5 mm. The allowable angle is again estimated from the lab experience, but further investigation would be required; the operative range was then calculated as the area limited by these values. About the semi-androgynous port, test results in terms of allowable lateral misalignment were scaled, due to the minor dimensions of the UDP, while angular values were maintained. Results are visible in figure 6.16: the semi-androgynous port (in green) shows larger limits respect to the MIT port, thanks to the different geometry and capture logic.

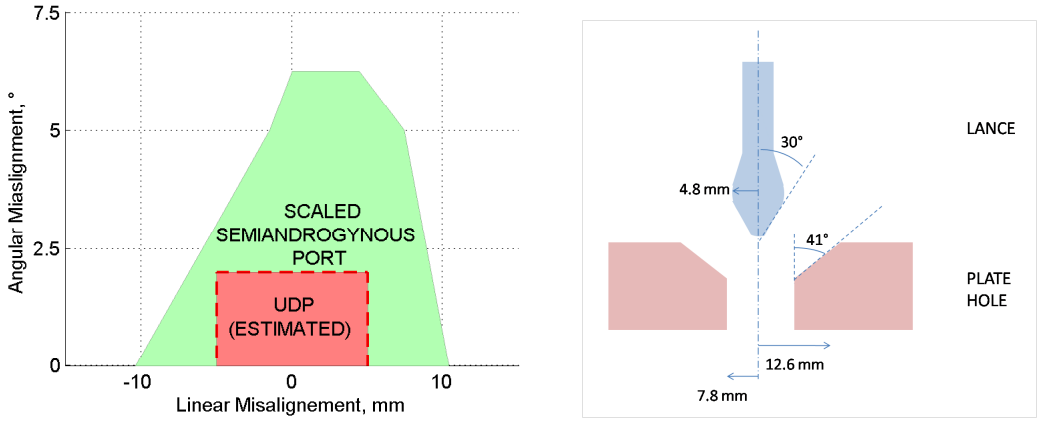

FIGURE 6.16: On the left, comparison between semi-androgynous port (scaled, in green) and UDP operative ranges (estimated, in red), on the right UDP lance and hole dimensions

Chapter 7

RESULTS AND CONCLUSIONS

The design and test process depicted in this work are here briefly summarized, presenting the advantages of the semi-androgynous configuration and the results collected in the laboratory analysis, that allowed to reach a Technology Readiness Level of 3-4. On the experience acquired during both the research and a visiting period at MIT Space Systems Laboratory, some observations are presented, related to the test in a more relevant environment and the design of dedicated sensors for close navigation and docking. In parallel, other activities on docking are reported. First, an improved version of the SAM is presented, with rotating actuation instead of the linear motor to reduce the interface bulk. Second, the concept of tethered soft docking is described, consisting in employing a magnetic tether probe to perform the soft docking procedure, significantly simplifying the spacecraft joining operations and reducing the system complexity; preliminary activities on such topic included the FELDs experiment, aiming to assess the automatic self-alignment of the probe in 0-g environment.
In conclusion, a long research work is still to be performed, aiming to reach higher TRLs; some indications on future development are introduced, considering the continuously increasing interest on small spacecraft rendezvous, docking and, more generally, proximity operations.

7.1 Results and Discussion

In this document the design and test of a novel docking system for small satellites was presented. A trade-off between requirements and constraints led to the definition of the semi-androgynous architecture as the most promising solution for spacecraft joining mechanisms: it merges the advantages of both gender-mate and androgynous solutions, allowing a simple geometry and the capability to dock with every similar interface,

thanks to its shifting from a close configuration to a drogue shape, that allows to enclose and capture another non actuated port to create the solid joint. The proposed solution uses only one actuator, capable to open and close eight petals thanks to sliding cam mechanisms, and can create a pre-load on the contact interface to increase the stiffen of the joint.

The utilization of a single linear motor to simultaneously actuate the eight petals is then one of the key features of the proposed mechanism; however, the advantages of simplicity and low mass were counterbalanced by a reliability issue, because the failure of one of the petal cams or of the motor could result in the hamming of the whole mechanism. On these considerations, a brief risk analysis was performed and some technical solutions to increase the mechanism reliability were analysed, although they were not implemented in the tested prototype.

Numerical simulations were developed to evaluate the effect of cam frictions on the actuation dynamics, analysing rigid bodies kinematics and defining low required forces (always under 1 N). Tests on a simplified test-bed demonstrate that simulations results were comparable with collected forces output, and allowed to define the mechanism working range in terms of maximal allowable angular and lateral misalignments that can still lead to a nominal docking, as reported in section 5.4.3 and in figure 7.1. It is visible that the docking ports can manage up to 5 ° or 15 mm of misalignment.

In parallel, a visiting period at MIT Space Systems Laboratory allowed to study the

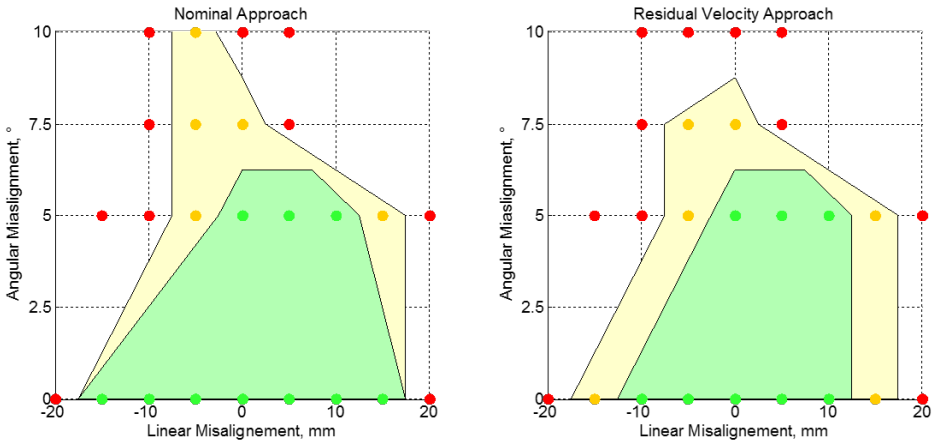

FIGURE 7.1: Alignment ranges to perform a complete docking procedure with null relative velocity (left) and residual relative velocity (right) in the axial direction between chaser and target, as reported in section 5.4.3

SPHERES test-bed, developing and simulating control codes for the Universal Docking Port ground test. The experience allowed to understand the UDP development and management strategy in the wider framework of SSL activities. At the end, a comparison between the SAM and the UDP demonstrates that the latter, due to the different working logic, has a smaller range in terms of accepted angular and lateral misalignments at

docking.
The developed port has reached a TRL of about 3-4, with the demonstration of a prototype on a simple test-bed in laboratory environment; this work produced other interesting outcomes, indicating the direction future investigation shall follow. First of all, a more relevant test environment is required, to increase the interface TRL and demonstrate its capabilities, and in parallel studies on rendezvous and docking sensors for small spacecraft shall be performed, to create a more complete system suitable for close navigation and joining.

7.2 Future works

Next steps in the development of the SAM are related to the test in a more relevant environment and the design of dedicated sensors for close navigation and docking; in this section, such task are briefly introduced, indicating the preliminary activities performed at the end of the research period and the foreseen following steps.

7.2.1 Test-bed

As reported in section 5.2.1, different test-beds can be used to perform docking simulations, with distinct outcomes in terms of collected data. The SAM was tested in controlled environment, in the lab, on a simple one-plus test-bed, allowing to measure involved forces during the actuation and docking procedure, but still being subject to gravity acceleration. Further test shall be performed in more performing test-bed, for example the 3-D robotic arm in development at CISAS, [76], in order to better analyse the contact dynamics between the two ports and simulate 0-g behaviour; similarly, parabolic flight tests could be the only milligravity facility in which flight duration (up to 30 seconds of low gravity, more than three times ZARM drop tower [89] despite higher residual gravity) and repeatability (usually several parabolas are performed in a single flight) should allow a complete verification of the docking mechanism.
Last, respect to the performed work, an important improvement to implement is the utilization of a closed-loop test facility, instead of the open loop one; advantages lies in the possibility to study the performance of the mechanism through navigation and control techniques, improving the accuracy of the collected results. This development would also require the study and the realization of dedicated sensors for close rendezvous and docking.

7.2.2 Close navigation Sensors

As previously introduced, sensors should be developed for the navigation and rendezvous of small satellites. At today, state-of-the-art technology consist in European ATV's navigation sensors suite, composed by GPS receivers for absolute and relative position determination in far rendezvous, and an optical sensor for close manoeuvres, called Videometer [90]; last, on ATV-5 some test were performed, to study the possible utilization of lidar technologies [91].
Thanks to the increasing miniaturization of Global Navigation Systems (GNS) antennas and electronics, CubeSat-based boards are being realized to determine absolute position [92]; the relative position estimation through GNS is also in development [93]. In parallel, at CISAS studies are being performed to include absolute GNS attitude determination for small satellites; preliminary results demonstrate that such technology has a promising future, and could be implemented for proximity operations and more generally CubeSat position and attitude determination.
In the optical navigation, preliminary studies were performed on ARCADE experiment [94], testing an optical sensor composed by an infrared LED transmitter mounted on the target, and two photodiode receivers mounted on the chaser. Laboratory tests assessed the sensor performance and range of application, showing an accuracy of less than 2 mm and 1° in the range of $0.2 - 0.4$ m.
In parallel, navigation based on visual imaging is under development by different research groups; for example, at MIT Space Systems Laboratory in the framework of the SPHERES program the Vertigo project aims to develop computer vision based navigation [83]. More interesting, the UDP port implements a navigation camera, to perform vision guidance in docking operations [85]: as visible in figure 6.3, each port camera uses four circular marks presents on the twin port to autonomously determine the relative distance and attitude.
In the framework of the SAM port development, it is planned to investigate navigation sensors following two different lines: GPS navigation for rendezvous and visual navigation for close manoeuvre. About the first one, a test board will be realized, to asses the real performance of absolute GNS attitude and position determination and compare results with of-the-shelf sensors for CubeSat and small spacecraft. Studies will be also performed to implement a hybrid system consisting in LED emitters and visual navigation: the preliminary concept is composed by four LEDs positioned on one interface to form a L shape, and a camera on the other port; using a simple filtering algorithm to elaborate the captured image it is possible to determine the relative distance and angular misalignment.

7.2.3 Docking sensors

Another investigation to be performed is related to the development of a suite of sensors that would be able to determine if a docking manoeuvre is correctly performed and the solid joint is created. In SPHERES UDP, an infra-red fork sensor positioned in the interface hole is used to verify that the lance penetrates the port, creating the solid joint. Being a peripheral mechanism with axis-symmetry, the SAM cannot implement a similar sensor, so different solutions shall be investigated; during the test campaign, only a visual check was performed to evaluate the manoeuvre results. Two different solutions should be investigated, to realize a good reliable sensor: the implementation of a peripheral system able to detect the contact between petals, consisting in a series of electric contacts that create a close circuit only if the docking procedure is positively concluded, or the measurement of the pre-load acting on the docking interface. Last solution could be implemented both on the current prototype (measuring the distance variation between the Actuating Disck and the docking interface) or in case of substitution of the spring system with an elastic interface (mounting embedded force or deformation sensors into it).

7.2.4 Refuelling interface

Last, one of the most critical operations in servicing missions is surely the refuelling [3] [4], due to the elevated involved pressure and the consequent need of watertight joints; at today, there is no standard refuelling interface nor it is planned to realize one common servicing valve, easy to access for fluids exchange. In this framework, studies should be performed to add a dedicated and independent refuelling mechanism to the SAM, that in the docking phase would be able to create the required sealed connection. In order to maintain the semi-androgyny concept, this system should be realized as a movable probe, that could be extracted from one interface to penetrate the other one, as visible in figure 7.2: in the non actuated configuration (left) the two refuelling interfaces are not active, and they are not involved in the docking procedure; after mating, one of them is moved, in order to penetrate the other port interface. Two seals are designed to create the watertight joint, allowing the fluid exchange. The most critical aspects that the design and the tests should evaluate are related to the actuating mechanism and to the maximal allowable pressure the interface could maintain without leaks.

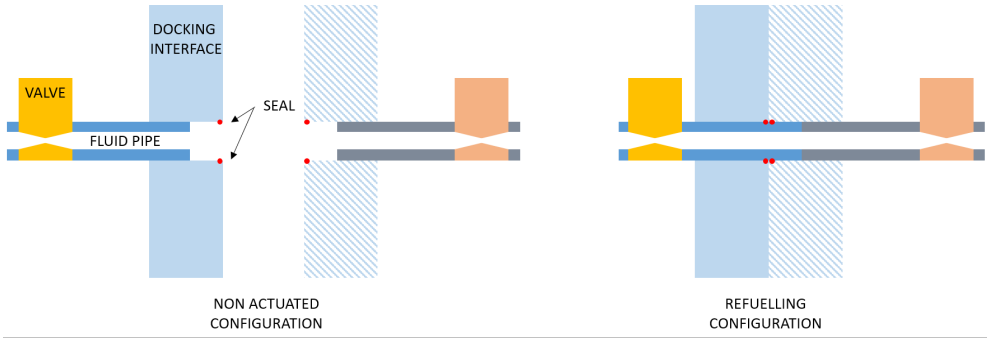

FIGURE 7.2: Preliminary concept of the refuelling mechanism: in the non actuated configuration (left) the two refuelling interfaces are not active; after mating (right), one of them is actuated to penetrate the other port interface, creating a watertight joint thanks to seals.

7.3 Related works

In parallel with the presented work, some other investigations are in development in the framework of small satellite docking. In this section, two different concepts will be introduced,(1) a more compact semi-androgynous port based on two rotative elements instead of a linear motor, and (2) the new idea of tethered soft-docking.

7.3.1 New semi-androgynous port

In the development of the semi-androgynous port, the utilization of a linear actuation was chosen to give the interface the shape-shifting capacity; to simplify the design, an off-the-shelf motor was implemented instead of a custom smart materials actuator. In this section, a different approach is proposed: considering that linear actuations usually require longer and bulker drivers than rotative ones, a new interface design was realized, using rotative cams to perform the petals opening and closing. In figure 7.3 a preliminary sketch of the actuation mechanism is showed: the two counter-rotative disks, actuated by independent motors (not showed), are able to open and close the petals, transforming the rotational movement into a translational one thanks to cam mechanisms.

The development of this concept into a testing model should pass through a complete dynamical simulation of the cam mechanisms, that would led to a optimized geometric design. The realization of the main elements could be again performed with 3-D printing, allowing fast prototyping to perform the preliminary test as soon as the geometries are defined.

The resulting mechanism should maintain the advantages of the already developed semi-androgynous interface, adding reduced bulk and mass thanks to the simpler design, simplifying its implementation in scaled versions for both CubeSat and larger spacecraft.

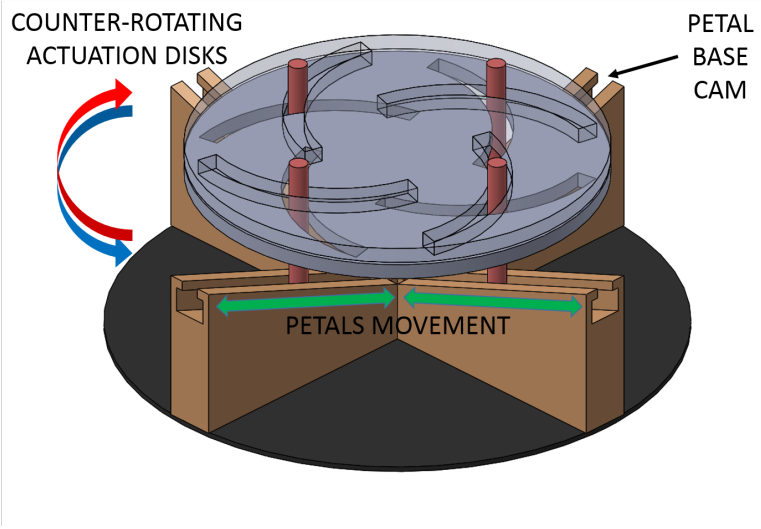

FIGURE 7.3: Rotative semi-androgynous port concept: the actuation to open and close the petals is given by two counter-rotative disks, actuated by independent motors (not showed), that transform the rotation into a linear movement thanks to a cam mechanism; petals heads are not inserted in figure.

7.3.2 Magnetic tethered soft-docking

An innovative approach to docking consists in employing a magnetic tether probe to perform the soft docking procedure, significantly simplifying the spacecraft joining operations and reducing the system complexity[95]. The concept, visible in figure 7.4, aims at reducing the proximity navigation and guidance requirements between chaser and target spacecraft, thanks to the use of a tethered probe that is ejected by the chaser and employs magnetic forces for automatic self-alignment and soft docking with the receiving interface on the target. After the achievement of soft docking, the tether provides a low stiffness connection between the two spacecraft, thus greatly reducing forces transfer. The tether finally allows to safely mate chaser and target simply by rewinding it, after the two-bodies dynamics has been stabilized. The advantages of the new concept will contribute to enable a large number of future on-orbit servicing missions; in particular, it will be possible to execute joining operations even between small satellites, despite of their limited resources.

In the past, the use of electromagnetic devices for docking has been poorly investigated. In addition, a great interest on tethered systems exists and has been recently focused on their application to space debris capture [96], as well as LEO spacecraft deorbiting at end-of-life [97]. This has brought to significant studies on tethers dynamics [98], although extensive research on the use of tethers to stabilize and pull space vehicles is still not available. More relevant for this project, the microgravity FELDs Experiment [99] on electromagnetic tethered docking has been performed to preliminarily evaluate the self-alignment concept using magnetic forces. Tests were conducted in ZARM drop

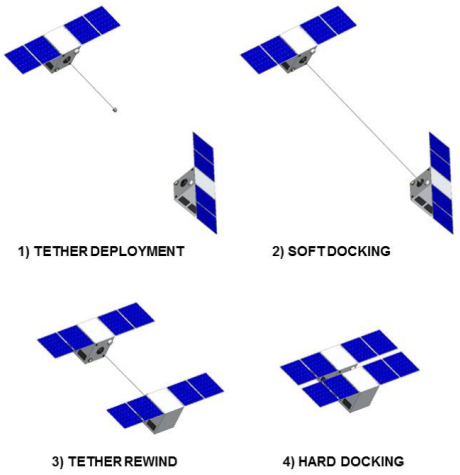

FIGURE 7.4: Artist's impression of the main steps of a tethered docking manoeuvre

tower, where a passive probe was shot towards an electromagnet to analyse its trajectory and to measure transmitted forces during free fall.

In details, the proposed technology to be developed during the project is innovative under two main aspects: (1) first, the use of tethered systems for cooperative docking has never been extensively studied, although the advantages of such techniques are well known and proven by the interest on tethered debris-capture systems. Several studies proposed the use of tethered devices for the capture of inoperative satellites, although only preliminary analysis have been conducted so far on the tether dynamics during the unreel phase, on the probe-to-target contact event and on the two-body leashed flight. (2) Second, the magnetic docking is an innovative concept that implies significant advantages due to the passive self-alignment, which can be successful in the low-forces orbital environment, determining a simplification of mission operations. The probe ejected from the chaser approaches the target with a controlled motion depending on the unreel time law and, in the final part, is passively guided towards the target interface by the magnetic field, which generates the self-alignment effect. These solutions imply reduction of chaser-to-target relative navigation and guidance requirements during rendezvous. Moreover, the extreme flexibility of the tether and the possibility to control its tensile force with the reel system null out the transmitted forces between the vehicles when connected, thus reducing the attitude disturbances on the chaser satellite and the loads on its structure. Once the tethered joining is obtained, the final approach toward hard connection can be performed easily and safely by reeling the wire with a controlled motion: a slightly modified version of the SAM can be designed to realize the solid joint.

7.4 Conclusions

As reported in this last chapter, the research performed in the framework of this PhD course permitted to design and realize a simple mechanical model of a docking interface for small satellites, and perform dynamical analysis and laboratory tests on a manufactured prototype, reaching a TRL of 3-4.
The experience acquired both in the development of the mating interfaces and in the visiting period at MIT allowed to foresee the next steps in the realization and test of a model with an higher TRL, from the improvement of laboratory facilities to the utilization of more relevant test-beds, to the design of a dedicated suite of sensors.
In parallel, some related activities were completed during the research period (i.e.: ARCADE-R2 - as team member - and FLEDs - as supporting scientist -) and others are still in development, for example the design of the refuelling interface and the further investigation of tethered docking.
With the main goal to develop and realize an in-space technological demonstrator of small satellites docking, a long research work is still to be performed, with most of it not already planned; in this work some advices on possible evolutions were introduced, with the aim to indicate a path to be followed for the next years. The run for space is at its beginning, and joining technologies are already a fundamental and unique enabler for most of the servicing activities, with positive and increasing opportunities for the next and far future, both in research and commercial fields. It is only matter of time before humankind will realize fleets of small spacecraft able to self assemble and repair each others or larger ones, or to move on interplanetary routes, transporting fuel, resources and scientific samples.

Appendix A

Large Space Structures and Booms

The high cost of space access led the technology research to adapt and develop new concept structures, in order to reduce the total mass and volume of space vehicles. Deployable systems can solve these requirements and improve the satellite storage in the launcher. Telecommunication antennas, solar panels, solar sails and beams are the main applications of packaging structures: different storage solutions can be implemented in order to obtain refolding [63] or only one-time deployment capability [64]. High precision structures like telescopes can also be realized with deployable structure, demonstrating all the potential of this technology. Industrial applications of deployable structures may also find in many sectors from truck mounted cranes to scaffolding; main differences between space and terrestrial systems are the different load conditions and the deployment power constraints, leading to unusual design solutions for on orbit operations. Deployable beams can be classified in three main categories: telescopic arms, folding trusses and winding bi-stable structures. Usually packaged beams (except telescopic ones) can reach 5% or less of their deployed dimensions [100]; the deployment can be realized with actuated mechanism or pre-loaded spring devices. A fourth class can include inflatable structures, with new concept solutions to deploy and actuate modular structures [101]. In next section some state-of-the-art technologies for space are briefly discussed.

A.1 Telescopic Arms

Telescopic structures in all their different forms work with the same deployment principle: concentric parts slides out till the boom is totally extended A.1. Usually a spindle

and nut mechanism control and actuate the boom, and latches lock it in order to maintain a sizeable stiffness.

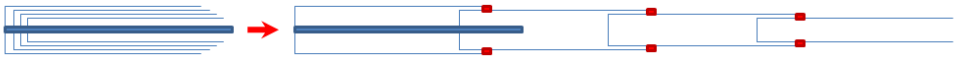

FIGURE A.1: Telescopic boom, stored (left) and deployed (right), in red the latches

Developed arms like ATK telescopic booms [102] have already been used in space. Main drawback of this system is its small storage ratio, due to the length of the larger concentric beam.

A.2 Folding Trusses

In this group various technology solution are collected. Different folding solutions allowed the storage of large structures like solar arrays mounted on beams. Usually a cable system is employed to actively deploy or refolding rod structures. Many examples of this kind of systems can be find in literature, from the Fast Auroral SnapshoT (FAST) satellite (1996) [64] to STS 99 radar topography mission (figure A.2). Recently, tensegrity structures as ADAMS mast [63] as well as STS-99 truss evolutions [100] are still used and investigated. Usually spring mechanisms at the joints between the rods, loaded folding the truss for storage, allow a totally passive deployment. High package ratio can be reached with this kind of beams. Innovative design solutions and material selection led to a considerable reduction of the truss mass.

A.3 Winding Bi-stable Structures

Bi-stable structures exploit the ability of thin walled shells to deform elastically between two stable conditions through a certain load. This condition allows to wind the beam like a flexible tape in a preloaded situation, and to deploy it in a three-dimensional rigid structure (see figure A.3), with the same principle of the measuring tape. Deployed beams present many different shapes and sections, from circular (created by one or two overlapping tapes [103]), to symmetric collapsible [104] [105]. Novel solutions present interlocking latches through the contact walls, improving torsional stiffness.
The main drawback of these beams is the dimension of the deployment-storage system, but in terms of storage ratio and specific weight the winding bi-stable structure is the best solution for extensible beams.

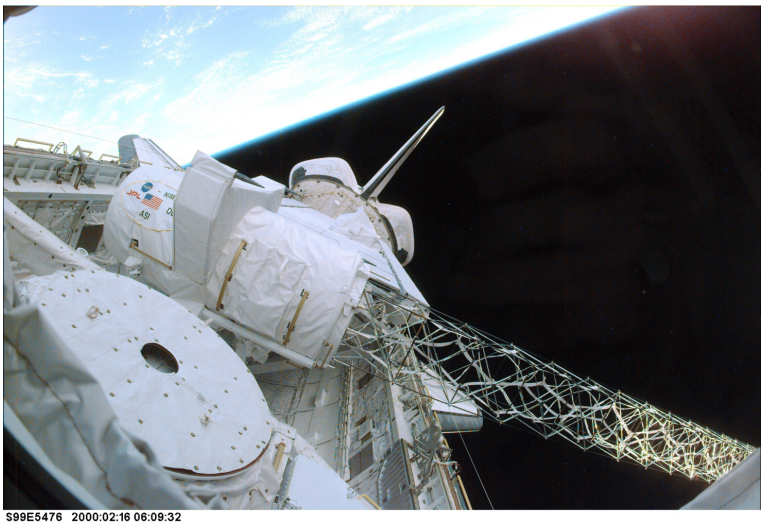

FIGURE A.2: STS-99 deployable truss (courtesy by NASA)

FIGURE A.3: Bi-stable structures: working principle (left) and different beam section configurations (right)

A.4 Inflatable Structures

In the last years inflatable structures are gaining interest thanks to their light mass in deployed configuration and small package volume: thin film materials can be used for these applications, with a calculated mass reduction of 50% over best competing technologies and a package volume reduction to 25% [101]. Thanks to their easiness of deployment, inflatable structures have a high reliability and simple mechanics. Main drawbacks of this technology are related to the internal pressure need: micro meteorites impacts or material ageing due to space environment can lead to structure failures and risk reduction solutions (like multi-cell configurations) should be realized.

Appendix B

ARCADE-R2 Docking mechanism modifications

Minor modifications were performed on ARCADE docking mechanism, as visible in figure B.1, in order to improve the possibility to perform successful procedures.
First, tests on ARCADE showed a small misalignment between SMAV and the drogue, due to the mounting process. To solve this issue, the SMAV front plate supporting the probe was modified (1), in order to allow alignment regulation.
To improve the magnetic force between the probe noise and the drogue, two more modifications were implemented: the drogue bottom was flatten (2), enhancing a better contact, and the probe iron tip was substituted with a magnetic one (3).
In parallel, three IR sensors, used to detect the actuation of the locking solenoids creating the solid joint, were replaced with off-the-shelf components, more reliable and easier to interface with ARCADE-R2 data acquisition system.

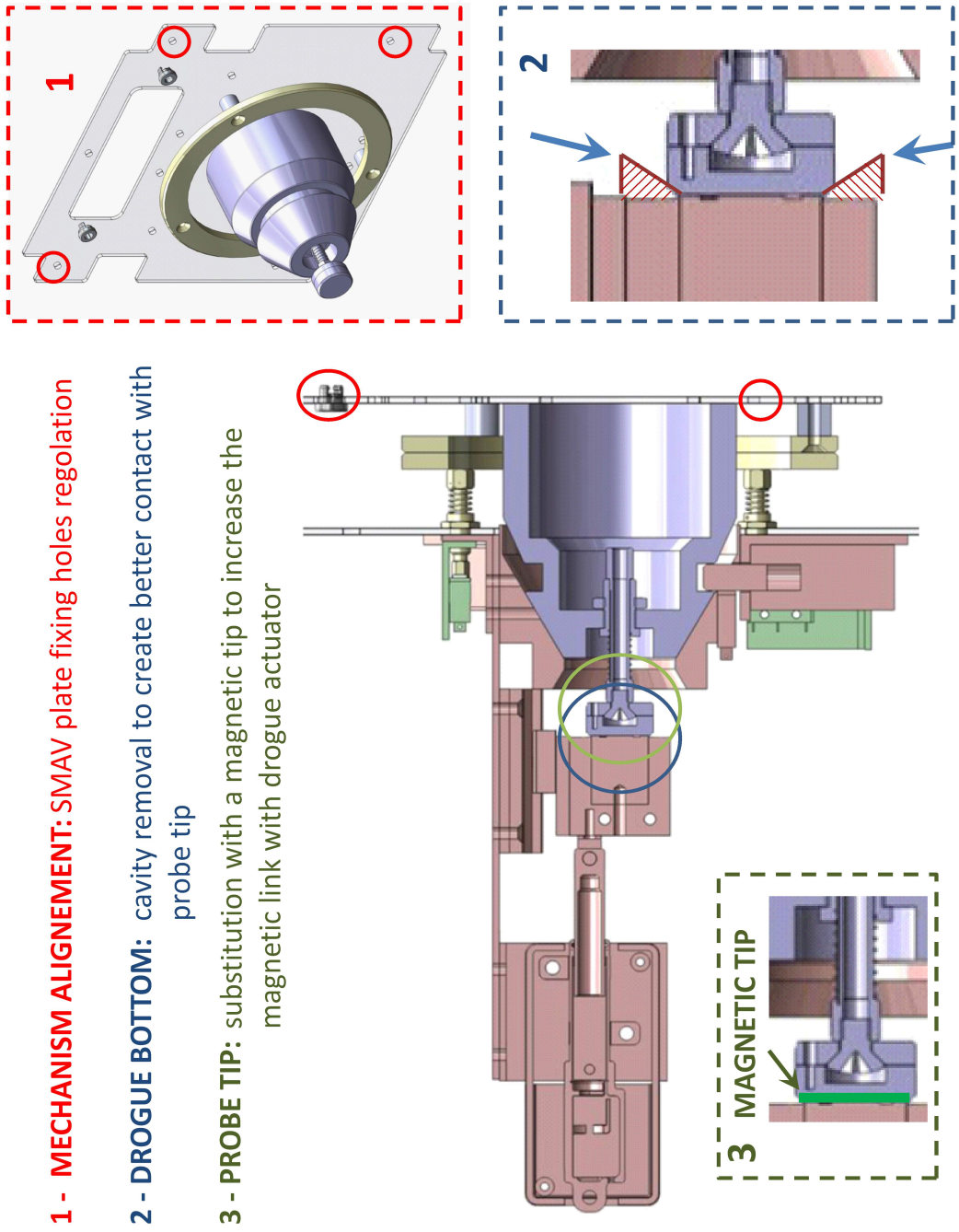

FIGURE B.1: ARCADE-R2 docking mechanism main modifications

Appendix C

Mechanical Drawings

List of inserted mechanical drawings:

Table C.1: Attached mechanical drawings

Part	Part Name	Part Number
Petal Body	PETAL01	Docking001
Petal Head	PETAL02	Docking002
Actuated Disc	Actuated Disc	Docking003
Actuated Disc Cam	AD CAM	Docking004
Base	BASE	Docking005

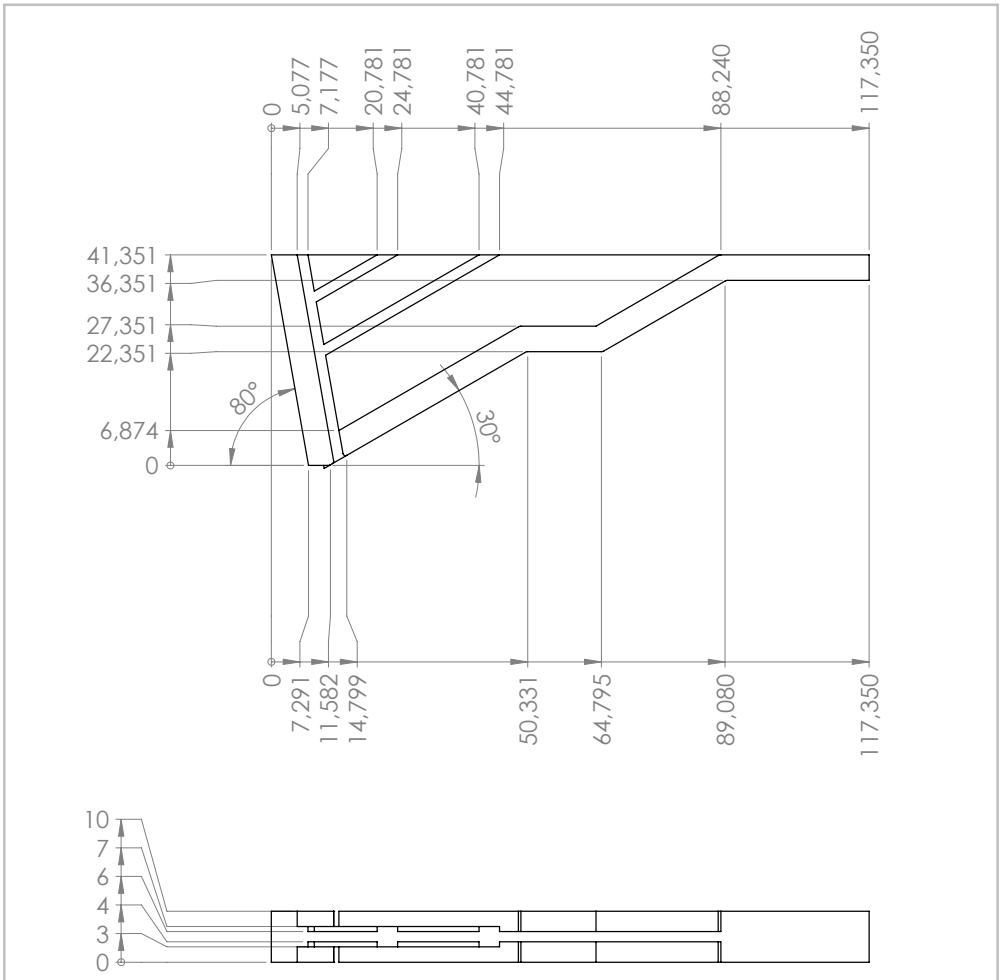

SE NON SPECIFICATO: QUOTE IN MILLIMETRI FINITURA SUPERFICIE: TOLLERANZE: LINEARE: 0.05 ANGOLARE: 0.5		FINITURA: 3.2		SBAVATURA E INTERRUZIONE DEI BORDI NETTI		NON SCALARE IL DISEGNO	REVISIONE
	NOME	FIRMA	DATA			TITOLO: PETAL01	
DISEGNATO	LO		20/6/14				
VERIFICATO	LO		14/11/14				
APPROVATO							
FATTO							
QUALITA'				MATERIALE: Al/ABS/PLA		N. DISEGNO Docking001	A4
PESO: /						SCALA:1:1	FOGLIO 1 DI 1

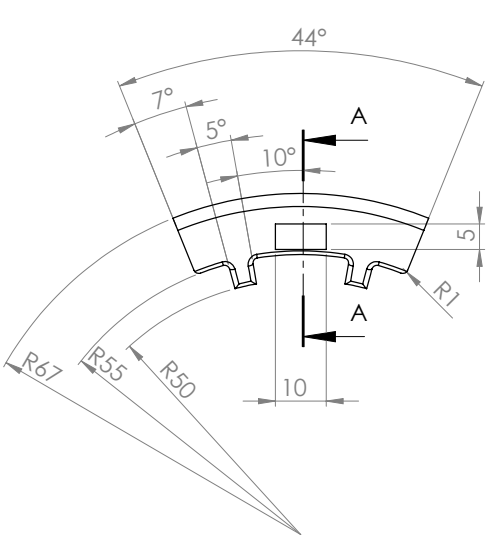

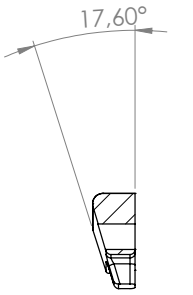

SEZIONE A-A

SE NON SPECIFICATO: QUOTE IN MILLIMETRI FINITURA SUPERFICIE: TOLLERANZE: LINEARE: 0.05 ANGOLARE: 0.5	FINITURA: 3.2				SBAVATURA E INTERRUZIONE DEI BORDI NETTI	NON SCALARE IL DISEGNO	REVISIONE
	NOME	FIRMA	DATA			TITOLO: PETAL02	
DISEGNATO	LO		20/6/14				
VERIFICATO	LO		14/11/14				
APPROVATO							
FATTO							
QUALITA'				MATERIALE: AI/ABS/PLA		N. DISEGNO Docking002	A4
PESO: /						SCALA:1:1	FOGLIO 1 DI 1

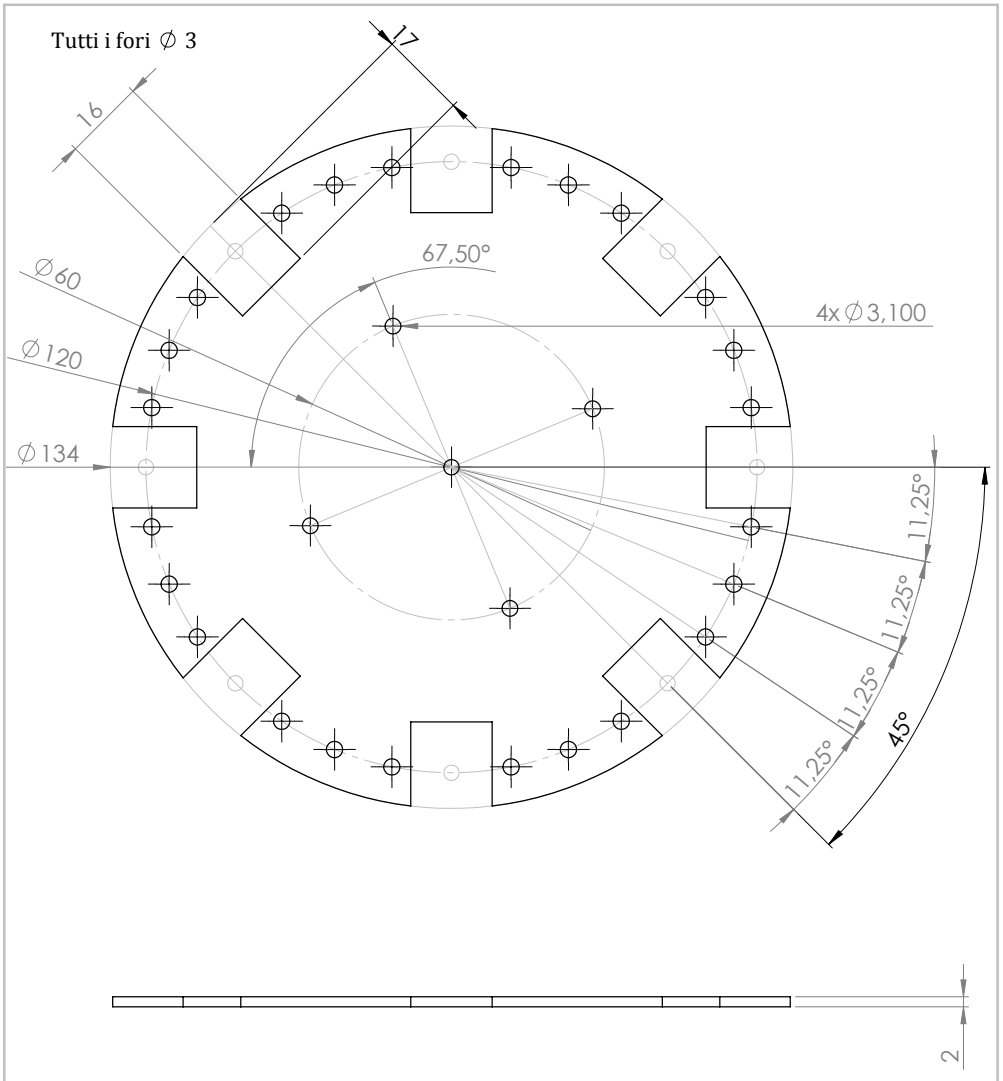

SE NON SPECIFICATO: QUOTE IN MILLIMETRI FINITURA SUPERFICIE: TOLLERANZE: LINEARE: 0.05 ANGOLARE: 0.5	FINITURA: 3.2		SBAVATURA E INTERRUZIONE DEI BORDI NETTI	NON SCALARE IL DISEGNO	REVISIONE	
	NOME	FIRMA	DATA	TITOLO: Actuated Disk		
DISEGNATO	LO		24/4/14			
VERIFICATO	LO		14/11/14			
APPROVATO						
FATTO						
QUALITA'				N. DISEGNO Docking003		A4
			MATERIALE: Al/ABS/PLA			
			PESO: /	SCALA:1:1	FOGLIO 1 DI 1	

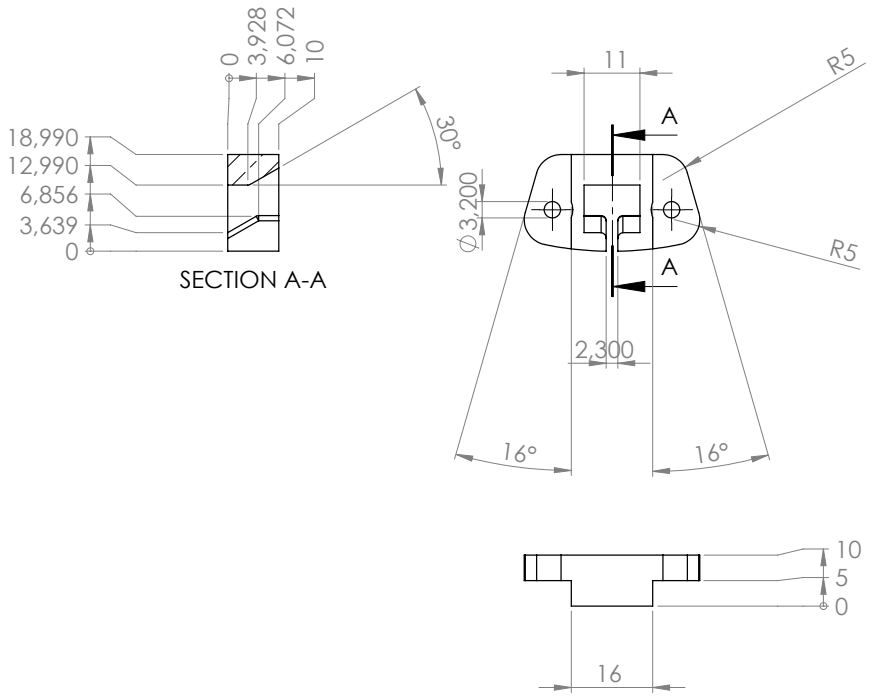

SE NON SPECIFICATO: QUOTE IN MILLIMETRI FINITURA SUPERFICIE: TOLLERANZE: LINEARE: 0.05 ANGOLARE: 0.5	FINITURA: 3.2				SBAVATURA E INTERRUZIONE DEI BORDI NETTI	NON SCALARE IL DISEGNO	REVISIONE
	NOME	FIRMA	DATA			TITOLO:	
DISEGNATO	LO		20/6/14			AD CAM	
VERIFICATO	LO		14/11/14				
APPROVATO							
FATTO							
QUALITA'				MATERIALE:		N. DISEGNO	A4
				Al/ABS/PLA		Docking004	
				PESO: /		SCALA:1:1	FOGLIO 1 DI 1

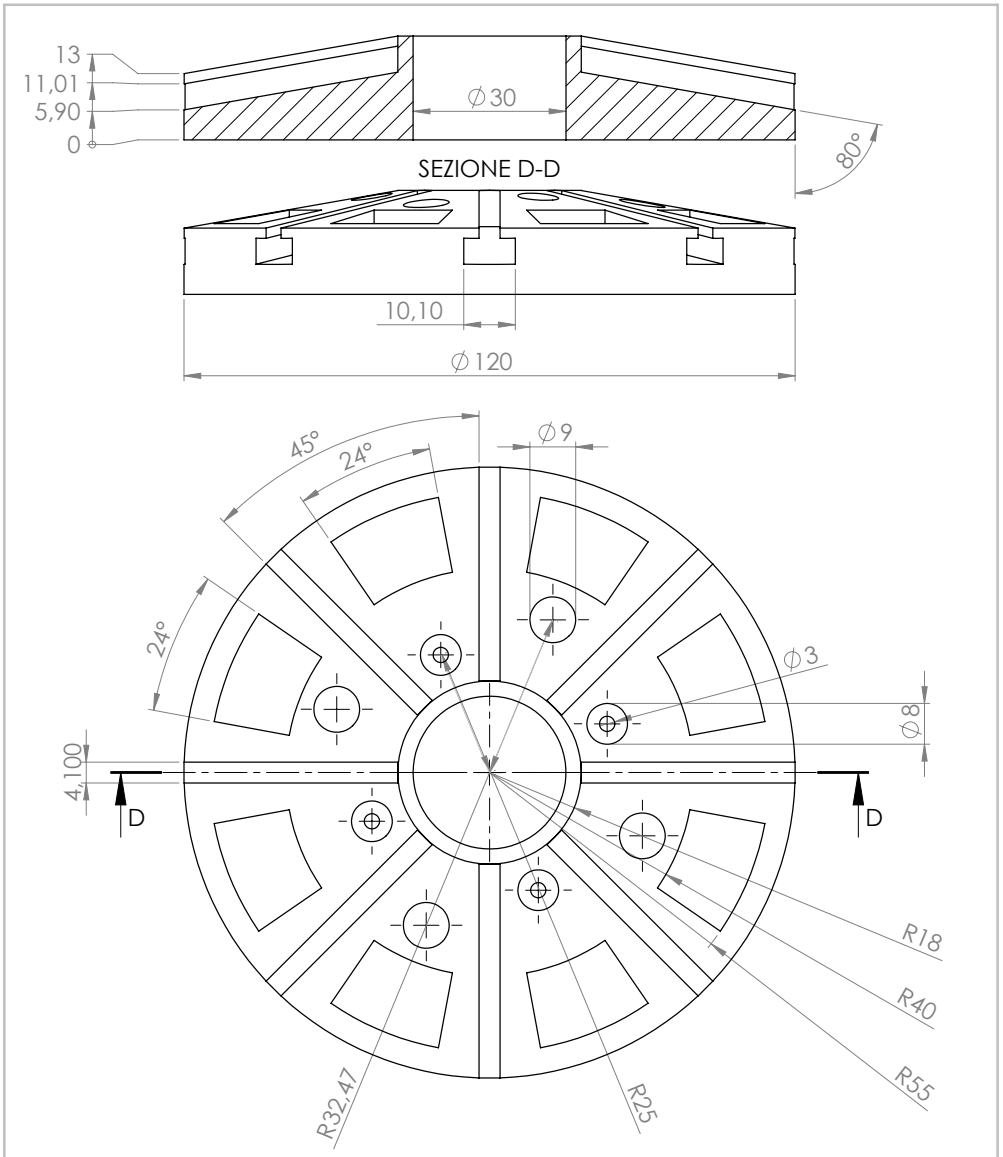

SE NON SPECIFICATO: QUOTE IN MILLIMETRI FINITURA SUPERFICIE: TOLLERANZE: LINEARE: 0.05 ANGOLARE: 0.5	FINITURA: 3.2		SBAVATURA E INTERRUZIONE DEI BORDI NETTI	NON SCALARE IL DISEGNO	REVISIONE	
	NOME	FIRMA	DATA	TITOLO: BASE		
DISEGNATO	LO		20/6/14			
VERIFICATO	LO		14/11/14			
APPROVATO						
FATTO						
QUALITA'				MATERIALE: Al/ABS/PLA	N. DISEGNO Docking005	A4
				PESO: /	SCALA:1:1	FOGLIO 1 DI 1

Appendix D

Test Table

TEST first level	TEST second level	TEST third level	#	CODEX	Y/N
Open-close mechanism	Slow closing: step by step	/	1	01t1ss_01	
		/	2	02t1ss_02	
		/	3	03t1ss_03	
	Slow continuous closing	/	1	04t1sc_01	
		/	2	05t1sc_02	
		/	3	06t1sc_03	
	Medium continuous closing	/	1	07t1mc_01	
		/	2	08t1mc_02	
		/	3	09t1mc_03	
	Fast continuous closing	/	1	10t1fc_01	
		/	2	11t1fc_02	
		/	3	12t1fc_03	
Aligned docking loads	Slow closing: step by step	/	1	13t2ss_01	
		/	2	14t2ss_02	
		/	3	15t2ss_03	
	Slow continuous closing	/	1	16t2sc_01	
		/	2	17t2sc_02	
		/	3	18t2sc_03	
	Medium continuous closing	/	1	19t2mc_01	
		/	2	20t2mc_02	
		/	3	21t2mc_03	
	Fast continuous closing	/	1	22t2fc_01	
		/	2	23t2fc_02	
		/	3	24t2fc_03	
Misaligned docking success	5°	v=0	/	25t305xx_00	
	5°	v=v1	/	26t305xx_v1	
	10°	v=0	/	27t310xx_00	
	10°	v=v1	/	28t310xx_v1	
	15°	v=0	/	29t315xx_00	
	15°	v=v1	/	30t315xx_v1	
	20°	v=0	/	31t320xx_00	
	20°	v=v1	/	32t320xx_v1	
	5 mm	v=0	/	33t3xx05_00	
	5 mm	v=v1	/	34t3xx05_v1	
	10 mm	v=0	/	35t3xx10_00	
	10 mm	v=v1	/	36t3xx10_v1	
	15 mm	v=0	/	37t3xx15_00	
	15 mm	v=v1	/	38t3xx15_v1	
	20 mm	v=0	/	39t3xx20_00	
	20 mm	v=v1	/	40t3xx20_v1	
	5° and 5 mm	v=0	/	41t30505_00	
	5° and 5 mm	v=v1	/	42t30505_v1	
	10° and 5 mm	v=0	/	43t31005_00	
	10° and 5 mm	v=v1	/	44t31005_v1	
	5° and 10 mm	v=0	/	45t30510_00	
	5° and 10 mm	v=v1	/	46t30510_v1	
	10° and 10 mm	v=0	/	47t31010_00	
	10° and 10 mm	v=v1	/	48t31010_v1	

Bibliography

[1] S. Gorevan, I. Yachbes, P. Bartlett, K.Zacny, G. L. Paulsen, T. Kennedy, B. Basso, J. Wilson. Comet and Asteroid Sample Acquisition, Containerization, and Transfer for Sample Return. *Workshop on Spacecraft Reconnaissance of Asteroid and Comet Interiors, LPI Contribution No. 1325*, pages 41–42, October 2006. URL `http://www.lpi.usra.edu/meetings/recon2006/pdf/3022.pdf`.

[2] International Docking System Standard (IDSS) Interface Definition Document (IDD) - Revision C. November 2013. URL `http://www.internationaldockingstandard.com/download/IDSS_IDD_Rev_C_11_22_13_FINAL.pdf`.

[3] A. Ogilvie, J. Allport, M. Hannah, J. Lymer. Autonomous Satellite Servicing Using the Orbital Express Demonstration Manipulator System. *International Symposium on Artificial Intelligence, Robotics and Automation in Space (i-SAIRAS) Proceedings*, February 2008. URL `http://robotics.estec.esa.int/i-SAIRAS/isairas2008/Proceedings/SESSION%2014/m113-Ogilvie.pdf`.

[4] D. King, B. Walker. Space Servicing: The Future is Now. *SOSTC AIAA Improving Space Operations Workshop*, April 2012. URL `https://info.aiaa.org/tac/SMG/SOSTC/Workshop%20Documents/2012/SOSTC_workshop_2012_abstracts_v05.pdf`.

[5] B. C. Hacker, J. M. Grimwood. *On the Shoulders of Titans: A History of Project Gemini —(NASA report SP-4203).*

[6] AIAA Guide for Berthing/Docking/Grasping Interfaces for Serviceable Spacecraft (G-056-1992). *AIAA Standards*, 1992.

[7] W. Fehse. *Automated Rendezvous and Docking of Spacecraft.*

[8] M. Caron, I. Mills. Planning and Execution of Tele-Robotic Maintenance Operations on the ISS. *The 12th International Conference on Space Operations Proceedings*, June 2012. URL `http://www.spaceops2012.org/proceedings/documents/id1272635-Paper-001.pdf`.

[9] E. Dupuis, E. Martin. An Overview of the Recent Canadian Space Agency Ativities in Space Robotics. *International Symposium on Artificial Intelligence, Robotics and Automation in Space (i-SAIRAS) Proceedings*, September 2012. URL `http://robotics.estec.esa.int/i-SAIRAS/isairas2012/Papers/Session%201/01_03_Dupuis.pdf`.

[10] S. Nishida, S. Kawamoto. Strategy for Capturing of a Tumbling Space Debris. *Acta Astronautica*, (68), 20121.

[11] H. Ueno, S. Dubowsky, C. Lee, C. Zhu,Y. Ohkami, S. Matsumoto, M. Oda. Space Robotic Mission Concepts for Capturing Stray Objects. *Proceedings 23rd Space Symposium on Space Technology and Science*, May 2002. URL `http://robots.mit.edu/publications/recent%20pubs/ists_paper.pdf`.

[12] T. Miyabe, A. Konno, M. Uchiyama. Automated Object Capturing with a Two-Arm Flexible Manipulator. *Proceedings of the IEEE International Conference on Robotics and Automation*, page 2529–2534, September 2003. URL `http://ieeexplore.ieee.org/xpls/abs_all.jsp?arnumber=1241973&tag=1`.

[13] B. Bischof, J. Starke, H. Guenther, W.P. Foth, L. Kerstein. ROGER - Robotic Geostationary Orbit Restorer. *Proceedings of the 8th ESA Workshop on Advanced Space Technologies for Robotics and Automation*, November 2004. URL `http://robotics.estec.esa.int/ASTRA/Astra2004/`.

[14] B. E. Kelm, J.A. Angielski, S.T. Butcher, N.G. Creamer, K.A. Harris, C.G. Henshaw, J.A. Lennon, W.E. Purdy, F.A. Tasker, W.S. Vincent, B.P. Whalen. FREND: Pushing the Envelope of Space Robotics. *Space Research and Satellite Technology, 2008 NRL REVIEW*, pages 239–241, 2008. URL `http://www.nrl.navy.mil/content_images/08Space_Kelm.pdf`.

[15] P. Rank, Q. Mühlbauer, W. Naumann, K. Landzettel. DEOS Automation and Robotics Payload. *Proceedings of the 11th Symposium on Advanced Space Technologies in Robotics and Automation*, April 2011. URL `http://www.spacetech-i.com/phase-b-69.html?.../04%20DEOS/02%20DEOS%2...%E2%80%8E`.

[16] N. Zinner, A. Williamson, K. Brenner, J. B. Curran, A. Isaak, M. Knoch, A. Leppek, J. Lestishen. Junk Hunter: Autonomous Rendezvous, Capture, and Deorbit of Orbital Debris. *Revolutionary Aerospace Systems Concepts Academic Linkage (RASC-AL) Conference*, May 2011. URL `http://nia-cms.nianet.org/RASCAL/2010-Winning-Papers/UC-Boulder-RASC-AL-2011.aspx`.

[17] G. Zhai, J. Zhang. Space Tether Net System for Debris Capture and Removal. *4th International Conference on Intelligent Human-Machine Systems and Cybernetics*, pages 257 – 261, August 2012. URL http://ieeexplore.ieee.org/xpls/abs_all.jsp?arnumber=6305675&tag=1.

[18] J. Reed, J. Busquets, C. White. Grappling System for Capturing Heavy Space Debris. *2nd European Workshop on Active Debris Removal*, June 2012. URL http://ieeexplore.ieee.org/xpls/abs_all.jsp?arnumber=6305675&tag=1.

[19] M. Andrenucci, P. Pergola, A. Ruggiero. Active Removal of Space Debris - Expanding foam application for active debris removal - Final Repor. , February 2011. URL http://www.esa.int/gsp/ACT/doc/ARI/ARI%20Study%20Report/ACT-RPT-MAD-ARI-10-6411-Pisa-Active_Removal_of_Space_Debris-Foam.pdf.

[20] C. Kaiser, F. Sjöbergb, J. M. Delcurac, B. Eilertsend. SMART-OLEV – An orbital life extension vehicle for servicing commercial spacecrafts in GEO. *Acta Astronautica*, 63(1-4):400–410, August 2008. URL http://www.sciencedirect.com/science/article/pii/S0094576507003633.

[21] V. Trushlyakov, V. Shalay, J. Shatrov. Aktiv De-Orbiting Onboard System from Leo of Upper Stages of Launchers. *Proceedings of the 5th European Conference on Space Debris*, April 2009.

[22] V. P. Legostaev. Russian space programs: Achievements and prospects of automatic control applications. *Annual Reviews in Control*, 29(Issue 1):1–11, 2005.

[23] *SMZA-03-BLOCK II (1) - Apollo Operational Handbook System Data – Section 2 – Subsectiom 2.13 Docking and Transfer*, .

[24] V. S. Syromyatnikov. Docking system of androgynous and peripheral type. *The 7th Aerospace Mechanism Symposium*, pages 27–35, November 1972. URL http://www.hq.nasa.gov/alsj/7thAerospaceMechanismsSymp_1973010139.pdf.

[25] D. Schwaab. NASA Docking System (NDS) Users Guide.

[26] R. J. McLaughlin, W. H. Warr. The Common Berthing Mechanism (CBM) for International Space Station. *31st International Conference On Environmental Systems*, 2001. URL http://spacecraft.ssl.umd.edu/design_lib/ICES01-2435.ISS_CBM.pdf.

[27] M. Oda. Space robot experiments on NASDA's ETS-VII satellite-preliminary overview of the experiment results. *Robotics and Automation, 1999. Proceedings.*

1999 IEEE International Conference on , 2, May 1999. URL 10.1109/ROBOT.1999.772555.

[28] D. Miller, A. Saenz-Otero, J. Wertz, A. Chen, G. Berkowski, C. Brodel, S. Carlson, D. Carpenter, S. Chen, S. Cheng, D. Feller, S. Jackson, B. Pitts, F. Perez, J. Szuminski, S. Sell. SPHERES: A Testbed for Long Duration Satellite Formation Flying in Micro-Gravity Conditions. *Proceedings of the AAS/AIAA Space Flight Mechanics Meeting,*, (AAS 00-110), January 2000. URL http://ssl.mit.edu/spheres/library/AAS-AIAA.pdf.

[29] Shuonan Dong, Katherine Allen, Paul Bauer, Brett Bethke, Amy Brzezinski, Thomas Coffee, Richard-Duane Chambers, Marcos Flores, Allison Gallagher-Rodgers, John Head, Michael Heiman, Nick Hoff, Colleen Horin, Michael Horvath, Elizabeth Jordan, John Keesee, SeongMin Kim, Edmund Kong, Agnieszka Koscielniak, Scott Lawrence, June Marquiss, Christopher McQuin, Jordan McRae, David Miller, James Modisette, Jasmin Moghbeli, Simon Nolet, Lennon Rodgers, Alvar Saenz-Otero, Audrey Schaffer, and Cemocan Yesil. Self-assembling wireless autonomously reconfigurable module design concept. *Acta Astronautica*, 62(2–3):246 – 256, 2008. ISSN 0094-5765. doi: http://dx.doi.org/10.1016/j.actaastro.2006.12.042. URL http://www.sciencedirect.com/science/article/pii/S0094576507001816.

[30] L. Rodgers, N. Hoff, E. Jordan, M. Heiman, D. W. Miller. A Universal Interface for Modular Spacecraft. *Proceedings of 19th Annual AIAA/USU Conference on Small Satellites*, 2005. URL http://ssl.mit.edu/spheres/library/small_sat_Lennon_Rodgers.pdf.

[31] P. Tchoryk Jr., A. B. Hays , J. C. Pavlich. A Docking Solution for On-Orbit Satellite Servicing: Part of the Responsive Space Equation. *1st Responsive Space Conference*, April 2003. URL http://www.responsivespace.com/Papers/RS1/SESSION2/TCHORYK/2001P.PDF.

[32] K. Ui, S. Matunaga, S. Satori, T. Ishikawa. Microgravity Experiments of Nano-Satellite Docking Mechanism for Final Rendezvous Approach and Docking Phase. *Microgravity - Science and Technology*, 17, Issue 3:pp 56–63, September 2005. URL http://link.springer.com/article/10.1007%2FBF02872088.

[33] A. Adomeit, M. Lakshmanan, P. Seefeldt, H. G. Reimerdes, J. Weise, K. Brieß. Structures for Modular and Serviceable Spacecraft Systems. *Proceedings of 12th European Conference on Spacecraft Structures, Materials and Environmental Testing*, 2012. URL http://esamultimedia.esa.int/multimedia/publications/SP-691/toc_SP-691.pdf.

[34] S. Gorevan, I. Yachbes, P. Bartlett, K.Zacny, G. L. Paulsen, T. Kennedy, B. Basso, J. Wilson. Comet and Asteroid Sample Acquisition, Containerization, and Transfer for Sample Return. *Workshop on Spacecraft Reconnaissance of Asteroid and Comet Interiors*, October 2006. URL `http://www.lpi.usra.edu/lpi/contribution_docs/LPI-001325.pdf`.

[35] A. Boesso, A. Francesconi. ARCADE small-scale docking mechanism for micro-satellites. *Acta Astronautica*, 86, May 2013. URL `http://www.sciencedirect.com/science/article/pii/S0094576513000180`.

[36] L. Olivieri, A. Francesconi. Design of a docking mechanism for small spacecraft. *63rd International Astronautical Congress*, October 2012.

[37] L. Olivieri, F. Branz, A. Francesconi. Conceptual design of small spacecraft docking mechanism actuated by electroactive polymers. *2nd IAA Conference on University Satellites Missions and Cubesat Winter Workshop*, February 2013. URL `http://www.sciencedirect.com/science/article/pii/S0094576513000180`.

[38] M. Fittock, A. Stamminger, M. Roth, K. Dannenberg, H. Page. REXUS/BEXUS: launching student experiments -a step towards a stronger space science community. *38th COSPAR Scientific Assembly*, July 2010. URL `http://adsabs.harvard.edu/abs/2010cosp...38.3891F`.

[39] TITLE XV—MATTERS RELATING TO ARMS CONTROL, EXPORT CONTROLS, AND COUNTER-PROLIFERATION, Subtitle B—Satellite Export Controls, PUBLIC LAW 105–261, .

[40] Aurora program, . URL `http://www.esa.int/Our_Activities/Human_Spaceflight/Exploration/The_European_Space_Exploration_Programme_Aurora`.

[41] Plans for asteroid mining emerge, . URL `http://www.bbc.com/news/science-environment-17827347`.

[42] Cubesat launches list, . URL `http://www.zarya.info/Diaries/Launches/Launches.php?year=2012`.

[43] Cubesat list, . URL `http://en.wikipedia.org/wiki/List_of_CubeSats`.

[44] E. Gill, P. Sundaramoorthy, J. Bouwmeester, B. Zandbergen, R. Reinhard. Formation flying within a constellation of nano-satellites: The QB50 mission. *Proceedings of 6th International Workshop on Satellite Constellation and Formation Flying*, 2010. URL `http://www.sciencedirect.com/science/article/pii/S0094576512001440`.

[45] E. P. Caillibot, C. C. Grant, D. D. Kekez. Formation Flying Demonstration Missions Enabled by CanX Nanosatellite Technology. *Proceedings of the 19th Annual AIAA/USU Conference on Small Satellites*, 2005.

[46] T. R. Krogstad, J. T. Gravdahl, K. Y. Pettersen, E. Børhaug. AUVSAT - an experimental platform for spacecraft formation flying. *Proceedings of 59th International Astronautical Congress*, 2008. URL `http://www.itk.ntnu.no/ansatte/Gravdahl_Jan.Tommy/papers/iac2008_paper.pdf`.

[47] M. Marszalek, O. Kurz, M. Drentschew, M. Schmidt, K. Schilling. Intersatellite Links and Relative Navigation: Pre-conditions for Formation Flights with Pico- and Nanosatellites. *Preprints of the 18th IFAC World Congress*, 2011. URL `http://www.itk.ntnu.no/ansatte/Gravdahl_Jan.Tommy/papers/iac2008_paper.pdf`.

[48] T. Vladimirova, X. Wu, A.H. Jallad, C. P. Bridges. Distributed Computing in Reconfigurable Picosatellite Networks. *Conference on Adaptive Hardware and Systems*, 2007. URL `http://www.itk.ntnu.no/ansatte/Gravdahl_Jan.Tommy/papers/iac2008_paper.pdf`.

[49] C.P. Bridges, L. Sauter, P. Palmer. Formation deployment and separation simulation of multi-satellite scenarios using SatLauncher. *IEEE Aerospace Conference, Big Sky, MT*, 2011. URL `http://www.itk.ntnu.no/ansatte/Gravdahl_Jan.Tommy/papers/iac2008_paper.pdf`.

[50] To the stars: Nasa selects small spacecraft technology demonstration missions, . URL `http://www.nasa.gov/home/hqnews/2012/aug/HQ_12-274_Small_Tech_Demo_Missions.html`.

[51] Robotic refueling mission, . URL `http://ssco.gsfc.nasa.gov/robotic_refueling_mission.html`.

[52] D. W. Miller, S. Mohan, J. Budinoff. Assembly of a Large Modular Optical Telescope (ALMOST). *The International Society for Optical Engineering*, July 2007. URL `http://dspace.mit.edu/handle/1721.1/52733`.

[53] D. L. Akin, J. C. Lanef, B. J. Roberts, S. R. Weisman. Robotic Capabilities for Complex Space Operations. *AIAA Space 2001 Conference and Exposition*, 2001. URL `http://spacecraft.ssl.umd.edu/publications/2001/2001.Akin.pdf`.

[54] Pierre Bely. *The design and construction of large optical telescopes*. Springer, 2003.

[55] James R Wertz and Wiley J Larson. Space mission analysis and design. 1999.

[56] C. E. Eyerman. A systems engineering approach to disturbance minimization for spacecraft utilizing controlled structures technology.

[57] Cira-2012 models of the earth's upper atmosphere, . URL `https://spaceweather.usu.edu/htm/cira/`.

[58] Backes P. Burdick J. Kennedy B. Kim J. Lee N. Malakhova G. Mukherjee R. Pellegrino S. Wu Y.-H. Hogstrom, K. A robotically-assembled 100-meter space telescope.

[59] Francesco Sansone, Livia Savioli, and Alessandro Francesconi. Economic benefits for leo telecom constellations due to modular spacecraft architecture.

[60] R. Shankar, T. K. Ghosh, R. J. Spontak. Dielectric elastomers as next-generation polymeric actuators. *Soft Matter*, Issue 9, 207.

[61] R. Zhang, P. Lochmatter, A. Kunz, G. Kovacs. Spring roll dielectric elastomer actuators for a portable force feedback glove. *Smart Structures and Materials 2006: Electroactive Polymer Actuators and Devices (EAPAD)*, SPIE 6168, 2006.

[62] G. Kovacs, S. Michel, R. Pelrine, Q. Pei. Study on core free rolled actuator based on soft dielectric EAP. *Smart Structures and Materials 2006: Electroactive Polymer Actuators and Devices (EAPAD)*, 6927.

[63] O. R. Stohlman. Repeatability of joint-dominated deployable masts.

[64] D. Pankow, R. Besuner, R.Wilkes, R. Ullrich. DEPLOYMENT MECHANISMS ON THE FAST SATELLITE: Magnetometer, Radial Wire, and Axial Booms. *Space Science Reviews*, v. 98, Issue 1/2:93–111, 2001. URL `http://sprg.ssl.berkeley.edu/fast/scienceprod/papers/pankow/FASTPaper.PDF`.

[65] R. Osiander, S. L. Firebaugh, J. L. Champion, D. Farrar, M. A. Garrison Darrin. Microelectromechanical Devices for Satellite Thermal Control. *IEEE SENSORS JOURNAL*, 4(4), August 2004.

[66] L. Johnson, et al. NanoSail-D: A solar sail demonstration mission. *Acta Astronautica*, 68(5-6), March–April 2011.

[67] M. Pignataro, N. Rizzi, A. Luongo. *Stabilità, Biforcazione e Comportamento Postcritico delle Strutture Elastiche.*

[68] S. P. Timoshenko, J. M. Gere. *Theory of Elastic Stability, 2^{nd} ed.*

[69] Friction and coefficients of friction, . URL `http://www.engineeringtoolbox.com/friction-coefficients-d_778.html`.

[70] J Schroeter. Risk management in esa's scientific directorate- a case study. *ESA Bulletin*, 107:64–71, 2001.

[71] Jana L Schwartz, Mason A Peck, and Christopher D Hall. Historical review of air-bearing spacecraft simulators. *Journal of Guidance, Control, and Dynamics*, 26(4):513–522, 2003.

[72] Heidi C. Schubert and Jonathan P. How. Space construction: an experimental testbed to develop enabling technologies, 1997. URL `http://dx.doi.org/10.1117/12.295583`.

[73] Saburo Matunaga, Keisuke Yoshihara, Takashi Takahashi, Shingo Tsurumi, and Kyoichi Ui. Ground experiment system for dual-manipulator-based capture of damaged satellites. In *Intelligent Robots and Systems, 2000.(IROS 2000). Proceedings. 2000 IEEE/RSJ International Conference on*, volume 3, pages 1847–1852. IEEE, 2000.

[74] T. Boge, T. Wimmer, O. Ma, M. Zebenay. EPOS:A Robotics-Based Hardware-in-the-Loop Simulator for Simulating Satellite RvD Operations . *i-SAIRAS 2010*, September 2010.

[75] Advanced robotic testbed for testing of space missions, . URL `http://www.gmv.com/en/Company/Communication/News/2013/09/platform.html`.

[76] A. Antonello, F. Sansone, A. Francesconi, R. Carli, A. Carron. A Novel Approach to the Simulation of On-Orbit Rendezvous and Docking Maneuvers in a Laboratory Environment through the Aid of an Anthropomorphic Robotic Arm. *IEEE International Workshop Metrology for Aerospace*, May 2014.

[77] Andrea Valmorbida, Francesco Scarpa, Mattia Mazzucato, Sergio Tronco, Stefano Debei, and Enrico C Lorenzini. Attitude module characterization of the satellite formation flight testbed. In *Metrology for Aerospace (MetroAeroSpace), 2014 IEEE*, pages 73–78. IEEE, 2014.

[78] S. Nolet. Development of a guidance, navigation and control architecture and validation process enabling autonomous docking to a tumbling satellite.

[79] A. Saenz Otero. Design principles for the development of space technology maturation laboratories aboard the international space station.

[80] A. R. Hilton, G. J. Eslinger, D. W. Miller. Dynamics Modeling of Electromagnetic Formation Flight. *36th ANNUAL AAS GUIDANCE AND CONTROL CONFERENCE*, February 2013. URL `http://www.usafa.edu/df/dfas/Papers/`

20122013/Dynamics%20Modeling%20of%20Electromagnetic%20Formation%20Flight%20-%20Hilton.pdf.

[81] F. Capolupo. Optical Staged Control for Separated Spacecraft Interferometry: from System Identification to Testbed Validation. *9th PEGASUS-AIAA Student Conference*, April 2014. URL https://www.pegasus-europe.org/AIAA_Pegasus/Papers/ISAE_Capolupo.pdf.

[82] J. Katz, S. Mohan, D. Miller. On-Orbit Assembly of Flexible Space Structures with SWARM. *AIAA Infotech@Aerospace 2010*, April 2010. URL http://arc.aiaa.org/doi/abs/10.2514/6.2010-3524.

[83] D. Fourie, B. Tweddle, S. Ulrich, A. Saenz Otero. Vision-Based Relative Navigation and Control for Autonomous Spacecraft Inspection of an Unknown Object. *AIAA GUIDANCE, NAVIGATION, AND CONTROL (GNC) CONFERENCE*, August 2013. URL http://arc.aiaa.org/doi/abs/10.2514/6.2013-4759.

[84] et al. M. Abel. Integrated Navigation Sensor Platform for EVA Control and Testing (INSPECT) for SPHERES.

[85] *Design Document Universal Docking Port*, .

[86] Buzz Aldrin. Line-of-sight guidance techniques for manned orbital rendezvous.

[87] D. J. Pearson. The glideslope approach.

[88] J. Enright, M. Hilstad, A. Saenz Otero, D. Miller. The SPHERES Guest Scientist Program: Collaborative Science on the ISS. *2004 IEEE Aerospace Conference*, March 2004.

[89] *ZARM Drop Tower Bremen User Manual*, .

[90] Didier Pinard, Stéphane Reynaud, Patrick Delpy, and Stein E. Strandmoe. Accurate and autonomous navigation for the {ATV}. *Aerospace Science and Technology*, 11(6):490 – 498, 2007. ISSN 1270-9638. doi: http://dx.doi.org/10.1016/j.ast.2007.02.009. URL http://www.sciencedirect.com/science/article/pii/S1270963807000624.

[91] Atv-5 set to test new rendezvous sensors, . URL http://www.esa.int/Our_Activities/Human_Spaceflight/ATV/ATV-5_set_to_test_new_rendezvous_sensors.

[92] Cubesat kit^{TM} gpsrm 1 gps receiver module, . URL http://www.cubesatkit.com/docs/datasheet/DS_CSK_GPSRM_1_710-00908-C.pdf.

[93] Oliver Montenbruck, Takuji Ebinuma, E Glenn Lightsey, and Sunny Leung. A real-time kinematic gps sensor for spacecraft relative navigation. *Aerospace Science and Technology*, 6(6):435–449, 2002.

[94] F. Sansone, F. Branz, A. Francesconi, M. Barbetta, and M.G. Pelizzo. 2d close-range navigation sensor for miniature cooperative spacecraft. *Aerospace and Electronic Systems, IEEE Transactions on*, 50(1):160–169, January 2014. ISSN 0018-9251. doi: 10.1109/TAES.2013.120295.

[95] L. Olivieri, R. Mantellato, F. Branz, F. Sansone, A. Cavinato, M. Gaino, D. Petrillo, A. Francesconi, E. C. Lorenzini. Cubesat mission concept for tethered electromagnetic docking demonstration. In *Tartu Conference on Space Science and Technology*.

[96] J. Reed and S. Barraclough. Development of harpoon system for capturing space debris. In *Proc. 6th European Conference on Space Debris*.

[97] E. Ahedo and J. R. Sanmartin. Analysis of bare-tether systems for deorbiting low-earth-orbit satellites.

[98] R. Mantellato, M. Pertile, G. Colombatti, A. Valmorbida, and E. C. Lorenzini. Two-bar model for free vibrations damping of space tethers by means of spring-dashpot devices.

[99] Meet the teams: Felds (2014), . URL `http://www.esa.int/Education/Meet_the_teams_FELDs_2014`.

[100] Articulated mast systems, . URL `https://www.atk.com/products-services/articulated-mast-systems/`.

[101] C. Cassapakis, M. Thomas. Inflatable Structures Technology Development Overview. *AIAA 1995 Space Programs and Technologies Conference*, 1995. URL `http://www.lgarde.com/assets/content/files/publications/overview.pdf`.

[102] Telescopic booms, . URL `https://www.atk.com/products-services/telescoping-boom/`.

[103] Stem products and programs, . URL `http://www.northropgrumman.com/BusinessVentures/AstroAerospace/Products/Documents/pageDocs/STEM_Hardware_Programs.pdf`.

[104] M. Leipold, D. Kassing, M. Eiden, L. Herbeck. Solar Sails for Space Exploration – The Development and Demonstration of Critical Technologies in Partnership. *ESA*

bulletin 98, June 1999. URL `http://www.esa.int/esapub/bulletin/bullet98/LEIPOLD.pdf`.

[105] F. Rehnmark, M. Pryor, B. Holmes, D. Schaechter, N. Pedreiro, C. Carrington. Development of a Deployable Nonmetallic Boom for Reconfigurable Systems of Small Spacecraft. *AIAA*, 2007. URL `http://ntrs.nasa.gov/archive/nasa/casi.ntrs.nasa.gov/20070031728.pdf`.